Josip Juraj Strossmayer University of Osijek

University of Dubrovnik

Ruđer Bošković Institute

University Postgraduate Interdisciplinary Doctoral Course of Molecular Biosciences

Tihana De Zan

The Role of Proteins RhoD and KIF20B in Sensitivity of Tumor Cell Lines to Anticancer Drugs

PhD Thesis

Osijek, 2021

Uloga proteina RhoD i KIF20B u osjetljivosti tumorskih staničnih linija na protutumorske lijekove

Tihana De Zan

Disertacija je izrađena u: Zavodu za farmakologiju, Sveučilište u Kyotu, Kyoto, Japan; Laboratoriju za staničnu biologiju i prijenos signala, Institut Ruđer Bošković, Zagreb, Hrvatska

Mentori: Dr. sc. Andreja Ambriović-Ristov, znanstvena savjetnica
                 Prof. Dr. sc. Toshimasa Ishizaki, redovni profesor

Kratki sažetak doktorske disertacije:
RhoD je atipična Rho GTPaza uključena u promet endosoma i dinamiku aktinskog citoskeleta. Njegov predloženi interakcijski partner, protein KIF20B, ima ulogu u završetku citokineze i povećano je eksprimiran u mnogim tumorima i tumorskim staničnim linijama. Uloga ovih proteina u osjetljivosti tumorskih staničnih linija na lijekove veoma je slabo ispitana. Ovisnost ekspresije proteina RhoD i KIF20B, njihova zajednička lokalizacija i uključenost u procesu stanične diobe ukazali su na potencijalnu sličnu ulogu u osjetljivosti odabranih staničnih linija na protutumorske lijekove, što je u ovoj studiji ispitano pomoću MTT testa nakon dodavanja lijekova cisplatine, paklitaksela i vinkristina stanicama s utišanim proteinima RhoD ili KIF20B.

Disertacija je pohranjena u: Nacionalnoj i sveučilišnoj knjižnici Zagreb, Ul. Hrvatske bratske zajednice 4, Zagreb; Gradskoj i sveučilišnoj knjižnici Osijek, Europska avenija 24, Osijek; Sveučilištu Josipa Jurja Strossmayera u Osijeku, Trg sv. Trojstva 3, Osijek

BASIC DOCUMENTATION CARD

Josip Juraj Strossmayer University of Osijek   **PhD thesis**
University of Dubrovnik
Ruđer Bošković Institute
University Postgraduate Interdisciplinary Doctoral Course of
Molecular Biosciences

Scientific Area: Biological Sciences
Scientific Field: Biology

The Role of Proteins RhoD and KIF20B in Sensitivity of Tumor Cell Lines to Anticancer Drugs

Tihana De Zan

Thesis performed at: Department of Pharmacology, Kyoto University, Kyoto, Japan; Laboratory for Cell Biology and Signal Transduction, Ruđer Bošković Institute, Zagreb, Croatia

Supervisors: Andreja Ambriović-Ristov, PhD, senior scientist
                                Prof. Toshimasa Ishizaki, PhD, full-time professor

Short abstract:
RhoD is an atypical Rho GTPase involved in endosome trafficking and actin cytoskeleton dynamics. Its proposed interacting partner, protein KIF20B, has a role in cytokinesis completion and is overexpressed in many tumors and tumor cell lines. The role of these proteins in sensitivity of tumor cell lines to anticancer drugs has barely been researched. The dependency of proteins RhoD and KIF20B expression, their mutual localization site and their involvement in the process of cell division, have suggested they may have a similar role in the sensitivity of selected tumor cell lines to antitumor drugs, which was tested in this study by performing the MTT cell viability assay after the addition of drugs cisplatin, paclitaxel and vincristine to cells with silenced RhoD or KIF20B.

Number of pages: 149
Number of figures: 55
Number of tables: 23
Number of references: 220
Original in: English
Key words: RhoD, KIF20B, cisplatin, paclitaxel, vincristin, cell division

Date of the thesis defense: 12 February 2021

Reviewers:
1. Prof. Maja Matulić, PhD, full-time professor, committee president
2. Prof. Vera Cesar, PhD, full-time professor, reviewer
3. Dragomira Majhen, PhD, senior research associate, reviewer
4. Jasminka Štefulj, PhD, senior research associate, substitute

Acknowledgements

I wanted to quit a million times. Life has thrown me so many curveballs, that sometimes it was difficult to stay on track. Thankfully, I had so many people around me who didn't stop believing in me, even when I did.

First of all, I would like to thank my Croatian mentor, Andreja Ambriović-Ristov, who was also my mentor for my diploma thesis. Dear Andreja, thank you so much for your overwhelming patience and understanding. Thank you for being a superb scientist and for being human at the same time. Thank you for your leadership and your support. Thank you for sharing your outlook on both science and life with all of us who have ever had the privilege to work with you. You live science with such passion and dedication and thank you for sharing it and passing it on to your students. And most of all, thank you for not giving up on me.

I would also like to thank my dear Croatian labmates. Dragomira, thank you for so many of your helpful talks and kindness. When I first met you, you were a PhD student and now you are a giant. Keep up the great work.

Sanjica, thank you so much for always being there and offering optimism and solution for any problem, be it life or life-science. You have taught me a lot about perseverence and dedication, while also being humble.

Anamaria, thank you for sharing your expertise and for encouraging talks. You are science with style!

Thanks to Ana, Mladen, Juran and Davor for the friendship and fun times during experiments. Special thanks go to my former mentor, Prof. Maja Osmak, who is an inspiration to all of us and who truly made a difference in Croatian science and all of our lives. Her unique leadership made the lab feel like a second home.

Thanks to Ljiljana, Snježana and Marina for technical assistance and much more than that, thank you for tying us all together and always doing your best to make us all feel like a big family.

Dear Ishizaki-Sensei, thank you so much for honoring me by being my mentor. Thank you for all of your patience, time and selflessness. Thank you for being both a great expert and a great teacher. I have learned so much from you and continue to learn each day. Thank you for your

understanding and for all the great advice and lessons. Thank you so much for the kindness and acceptance you have shown numerous times and for enabling me to learn so many new techniques.

Thank you to Narumiya-Sensei, who has welcomed me to his lab in Kyoto and who is truly a great person and a great scientist. As you have taught us all: It's all there. We just have to find it. Thank you for your tireless pursuit of knowledge and for teaching it to so many of us.

Thanks to my Japanese lab partners: Sada, we all strive to be the scientist you are some day; committed, knowledgeable, humble and persistent. It was great working with you. You taught me a lot.

Sakamoto-San, thank you for all your great advice and for your friendship. It has really meant a lot to me. Thank you for your readiness to explain facts about Rho GTPase and Japanese customs.

Maekawa-San, thank you for being so kind and such a great friend and teacher. It was fun learning from you, both about science and also Japanese culture. Thank you for all the support talks and for embracing both me and my husband as friends. It isn't easy being a „gaikoku-jin" in Japan, so it was great to have friends like you.

Aliza and Somayeh, thank you for your friendship and introducing my husband and me to a life in Japan as strangers. It is nice to have someone who is in the same boat as you.

To Dean-Sensei, Furuyashiki-Sensei, Fujita-Sensei, Deguchi-San, thank you for acknowledging me as a valued member of your lab and welcoming my opinions in lab discussions.

To Nonomura-San, thank you so much for sharing your enormous expertise, for your inexhaustive willingness to help others and for your kindness.

To Arai-San, thank you for making all the necessary paperwork for coming to Japan look easy. Thank you for your patience and your good work.

To all the post-docs and PhD students: Joan, Kathy, Kamijo-San, Shinohara-Sun, Hiro, Shirakawa-kun, thank you for being good coworkers and for making my stay in Japan feel valued.

Thank you to all the Narumiya Lab for truly doing remarkable science, for addressing every problem bravely and seriously, for being the cultivating place of knowledge and for making a small PhD student from Croatia feel like really contributing to the world science. I miss you all and I will never forget you!

"The path to heaven runs through miles of clouded hell right to the top"

"And I know it's hard when you're falling down
And it's a long way up when you hit the ground
Get up now, get up, get up now"

Imagine Dragons

Table of Contents

1. Introduction

1.1. Anticancer Drugs

Today cancer is one of the biggest causes of morbidity and mortality worldwide. Due to the versatility of the disease, which arises from different mutations in the genome, there are also various types of cancers, specific to tissues and cells of the organism. The most common courses of action in tumor treatment are surgical excision, radiotherapy and chemotherapy. Chemotherapy encompasses treatment by immunotherapy, hormonal therapy and antitumor drugs. Antitumor drugs may be natural compounds or their derivatives and synthetic molecules. In both cases, aside from chemical modifications to the drugs, they can also be encapsulated or conjugated to a carrier system to enhance their efficiency of distribution in target tissues and entry in tumor cells. Classified by their structure and mode of action, they can be subdivided into alkylating agents, antibiotics, antimetabolites, topoisomerase I and II inhibitors, mitosis inhibitors, platinum compounds and others (Espinosa et al., 2003).

1.1.1. Cisplatin

Cisplatin, cisplatinum, or *cis*-diamminedichloroplatinum(II), is a metallic coordination compound with a square planar geometry (Figure 1.1.1.1.). It was first synthesized by Peyrone in 1844 and its structure was identified in 1893 by Alfred Werner. After observations that an electrolysis product of cisplatin inhibited division in *E. coli* by Rosenberg and coworkers in 1965, it underwent further studying, especially in attempts to use it as antitumor drug (Dasari and Tchounwou, 2015). Today cisplatin is widely used in clinic in treatment of different types of cancers including sarcomas, cancers of soft tissue, bones, muscles, and blood vessels (Desoize and Madoulet, 2002).

1.1.1.1. Cisplatin Uses in Clinic

Aside from cisplatin, several thousand analogs were synthesized, of which 13 are extensively used in clinical applications, most notable one being carboplatin, because of its advantages over cisplatin in regards of reduced side effects (Dasari and Tchounwou, 2015). Cisplatin is also being used in conjuncture with some other cytotoxic drugs and compounds in combination therapy, such as paclitaxel, doxorubicin, tegafur-uracil, gemcitabine, vitamin D, honeybee venom, vinblastine, methotrexate etc.
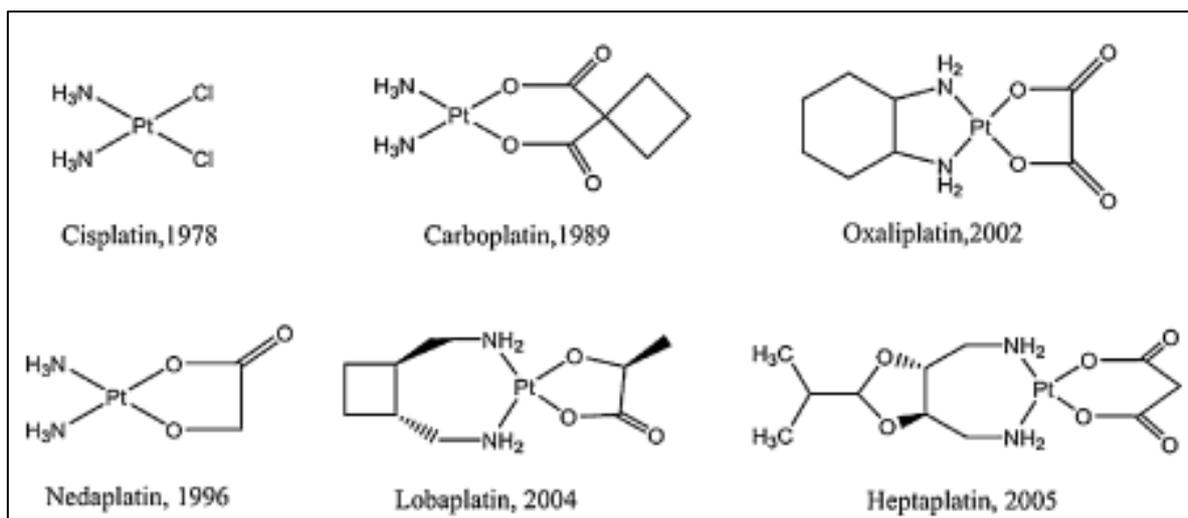
Figure 1.1.1.1. The chemical structure of cisplatin and most notable classical cisplatin analogs used in clinic; carboplatin, oxaliplatin, nedaplatin, lobaplatin and heptaplatin. The years indexed in compound names indicate the year each drug was entered in clinical use. Reprinted from Ma et al., 2015.

Alongside carboplatin, cisplatin is the most prevalent treatment in SCLC chemotherapy (Go and Adjei, 1999), however it exhibits renal toxicity, nausea and vomiting in patients (Iwasaki et al., 2005; Kosmas et al., 2001). Cisplatin and its derivatives are still the principal treatment for ovarian cancer, despite their adverse symptoms and emergence of resistance. However, the new formulations of liposomal cisplatin display less of the severe side effects in patients and also circumvent resistance (Koch et al., 2013). Since cisplatin is not effective as a standalone drug in the treatment of head and neck squamous cell carcinoma (HNSCC) and other types of carcinoma in general, it is still being used in combination therapy in their treatment, along with methotrexate, vinblastine, doxorubicin and gemcitabine (Dasari and Tchounwou, 2015). It is also widely used in the treatment of breast, testicular, cervical, prostate, bladder and lung malignancies and refractory non-Hodgkin's lymphoma (Tsimberidou et al., 2009), as well as for childhood brain tumors, gastric cancer, anal cancer and leukemias (Dasari and Tchounwou, 2015).

1.1.1.2. Cisplatin mechanisms of action

In part, cisplatin can enter the cell via passive diffusion through the plasma membrane, however the import depends on the cell energy state. By introducing Na/K pump inhibitors the sodium gradient across plasma membrane becomes destabilized which then inhibits the facilitated or active transport of cisplatin into the cell (Hall et al., 2008). The principal mode of cisplatin uptake into the cell is by the copper transporter (CTR1) (Ishida et al., 2002), a solute carrier importer, which is analogous to the MDR1 (multidrug resistance receptor).

Cisplatin uptake is also carried out by the organic cationic transporters (OCT1-3), which are involved in the absorption and secretion of various compounds in organs and tissues (Hall et al., 2008). On the other hand, cisplatin is excreted from cells by copper transport ATPase proteins ATP7A and ATP7B, and transporters involved in the expulsion of toxins, such as the multidrug resistance associated proteins (Hall et al., 2008) (Figure 1.1.1.2.).
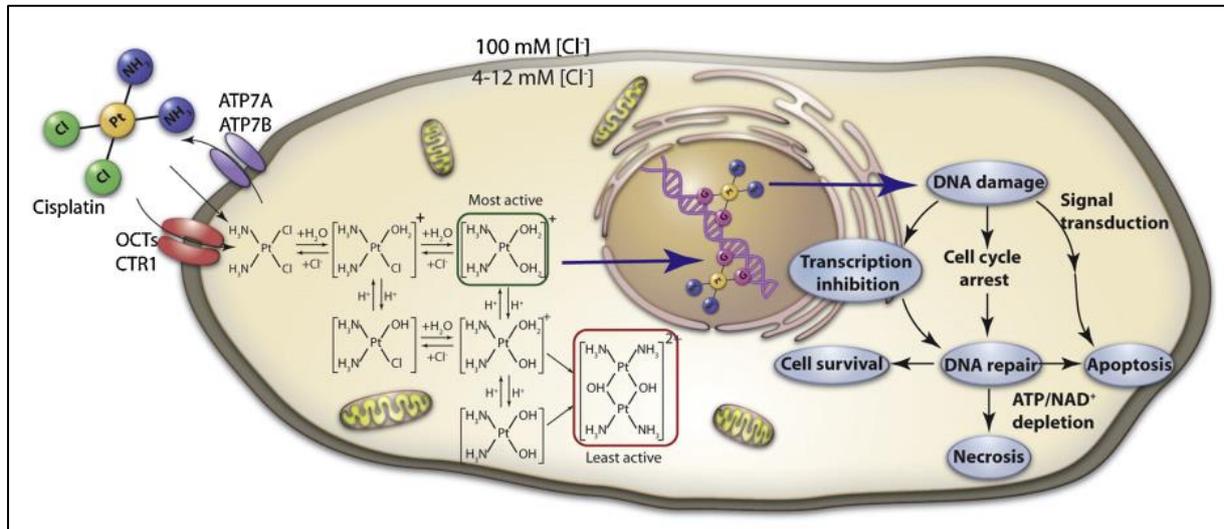
Figure 1.1.1.2. Cisplatin internalization into the cell, activation and effects on vital cell processes. After uptake by CTR1 transporters, cisplatin is activated inside a cell by displacement of chloride ions with water. The most active cisplatin species attacks the nucleophile DNA strand, causing DNA crosslinks and adducts which leads to DNA damage and subsequently cell death by apoptosis or necrosis, unless there are other mechanisms active in cell to prevent cell death and ensure cell survival. Reprinted from Ma et al., 2015.

Once cisplatin enters the cell, it becomes activated by displacement of its chloride ions by water molecules, thus becoming hydrolyzed and a powerful electrophile. This electrophile can react with sulfhydryl groups from proteins and nitrogen atoms incorporated in nucleic acids. Cisplatin is applied intravenously in clinic, and in blood (which has a high concentration of chloride ions, approximately 100 mM) it is coordinated with chloride ligands. Inside the cells, however, chloride concentration is low (4-12 mM), and the chloride ligands are displaced by water (Kartalou and Essigmann, 2001). By binding to nitrogen containing purine sites, cisplatin can cause DNA damage in cells, which in turn blocks cell division and results in apoptosis. Cisplatin is responsible for creating intrastrand crosslinks between purine bases in DNA, and nonfunctional adducts, which contribute to its toxicity. Another mechanism of cisplatin toxicity is the induced oxidative stress which can deter normal biological functions of the cell (Saad et al., 2004). The induced reactive oxygen species (ROS) can also trigger cell death by activating a number of signaling pathways. ROS formation depends on cisplatin concentration in the cell, as well as length of treatment (Brozovic et al., 2010). Cisplatin can

also disrupt calcium homeostasis which contributes to lipid peroxidation and enzyime inhibition events. The affected cells suffer mitochondrial damage which then probably leads to apoptosis and tissue necrosis (Aggarwal, 1998).

There are also numerous signaling pathways activated by cisplatin, which finally lead to apoptosis (Figure 1.1.1.3.). Cisplatin activates ERK (extracellular signal regulated kinase) which phosphorylates p53 and upregulates p21, GADD45 (45 kd growth arrest and DNA damage) and Mdm2 (mouse double minute 2 homolog) (Dehaan et al., 2001). This signaling cascade can arrest the cell cycle and enable DNA damage repair. DNA damage induced by cisplatin is another stress stimulus for the cell which can also activate the SAPK (stress activated protein kinase) and in turn the JNK (c-Jun N-terminal kinase) pathway, ultimately leading to apoptosis (Jones et al., 2007). The p38-MAPK (mitogen activated protein kinase) pathway is also involved in cisplatin induced apoptosis. After activation by cisplatin, p38 MAPK phosphorylates EGFR (epithelial growth factor receptor), regulates the p18 (Hamlet) protein which interacts with p53 and stimulates the proapoptotic genes PUMA and NOXA to transcription (Cuadrado et al., 2007). In cells with cisplatin induced DNA damage Akt phosphorylates Bad, which is necessary for cell viability in both cisplatin sensitive and resistant cells (Hayakawa et al., 2000). When DNA is damaged after treatment with cisplatin, cell cycle check point proteins become activated. The cell cycle itself is then delayed until the DNA damage is repaired or the situation is resolved by pushing the cell into apoptosis, depending on survival mechanisms that may be in place in the treated cells (Basu and Krishnamurthy, 2010).

One such example is the activation of ATM (ataxia telangiectasia mutated) upon DNA damage, which in turn activates p53 by phosphorylation and subsequently Mdm2. p53 transactivates genes involved in cell cycle progression, DNA damage repair and apoptosis and as such has a role in cisplatin induced DNA damage response, however, the p53 negative cells also respond to cisplatin induced DNA damage (Dasari and Tchounwou, 2015). Cisplatin can also induce cleavage of c-Abl (Abelson tyrosine-protein kinase 1), a tyrosine kinase receptor which is recruited from plasma membrane to nucleus after DNA damage. It is a substrate for caspase and hence crucial for cisplatin induced apoptosis (Machuy et al., 2004).
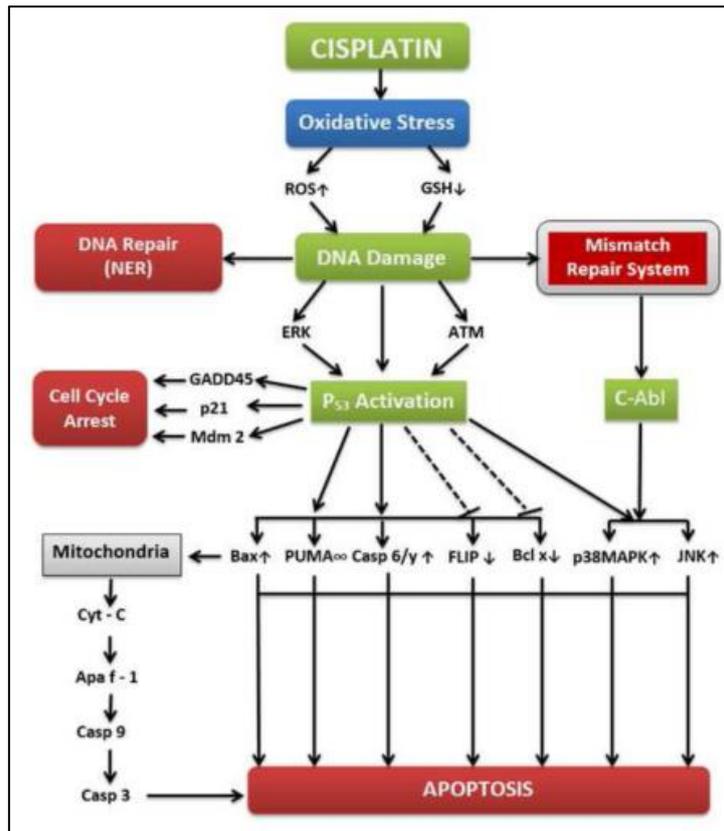
Figure 1.1.1.3. The schematic representation of molecular mechanisms and pathways activated by cisplatin in cancer cells.
Reprinted from Dasari and Tchounwou, 2015.

1.1.1.3. Mechanisms of cisplatin resistance

One of the major problems arising in cisplatin administration and a major obstacle to effective treatment, is the innate/primary (an already present resistance) or acquired resistance of tumor cells to cisplatin. There are several different mechanisms implicated in the resistance of cancer cells to cisplatin, which are schematically represented in Figure 1.1.1.4.

The basic mechanisms of cisplatin resistance are associated with efficiency of drug accumulation inside the cells, which directly depends on the levels of drug uptake and drug export. This accumulation may be low because of decreased drug uptake or increased drug export in cancer cells (Y. Hu et al., 2018). Reduced cisplatin uptake can occur because of copper transporter 1 (CTR1) downregulation (Howell et al., 2010). The upregulation of the P-type adenosine triphosphatases ATP7A and ATP7B or multidrug resistance associated proteins (MRP) in the cell membrane, which are involved in cisplatin cellular export, is also directly related to cisplatin resistance (Guminski et al., 2006). Another metabolic mechanism of cisplatin resistance is related to cisplatin scavenging by the glutathione detoxification

5
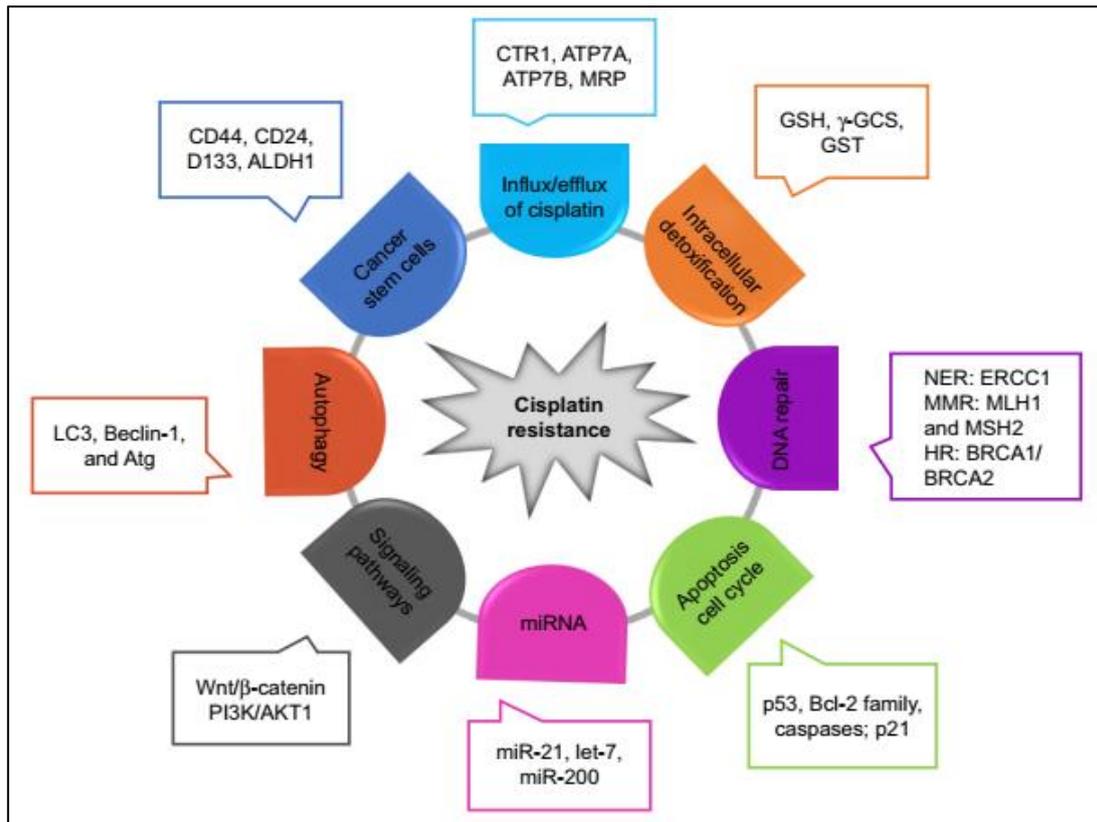
Figure 1.1.1.4. The mechanisms of cisplatin resistance. *The major genetic and epigenetic factors contributing to cisplatin chemoresistance are illustrated in the figure. These mechanisms include irregularities of the cell cycle, apoptosis, autophagy, intracellular detoxification and drug influx and efflux. Reprinted from* Hu et al., 2018.

system, where overexpression of enzymes involved in GSH synthesis and GSH conjugation are associated with resistance (Brozović et al., 2008; Galluzzi et al., 2014). One of the most prominent mechanisms of cisplatin resistance is the upregulation of DNA damage repair proteins which occurs through several different DNA damage control processes, like the nucleotide excision repair (NER), homologous recombination (HR) and mismatch repair (MMR). Increased expression of NER proteins, including the XPF (Xeroderma pigmentosum type F) – ERCC1 (excision repair cross-complementing rodent repair deficiency, complementation group 1) complex mediates DNA damage repair and hence contributes to cisplatin resistance (Arora et al., 2010). By downregulation or mutation in MMR related genes MLH1 (MutL homolog 1) and MSH2 (MutS homolog 2), the MMR which detects cisplatin induced DNA lesions and activates apoptosis becomes defective and cells overcome sensitivity to cisplatin (Fink et al., 1996). BRCA 1 and 2 (breast cancer susceptibility proteins 1 and 2) are essential components of the HR repair, which can also detect cisplatin induced DNA damage. Their deficiency mediates cancer cell sensitivity to cisplatin (Turner et al., 2012). The tumor suppressor protein p53 expression in cancer cells also mediates cisplatin cytotoxicity

and p53 deletions lead to acquired cisplatin resistance in cancer cells. Since cisplatin can induce apoptotic signals in cells, the levels of proapoptotic and apoptotic proteins such as Bcl2, caspases and mitochondrial intermembrane proteins have a direct effect on tumor cell response to cisplatin (Y. Hu et al., 2018).

1.1.2. Paclitaxel

Paclitaxel is a diterpene compound with a taxane skeleton (Figure 1.1.2.1.), isolated from the bark of *Taxus brevifolia*, the Pacific yew. The compound was identified in a large screening study of natural substances for antitumor purposes from plants, funded by the NCI (National Cancer Institute), in 1964 (Wani and Horwitz, 2014). Initially, it was very difficult to extract sufficient amounts of paclitaxel from the yew bark, in an isolation process that yielded 0,5 g of paclitaxel from 12 kg of raw material, which was a yield of only 0,004%. The isolated compound showed moderate efficiency in treatment on animal models and the research was put to rest for about a decade. The interest for paclitaxel was sparked in the 1970s, upon discovery that paclitaxel arrested cells in the metaphase of mitosis, by stabilizing microtubules (Schiff et al., 1979). When clinical trials started, it was determined that paclitaxel may cause hypersensitivity and anaphylactic shock. Due to these issues and its high hydrophobicity, paclitaxel is administered today to patients via polyethoxylated castor oil (Cremophor EL, CrEL) or albumin-bound (Abraxane), while novel formulations with nanocarriers, liposomes, micelles and emulsions are being intensively investigated (Barbuti and Chen, 2015). The clinical trials with paclitaxel started in 1984 and it was approved by FDA for medical use in 1993 (Kampan et al., 2015).
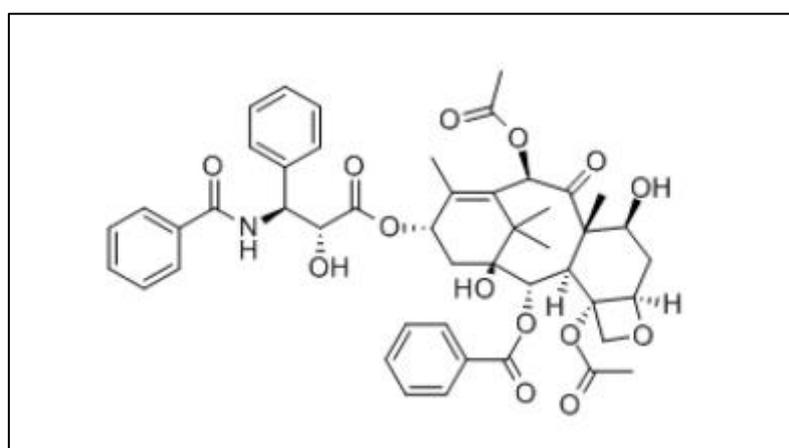
Figure 1.1.2.1. Chemical structure of paclitaxel. Reprinted from Barbuti and Chen, 2015.

1.1.2.1. Paclitaxel uses in clinic

When paclitaxel entered clinical trials in 1984, the first results found that 30% of ovarian cancer patients with platinum-resistant ovarian cancer completely or partially responded to paclitaxel therapy (McGuire et al., 1990). A problem in its administration was encountered when the hypersensitivity reactions to Cremophor led to two patient deaths, which almost stopped the clinical trials. This was overcome by increasing administration time to 24 hours to slowly introduce the drug to patients (Wiernik et al., 1987). A major problem in the availability of paclitaxel stemmed from very poor yields obtained by extraction from the already endangered *Taxus brevifolia*. To avoid this lengthy, costly and species endangering procedure, a commercially viable semisynthetic paclitaxel was developed by Holton and colleagues (Kampan et al., 2015). Finally, in 1992, nearly 30 years after its identification, paclitaxel was registered as a chemotherapeutic agent for treatment of ovarian cancer. In 1994 FDA approved the use of paclitaxel against breast cancer. Today paclitaxel is used alone or in combination with other chemotherapeutics (like cisplatin or carboplatin) in therapy of ovarian, breast and non-small cell lung cancer (NSCLC) (Piccart and Cardoso, 2003; Kampan et al., 2015).

1.1.2.2. Paclitaxel modes of action

Paclitaxel is a microtubule targeting agent (MTA). It specifically binds several sites on microtubules, namely on its β-tubulin subunit. Microtubules are polymers consisting of α and β subunits. They have multiple roles in the cell, including forming the mitotic spindle, maintenance of cell structure, motility and cytoplasmic traffic inside of the cells. At the beginning of mitosis microtubules become unstable (Kampan et al., 2015). The mechanisms of action of paclitaxel that are currently known are summarized in Figure 1.1.2.2. At low concentrations, less than nanomolar, paclitaxel inhibits microtubule depolymerization, while at high concentrations it increases microtubule stability by blocking detachment of minus microtubule ends (slow polymerizing ends in the proximity of cellular structures, like the nucleus) from centrosomes (Ganguly et al., 2010). Other than the microtubule stabilizing effect, paclitaxel can induce apoptosis, independently of the microtubule binding mechanism. This process depends on its concentration and duration of exposure, particularly in the case of administration to patients. At minimum concentrations of 10 nM and 12 hours exposure, paclitaxel can induce apoptosis already in the S phase, without arresting the cells in mitosis.

At concentrations greater than 9 nM paclitaxel mediates Raf-1 activation, responsible for apoptotic control. However, at concentrations less than 9 nM, Raf-1 is not involved in apoptosis, which in turn occurs because of p53 and p21 activation (Sevko et al., 2012). At exposure of 24 hours, both apoptosis and mitotic arrest occur (Giannakakou et al., 1997).

Paclitaxel also activates a number of signaling pathways which may finally lead to apoptosis. These pathways include the TLR-4 dependent pathway, c-Jun N-terminal kinase (JNK), p38 MAPK, nuclear factor kappa B (NFκB) and Janus kinase – signal transducer and activator of transcription factor (JAK-STAT) signaling pathways. Changes in these pathways may contribute to the development of paclitaxel resistance (Kampan et al., 2015). Paclitaxel can also induce ROS and increase hydroperoxide status of the cell by enhancing activity of nicotinamide adenine dinucleotide phosphate oxidase (Alexandre et al., 2007), but the mechanism by which ROS induction contributes to paclitaxel cytotoxicity is still unknown.

Paclitaxel administration on weekly basis has also shown high inhibitory activity on angiogenesis (Belotti et al., 1996), which was proven both by murine and clinical studies.
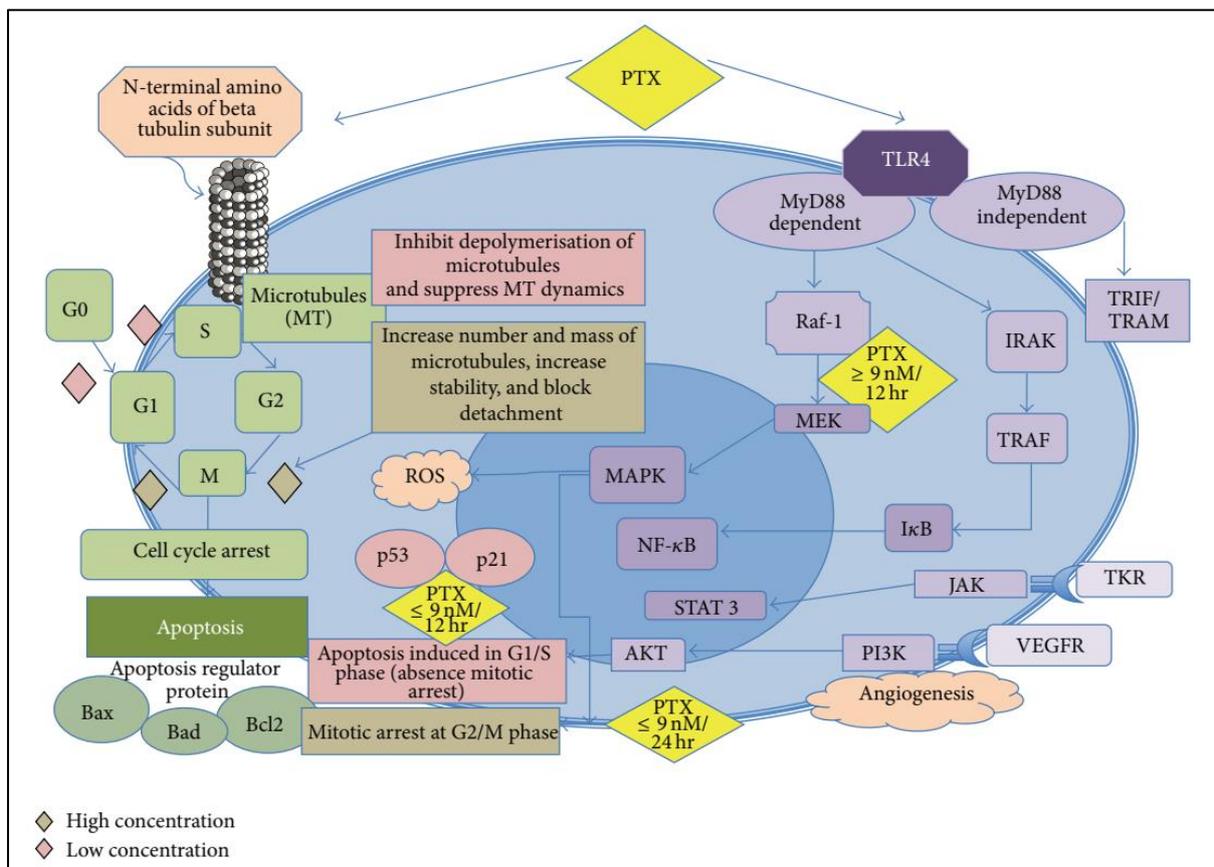
Figure 1.1.2.2. Paclitaxel mechanisms of action. Paclitaxel targets microtubules. At high concentration, it causes mitotic arrest at G2/M phase. At low concentration, apoptosis is induced at G0 and G1/S phase by Raf-1 kinase activation or p53/p21 depending on dosage. Paclitaxel also activates multipleproapoptotic pathways. Reprinted from Kampan et al., 2015.

In mice, the low noncytotoxic doses suppressed the expression of VEGF (vascular endothelial growth factor) (Klauber et al., 1997). The low doses of weekly paclitaxel have been studied in patients with advanced ovarian cancer, metastatic melanoma and advanced head and neck cancer, which was considered as metronomic, or maintenance treatment, keeping cancer under control (Kampan et al., 2015).

1.1.2.3. Resistance mechanisms to paclitaxel

There are several different mechanisms of paclitaxel resistance, some arising from its specific mode of action by targeting microtubules, others are linked to multidrug resistance and some arise from changes in tumor microenvironment and signaling pathways linked to cell metabolism and survival, as well as to drug accumulation and efflux (Kampan et al., 2015). The changes involved in paclitaxel resistance are those in mRNA and protein synthesis, oxidative stress, glycolysis, glutathione metabolism and leukocyte transendothelial migration pathways (Agarwal and Kaye, 2003). For instance, the rapid tumor growth causes formation of tumor centers which are devoid of oxygen, hence becoming hypoxic and acidic and developing different regulations linked to the hypoxia. These changes promote tumor proliferation, dissemination and progression by also inducing resistance to the drug (Acker and Plate, 2003). This genomic instability induced by hypoxia promotes inhibition of apoptosis and highly induces angiogenesis, upregulates production of growth factors (like VEGF-vascular endothelial growth factor, PDGF-platelet derived growth factor and IGF-the insulin like growth factor) and induces anaerobicity and glycolysis, ultimately preventing tumor cell demise (Kampan et al., 2015). Hypoxia may induce a p53-independent apoptosis in tumor cells mediated by hypoxic inducible factor 1 (HIF-1) and Bcl-2. HIF-1 concentration increases in hypoxic environment and it can arrest cell cycle at G0/G1 transition, thereby reducing sensitivity to chemotherapeutics, including paclitaxel (Rohwer and Cramer, 2011). Hypoxia also activates NFκB and STAT-3 pathways, involved in inflammation, angiogenesis, cell survival, proliferation and metastasis. STAT-3 was found to be overexpressed in the majority of paclitaxel resistant ovarian cancer cells, and its inhibition diminished resistance to paclitaxel (Duan et al., 2006).

One of the major problems of resistance development on many drugs, (including paclitaxel), are reduced drug accumulation, increased efflux of drug from the cells and the changes in pharmacokinetics. The latter may arise from inadequate drug concentrations

administered, shorter drug exposure, increased hepatic or renal clearance, or poor binding to tubulin or microtubules) (Kampan et al., 2015). Drug efflux from cancer cells is mediated by the ATP binding cassette transporters, like P-glycoprotein (ABCB1/MRP, encoded by the MDR-1 gene). P-gp was found to be overexpressed in paclitaxel resistant cell lines and also in chemoresistant ovarian cancer patients. This overexpression also correlated negatively with the overall survival time (Kampan et al., 2015).

Since paclitaxel specifically binds sites on tubulin, it is natural to expect that changes in tubulin may significantly deter sensitivity of tumor cells to paclitaxel. These changes include reduced intracellular tubulin concentration (effectively producing less targets for paclitaxel activity), point mutations in tubulin genes or alterations in tubulin isotypes, like Class III β-tubulin (Mozzetti et al., 2005; Kavallaris et al., 1997). These changes can also affect microtubule stability and dynamics, which can cause cell cycle arrest, apoptosis and also resistance to drugs.

Other signaling pathways that are also involved in paclitaxel resistance include inhibition of apoptosis, activation of MAPK, Raf or PI3K, increase in expression of proinflammatory cytokines and activation of lipopolysaccharide inducible genes and p53 (Kampan et al., 2015).

1.1.3. Vincristine

Like paclitaxel, vincristine is also a microtubule targeting agent (MTA), however, contrary to paclitaxel's microtubule-stabilizing activity, vincristine harbors a microtubule depolymerizing/destabilizing activity. Although both molecules target the β-subunit of tubulin, their mechanisms of interference with normal microtubules dynamics are highly different (Figure 1.1.3.1). The microtubule stabilizers, like paclitaxel, bind to the "so called" taxane binding site of the β-tubulin chain, which stabilizes the microtubules and prevents their disassembly. This leads to cell death by apoptosis. On the other hand, the microtubule destabilizing drugs, like vinca alkaloids, bind to the specific vinca binding site, on the central portion of β-tubulin, which prevents polymerization into microtubules (Morris & Fornier, 2008).

Vincristine, as well as vinblastine, is a vinca alkaloid, a natural compound with antitumor properties isolated from plants. The interest for medical uses of vinca alkaloids first appeared in the 1950s. Scientists Noble and Beer were interested in tea made from the Madagascar periwinkle plant (*Vincarosea*/*Catharanthus roseus*), that was used as a diabetes
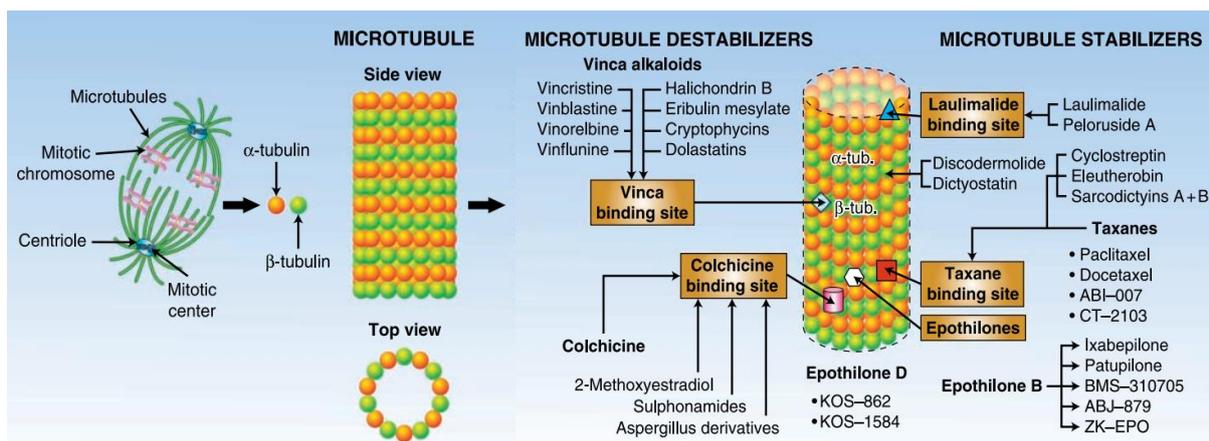
Figure 1.1.3.1. Schematic representation of binding sites of several microtubule targeting drugs, including paclitaxel and vincristine, on microtubules. *Microtubule structure is depicted as polymerized chains of α and β-tubulin, providing different sites of binding for various MTA drug groups. Adapted from Morris and Fornier, 2008.*

remedy in Jamaica, and they wanted to test its effects more thoroughly (Florian et al., 2016). Contrary to their expectations, after conducting experiments with the plant extract in rats, they found no effects to glucose levels in blood, instead they found that treated animals developed a severe decrease in white blood cell count and became susceptible to lethal infections (Noble et al., 1958). They have managed to isolate both vincristine and vinblastine from the plant extract in a stepwise fractionation process. The only difference in structures of vincristine and vinblastine lies in a substitution of a single methyl/formyl group (Figure 1.1.3.2.), however this slight chemical modification has immense clinical repercussions – vincristine and vinblastine have very different clinical efficiencies and side effects. (Florian et al., 2016). Vincristine was later isolated in larger quantities from leaves of Madagascar periwinkle at Ely Lilly, where it began to be marketed under the name Oncovin. Initially they needed one ton of dried periwinkle leaves to obtain approximately 28 g of vincristine. In 1963 vincristine use in medical applications was approved by FDA. Since the yield of vincristine extraction from the periwinkle plant is very low (0,0003%), it was necessary to develop synthetic procedures of its manufacturing. One such approach is the stereocontrolled total synthesis technique (Kuboyama et al., 2004).

1.1.3.1. Vincristine uses in clinic

Today vincristine is used in clinic in the treatment of various types of malignancies, for example in therapy against Philadelphia chromosome-negative acute lymphoblastic leukemia (ALL), B-cell lymphoma, metastatic melanoma, estrogen-receptor negative breast cancer, glioma, colorectal cancer, non-Hodgkin's and Hodgkin's lymphoma, neuroblastoma,
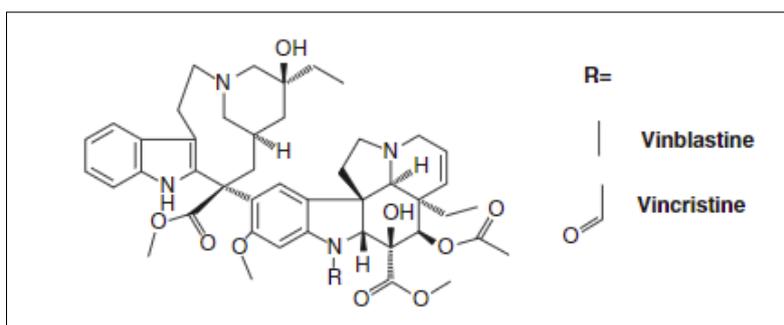
Figure 1.1.3.2. Chemical structure of vincristine and vinblastine. Reprinted from Florian et al., 2016.

rhabdomyosarcoma, multiple myeloma and Wilms' tumor (Martino et al., 2018). It may be used as a single agent or in combination chemotherapy. However, vincristine is being used more frequently and effectively in pediatric oncology than in adults with cancer, which is probably due to the fact that pediatric tumors exhibit higher sensitivity to vincristine and due to the better tolerance of pediatric patients to higher doses of the drug (Gidding et al., 1999). The clinical response in pediatric malignancies ranges from 40% in solid tumors and more than 75% in hematologic tumors, especially ALL (Said and Tsimberidou, 2014). The dose limiting factors, naturally, are the side effects, the most important being peripheral neuropathy, nausea, vomiting, diarrhea, bloating, stomach/abdominal pain and cramping, constipation, mouth sores, dizziness, hair loss, headache, loss of appetite, changes in sense of taste and weight loss (Martino et al., 2018).

Vincristine is administered intravenously, as a bolus injection (the administration of a discrete amount of medication, within a specific time frame). To circumvent some known issues of vincristine and other vinca alkaloids regarding limiting side effects and enhancing its uptake and possibly specificity, as well as avoiding the Pgp-mediated resistance, novel formulations using drug conjugates with microspheres, nanoparticles and liposomes have started being used in clinical applications (Ling et al., 2010; Martino et al., 2018).

1.1.3.2. Vincristine mode of action

The vinca alkaloids' tubulin targeting mechanism is specifically well suited to battle the fast-dividing cancer cell profiles, since they inhibit microtubule polymerization, and thus prevent the onset of anaphase, which leaves cancer cells in a senescence-like G1 state, or in a prolonged arrested state which ends in cell death (Liu et al., 2014). *In vitro* vincristine induces apoptosis in tumor cells, while in animal models it can interfere with tumor blood flow, resulting in necrosis (Gidding et al., 1999). By binding to β-tubulin, vincristine inhibits

the polymerization of mitotic spindle microtubules, which damages the spindle microtubules in a concentration dependant manner (Martino et al., 2018). At low concentrations vincristine stabilizes the microtubules, resulting in failure of chromosomes to segregate leading to metaphase arrest and inhibition of mitosis. At high concentrations vincristine disrupts and depolymerizes microtubules. This process is described in more detail in Figure 1.1.3.3. Besides the concentration dependent clinical efficiency of vincristine, the duration of exposure to vincristine is also important in vincristine therapy. Effects of short-duration vincristine exposure are reversible if the drug is discontinued, while at long exposure it has an irreversible lethal effect (Said and Tsimberidou, 2014). Vincristine was also reported to have apoptotic, antiangiogenic and other biochemical effects on tumor cells (Harmon et al., 1992; Takano et al., 1993; Jordan et al., 1991).
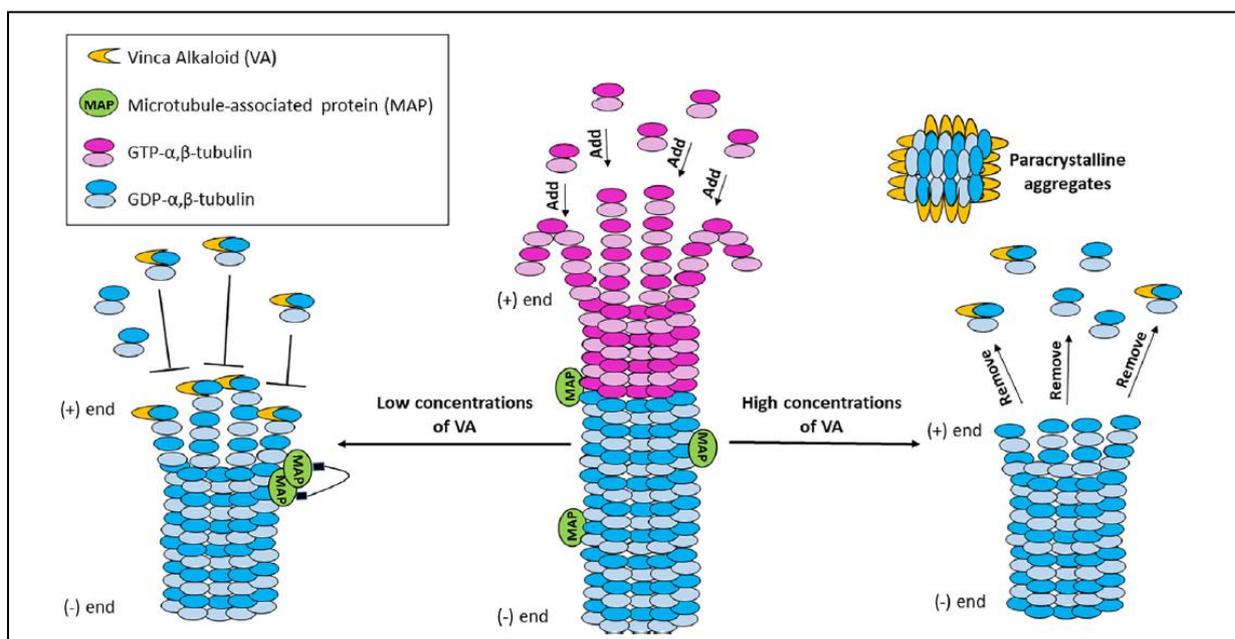
Figure 1.1.3.3. Mechanism of action of vinca alkaloids. At low concentrations vinca alkaloids inhibit microtubule formation by directly binding to + microtubules, which impedes attachment of GTP and causes crosslinking of microtubule associated proteins (MAP). At high concentrations, vinca alkaloids form paracrystaline aggregates with GDP tubulin, which causes microtubule depolymerization. Reprinted from Martino et al., 2018.

1.1.3.3. Mechanisms of resistance to vincristine

Resistance to all microtubule targeting drugs can arise from several pharmacodynamic levels of MT drugs. These are the cellular efflux of the drug, ineffective interaction with the drug target and faulty induction of apoptosis. There may also be present changes in different proteins and microRNA expression levels, dependent upon cell and tumor type (Dumontet

and Jordan, 2010). The main three types of resistance mechanisms are summarized in Figure 1.1.3.4.

The transporter responsible for both vinca alkaloid and taxane efflux from the cell is the Pgp, the product of the mdr1 gene, which causes the classic multidrug resistance phenotype by their transport out of the cell, thereby reducing the cellular concentration of these drugs. However, aside from the classical Pgp-mediated efflux, there are also transporters which specifically transport only some types of antitubulin agents, like the MRP1 protein (Breuninger et al., 1995).

The second line of tumor cell resistance to vincristine is associated with alterations in microtubules, which comprise of qualitative or quantitative changes in microtubules. Such changes can influence drug binding, the effects of drug binding on tubulin conformation, and GTPase activity of tubulin polymerization. These changes may include variations in proteins responsible for tubulin protein folding, dimer sequestration, microtubule dynamics or involved in microtubule/tubulin regulatory pathways, like FHit, surviving, MAP2, MAP4, stathmin and STOP (Dumontet and Jordan, 2010). The quantitative tubulin isotype
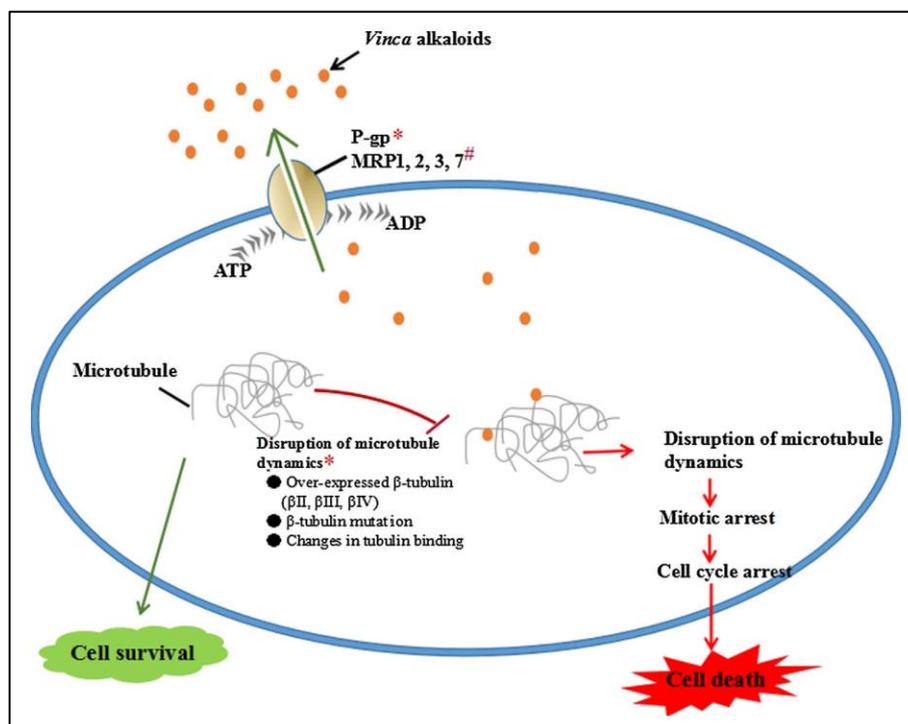
Figure 1.1.3.4. The summary of tumor cell resistance mechanisms to vincristine. *denotes acquired resistance mechanisms, while # denotes intrinsic resistance mechanisms. Adapted from* Zhang et al., 2017.

composition of microtubules influences sensitivity to MTAs. Specifically, in vinca alkaloid resistant cell lines decreased expression of class III β-tubulin has been observed, as well as

increased levels of MAP4 protein and increased microtubule stability (Kavallaris et al., 2001). In contrast, siRNA mediated knockdown of class II or class IVb β-tubulins hypersensitized lung cancer cells to vinca alkaloids (Pei et al., 2007).

The third mechanism of vinca alkaloids resistance in tumor cells involves apoptotic signaling. Thus far this research area regarding vincristine resistance has been scarce. Simonian and colleagues reported that Bcl-2 and Bcl-XL provided protection against vincristine and vinblastine in lymphoid cells (Simonian et al., 1997). In another article by Zhang et al., it was confirmed that overexpression of Bcl-2 provided near total protection to vincristine induced cell death in ALL-697 leukemia cells (I. Zhang et al., 1996).

1.2. RhoD

RhoD is a small GTPase protein, which belongs to the Rho (Ras homologous) family of proteins. It is a relatively new addition to the Rho family, with features that are still being discovered, ranging from the most recent functional properties in endosome traffic and mobility, through Golgi homeostasis and centrosome duplication, to alterations in actin cytoskeleton dynamics. This chapter will introduce RhoD and its difference regarding other well-known family members.

1.2.1. Rho family and protein regulation

The Ras superfamily of proteins contains 167 member proteins, which can be grouped into 6 broad subfamilies: Ras, Ran, Rad, Rab, Arf and Rho, according to homology and function (Rojas et al., 2012). Rho GTPases were first identified as a separate family by Madaule and Axel in 1985. Rho GTPases are GTP-hydrolyzing enzymes which cycle between an active GTP-bound conformation and the inactive GDP-bound conformation. They are highly conserved and found in nearly all eukaryotes. They are activated by numerous growth factors, cytokines, adhesion molecules, hormones, integrins, G-bound proteins and also biologically active substances (Narumiya and Thumkeo, 2018). The most prominent roles of the Rho family of proteins are in cell proliferation, apoptosis, cell division, vesicle trafficking, phagocytosis, gene expression, organization of microtubule cytoskeleton and especially actin cytoskeleton dynamics, through which most of these and other important cellular functions (as focal adhesion, stress fiber formation, directed cell migration, filopodia and lamellipodia formation) are achieved (Haga and Ridley, 2016). Today, the Rho family consists of 20

identified proteins divided into 8 subfamilies (Figure 1.2.1.1.). The cornerstone families that were first identified and researched the most, are the three classical Rho GTPase familes: Rho, Rac and Cdc42, each exerting different functions in cell proliferation and actin cytoskeleton dynamics.
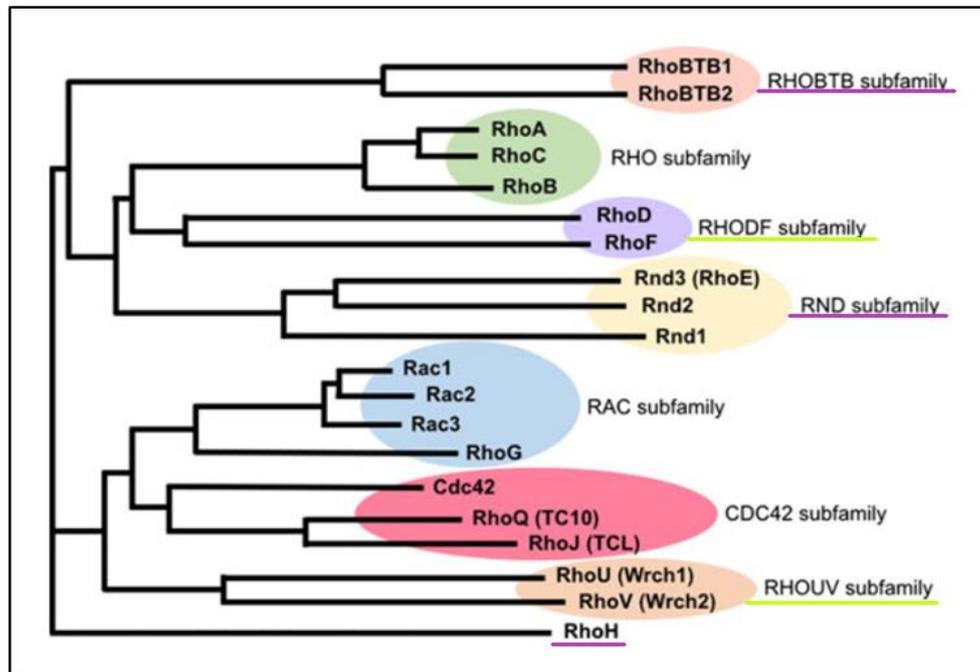
Figure 1.2.1.1. The phylogenetic tree of the human Rho protein family divided into 20 proteins across 8 subfamilies. The tree differentiates the 3 classical Rho subfamilies: Rho, Rac and Cdc42 and outlines the atypical Rho GTPase subfamilies, with respect to the regulation of GTPase activity of each subfamily. The atypical Rho subfamilies are underlined purple for GTPase defective subfamilies (RhoBTB, Rnd and RhoH) and green for fast-cycling Rho GTPase subfamilies (RhoU/V and RhoD/F subfamilies). Modified from Narumiya and Thumkeo, 2018.

The first orthologues of human Rho proteins stemmed from plants, which, interestingly have a larger number of Rac proteins than other organisms (Rac1 – Rac11). By duplication of the ancestral RAC gene in fungi/metazoans, CDC42 and RHO genes emerged, with roles in control of cell polarity and cytokinesis, respectively (Yang, 2002; Jaffe and Hall, 2005). The basic Rho GTPase structure is highly conserved among individual family constituents, and it comprises several regions important for proper protein function, localization and regulation. The most important parts of these 20 to 40 kDa proteins are coding for regions involved in GTP and GDP binding (G domains), effector binding domain, the Rho insert domain, the hypervariable region (which varies among different Rho GTPase family members) and the CAAX box (short for cysteine, alyphatic amino acid and any amino acid, X) on the C-terminus of the proteins (which undergoes a variety of post-translational

modifications important for membrane targeting) (Hodge and Ridley, 2016). The schematic representation of Rho GTPase basic structure is illustrated in Figure 1.2.1.2.
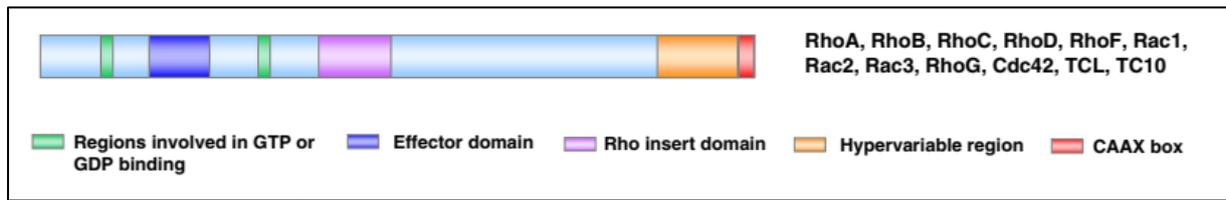
Figure 1.2.1.2. The protein structure of Rho GTPase family members. The basic structure includes G domains (green), effector domains (blue), insert domain (magenta), hypervariable region (orange) and the CAAX box (red). This basic structure is shared by most of the Rho GTPase family member proteins. Modified from Vega and Ridley, 2008.

Today, Rho GTPase family of proteins is divided into typical (classical) and atypical subfamilies, based on the regulation of their GTPase/GDPase cycle. The Rho, Rac and Cdc42 subfamilies fall into the classic category of subfamilies. Rho GTPases act as molecular switches, by cycling between their active GTP-bound and inactive GDP-bound form (Haga and Ridley, 2016). The ratio of GTP- and GDP-bound forms is regulated, in the case of classic Rho GTPases, by three different groups of proteins: the guanine nucleotide exchange factors (GEFs), GTPase activating proteins (GAPs) and guanine nucleotide dissociating inhibitors (GDIs), whose actions on Rho are illustrated in Figure 1.2.1.3. The GEFs displace the GDP bound in the active site of the Rho GTPase, which allows GTP binding. The binding of GTP alters the conformation of the GTPase, allowing it to interact with downstream effector molecules. GEFs have also been thought to contribute to signaling specificity through scaffolding upstream and downstream interactors (Porter et al., 2016; Haga and Ridley, 2016; Aspenström, 2018). Conversely, GAPs activate the weak intrinsic GTPase activity of Rho proteins leading to the hydrolysis of bound GTP, switching the GTPase to an inactive conformation. Guanine nucleotide dissociation inhibitors (GDIs) are a third class of regulators of Rho proteins. They sequester inactive GTPases in the cytoplasm by masking their C-terminal lipid moieties that mediate plasma membrane localization, which can inhibit their activation. They can also protect GTPases from degradation and also have more subtle effects, such as directing activation of Rho GTPases to specific membrane compartments (Porter et al., 2016).

Rho GTPases expression can also be regulated at transcriptional level epigenetically, and at translational level by micro RNAs (miRNAs). Rho GTPases may also be activated or inactivated by post-translational modifications, like phosphorylation and sumoylation, which

depends on the cellular context. On the protein level, Rho GTPases are regulated by the ubiquitin-proteasome system (Hodge and Ridley, 2016).
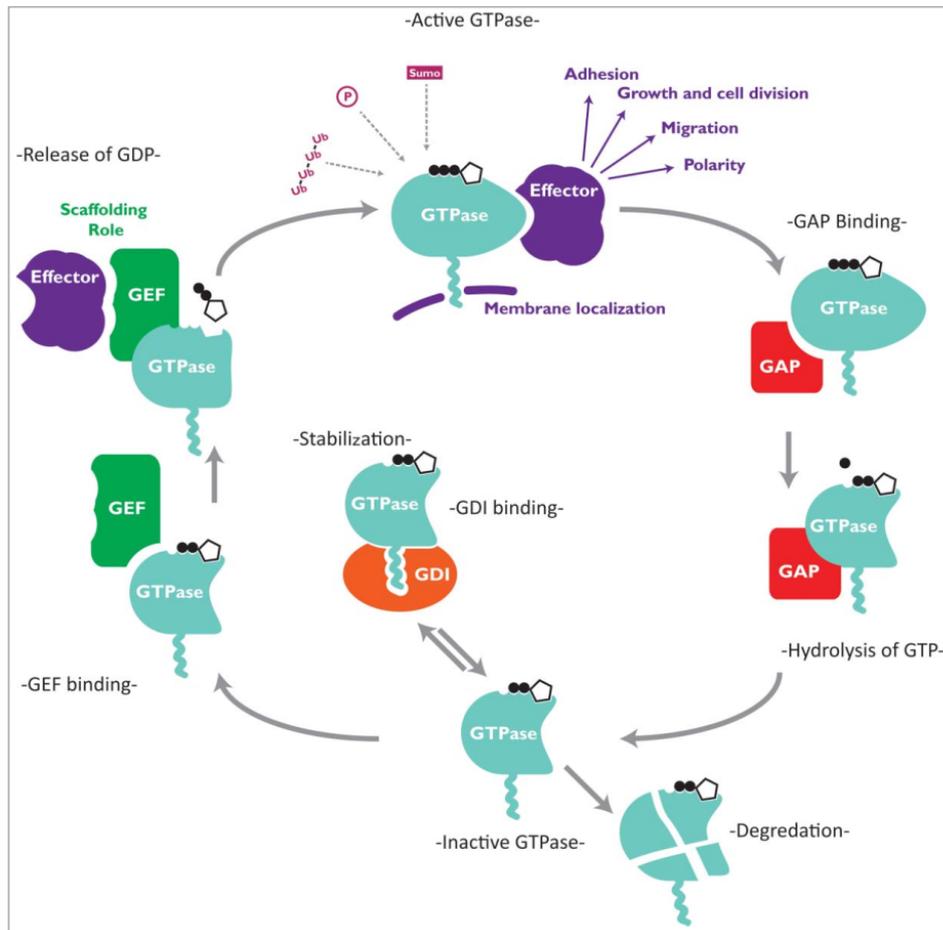
Figure 1.2.1.3. The regulation of classical Rho GTPases by GEF, GAP and GDI proteins. In their active form, Rho GTPases bind a variety of effector molecules and hence mediate a large number of cellular processes like cell migration, cell-cell adhesion, transcription and proliferation. Inactive Rho GTPases are mainly found in the cytoplasm, where they can be degraded or stabilized by binding to Rho GDIs, which act as chaperones and prevent activation by sequestering the GTPases away from GEF proteins. Reprinted from Porter et al., 2016.

Classical Rho GTPases also succumb to regulation by lipid modifications. Specifically, the CAAX motif at the carboxy terminus of the proteins undergoes post-translational modifications, which are crucial for membrane targeting. These modifications consist of isoprenylation, and include farnesylation, geranylgeranylation and palmitoylation. The added lipid group then tethers the Rho GTPase to the membrane and prevents its free diffusion through the cytoplasm (Hodge and Ridley, 2016). The atypical Rho GTPases are mostly GTP-bound and thus far no evidence has been found of their regulation by GEF and GAP proteins. It is suggested they are regulated by other mechanisms, like expression and post-translational modifications. Some of them also consist of additional domains that are not present in the basic outline of the classical Rho GTPase structure (Aspenström et al., 2007). The atypical Rho

GTPases can be further divided into two subgroups: the GTPase defective and the fast-cycling Rho GTPases. The GTPase defective Rho GTPases have different amino acid sequences in the G binding domains, which probably arose by mutations in the specific residues responsible for GTP/GDP binding. These GTPases have a very limited capacity of GTP hydrolysis and they are constitutively GTP-bound. The subfamilies befalling into this group are RhoH, RhoBTB (Rho BTB1 and BTB2) and Rnd (Rnd1, Rnd2 and RhoE/Rnd3) (Aspenström, 2017).

The concept of fast-cycling Rho GTPases was first mentioned in the context of Cdc42 mutated protein, which gained a high intrinsic GDP/GTP exchange activity. Specifically, the Cdc42 protein with the F28L mutation exhibited oncogenic properties through a constitutively active GTPase activity which induced anchorage-independent growth of Cdc42^{F28L} expressing NIH-3T3 cells in soft agar experiments (R. Lin et al., 1997). Since the intracellular levels of GTP nucleotides in 10-fold that of GDP (Traut, 1994), this is probably the reason why high GDP/GTP exchange rates result in a constitutively active GTPase (active) form of the protein. The fast-cycling Rho GTPases do possess the intact GTPase activity, however the GTP/GDP exchange activity is so high in their case, that it overrides the GTPase activity (Fidyk et al., 2006). The members of the fast-cycling Rho GTPase subfamilies include the RhoU/V (RhoU/Wrch-1 and RhoV/Chp) and the RhoD/F families (RhoD and RhoF/Rif) (Aspenström, 2017).

The mutations in the HRas protein as well as in the Rho GTPase family also have multiple implications on various cellular processes, as well as tumorigenesis. This is best observed on the mutations which render HRas and the Rho GTPases constitutively active. In the case of HRas, for example, the constitutively active mutants G12V and G12D contribute to formation of bladder cancer, Costello syndrome and congenital myopathy with excess of muscle spindles (Aoki et al., 2005; Van Der Burgt et al., 2007; Lo et al., 2008). It has been acknowledged that mutations in HRas at the amino acid sites 12, 13 and 61 especially activate the potential of HRas to transform cultured cells and are implicated in a variety of human tumors (Honkawa et al., 1987). Reflecting the similarity in sequences of the Rho GTPase proteins and HRas, this protein family also possesses mutation sites which, when altered, may induce tumorigenesis (Wennerberg and Der, 2004). For instance, the constitutively activated RhoA and even constitutively activated RhoB, can transform rodent fibroblast (Prendergast et al., 1995; Wang et al., 2003). In humans the most common substitutions that render constitutive GTPase activity are the G → V and the Q → L mutations. In Rac1 and Cdc42 these are the G12V and Q61L, at the same site as in the HRas protein. In RhoA and RhoB these are

the G14V and Q63L (Wherlock et al., 2004; Chatterjee and Van Golen, 2011). Regarding mutations in RhoD, thus far the constitutively active G26V mutation (GTPase deficient mutant) was found to induce formation of filopodia, which is similar activity seen in GTPase deficient RhoF of endothelial cells (Aspenström et al., 2004; Koizumi et al., 2012). As illustration of sequence similarity, an alignment of the most extensively studied members of RhoGTPase family and HRas is shown in Figure 1.2.1.4.
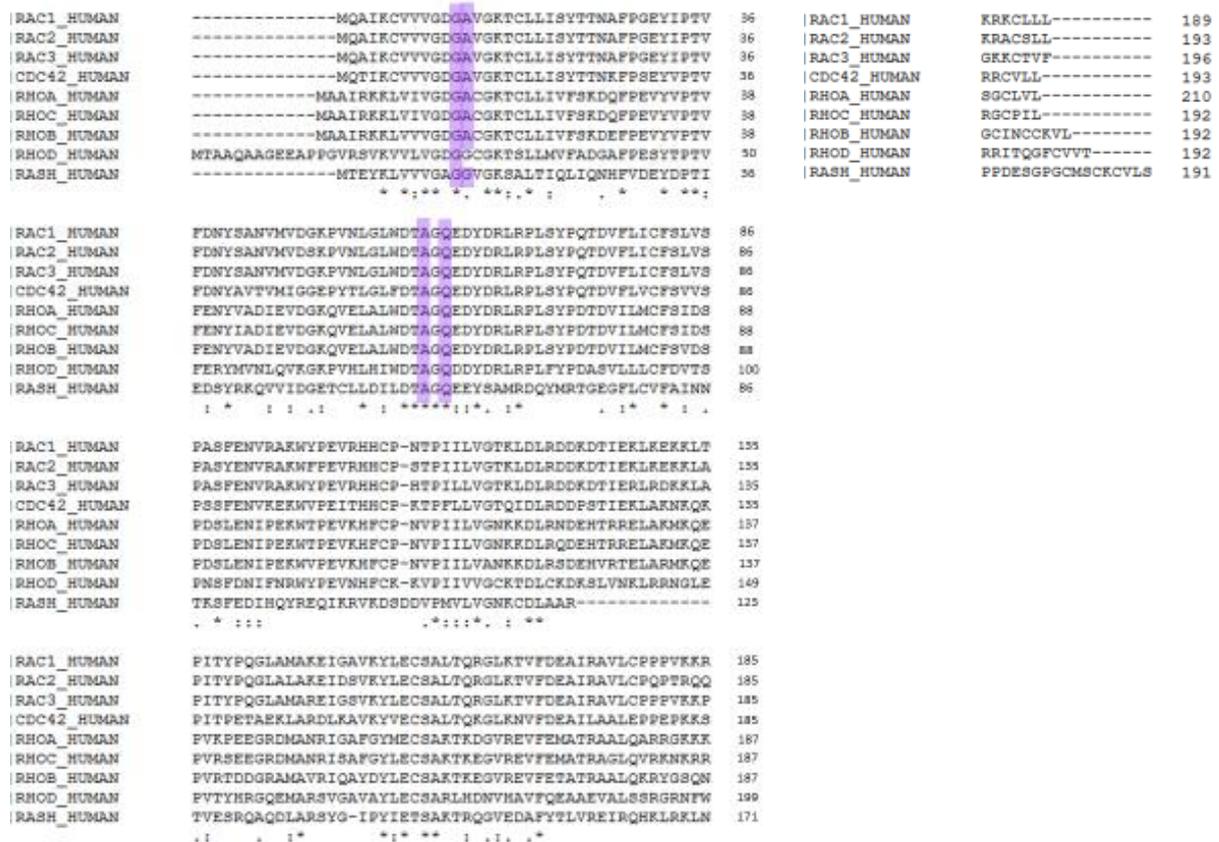
Figure 1.2.1.4. Multiple alignment of the Rho family proteins and HRas. *The amino acid sequences of the 8 described Rho-family gene members and HRas (main isoforms) were aligned by Clustal W 2.1. The residues highlighted in violet are important for GTPase activity. The protein sequences used correspond to the following UniProt identifiers (from top to bottom): P63000, P15153, P60763, P60953, P61586, P08134, P62745, O00212, P01112. Source: UniProt last modified October 15, 2019.*

1.2.2. Rho GTPases in cancer

The functions of Rho GTPases were initially ascribed to regulation of cytoskeleton dynamics, cell shape, polarity and cell migration, while later they were also linked to cell cycle progression, survival, angiogenesis, neurogenesis and even immune responses and vascular reactivity (Bustelo, 2018). Taking all of these processes into account, it is not surprising that Rho GTPases have implications in tumor biology and progression. The area of Rho GTPases and their deregulation in cancer has been investigated for more than 20 years and significant

advances in the understanding of their involvement in cancer were made. There are several obvious mechanisms by which Rho GTPases may become deregulated and push the cell towards a cancer phenotype, and these include direct mutations of Rho GTPases (which may render them GTPase deficient or constitutively active), altered expression of their regulating proteins (in the case of classical Rho GTPases) such as overexpression of GEFs and downregulation of negative regulators GAPs and GDIs; altered post-translational modifications and emergence of alternative splice forms, and finally, the overexpression of the Rho GTPases themselves (Porter et al., 2016).

Quite a few Rho GTPases were found to be overexpressed in human tumors, which also correlated with cancer progression and prognosis in some cases. RhoA overexpression is linked with the progression of testicular and breast cancers (Fritz et al., 2002; Fritz et al., 1999). Increased expression of RhoA was also found in colon cancers, lung cancers, head and neck squamous cell carcinoma and liver cancer (Orgaz et al., 2014). Similar to RhoA, RhoC was also found to be overexpressed in several different tumor types, namely in inflammatory breast cancer and colorectal carcinoma. Correlation was also found between cancer progression and poor prognosis in melanoma and pancreatic adenocarcinoma (Orgaz et al. 2014).

Intriguingly, RhoB, which belongs to the same subfamily as RhoA and RhoC, has quite the opposite effects. There have been implications of RhoB overexpression in progression of breast cancer (Fritz et al., 2002), however, other studies report downregulation of RhoB in squamous cell carcinoma and loss of its expression in lung cancer progression, suggesting a tumor suppressing role for this particular Rho GTPase. The downregulation of RhoB in human laryngeal carcinoma cells (Hep2) has also been linked to development of resistance to cisplatin (Čimbora-Zovko et al., 2010). This decreased RhoB expression was also found to be responsible for increased Ad5 (Adenovirus type 5) mediated transgene expression, while also making a connection to the endosomal trafficking roles of RhoB (Majhen et al., 2014). Moreover, expression of RhoB is downregulated in several malignancies and promotes apoptosis in cancer cell lines, while its depletion stimulates cancer cell migration (Huang and Prendergast, 2006; Vega et al., 2012; Croft and Olson, 2011; Prendergast, 2001).

Out of other prominently researched Rho GTPase family members, Rac1 was found to be overexpressed in testicular cancer, breast cancer and various leukaemia. Its splice variant Rac1b was found highly expressed in colon, breast and non-small cell lung carcinomas and is

thought to mediate epithelial-mesenchymal transition in lung cells. Cdc42 was found overexpressed in non-small cell lung cancer, colorectal adenocarcinoma, melanoma, breast and testicular cancers (Orgaz et al., 2014). It is involved in signaling regulating cell polarity, migration and proliferation and hence is regarded as pro-oncogenic (Stengel and Zheng, 2011; Jansen et al., 2018).

1.2.3. RhoD

RhoD was first described in a study carried out by the group of Marino Zerial, who attempted to identify novel Rab and Rho GTPases with functions in membrane traffic and cytoskeleton interaction, by a PCR-cloning aproach (Chavrier et al., 1992). Their result yielded a previously unknown Rho GTPase, termed RhoD, whose functions were further described in a paper by Murphy and colleagues (Murphy et al., 1996). The group established a connection between membrane traffic and cytoskeleton since they found that activated RhoD causes rearrangements of the actin cytoskeleton and cell surface, and also reduces early endosome motility and affects their distribution. Activated mutant or wild type RhoD induced disappearance of actin stress fibers from the cell body and disassembly of focal adhesions, while causing formation of thin cell protrusions (Murphy et al, 1996).

Subsequent research on active forms of RhoD found that overexpression of RhoD suppresses cell migration and cytokinesis. Tsubakimoto and colleagues (1999) postulated that cytoskeletal alterations including loss of actin stress fibers and focal adhesions by RhoD lead to retardation of cell migration, and that RhoD probably prevents the assembly of contractile actin ring necessary for cytokinesis (Tsubakimoto et al., 1999). This research cemented RhoD's antagonistic roles to RhoA, a known oncogene. It was later further confirmed that active RhoD limits vesicular movement and endothelial cell motility (Murphy et al., 2001).

Aside from RhoB, RhoD is thus far the only other identified Rho GTPase subfamily member localized to the endosome compartment of the cell (Ellis and Mellor, 2000). In light of RhoD impeding migratory phenotypes, a research emerged where RhoD was used as a RhoA inhibitor in the process of cellular invasion induced by the Src oncogene. In particular, it was proposed that RhoA and RhoD act as a molecular switch of cellular invasion in pre-malignant and Src-transformed kidney and colon cancer cells (Nguyen, 2002), highlighting the potential of RhoD in abrogating RhoA mediated tumorigenesis and transformation processes.
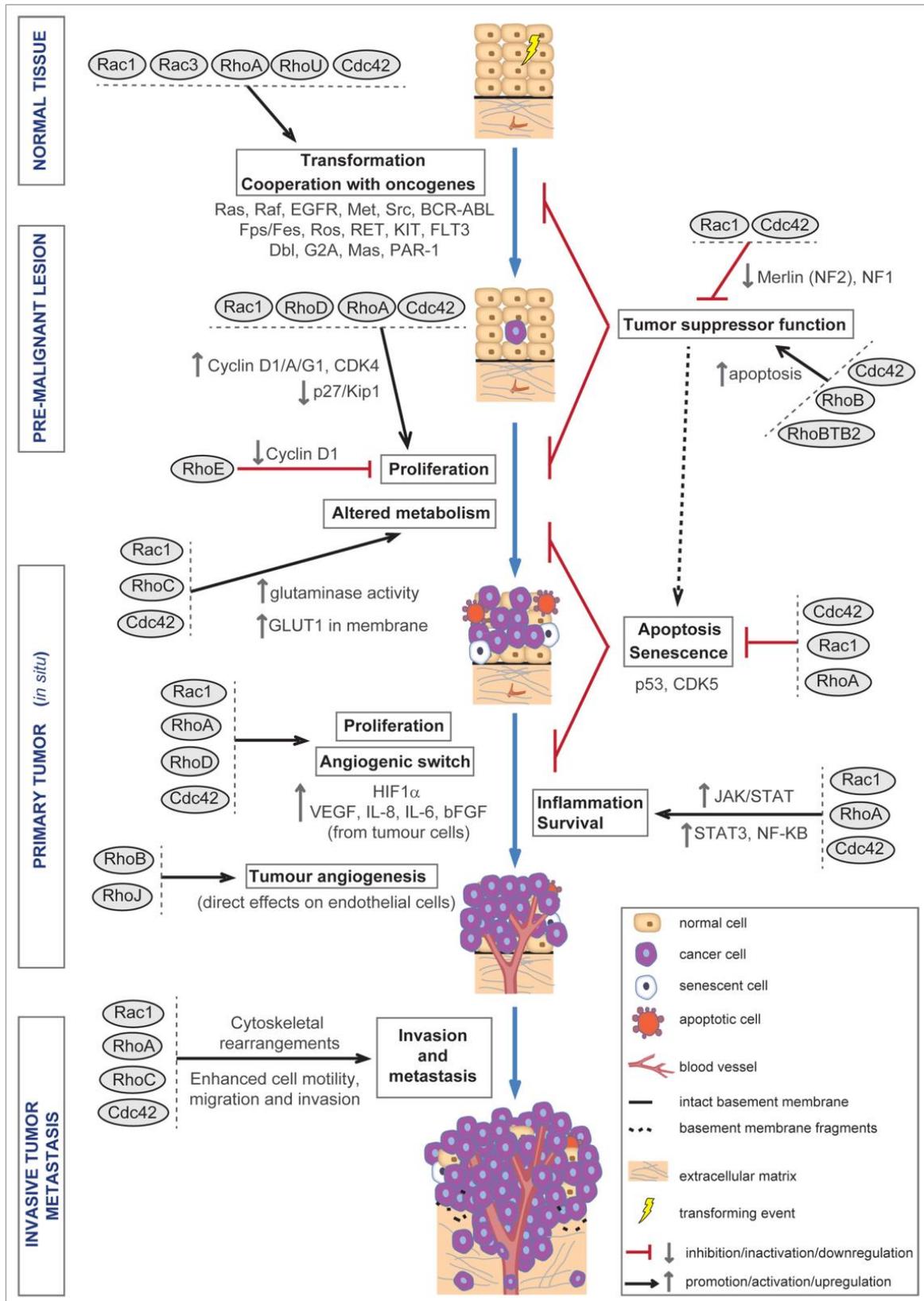
Figure 1.2.2.1. *Roles of Rho GTPases in malignant transformation and tumor progression.* *Reprinted from Orgaz et al. 2014.*

The connection between RhoD and Src was emphasized when it was discovered that a human Diaphanous splice variant, hDia2C, binds to RhoD, which then activates Src kinase. This sequential activation of hDia2C and Src appears to regulate the motility of early endosomes through interactions with the actin cytoskeleton (Gasman et al., 2003). This notion was developed further in a mini review article by Randazzo (2003), who proposes a mechanism of regulatory machinery that transfers early endosomes from microtubules to F-actin, involving the RhoD-hDia2C-Src signaling axis.
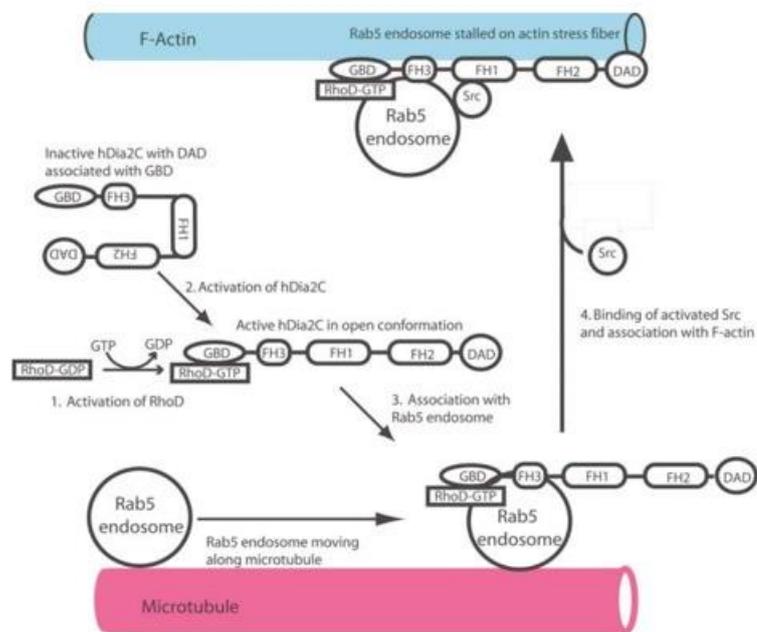
Figure 1.2.3.1. RhoD, hDia2C and Src in endosome motility. Activated RhoD (1.) binds the activated hDia2C (2.) and the complex associates with Rab5 endosome (3.). Active Src binds the complex which then associates with F-actin (4.). Reprinted from Randazzo, 2003.

In this model, RhoD is activated by nucleotide exchange into its GTP form which then binds hDia2C. This activates hDia2C, causing it to assume an open conformation, that allows the entire RhoD-hDia2C complex to bind the early (Rab5 positive) endosome, which was moving along the microtubule. The complex dissociates from the microtubule and activated Src binds the hDia2C FH1 domain and the newly formed RhoD-hDia2C-Src complex now associates with F-actin, thereby mediating the reduction of endosomal motility (Randazzo, 2003) (Figure 1.2.3.1.).

RhoD was also found to be important for proper targeting of Src, Yes and Fyn family proteins to the cell membrane. Fyn is generally present on RhoD positive endosomes, while palmytoilated Src localizes predominantly to RhoD endosomes. RhoD depletion also inhibits localization of Src and Fyn to such vesicles (Sandilands et al., 2007). RhoD was also shown to

interact with the Plexin protein B1 effector domain, which is important for actin cytoskeleton remodeling and cell movement (Tong et al., 2007).

In the latest paper published regarding RhoD, it was demonstrated that RhoD possesses a unique N-terminal motif, absent from the classical Rho GTPases (RhoA, Cdc42 and Rac1), which is critical for regulation of RhoD positive vesicle dynamics, as deletion of this motif caused clustering of RhoD positive vesicles and their accumulation at the peripheral membrane border, in transformed human foreskin fibroblasts (Blom et al., 2018).Other than just early endosome motility, it was found that RhoD also participates in targeting of PAK5 to different subcellular locations. PAK5 (p21-activated kinase 5), is a serine/threonine protein kinase that plays a role in cytoskeleton regulation, cell migration, proliferation and cell survival. It shuttles between the nucleus and mitochondria, and its mitochondrial localization is crucial for the role in cell survival (Wu and Frost, 2006). All of these early papers on RhoD therefore collectively add to the importance of RhoD in cell migration, proliferation and intercellular traffic and cytoskeletal organization, underlying a possible role of RhoD in cancer biology.

Since 2010 more groups started taking interest in RhoD. Many papers were published dealing with biological functions of RhoD within the cell, and also identifying novel RhoD interacting partners. RhoD was reported to have a role in the organization of actin dynamics that is diverse to the roles of other Rho GTPases (Cdc42, RhoA and Rac1) involved in these processes (Gad et al., 2012). RhoD binds the actin-nucleation promoting factor *WASp homologue associated with actin of Golgi membranes and microtubules* (WHAMM) and also interacts with FILIP1 (filamin A binding protein). WHAMM also binds the Arp2/3 complex, which initiates growth of new actin filaments, and was found to act downstream of RhoD in the regulation of cytoskeletal dynamics. FILIP1 binds filamin A, which crosslinks actin filaments and participates in the anchoring of membrane proteins for the actin cytoskeleton. It was later shown that RhoD and WHAMM also participate in proper localization of Golgi stacks, and hence, Golgi homeostasis (Blom et al., 2015). Later another interacting partner of RhoD, the ZIPK (Zipper Interacting protein Kinase) was identified and associated with reorganization of focal adhesions and increased adhesion size (Nehru et al., 2013). It is being speculated that RhoD might be involved in interplay with FAK in focal adhesion dynamics, since adding evidence suggests it is a negative regulator of focal adhesion assembly (Murphy et al., 1996; Tsubakimoto et al., 1999). The same research group found that RhoD also

interacts with Rabankyrin 5, a Rab5 effector protein, and that together they share a role in internalization and trafficking of activated tyrosine kinase receptors (Nehru et al., 2013).

It was further elucidated that RhoD is important for directed cell migration. It was shown by Blom and colleagues that RhoD depletion leads to increase in actin-containing structures, but also reduces cell migration and proliferation (Blom et al., 2017). In vaccinia virus infection, it was also found that RhoD recruits its interacting partner Pak6 to the plasma membrane, which antagonizes the RhoC-ROCK-myosin signaling axis which enables cell contraction and blebbing (Durkin et al., 2017). Another example of infection by pathogens where RhoD is involved was demonstrated on Henle 407 intestinal cells, where it was shown that bacterial protein SopB from *Salmonella typhimurum* can recruit RhoD to bacterial invasion sites, among other Rho GTPases (Truong et al., 2018).

Upon activation with high concentrations of FGF (Fibroblast Growth Factor), RhoD was found to bind and activate the actin nucleator mDia3C at the plasma membrane and induce the formation of cytoneme-like protrusions (thin cellular protrusions specialized for exchange of signaling proteins between cells) (Koizumi et al., 2012). RhoD was also found to be involved in the regulation of G1/S phase progression during the cell cycle through the effector protein Diaph1, and centrosome overduplication, in HeLa and U2OS cells (Kyrkou et al., 2012).

In 2017, on the melanoma cell line model it was shown that RhoD was downregulated in three melanoma cell lines (M14, A375 and MV3), when compared to normal melanocyte cells (MC). Consequentially, the normal melanocytes exhibited no actin stress fibers or adhesion plaques, while both were present in the melanoma cell lines. Also, the migration rates of melanoma cell lines were high, while MC had no ability to complete the transwell migration test. Hence, it was concluded that RhoD, through its interacting partner Diaph2, influences the migration and invasion of melanoma cells through regulating filopodia, lamellipodia, stress fiber and adhesion plaques (Wen et al., 2017).

Strikingly, not much focus has been given to the role of RhoD in cancer and anticancer treatments. Only a couple of papers deal with this aspect of RhoD biology. In one of them, an expression microarray analysis on the MCF-7 cell line model revealed that the expression of RhoD was approximately threefold decreased in MCF-7 cisplatin resistant cell line, compared to the parental cell line (Watson et al., 2007). Another study found that RhoD was overexpressed in tumor plasma cells of multiple myeloma patient samples, compared to normal (healthy) plasma cells (Andrade et al., 2010). In this research the levels of integrin

subunit α5 were found to be underexpressed and RhoD upregulation was associated here with disruption of the focal adhesion pathway in multiple myeloma. Taken together with research in which RhoD was associated with defects in cell proliferation and centriole number (Kyrkou et al., 2012) and research linking RhoD to cell invasiveness (Nguyen et al., 2002), which are often phenotypes displayed by cancer cells (Long and Simpson, 2017), there is emerging evidence of RhoD having a role in cancer biology and antitumor therapies. Considering that specific research dealing with RhoD in this aspect is still largely unavailable, it is becoming increasingly important to elucidate possible roles RhoD might have in this field and to conduct research regarding its potential in anticancer drug approaches.

1.3. KIF20B

KIF20B is a kinesin family protein, with a size of 210 kDa. It is a large positive oriented motor protein subclassified into kinesin family 6, alongside KIF20A (MKLP2, RAB6KIFL) and KIF23 (MKLP1, CHO1), important regulators of cell division and cytokinesis. This chapter will cover the kinesin family of proteins with a focus on subfamily 6 and functions of KIF20B and its importance in cell division and proliferation.

1.3.1. Kinesins

Kinesins are a large motor protein family, which consists of 14 subclasses comprising 45 kinesin proteins in total in humans (Figure 1.3.1.1.). Across known species, over 650 kinesins have been identified to date. They are present in all eukaryotes, but absent from archaea and bacteria (Rath and Kozielski, 2012). They were discovered and differentiated from dynein in 1985 by Ron Vale and colleagues (Klinman and Holzbaur, 2018). Much work on kinesin orthologues, especially on *Drosophila melanogaster*, has shown that they possess functions essential for the execution and completion of mitosis and meiosis. They have important roles in separation of chromosomes, microtubule dynamics, mitotic spindle formation, cytokinesis and cell cycle progression. Kinesins generally move in a plus directed manner along microtubules – from cell nucleus towards the periphery (Klinman and Holzbaur, 2018).

Kinesins can be monomeric, dimeric, trimeric or even tetrameric proteins structured from two domains: an ATP hydrolysis domain which allows movement along microtubules, and a tail domain which binds cargo (Camlin et al., 2017). They usually use scaffold proteins to bind
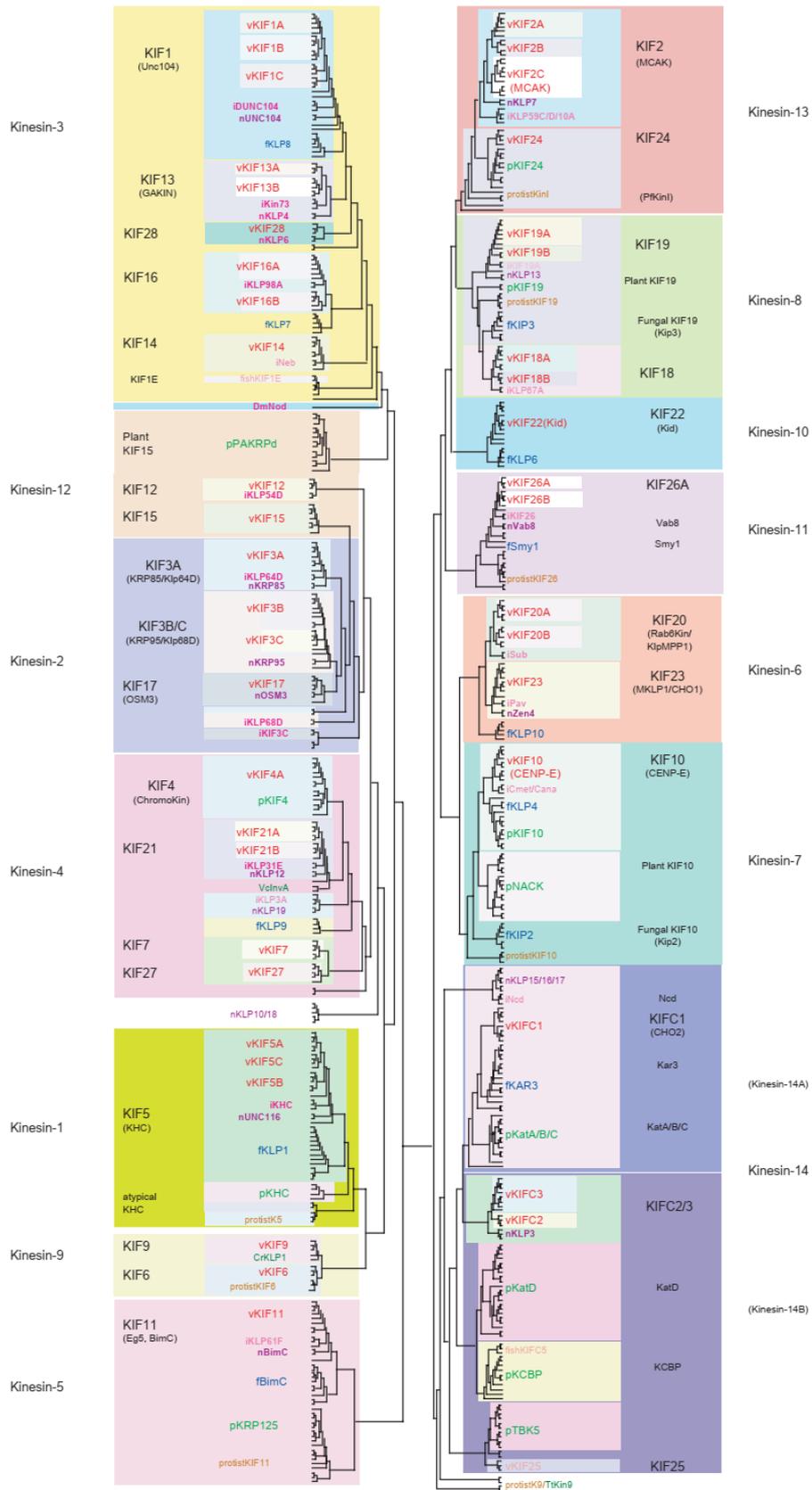
Figure 1.3.1.1. The kinesin superfamily tree depicting phylogenetic relationships between different kinesin subfamilies across several different species. *Code: v (red): vertebrate; i (pink): insect; n (purple): nematode; p (green): higher plant; f (blue): fungi. Reprinted from Miki et al., 2005.*

cargo, or sometimes bind cargo directly (Hirokawa and Tanaka, 2015). The motor domain is conserved in different kinesin families, and the tail domains are more divergent (Vicente and Wordeman, 2015). Since kinesins are one of the three major groups of cargo transporting proteins (the other two being myosins and dyneins), they are exceedingly important in neuronal transport along the axon fibers, which is important for neural functions such as learning, memory and brain development. They have also been found important in regulating development, in particular the left/right asymmetry of the body, and organogenesis (Hirokawa and Tanaka, 2015). Kinesins transfer cargo by moving along the microtubule tracks while hydrolyzing ATP for energy (Klinman and Holzbaur, 2018). Aside from just "walking" along microtubules, some kinesins can also control microtubule dynamics through promoting polymerization, depolymerization or pausing polymerization (Vicente and Wordeman, 2015).
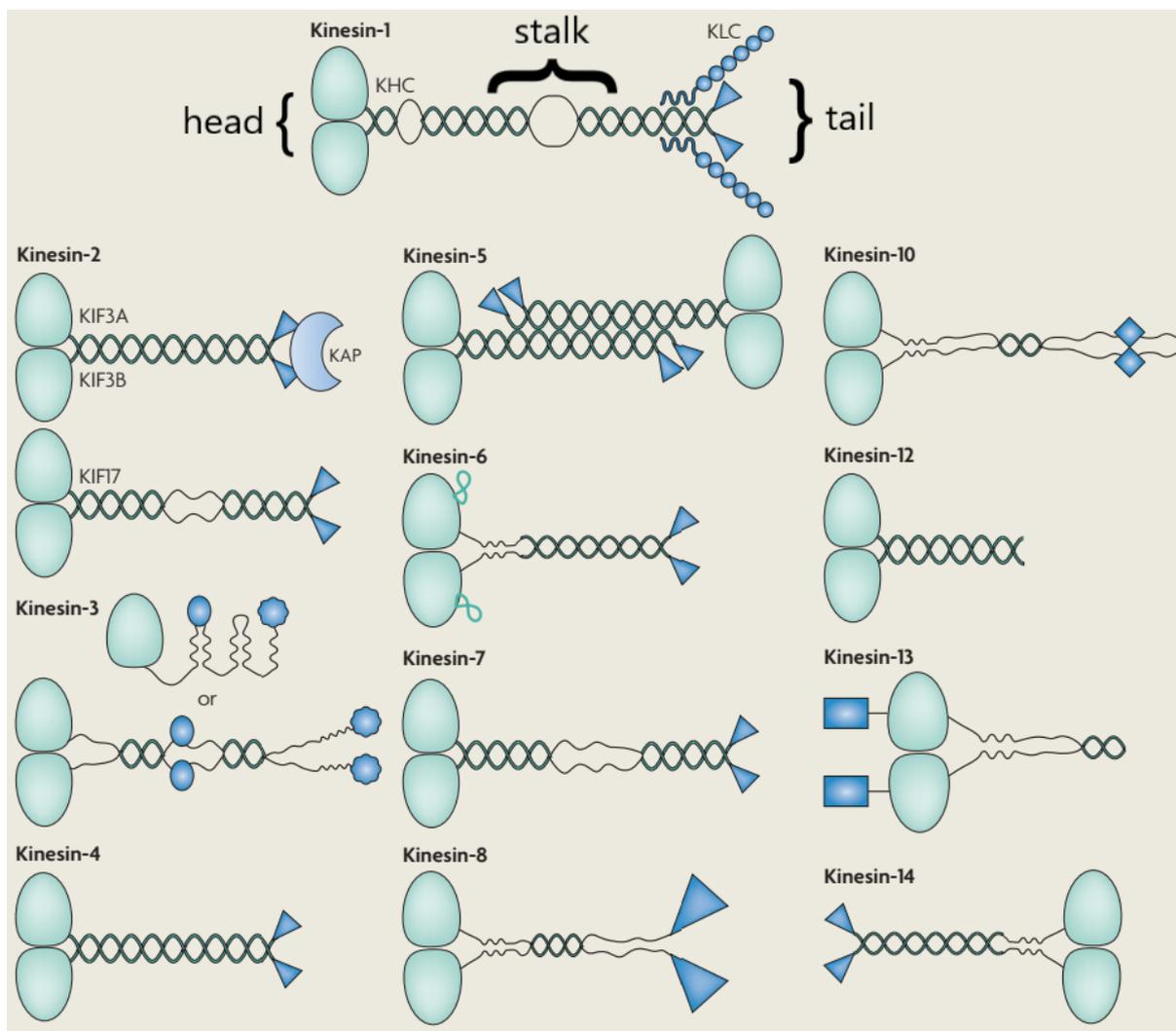
Figure 1.3.1.2. Basic kinesin structure across all kinesin families. *The main domains are outlined on the example of Kinesin-1 (namely the head, stalk and tail regions). Adapted from* Verhey and Hammond, 2009.

All kinesin motors feature a 360-residue globular domain, a conserved domain which is responsible for ATP hydrolysis and microtubule binding. It is often called the "catalytic core" of the kinesins (Miki et al., 2005). This area is identified as the protein "head", which is followed by a long filamentous "stalk" region, finishing in a "tail" region, as depicted in Figure 1.3.1.2.

All kinesin families share similarities in both their localization and function in the cell, which are predominately linked to mitosis/meiosis and cargo transport. Various kinesin families participate in vital parts of mitosis (Figure 1.3.1.3.), from the first steps of centrosome separation, microtubule crosslinking and formation of the bipolar spindle (kinesin family 5, 12 and 14), through capture and congression of chromosomes (families 4, 7, 8, 10, 13 and 14), correct chromosome alignment (kinesin family 8), microtubule depolymerization important for chromosome segregation in anaphase (families 5 and 13) and finally, in cytokinesis (kinesin families 3, 6 and 7) (Vicente and Wordeman, 2015).
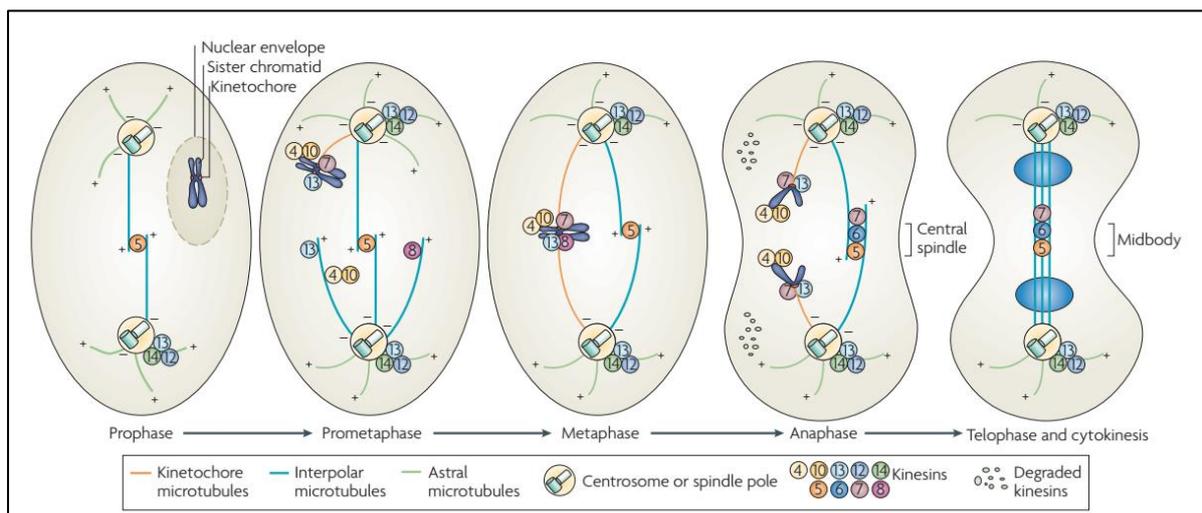
Figure 1.3.1.3. Localization of various kinesin families in mammalian cells during mitosis. *Reprinted from Verhey and Hammond, 2009.*

1.3.2. Kinesins in cancer

Since kinesins have crucial roles in the processes of cell division, it is not surprising that the variability in their activity in the cell may influence tumorigenesis and cancer progression. Recently, the potential of kinesins as novel drug targets in cancer has been identified and exploited. Kinesin inhibitors have come into the spotlight as important drugs that could help diminish excessive cell proliferation in cancer. Two of such drugs have already started clinical trials as monotherapies or in combination with other drugs: the Eg5 (KIF11)

inhibitor and CENPE (Centromere-associated protein E/ KIF10) (Rath and Kozielski, 2012). Eg5 is involved in the formation of the bipolar spindle, and CENPE is required for progression from metaphase to anaphase. Inhibition of Eg5 in human cells by siRNA, antibodies or inhibitors directed towards this protein, causes the activation of the spindle checkpoint and mitotic arrest leading to tumor cell death in some tumor cell lines (Rath and Kozielski, 2012). Deletion of CENPE results in the chromosomal instability phenotype (CIN). Intriguingly, CENPE is considered both a tumor suppressor and oncogenic protein. Aside from malignancy associations of kinesins, some kinesin proteins are also implicated in drug resistance of solid tumors. For example, several mitotic kinesins like KIF2A, KIF2B, CENPE and HSET, have been implicated in development of resistance to microtubule poisons, such as epothilone A and B, docetaxel and colchicine (De et al., 2009, Ganguly et al., 2011, Liu et al., 2013, Rath and Kozielski, 2012). Some non-mitotic kinesins are also involved in resistance to paclitaxel and docetaxel, for example overexpression of KIF1A, KIF5A or KIFC3 increased resistance to paclitaxel derivatives in breast cancer cell lines (De et al., 2009).

Table 1.3.1.1. Kinesin family members and their tumorigenic characteristics, adapted from Liu et al., 2013. The numbers in parentheses denote affiliation of each kinesin protein to their proper kinesin protein family.

Kinesin member (family)	Tumorigenic properties
KIF5B (1)	Overexpressed in bladder, stomach, skin and breast cancers
KIF3A, KIF3B (2)	Oncogenesis and metastasis of breast cancer and renal cell carcinoma
KIF1B (3)	Metastasis of nervous system tumor
KIF14 (3)	Overexpression promotes development of breast, lung and retinoblastoma tumors
KIF4A (4)	Oncogenesis of cervical and non-small-cell lung cancer
KIF7 (4)	Oncogenesis and metastasis of multiple cancers
Eg5/KIF11 (5)	Overexpression promotes development of multiple cancers
MPHOSPH1/KIF20B (6)	Overexpressed in bladder, colorectal and hepatocellular cancers
MKLP1/KIF23 (6)	Downregulation causes cytokinesis defect in tumor cells
MKLP2/KIF20A (6)	Overexpressed in pancreatic ductal adenocarcinoma cells, downregulation inhibits growth of gastric cancer cells
CENPE/KIF10 (7)	Downregulation inhibits growth of multiple cancer cells
MCAK/KIF2C (13)	Overexpressed in many cancers and linked to taxane resistance of tumor cells
KIF2A (13)	Upregulation promotes tongue squamous cell carcinoma development
HSET/KIFC1 (14)	Associated with brain metastasis of lung cancer
KIFC3 (14)	Upregulation causes docetaxel resistance in breast cancer cells

Various kinesins are overexpressed in many cancer cell lines and may also be associated with poor prognosis. The protein levels of these kinesins can also serve as prognostic indicators, usually outlining a poor disease outcome correlating with KIF overexpression, as overexpressed kinesins tend to be linked to tumor progression, invasion and metastasis (Liu et al., 2013). As example, the most prominently cancer-associated kinesins from several families and their tumorigenic characteristics have been listed in Table 1.3.1.1., adapted from Liu et al., 2013.

1.3.3. Kinesin family 6

Kinesin family 6 comprises 3 members whose activities are essential in cell division. Not only are they deeply involved in mitosis, but also in cargo transport, as is the case with KIF20A. Kinesin family 6 in humans consists of three proteins: KIF23 (MKLP1, CHO1), KIF20A (MKLP2, RAB6KIFL) and KIF20B (MPHOSPH1, MPP1, KRMP1) (Miki et al., 2005). The members of this family can be further subdivided into KIF20 and KIF23 subfamilies. KIF20 subfamily members appear in fungi, slime mold and animals, while KIF23 subfamily has diverged in animals. No plant kinesin members of family 6 have been identified in plants so far (Miki et al., 2005). The major structural characteristic of this family is the long insert of 8 to 10 kDa inside the catalytic core, at the L6 loop site, which is situated on the opposite side of the microtubule-binding surface and might regulate the protein's motor activity (Figure 1.3.3.1.). Targeting this site may harbor highly specific kinesin 6 inhibitors, and result in obtaining novel cancer drug targets (Rath and Kozielski, 2012).
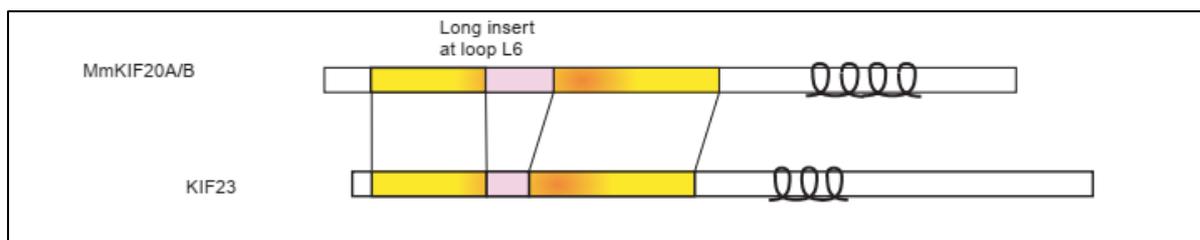
Figure 1.3.3.1. Schematic representation of kinesin family 6 protein structure. Adapted from Miki et al., 2005.

Kinesin family 6 has essential roles in cytokinesis and microtubule transport. KIF20A, or RAB6KIFL, was the first kinesin reported to bind a Rab GTPase protein (Echard et al., 1998). Later studies revealed that KIF20A also has an essential role during cytokinesis (Hill et al., 2000).

KIF23 is the component of centralspindlin complex. Two splice variants (MKLP1 and CHO1) were reported so far, and an orthologue named *Pavarotti* was identified in *Drosophila melanogaster*, that organizes the central spindle and contractile ring for cytokinesis (Mishima et al., 2002, Rath and Kozielski, 2012). The chromosomal passenger protein INCENP (Inner Centromere Protein) recruits KIF23 to the spindle midbody (Zhu et al., 2005). KIF23 is regulated by important proteins of the cell cycle and cell division – CDK1 (Cyclin Dependent Kinase 1), Aurora B and PLK1 (Polo-Like Kinase 1) (Liu et al., 2004). KIF23 depletion causes incomplete cytokinesis in affected cells and a binucleated or multinucleated phenotype (Neef et al., 2006). No redundancy roles have been reported between KIF23 and KIF20A/B proteins. KIF23 downregulation suppresses glioma proliferation and it has been proposed as a target for glioblastoma (Takahashi et al., 2012). KIF23 was also found to be upregulated in non-small cell lung carcinoma (Rath and Kozielski, 2012).

KIF20A was first isolated as the interacting partner of Rab6A (Echard et al., 1998). Through further research it was established however, that this protein's primary function was during cytokinesis. Introduction of KIF20A antibodies into mammalian cells leads to cytokinesis defects (Fontijn et al., 2001; Hill et al., 2000). KIF20A is important for cleavage furrow ingression during early cytokinesis stages. PLK1 directly phosphorylates KIF20A, thereby regulating its motor properties (Neef et al., 2003). In turn, KIF20A is essential for normal PLK1 localization to the central spindle. One of the most important roles of KIF20A during cell division is that it is required for translocation of the chromosome passenger complex from the kinetochores to the central spindle (Gruneberg et al., 2004; Hümmer and Mayer, 2009). The passenger complex proteins are essential for completion of cytokinesis. KIF20A mRNA is overexpressed in pancreatic ductal adenocarcinoma (PDAC) and its inactivation leads to inhibition of pancreatic tumor cell growth (Taniuchi et al., 2005). These characteristics of KIF20A make it a potential drug target to selectively affect cell division. Interestingly, an orthologue named *Subito* was found in *Drosophila melanogaster*, which is corresponding in roles to both KIF20A and KIF20B (Cesario et al., 2006), indicating that for some reasons KIF20 proteins diverged to form KIF20A and KIF20B in higher animals.

1.3.4. KIF20B

KIF20B is a 210 kDa plus-end oriented motor kinesin. In 1994 Westendorf et al. reported a partial cDNA they identified as an epitope sequence for the antimitotic protein

MPM-2 monoclonal antibody after phosphorylation by the M-phase kinases (Westendorf et al., 1994). The sequence was named MPP1 (MPM-2 reactive phosphoprotein 1). Five years later, another group reported this sequence of 566 amino acids at the carboxy terminus was identical to their newly discovered protein KRMP-1 (kinesin-related motor interacting with Pin1). In this research the group placed KRMP1 in the same kinesin family as KIF23. They have actually identified KIF20B through its *in vivo* interaction with mitotic peptidyl-prolylisomerase PIN1, which is regulated by CDK1. The paper also reported localization of KIF20B for the first time: endogenous KIF20B localized predominately in the cytoplasm of interphase cells and dispersed throughout the cell during mitosis. Interestingly, the overexpressed KRMP1/KIF20B localized also to the nucleus, revealing a possible association with nuclear pores. Overexpression of KRMP1/KIF20B also caused COS-7 cells to arrest in G2/M phase transition, which further underlined the importance of KIF20B during mitosis (Kamimoto et al., 2001).

In 2003 KIF20B was first characterized as a plus-end-directed kinesin motor, which moves slowly along microtubules and also exhibits microtubule bundling properties and microtubule-stimulated ATPase activity. The same research paper corroborated the previous localization finds of KIF20B situating to the nucleus during interphase. However, in dividing cells it was found for the first time that KIF20B localized to the spindle midzone during anaphase, and subsequently concentrated on the midbody in telophase. This localization pattern prompted the group to investigate the influence of KIF20B on the outcome of cell division and they found that KIF20B depletion by siRNA induced failure of division in late stages of cytokinesis, in HCT-116 cell model. Defects in mitotic exit, daughter cell separation and appearance of apoptosis were observed in KIF20B depleted cells (Abaza et al., 2003).

KIF20B has been found in many tissues and different cell types. It is abundantly expressed in human brain, kidneys and testes, and has been found overexpressed in many tumor cell lines: HeLa, HCT-116 (Abaza et al., 2003), BEL7404, A549, SW620, T24 (X. R. Liu et al., 2012) and a wide range of bladder cancer cell lines: HT-1197, UM-UC-3, J82, HT-1376, SW780 and RT4 (Kanehira et al., 2007), compared to normal tissues. Subsequently it has been elucidated that KIF20B is also overexpressed in hepatocellular carcinoma samples obtained from patients, and also in hepatocellular cancer cell models HepG2, Hep3B, BEL7404 (X. Liu et al., 2014) and HuH-7 (X. Liu et al., 2018). KIF20B was also found to be overexpressed in colorectal cancer samples from patients and established colorectal carcinoma cell lines LOVO

and SW480 (W. F. Lin et al., 2018). Most recently, high expression of KIF20B has been confirmed in clear cell renal carcinoma (ccRCC) tissues and ccRCC established cell lines 786-O and CRL-1932. Moreover, depletion of KIF20B in these cell lines by a lentiviral vector with KIF20B shRNA, caused a decrease in the amount of proliferation markers Ki67 and PCNA (G. Li et al., 2019).

KIF20B has come into the spotlight as a promising target of various epithelial – type cancers. High expression of KIF20B was found in tongue cancer patients and consequentially in oral squamous carcinoma cell lines CAL-27 and TCA-8113 (Z. Y. Li et al., 2019). In all of the aforementioned cases, KIF20B high expression was correlated with poorer prognosis and KIF20B depletion, by means of either viral vectors, shRNA or siRNA, has reduced the proliferation rates of tumor cells *in vitro*, or decreased tumor size in animal models. KIF20B depletion by shRNA was also reported to negatively affect levels of proliferation associated proteins Ki67 and PCNA in oral squamous carcinoma cells (Z. Y. Li et al., 2019). Interestingly, KIF20B has been identified as upregulated even by deep sequencing in pancreatic cancer patients (Ansari et al., 2015).

Except for its role in tumor proliferation, KIF20B has an essential role in the regulation of cerebral cortex growth. In developing mice embryos, the most Kif20b mRNA was found in neural stem/progenitor cells. On the mouse model it was found that Kif20b is required for normal cytokinesis of polarized cortical stem cells and normal cerebral cortex size, as the Kif20b loss of function mutants developed microcephaly. Interestingly, in the mutant mice there was no change in mitosis, but a difference in the number and positioning of apical midbodies of polarized cortical stem cells was observed. Disruption in abscission didn't result in binucleate cells, but in apoptosis (Janisch et al., 2013). Another example further illustrates the significance of KIF20B in neural development, and that is the interaction that was found between KIF20B and Shootin 1. Shootin 1 has a role in regulating polarization of primary hippocampal neurons and downregulation of either Kif20b or Shootin 1 in mice hindered the transition from multipolar to bipolar cells (Sapir et al., 2013).

Further study on KIF20B localization revealed it to have a similar pattern to KIF20A during cell division. During interphase the localization on the nucleus was confirmed, which then shifted from chromosomes to the spindle midzone throughout anaphase and finally resulted in condensed KIF20B signals on the midbody during telophase, all the way through cytokinesis, which was demonstrated on bladder cancer

cells UM-UC-3 (Kanehira et al., 2007), MEF cells (Janisch et al., 2013), and HeLa cells (Sapir et al., 2013; Janisch et al., 2018). Localization of KIF20B was further elaborated on both immunofluorescence and live- imaging in HeLa cells, and directly compared to localization patterns of other kinesin 6 family members KIF20A and KIF23. The authors displayed KIF20B localization to be very similar to that of KIF20A and KIF23 during anaphase and telophase, but with slight variations. This difference is most striking in early anaphase where both KIF20A and KIF23 localize in the spindle midzone, but KIF20B also localizes on microtubules emanating from kinetochore regions of the chromosomes, and also the ones leading from chromosomes to centrioles. Another difference is visible during late telophase/cytokinesis, where KIF20B appears as two distinct signals on the midbody, while KIF20A sports only one signal inbetween two KIF20B signals. Interestingly, KIF23 has signals similar to KIF20B in this stage (Janisch et al., 2018).

KIF20B depletion on HeLa cells by siRNA-mediated knockdown affects both the speed of furrow ingression and abscission. KIF20B is not required for the assembly of the midbody, but may accelerate or coordinate midbody maturation, in particular the late steps of maturation including anillin dispersal, recruitment of ESCRT-III and formation of microtubule constricting sites (Janisch et al., 2018). The phenotype elicited by KIF20B knockdown exhibits mild multinucleation rates, ranging from 1 to 5%, and affected cells mostly end in apoptosis. Other than in HeLa cells, this was also shown recently on AGS gastric and HCT-116 colorectal carcinoma cell lines (Georges et al., 2019). The same research has found that KIF20B interacts with the F-box protein FBXO38, which also interacts with the ubiquitin specific protease 7 (USP7). Interestingly, USP7 knockdown in AGS and HCT-116 cells affects both the levels of KIF20B and FBXO38 proteins, by decreasing them and inducing the cytokinesis-defect phenotype characteristic for KIF20B.

In 2007 KIF20B was referred to as the "cancer-testis antigen 90"/CT90 (Kanehira et al., 2007). This particular designation comes from a large family of tumor-associated antigens expressed in human tumors, but not in normal tissues except for testes or placenta (Fratta et al., 2011). Although KIF20B was not officially recognized as a characteristic CTA, its tumorigenic potential is highlighted through this initial "nickname". The first research employing KIF20B as a target in tumor therapies focused on an shRNA depletion approach by means of an oncolytic adenoviral vector. In combination with the anti-tumorigenic gene interleukin 24 (IL-24), this vector showed great anti-tumor effect on numerous cancer-cell

lines *in vitro*, and also *in vivo*, on a nude-mice xenograft with SW620 human cells (X. R. Liu et al., 2012).

Furthermore, a HLA-A24-restricted peptide epitopes corresponding to parts of KIF20B were identified using a genome-wide expression profile analysis for bladder cancer. These peptides may induce a cytotoxic lymphocyte response specific to KIF20B, which would enable them to be used as cancer peptide vaccine oncotherapy. These peptide epitopes were even used in a clinical trial with patients suffering from advanced bladder cancer. The peptide vaccine was well-tolerated in patients, without any serious adverse effects, and effectively induced cytotoxic T-lymphocytes *in vivo* (Obara et al., 2012).

Regarding research of KIF20B in response to anticancer agents, an expression profile study on breast cancer patient samples showed that among other kinesin proteins, KIF20B was generally overexpressed in the basal and Her2+ tumor subtypes. The same research also reported that KIF20B expression in breast cancer patient samples inversely correlated with taxane response, meaning that KIF20B was overexpressed in tumor tissues resistant to taxane compounds, compared to normal breast tissues (Tan et al., 2012). Following the research based on adenoviral oncolytic vector bearing KIF20B shRNA, in 2014 another study from the same group confirmed that KIF20B is the oncogenic driver in hepatocellular carcinoma and they found that KIF20B shRNA initiated HCC proliferation arrest, induction of apoptosis and also increased sensitivity to paclitaxel toxicity, which was demonstrated on two HCC cell lines HepG2 and Hep3B. The group delved a bit deeper towards a mechanism behind the find and they discovered that KIF20B depletion stabilized p53, blocked STAT3 phosphorylation and prolonged mitotic arrest (X. Liu et al., 2014).

A novel KIF20B localization in pseudopodia of colorectal carcinoma cells finding led to a hypothesis that KIF20B may promote Gli1 (glioma associated oncogene 1)-induced epithelial-mesenchymal transition (EMT) in human colorectal cancer. They also found that KIF20B promoted migration and invasion of colorectal carcinoma cells. They proposed a mechanism where KIF20B mediated the cooperation of actin and microtubules necessary for the elongation process of the pseudopodia (invadopodia), and also might induce Gli1-mediated EMT and EMT-related protrusion formation through pseudopodial actin dynamics (Lin et al., 2018).

In hepatocellular carcinoma cell lines HepG2, Hep3B and HuH-7 it was recently found that KIF20B depletion by shRNA-bearing oncolytic adenoviral vector induced sensitivity of

cells to paclitaxel and acted synergistically with two other microtubule-targeting agents Epothilone B and vincristine. In addition to MTAs, KIF20B reduction also enhanced the toxicity of drugs hydrocamptothecin and mytomicin C (X. Liu et al., 2018).

The abundance of recent research which profiles KIF20B as a tumor-cell proliferation promoting molecule has brought about the need to more seriously explore KIF20B as a valuable target in anticancer therapy, and also as a prognostic marker. More research investigating KIF20B effects on commonly used tumor therapies is becoming increasingly necessary, especially with today's advances in personalized medicine. With emerging resistance and adaptability of cancer cells, it becomes increasingly important to address what kind of response to anticancer drugs KIF20B depletion would yield.

1.4. Cell division and cytokinesis

Cell division, mitosis or M phase, is a part of the cell cycle. Chromosomes duplicate once per cell cycle, in S phase, preceded by G1 and followed by G2 phase. Interphase encompasses phases G1, S and G2. Some cells may exit the cell cycle in G1 phase and stay in a metabolically active state – the G0 phase, until extracellular signals reactivate them. The cell cycle is precisely regulated by the activity of cyclin-dependent kinases (Cdk). They are involved in the checkpoint system, which assures that progression through the cell cycle is blocked if abnormalities have occurred in the steps so far. For discovering the key molecular principles coordinating the cell cycle Tim Hunt, Paul Nurse and Lee Hartwell were awarded with a Nobel prize in 2001. Mitosis was first described and named by Walther Flemming in 1882, who also named its 4 characteristic stages: prophase, metaphase, anaphase and telophase.

The master regulator of the cell cycle is the cyclin-dependent kinase 1 (Cdk1). It is a serine/threonine kinase made up of a catalytic Cdk subunit and an activating cyclin subunit (cyclin A or B) (Morgan, 1997). Entry into mitosis (M-phase) is mediated by active Cdk1 which is associated with cyclin B – the two key components of the maturation promoting factor (MPF) (Heim et al., 2017). Exit from M phase follows the inactivation of MPF. The activation of Cdk1/cyclin B complex begins in the cytoplasm, particularly at the centrosomes. In late prophase, a nuclear translocation of the complex occurs, resulting in the breakdown of the nuclear envelope and marking the start of M phase. Mitotic exit occurs upon inactivation of
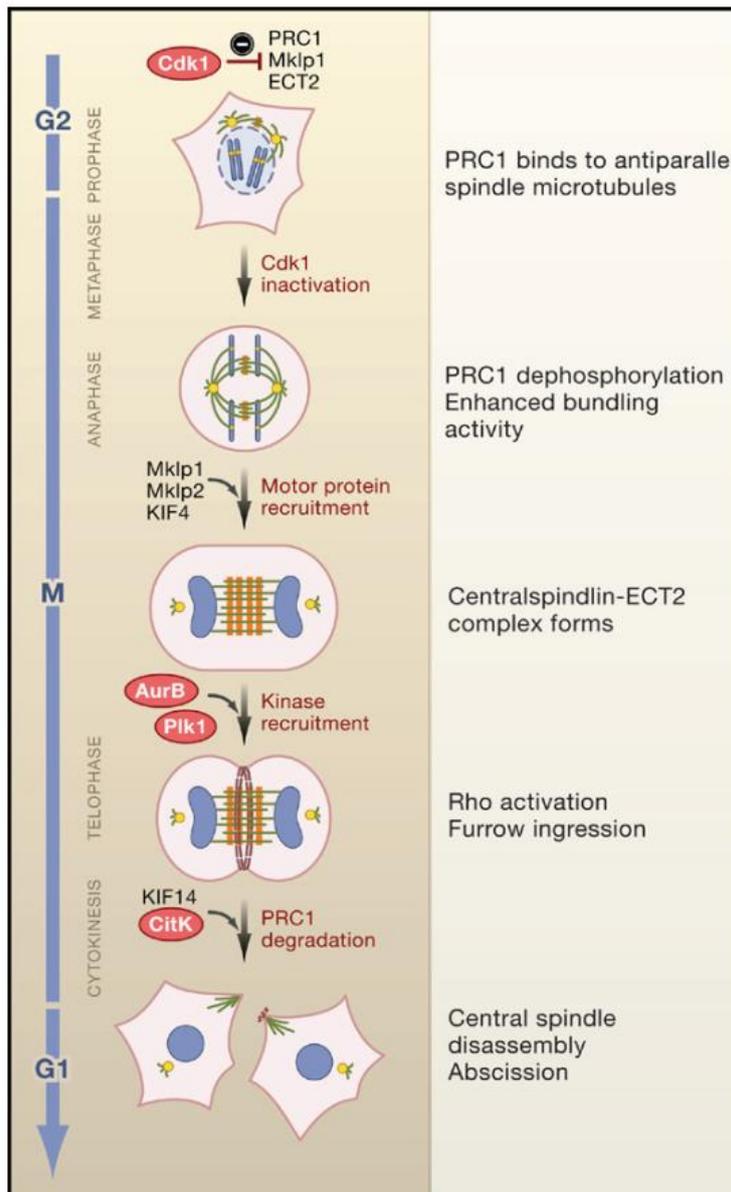
Figure 1.4.1. A brief depiction of the major cell division events. PRC1, kinesin Mklp1, and ECT2 are inhibited by Cdk1. PRC1 is able to bind antiparallel microtubules in the forming spindle, but cannot bundle them. At the anaphase onset, Cdk1 is inactivated. PRC1 promotes microtubule bundling and helps recruit centralspindlin, Mklp2, and KIF4. Together they define and extend the forming central spindle microtubule bundles. PRC1 recruits Plk1 to the microtubules where it phosphorylates substrates required for cytokinesis. Mklp2 helps relocate Aurora B to the central spindle, where it phosphorylates centralspindlin which promotes its assembly. The active band of Rho controls actomyosin ring assembly and furrow ingression. These proteins are subsequently degraded and later stages of cytokinesis, following midbody formation, start to unfurl. The late factors involved in cytokinesis, KIF14 and Citron kinase (CitK) act downstream of Rho in abscission. Finally, membrane fusion occurs to promote abscission. Reprinted from Barr and Gruneberg, 2007.

Cdk1/cyclin B complex by destruction of cyclin B via degradation by ubiquitylation. This process requires the activated ubiquitin E3 ligase anaphase-promoting complex/cyclosome (APC/C) (Heim et al., 2017). The onset of anaphase needs to occur only once after all the chromosomes are attached to the spindle microtubules. To ensure that it does, the spindle assembly checkpoint pathway (SAC) prevents APC/C activation in the presence of improperly attached chromosomes. Unattached kinetochores cause the formation of the mitotic

checkpoint complex (MCC), consisting of Mad2, Bub3, BubR1 and Cdc20, that strongly inhibits the APC/C mediated poly-ubiquitylation of cyclin B. After chromosome separation, mitotic exit takes place (Heim et al., 2017). The complex regulation behind cell division checkpoints has been an object of intensive research and will not be elaborated further here. The major events of cell division are briefly depicted in Figure 1.4.1.

Following anaphase onset, the division plane is positioned between segregating chromosomes. The mitotic spindle is reorganized into the central spindle, an array of interdigitating and antiparallel microtubules. The central spindle originates from microtubules being released from centrosomes in anaphase. These microtubules become tightly bundled at their plus ends in a structure known as the spindle midzone. Many proteins are implicated in the assembly and organization of the central spindle. The most important proteins involved in these processes include several protein complexes and different protein families, like the chromosomal passenger complex (CPC), the centralspindlin complex, microtubule associated protein (MAP, protein regulator of cytokinesis (PRC1) and several kinesin family members (KIF4A, KIF20A and KIF23), Rho and Diaphanous family members, spastin and anillin (D'Avino et al., 2015). PRC1 crosslinks microtubules while the KIF4A protein regulates microtubule dynamics and controls the size of the central spindle (Bieling et al., 2010; Subramanian et al., 2010; C.-K. Hu et al., 2011; Bastos et al., 2013). KIF4A is responsible for transporting PRC1 to the spindle midzone (Kurasawa et al., 2004; Zhu and Jiang, 2005; Zhu et al., 2006. Cdk1 inhibits their interaction before the onset of anaphase, which is later promoted by Aurora kinase B (component of the CPC) (Zhu and Jiang 2005; Bastos et al. 2013).

The centralspindlin complex is a conserved heterotetramer which consists of KIF23 and RacGAP1 (Rho family GTPase activating protein) dimers and is responsible for bundling microtubules (Adams et al., 1998; Mishima et al. 2002; D'Avino et al., 2006). In metaphase Cdk1 phosphorylation inhibits KIF23 binding to microtubules, while after anaphase onset KIF23 localizes to the spindle midzone, which depends on CPC. KIF20A recruits CPC to the spindle midzone, by which an active pool of Aurora B is created, which is necessary for the subsequent control of KIF4A and KIF23 activity (Gruneberg et al., 2004; Fuller et al., 2008). To achieve proper nuclear and cytoplasmic division the cleavage plane and the mitotic spindle need to be properly aligned. In animal cells actomyosin filaments assemble at the cleavage furrow, forming the contractile actin ring. Their contraction is one of the driving forces behind furrow ingression (H. Wang et al., 2005). Rho GTPase RhoA controls the formation of the

contractile actin ring through two signaling pathways: by stimulating actin polymerization via activation of diaphanous proteins (Dia), and by activating the Rho-associated kinase (ROCK). ROCK subsequently phosphorylates the myosin regulatory light chain (MRLC) which promotes myosin contraction (D'Avino et al., 2015). Citron Kinase (CITK/CRIK) and anillin are proteins which are essential for connecting the contractile ring to the membrane and the central spindle.

Aside from constriction of the actomyosin ring to complete a successful cytokinesis, membrane traffic has also proven to be quite indispensable. Vesicle traffic is important for both insertion of vesicles at the cleavage site and also timely delivery of proteins required for proper progression of cytokinesis (Neto et al., 2011). The vesicle pathways involved in cytokinesis include secretory and endocytic/recycling endosomes (Prekeris and Gould, 2008; D'Avino et al., 2015). The secretory pathway begins in the endoplasmic reticulum (ER), transfers to the Golgi apparatus from where it goes to the plasma membrane. On the other hand, the endocytic pathway starts with vesicle budding at the plasma membrane, which occurs through several different types of vesicles: first the early and then the recycling endosome. Finally, they are directed to the plasma membrane (Mckay and Burgess, 2011). An example of this was found in HeLa cells, where secretory vesicles moved to the cleavage site suggesting that the endocytic vesicles fuse with the furrow plasma membrane (Gromley et al., 2005).

The endocytic and recycling proteins also have an important role in furrow ingression and abscission processes (Prekeris and Gould, 2008). Rho GTPases Rab11, Arf6 and Rab35 are needed for completion of cytokinesis in various cell types (Schiel and Prekeris, 2013). By successive constriction of the actin ring, the central spindle finally compacts into a structure, an organelle, called the midbody (or the Flemming body, named after its discoverer in 1891). The midbody is an electron-dense structure composed out of tight bundles of microtubules. This area is difficult to penetrate with tubulin antibodies and this is why it appears as a dark region in cells immunostained for microtubules. After the completion of furrowing, constriction sites appear on the both sides of the midbody, which can be readily observed as tubulin fibers emanating from a dark area of the midbody. The microtubule bundles become thinner and finally a distinct abscission site appears usually at one side of the midbody (D'Avino et al., 2015).
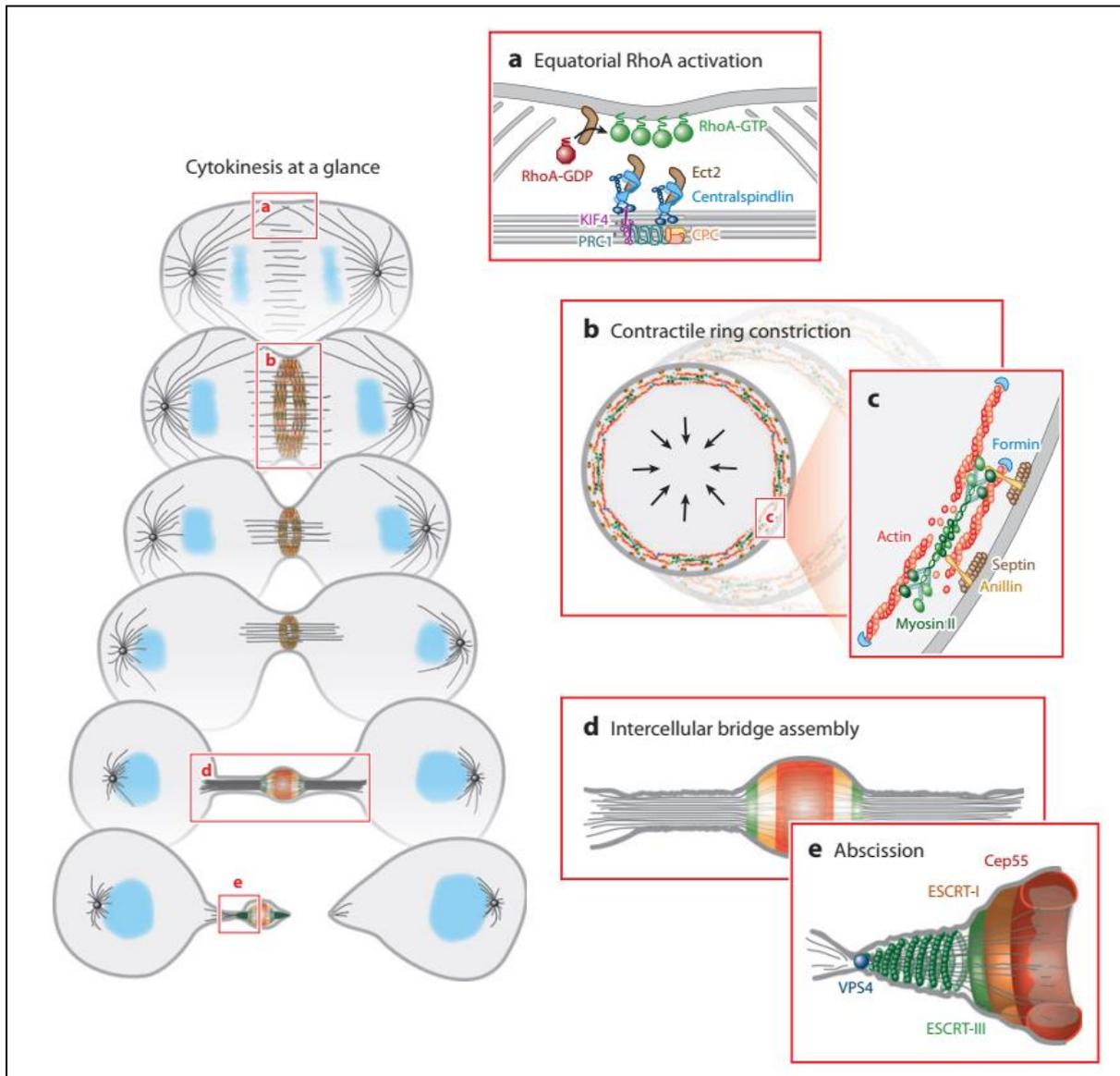
Figure 1.4.2. Events during cytokinesis: a) Cytokinesis begins with signaling between anaphase spindle and cortex to generate an equatorial zone of active RhoA (b) Active RhoA directs assembly of the contractile ring (c) The contractile ring is a filamentous network composed of formin-nucleated actin filaments, bipolar filaments assembled from the motor, myosin II, membrane-associated septin filaments, and the filament cross-linker, anillin. (d) As the contractile ring constricts, the spindle midzone matures to form the midbody, which organizes the intercellular bridge. (e) During abscission, ESCRT-III catalyzes membrane scission on either side of the midbody to generate two daughter cells. (Reprinted from Green et al., 2012)

At the end of cytokinesis the mechanism which mediates membrane fission includes the components of the ESCRT complex (endosomal sorting complex required for transport). The ESCRT proteins localize to the midbody, along with the protein Cep55 at a late stage of cytokinesis (Morita et al., 2007; D'Avino et al., 2015). The crucial events of cytokinesis are illustrated in Figure 1.4.2.

2. Research Objectives

The aims of this research were:

-to determine if knockdown of either KIF20B or RhoD affect the expression of the other protein, because of their postulated interaction

-to determine where in the cell this interaction takes place and why it would be important for cell processes or homeostasis

-to find other possible localization patterns of proteins RhoD and KIF20B during cell division

-to find if RhoD and KIF20B have a role in tumor cell sensitivity to anticancer drugs cisplatin, paclitaxel and vincristin, and if the cellular response is comparable between the two proteins.

3. Materials and Methods

This work was done in part at the Kyoto University, Kyoto, Japan, and at the Ruđer Bošković Institute, Zagreb, Croatia. Due to this reason, some reagents that were used in the experimental procedures might differ between the institutions, but precautions were used to ensure same results were obtained. That is why for some methodologies two sets of materials are presented.

3.1. Cell lines

In this work the following cell lines obtained from the ATCC (American Type Culture Collection) repository were used: HeLa (cervical adenocarcinoma; ATCC CCL-2), CaCO-2 (colorectal adenocarcinoma; ATCC HTB-37), HCT-116 (colorectal carcinoma; ATCC CCL-247), MDA-MB-231 (mammary gland/breast adenocarcinoma; ATCC HTB-26), MDA-MB-468 (mammary gland/breast adenocarcinoma; ATCC HTB-132) and MCF-7 (mammary gland/breast adenocarcinoma; ATCC HTB-22). The cisplatin resistant HeLa subline, HeLa CK, was derived from HeLa cells by exposing them to increasing concentrations of cisplatin during the course of 24 hours. The starting concentration of cisplatin used was 0,3 μM and the final 2,4 μM (Osmak and Eljuga, 1993). All cell lines were grown as a monolayer culture in 10 cm Petri dishes or T-25/T-75 flasks in Dulbeccos's Modified Eagle's Medium (DMEM, D5976, Sigma Aldrich, USA) supplemented with 0,01% w/v penicillin/streptomycin, pH 7 and 10% Fetal Bovine Serum (20% FBS for CaCO-2 cells) (GIBCO, UK) – DMEM FBS, in humid atmosphere at 37°C and in the presence of 5% CO_2. For CaCO-2 and MCF-7 cells DMEM was additionally supplemented with non essential amino acids (1X NEAA, GIBCO, UK). The 0,25% trypsin solution was used for detaching cells from culture dishes during cell passaging.

3.2. Chemicals and reagents

Chemicals and reagents used in experimental procedures are given in Table 3.2.1.

Table 3.2.1. Used chemicals and reagents

	Chemical or Reagent	Manufacturer
Cell culture	DMEM (Dulbecco's Modified Eagle's Medium), D5976	Sigma Aldrich, Germany
	Trypsin from porcine pancreas	Sigma Aldrich, Germany
	FBS (Fetal Bovine Serum)	GIBCO, UK
	10x NEAA (Non Essential Amino Acids)	GIBCO, UK
	Penicillin/Streptomycin	GIBCO, UK
Transient transfection	OptiMem Reduced Serum Media	GIBCO/ThermoFisher Scientific, USA
	Lipofectamine RNAiMAX Transfection Reagent	Invitrogen/ThermoFisher Scientific, USA
	Lipofectamine LTX Transfection Reagent	Invitrogen/ThermoFisher Scientific, USA
	Lipofectamine 2000 Transfection Reagent	Invitrogen/ThermoFisher Scientific, USA
RNA isolation	TriZol Reagent	Ambion/ThermoFisher Scientific, USA
	Chloroform	Kemika, Croatia; Nacalai Tesque, Japan
	Ultra Pure phenol-chloroform-isoamyl alcohol solution (25:24:1, v/v)	ThermoFisher Scientific, USA
	Isopropanol	Sigma Aldrich, Germany
	Ethanol	Kemika, Croatia; Nacalai Tesque, Japan
	High Pure RNA isolation kit	Roche, Switzerland
Reverse transcription, qPCR	Takara PrimeScript Perfect Real Time RNA transcription kit (PrimeScript RT kit and SYBR Ex Taq Premix for qPCR)	Takara, Japan
Reverse transcription	High Capacity cDNA Reverse Transcription Kits	Applied Biosystems, USA

	Chemical or Reagent	Manufacturer
qPCR	Power SYBR Green PCR Master Mix and Power SYBR Green RT-PCR Reagents Kit	Applied Biosystems, USA
Western blot	Acrylamide	Serva, Germany
	Bisacrylamide	Serva, Germany
	Ammonium persulfate (APS)	Serva, Germany
	TEMED (Tetramethyethylenediamine)	Sigma Aldrich, Germany
	SDS (Sodium Dodecyl Sulfate)	Serva, Germany
	Powdered milk	Roth, Germany; Nacalai Tesque, Japan
	Amersham Protran Premium 0,2 μm Nitrocellulose Membrane	Amersham/GE Healthcare, Germany/USA
	Western Lightning Plus-ECL	PerkinElmer Life Science, USA
	Medical X-ray developer	G138I, Agfa, Belgium
	Kodak Readymatic Fixer	Kodak, USA
	Amersham Hyperfilm ECL	Amersham/GE Healthcare, Germany/USA
Western blot, IF	Bovine Serum Albumine (BSA)	Sigma Aldrich, Germany
	Tween 20	Sigma Aldrich, Germany
Immunofluorescence	Paraformaldehyde	Sigma Aldrich, Germany
	PIPES (1,4-Piperazinediethanesulfonic acid)	Sigma Aldrich, Germany
	Triton X-100	Sigma Aldrich, Germany
	EGTA (ethylene glycol tetraacetic acid)	Sigma Aldrich, Germany
	$MgCl_2$	Kemika, Croatia/Nacalai Tesque, Japan
	Formaldehyde	Gram Mol, Croatia
	Hoechst 33342	Sigma Aldrich, Germany
	TO-PRO-3 iodide	Invitrogen, USA
	ProLong DAPI Gold mounting medium	ThermoFisher Scientific, USA
	DAKO Fluorescent mounting medium	DAKO, Denmark
	Alexa Fluor 594 phalloidin A12381	Invitrogen/ThermoFisher Scientific, USA

	Chemical or Reagent	Manufacturer
MTT assay	Cisplatin/*cis*-diamminedichloridoplatinum (CDDP)	Sigma Aldrich, Germany
	Paclitaxel	Sigma Aldrich, Germany
	Vincristine	Oncovin, Eli Lily, Indianapolis, USA
	MTT (3-(4,5-dimethylthiazol-2-yl)-2,5-diphenyltetrazolium bromide)	Sigma Aldrich, Germany
	DMSO (dimethyl sulfoxide)	Gram Mol, Croatia
Cell synch.	Thymidine	Sigma Aldrich, Germany
Flow cytometry	Propidium iodide	Sigma Aldrich, Germany
	RNAse	Sigma Aldrich, Germany
	IsoFlow Sheath Fluid	Beckman Coulter, USA
Agarose gel electrophoresis	Agarose	Sigma Aldrich, Germany
	Acridine orange	Serva, Germany
	Ethidium bromide	Sigma Aldrich, Germany
Misc.	Ethylenediamine tetraacetic acid (EDTA)	Kemika, Croatia
	Tris base	Sigma Aldrich, Germany
	Tris HCl	Serva, Germany

Standard chemicals, like the ones for preparation of phosphate buffer saline (PBS) were purchased from Nacalai Tesque (Japan) or Kemika (Croatia) and Gram Mol (Croatia).

All of the listed chemicals were dissolved and stored per manufacturer's instructions.

3.3. Buffers and solutions

The recipes for buffers and solutions used in this research are given in Table 3.3.1.

Table 3.3.1. Used buffers and solutions

Buffer/Solution	Constituents
PBS	137 mM NaCl, 2,7 nM KCl, 1,5 mM KH_2PO_4, 8 mM Na_2HPO_4
PBS with Calcium and Magnesium	137 mM NaCl, 27 mM KCl, 4,3 mM Na_2HPO_4 x $2H_2O$, 1,4 mM KH_2PO_4, 3 mM $CaCl_2$ x $2H_2O$ 2,4 mM $MgCl_2$ x $6H_2O$, pH 7,2
6x Laemmli Buffer	2% SDS, 0,06% bromophenol blue, 50% glycerol, 60 mM Tris-HCl, pH 7,5
Stacking gel for western blot	5% mixture of acrylamyd/bisacrylamyd (30%), 0,125 M Tris HCl pH 6,8, 0,05% APS, 0,0625% TEMED
Separating gel for western blot	8-15% mixture of acrylamyd/bisacrylamyd (30%), 0,375M Tris HCl pH 8,8, 0,035% APS, 0,5% TEMED
SDS running buffer	0,025 M Tris, pH 8,3, 0,192 M glycine, 0,1% SDS
Towbin/Transfer buffer	25 mM Tris, 192 mM glycine, 20% methanol, pH 8,3
TBS-T	20 mM Tris, 137 mM NaCl, 3,8 mM HCl, 0,1% Tween 20
1x PTEM buffer	20 mM PIPES-KOH, 0,2 % Triton X-100, 10 mM EGTA, 2 mM $MgCl_2$, pH 6,8
1x PTEMF buffer	1x PTEM buffer with added formaldehyde, 4% w/v

3.4. Antibodies

The antibodies used in the experimental procedures are described in Table 3.4.1.

Table 3.4.1. Information on used antibodies

Antibody information	Manufacturer
polyclonal rabbit antibody against KIF20B ab122165	Abcam, UK
polyclonal rabbit antibody against KIF20A ab70791	Abcam, UK
polyclonal rabbit antibody against RhoD ARP42413_P050	Aviva Systems Biology, USA
monoclonal mouse antibody against RhoD 2F7 ab119301	Abcam, UK
purified mouse monoclonal antibody against Rabaptin 5 610676	BD Biosciences, USA
purified mouse monoclonal antibody against EEA1 610456	BD Biosciences, USA
monoclonal mouse antibody against Tubulin α, clone DM1A CP-06	Merck/Millipore, Germany/US
secondary sheep antibody against mouse conjugated to horseradish peroxidase NA931	Amersham, GE Healthcare, USA

Antibody information	Manufacturer
secondary bovine antibody against rabbit conjugated to horseradish peroxidase sc-2370	Santa Cruz Biotechnologies, USA
fluorescent donkey secondary antibody against rabbit Alexa Fluor 488, A21206	Invitrogen/Thermo Fisher Scientific, USA
fluorescent goat secondary antibody against mouse Alexa Fluor 546, A11030	Invitrogen/Thermo Fisher Scientific, USA
fluorescent donkey secondary antibody against mouse Alexa Fluor 594, A21203	Invitrogen/Thermo Fisher Scientific, USA
fluorescent donkey secondary antibody against mouse Alexa Fluor 488	Invitrogen/Thermo Fisher Scientific, USA
fluorescent donkey secondary antibody against mouse Alexa Fluor 647, A31571	Invitrogen/Thermo Fisher Scientific, USA
fluorescent donkey secondary antibody against rabbit Alexa Fluor 647, 4414S	Cell Signaling Technology, USA
fluorescent donkey secondary antibody against rabbit Alexa Fluor 555, A31572	Invitrogen/Thermo Fisher Scientific, USA

3.5. Transfection with plasmid constructs and small interfering siRNAs

3.5.1. Transient transfection of EGFP-RhoD plasmid constructs

The RhoD antibody of acceptable quality for immunofluorescence is not yet commercially available. Therefore, to analyse the localization of RhoD in cells, plasmids expressing exogenous RhoD and mutants RhoD^{Q75L} and RhoD^{G26V} fused with EGFP were transfected by Lipofectamine 2000 or LTX reagent (ThermoFisher Scientific, USA). The EGFP RhoD^{Q75L} and EGFP RhoD^{G26V} plasmids are RhoD mutants with constitutively active GTPase activity. The pEGFP-RhoD construct plasmids were a kind gift from Prof. Toshimasa Ishizaki. The plasmid pEGFP-C1 was used as the plasmid backbone for the RhoD constructs. cDNA of RhoD was isolated by PCR using cDNA of HeLa cells as a template. Then, RhoD sDNA was inserted into pEGFP-C1 using BamHI and XhoI restriction endonucluase.

For evaluating EGFP RhoD localization in non-silenced HeLa and CaCO-2 cells, a classic transfection protocol with Lipofectamine LTX reagent was used, following the manufacturer's instructions, as demonstrated in Table 3.5.1. Cells were plated in 6 well dishes with pre-sterilized

glass coverslips (18x18 mm, Matsunami, Japan) in 2 mL DMEM medium with addition of appropriate supplements and antibiotics and incubated for 24 hours, after which medium was

replaced with 1,5 mL medium without antibiotics. To each well a mixture consisting of OptiMem, Lipofectamine Plus Reagent, Lipofectamine LTX and plasmid DNA, was added. 48 hours after transfection medium was removed and cells were processed further for immunofluorescence.

Table 3.5.1. Conditions for EGFP-RhoD plasmid transfection in HeLa and CaCO-2 cells

	Cell number	DMEM without AB	OptiMem	Lipofectamine Plus	LTX reagent	Plasmid DNA
Amount	2×10^5	1,5 mL	500 µL	3 µL	2,5 µL	1 µg

3.5.2. Gene knockdown by small interfering RNA (siRNA)

For knockdown experiments the following commercially available small interfering RNAs (Stealth Select siRNA), produced by Invitrogen, USA were used:

Table 3.5.2. Small interfering siRNA sequences used

Stealth Select siRNA	Sequence
Negative Universal control, low GC #2	Thermo Fisher Scientific, USA
KIF20B/HSS114314	5'-CCACAUAGAUCCAGAGAAUACUUAA-3'
KIF20B/HSS114315	5'-GGGAGUACCUCGACCAUCUUAUGUU-3'
KIF20B/HSS190436	5'-GAGCAUGCAAAGAUCUAAAUGUUAA-3'
RHOD/HSS179133	5'-GGUGGUACCCAGAAGUGAAUCAUUU-3'
RHOD/HSS121171	5'-UCACCAGCCCGAACAGCUUUGACAA-3'
RHOD/HSS121172	5'-GCGCAAGGACAAAUCACUGGUGAAC-3'

Gene knockdown by siRNA uses the already present cellular machinery to degrade the target mRNA and henceforth stop translation into proteins.

In the experimental procedures forward or reverse transfection protocols were used, depending on experiment purpose. Cell number was adjusted accordingly for each experiment.

Cells were seeded in either 6-well or 12-well dishes. Twenty-four hours after seeding, when cell density reached 30-50% confluency, cells were transfected with specific or control siRNA

according to Table 3.5.3. OptiMem was added to the wells to make 1 or 10 nM final concentration of siRNA. Cells were incubated for 48 to 72 hours, before starting with the desired experiment. The efficiency of transfection was verified by either western blot or RT-qPCR at 48 or 72 hours post transfection.

Table 3.5.3. Conditions for transfection of gene-specific siRNAs in knockdown experiments

Vessel	DMEM-FBS (no AB)	Lipofectamine RNAiMax	OptiMem
6 well	1,5 mL	3 to 5 µL	500 µL
12 well	0,75 mL	1,5 µL	250 µL

3.5.3. Transfection of KIF20B-knocked down cells with EGFP RhoD plasmid constructs

To evaluate if KIF20B knockdown affects localization patterns of RhoD, cells were either silenced first with KIF20B siRNA and then transfected with EGFP-RhoD plasmids on the following day, or cotransfected with both KIF20B siRNA and plasmid DNA at the same time. In the first case, appropriate amount of cells ($2x10^5$ for HeLa and $3x10^5$ for CaCO-2 cells) was plated in 6 well format, on sterilized 18x18 or 10 mm coverslips in a reverse transfection protocol. First, the mixture containing 500 µL OptiMem, siRNA and the 5 µL Lipofectamine RNAiMAX reagent was added to the well and incubated for 20 min at room temperature. Then cells diluted in 1,5 mL medium without antibiotics were plated into the wells. The final concentration of siRNA was 10 nM. The next day cell medium was replaced with fresh medium with antibiotics and incubated for 5 hours. The medium was replaced again, just before cells were transfected with a mixture of plasmid DNA (1 µg), 3 µL Lipofectamine Plus and 2,5 µL LTX reagent in 500 µL OptiMem. After 24 hours of transfection with plasmid DNA, and 48 hours after transfection with siRNA the desired experiment was carried out.

In case of cotransfection, a reverse transfection protocol was followed according to the manufacturer's protocol. Sterilized 10 mm coverslips were inserted into 24 well plate wells. The mixtures of 50 µL OptiMem with Lipofectamine 2000, and 50 µL OptiMem with plasmid DNA and siRNA (final concentration 20 nM, higher than usually used 10 nM, because plasmid DNA may abrogate knockdown) were prepared separately. The two solutions were mixed and incubated for 30 min at room temperature. The used reagent amounts are given in Table 3.5.4.

Volume cells plated	Total transfection volume /well	Volume siRNA stock (20 µM) solution/well	Final concentration siRNA in well	Plasmid DNA amount/well	Lipofectamine 2000 volume/well
400 µL	100 µL	0,5 µL	20 nM	250 ng	1 µL

Cells were plated on the wells with transfection mixture, in medium without antibiotics. 48 hours after cotransfection, cells were used for further experiments. Cell number amounts for this protocol are given in Table 3.5.5.

Table 3.5.5. Appropriate cell numbers for cotransfection protocol

Cell line	Required cell number/well in 24 well dish
HeLa/HeLa CK	5×10^4
HCT-116	$1,25 \times 10^5$
MDA-MB-231	$1,5 \times 10^5$
MDA-MB-468	$1,1 \times 10^5$
MCF-7	$1,5 \times 10^5$

3.6. Quantitative PCR primer design and verification

For the purpose of determining expression levels of either KIF20B or RhoD in selected cell lines by RT-qPCR, custom primer pairs were designed specifically for KIF20B or RhoD and presented in Table 3.6.1, along with the reference GAPDH primers.

Table 3.6.1. Custom designed primer pairs for qPCR reaction for KIF20B and RhoD

Lane	Primer set	Product size(bp)	Fw (5'-3' direction)	Rv (5'-3' direction)
1	KIF20B H B	255	gcgaagtttgcagaatggaatcta	acacagccctcagactcaagttct
2	KIF20B H G	209	cttcaagatgagttacaggagtctgaacag	actatctttctctgtcagctgggct
3	KIF20B H R	232	aggtatctgtaatgcgtgatgagga	ttctagtgtcattcgcatgtcttca
4	RhoD H B	288	atctttaaccggtggtacccagaa	taatccgccgccagaagtt
5	RhoD H R	221	acacagcagggcaagatgactatg	tcggagcttgttcaccagtgat
6	GAPDH	nd	agaacatcatccctgcctctactg	tgtcgctgttgaagtcagaggaga

Primer specificity was verified in a conventional PCR reaction, by subjecting the reaction products to a 2% agarose gel electrophoresis and inspecting the obtained fragment length. The reaction was performed according to the following protocol described in Table 3.6.2.:

Table 3.6.2. Reaction setup for conventional PCR of cDNA after reverse transcription

Reagent	Amount
ExTaq enzyme	0,2 µL
ExTaq buffer	4 µL
dNTPs	6,4 µL
Primer 1 (10 µM)	0,2 µL
Primer 2 (10 µM)	0,2 µL
mqH₂O	27 µL
Template (cDNA)	2 µL
Total reaction volume per sample	40 µL

Upon reaction setup, the subsequent PCR program was used:

Table 3.6.3. Thermal cycler protocol used for validating PCR fragment sizes

Temperature (°C)	Duration (min)	Number of repeats (cycles)
98	1	1
98	0,5	
60	0,5	35
72	0,5	

3.7. Determining mRNA expression levels by RT-qPCR

3.7.1. RNA isolation and reverse transcription

Forty-eight hours upon knockdown with RhoD or KIF20B gene-specific siRNAs, cells were collected for RNA isolation either by TriZol reagent (Ambion, ThermoFisher Scientific, USA) or by the High Pure RNA Isolation kit (Roche, Switzerland), following the manufacturer's

instructions. The TriZol reagent was used when the cell number for isolation of mRNA was higher than 1×10^6 cells, and the commercially available kit (High Pure RNA isolation kit, Roche, Switzerland) when the cell number was lower than this limit.

In the TriZol method, medium was removed from wells and cells were washed briefly with ice cold PBS and 500 or 1000 µL of TriZol reagent was added per well of 12-well or 6-well dish, respectively). All the subsequent steps were carried out as per manufacturer's protocol.

As for the High Pure RNA isolation kit (Roche, Switzerland), the cells were trypsinized, resuspended in medium and centrifuged for 8 minutes at 1000 x g after which the supernatant containing medium was removed and the cells were subjected to two more rounds of PBS washing and centrifugation. In the final step before proceeding to RNA isolation protocol by kit, the cells were resuspended in 200 µL of PBS. The total RNA obtained after isolation with either method was diluted in 20 – 50 µL of RNAse free diH$_2$O. RNA concentration and quality was determined spectrophotometrically (the absorbance at 260 nm, ratio of absorbance at 260 and 280 nm and at 260 and 280 nm) by a nano UV-spectrophotometer (NanoPhotometer N50, Implen, Germany and DU730 spectrophotometer, Beckman Coulter, USA), from 1 µL of sample. The A$_{260/280}$ ratio of 1,8-2,0 and A$_{260/230}$ ratio of 2,0-2,2, generally accepted as pure for RNA, were considered appropriate. The isolated RNA was stored at -80°C until further use.

The synthesis of cDNA was performed by reverse transcription of the obtained RNA using the commercially available kits PrimeScript RT reagent kit (Takara, Japan) or High capacity cDNA reverse transcription kit (ThermoFisher Scientific, USA), according to the manufacturer's instructions. 500 ng of RNA template was used for reverse transcription in a 20 µL reaction volume. 1 µL of the reverse transcription reaction product was used in the subsequent qPCR reaction.

3.7.2 qPCR using SYBR Green

The qPCR reaction using the SYBR Green assay is a quantitative system, where products of the reverse transcription reaction (cDNA) are detected as the PCR reaction progresses through each cycle in real time. Fluorescence is emitted each time that the SYBR green dye incorporates into DNA during the polymerization process. This fluorescence is then detected in the thermal cycler machine and increases as the number of DNA copies also increases. This is visualized as a sigmoid type curve which indicates the progress of reaction in each sample.

Table 3.7.1. Reaction setup for real time PCR

ExTaq SYBR Premix		Power SYBR green PCR Master Mix	
Reagent	**Amount**	**Reagent**	**Amount**
SYBR Premix ExTaq (2X)	10 µL	Power SYBR green PCR Master Mix (2X)	7,5 µL
PCR Forward primer (10 µM)	0,4 µL	PCR Forward primer (10 µM)	0,3 µL
PCR Reverse primer (10 µM)	0,4 µL	PCR Reverse primer (10 µM)	0,3 µL
dH$_2$O	8,2 µL	dH$_2$O	5,4 µL
Template cDNA	1 µL	Template cDNA	1,5 µL
Total reaction volume	20 µL	Total reaction volume	15 µL

The conditions for the qPCR reaction were optimized by performing the reaction with cDNA of different dilutions. GAPDH was used as reference gene for quantification.

qPCR reactions were prepared separately for each gene (RhoD and/or KIF20B and GAPDH) according to the manufacturer of the SYBR Green premix used. The volumes of each reaction component are given in Table 3.7.1. for each of the two qPCR premixes that were used in this research: Takara ExTaq SYBR Premix (Takara, Japan) and the Power SYBR green PCR Master Mix (Applied Biosystems, USA).

Each sample was run at least in duplicate on the microtiter plate, on a Bio-Rad CFX96 Thermal cycler machine (Bio-Rad Laboratories, USA), by using the thermal protocol suggested by the manufacturer of each SYBR Green real time PCR premix (Table 3.7.2.).

The data was analyzed using the Bio-Rad CFX96 Manager Software, version 3.1 (Bio-Rad Laboratories, USA).

Table 3.7.2. Thermal cycler Bio-Rad CFX96 protocols used

ExTaq SYBR			Power SYBR green		
Temperature (°C)	**Duration**	**Number of cycles**	**Temperature (°C)**	**Duration**	**Number of cycles**
95	30 sec	1	95	10 min	1
95	10 sec	40	95	15 sec	40
60	20 sec	40	60	1 min	40

3.8. Determination of protein expression using SDS-PAGE and Western blot

3.8.1. Preparation of whole cell lysates by hot Laemmli buffer method

The whole cell lysates were prepared from the samples 48 or 72 hours after siRNA transfection. Appropriate number of cells was seeded beforehand in a 6- or a 12-well dish, as described in the section 3.6. of this chapter. Medium was removed from wells and cells were washed 2 times with ice cold PBS. All the subsequent steps were carried out on ice. PBS was then aspirated from the wells and 200 µL/6 well or 120 µL/12 well of 1X Laemmli Buffer with reducing agent 2-mercaptoethanol, preheated at 96°C, was added to each well. The wells were scraped with the policeman scraper and the cell lysates were collected into 1,5 mL eppendorf tubes. The samples obtained by this manner were sonicated three times at 30% amplitude, with 10 pulses each with the Ultrasonic Processor, Cole-Parmer, USA. After this samples were stored at -20°C until further use.

3.8.2. Protein separation by SDS-PAGE

Sodium Dodecyl Sulfate-Polyacrylamide Gel Electrophoresis (SDS-PAGE) is a method of separating proteins in a polyacrylamide gel system based on the differences in protein molecular weight (Laemmli, 1970). This is enabled by the treatment of proteins within the sample with chemical denaturant SDS (Sodium Dodecyl Sulphate, a mild anionic detergent which can bind proteins electrostatically) which turn proteins into unstructured molecules whose mobility depends only on their length. In this procedure two gels were used, the stacking gel and the separating gel. The stacking gel always has the same composition, while the percentage of acrylamyde/bisacrylamide in the separating gel can vary depending on the molecular weight of the proteins to be analyzed. Lower percentage of the gel like 8% up to 10% has a thinner mesh of pores which allows proteins of higher molecular weight to pass through. On the other hand, higher acrylamyde/bisacrylamyde percentages of the gel, like 12 to 15%, have smaller pores and only proteins of lower molecular weight can pass through freely, while higher molecular weight proteins are stalled at the beginning of the gel. The gels were cast on the Bio-Rad casting system (Mini Protean 3 multi-caster, Bio-Rad Laboratories, USA) and stored in damp tissues at +4°C until use on the following day.

For determining the basal levels of KIF20B protein in tested samples, gels with 10% of acrylamyde/bisacrylamyde were used. Samples that were previously sonicated were preheated before loading, 5 minutes at 96°C and centrifuged briefly to spin down the droplets

on the tube walls. Since there was no substantial difference in silenced cells growth compared to controls after 48 or 72 hours post transfection, equal volumes of proteins were loaded in the wells of the gel. Usually 20 µL of protein lysate was used per well for each sample. Samples were loaded sequentially onto the gel, with appropriate negative and positive controls and protein molecular weight marker (Bio-Rad Precision Plus Protein Dual Color Standard, Bio-Rad Laboratories, USA).

Gel electrophoresis was run in SDS buffer, for approximately 2 hours, at a constant voltage of 100 V.

3.8.3. Western blotting

After SDS-PAGE the separated proteins were transferred to a nitrocellulose membrane with 0,2 µm pores (Amersham Protran Premium 0,2 μm NC, GE Healthcare, Germany) in Towbin buffer with the Bio-Rad Mini PROTEAN Tetra system (Bio-Rad Laboratories, USA) wet transfer system. The transfer was conducted for 90 minutes at a constant amperage of 400 mA.

The membrane was blocked with 5% skimmed milk (Powdered milk, Roth, Germany) in the TBS-T buffer. Afterwards, membrane was briefly washed in TBS-T buffer and then incubated with the appropriate primary antibody diluted in 2,5% skimmed milk in TBS-T buffer, according to optimized conditions of each antibody, with shaking. After necessary incubation time, the primary antibody was removed from the membrane and membrane was washed with TBS-T (2x briefly, 1x10 min, 3x5 min). Appropriate secondary antibody was then added to the membrane. Both of the secondary antibodies, listed in the Antibodies section of this chapter, were diluted (1:5000) in 2,5% skimmed milk in TBS-T and incubated for 1 hour at room temperature with shaking. The membrane was then washed with TBS-T buffer (2x briefly, 1x10 min, 3x5 min) and the signal of the desired protein was detected by a chemiluminescence reagent (Western Lightning Plus-ECL, PerkinElmer Life Science, USA). According to manufacturer's instructions the membrane was devoid of residual TBS-T buffer and it was incubated for 1 min with the combined reagents from the aforementioned chemiluminescence kit, wrapped in cellophane foil and put in a film developing cassette. In the dark room, at red light illumination, the photosensitive film (Amersham Hyperfilm ECL, GE Healthecare, USA) was placed on the membrane. After exposition time depending on the

optimized conditions for each tested antibody, the film was immersed in the developer solution (Medical X-ray developer, G138I, Agfa, Belgium), rinsed in water after

Table 3.8.3.1. Incubation time and temperature conditions for primary antibody incubation.

Antigen	Host	Dilution	Incubation time
α-tubulin (DM1A)	mouse	1:1000	3 h, RT
KIF20B	rabbit	1:500	ON, +4°C
EEA1	mouse	1:500	3 h, RT
RhoD (AVIVA)	rabbit	1:1000	2 h, RT

appearance of signal and fixed with the fixer solution (Kodak Readymatic Fixer, Kodak, USA). Finally the film was washed again with diH$_2$O and dried.

The effective dilutions and incubation time of each antibody used in western blot are given in Table 3.8.3.1.

3.9. Immunofluorescence and confocal microscopy

The cells were previously plated on glass coverslips in appropriate numbers and processed by siRNA mediated knockdown and or plasmid DNA transfection, after which they were incubated 48 to 72 hours prior to fixation. In this study, two similar fixation protocols were used for immunofluorescence, 4% PFA and PTEMF fixation. The 4% PFA fixation is a classic protocol used for most applications. The PTEMF protocols encompasses both fixation and permeabilization at the same time, which is more suitable for analysis of kinesin proteins localization.

In the classic PFA protocol, medium was removed from cells and the cells were washed briefly with PBS with Ca and Mg. The coverslips were then fixed with 4% PFA for 15 min at 37°C. After this, the slides were extracted from wells and put in a humid dish, on a glass plate covered with parafilm. The coverslips were washed three times with PBS and then permeabilized with 0,2% Triton X-100 in TBS, for 5 min at 4°C. After this, coverslips were blocked with 3% BSA in PBS, for 30 min at room temperature. The primary antibodies diluted in PBS at appropriate concentrations were added to coverslips and incubated for 2-4 hours at room temperature. Then the slides were washed 3 times with PBS and incubated for 30 min

at room temperature, in the dark, with suitable fluorescent labelled secondary antibodies (diluted in PBS at 1:1000) or phalloidin (diluted in PBS at 1:200). The slides were washed 3 times with PBS and finally incorporated on microscopy slides with fluorescent mounting medium containing DAPI. The slides were dried and sealed with rubber cement and stored at 4°C before confocal microscopy, which was conducted on a Leica SP5 confocal imaging system, using 630x magnification under immersion. The micrographs were taken at the resolution of 512x512 pixels, or 1024x1024 pixels.

In the PTEMF fixation protocol, fixation and permeabilization are conducted at the same time.

Table 3.9.1. Antibody dilutions and incubation time in immunofluorescence

Antigen	Host	Dilution	Incubation time
Alexa Fluor 594 Phalloidin (F-actin)	*Ammanita phalloides*	1:200	30 min, RT, dark
KIF20B, KIF20A	rabbit	1:500	ON, +4°C
α-tubulin	mouse	1:1000	2h, RT
EEA1	mouse	1:500	2h, RT
Rabaptin 5	mouse	1:500	2h, RT
RhoD (Aviva)	rabbit	1:1000	2h, RT
RhoD (2F7, ab)	mouse	1:500	2h, RT
Alexa Fluor 594 anti mouse	donkey	1:200	30 min, RT, dark
Alexa Fluor 546 anti mouse	goat	1:1000	30 min, RT, dark
Alexa Fluor 488 anti mouse	donkey	1:200	30 min, RT, dark
Alexa Fluor 488 anti rabbit	donkey	1:200	30 min, RT, dark
Alexa Fluor 647 anti mouse	donkey	1:200	30 min, RT, dark
Alexa Fluor 647 anti rabbit	goat	1:1000	30 min, RT, dark
Alexa Fluor 555 anti rabbit	donkey	1:200	30 min, RT, dark

In the experimental procedure the medium was removed from wells and they were washed briefly with PBS with Ca and Mg. After this they were washed once with 1x PTEM buffer and then fixed and permeabilized with 1x PTEMF buffer. The fixation lasted for 15 min at 37°C after which the cells were immediately blocked with 3% BSA in PBS, for 30 min at room temperature. The PTEM buffer was prepared in 2x concentration and stored at 4°C until application in immunofluorescence. Each time before immunofluorescence, it was diluted to 1x concentration and fresh formaldehyde in liquid form was added into the solution to make up 4% w/v. All of the other steps of immunofluorescence were essentially the same to the standard 4% PFA protocol.

In all steps, 60 or 200 μL of each solution was added to the coverslides, depending on its surface.

Working antibody dilutions for immunofluorescence and incubation times are given in Table 3.9.1.

3.10. HeLa cell synchronization in G1/S phase by Double Thymidine Block

To evaluate if there was a delay in some of the mitotic events in HeLa cells after RhoD or KIF20B knockdown, cell synchronization was performed. Excess thymidine added to the culture medium inhibits DNA synthesis and arrests cells in late G1 or early S phase after second block, after which they synchronously progress through G2 and M phases of the cell cycle. For cell synchronization a 10 cm culture dish was prepared, containing 10% confluency cells. The cells were subjected to the first Thymidine block at 19:00 hours of the first day of experiment. The cell medium was simply replaced with Thy containing medium (5% FBS, 10% antibiotic Penicillin Streptomycin and 10 mM Thy, in DMEM). 14 hours after first Thy block, the cells were transfected with gene specific and control siRNA in 6-well plates by using the reverse transfection protocol. After 8 hours the medium was replaced once more with Thy medium for the second Thy block. After 14 hours of this last block, the cells were released by replacing the medium with the standard DMEM with 10% FBS and antibiotics. Approximately 10 hours after second release from Thy, cells were checked under inverted microscope to confirm the majority of the cells has entered division, and then they were collected at 11 and 12,5 hours after release. The cells were fixed and stained for α-tubulin as described in the

previous section. The stained cells were then counted for each phase of cell division under confocal microscope.

3.11. Cell cycle analysis by flow cytometry

HeLa cells were plated and silenced in 6 cm culture dishes following the described reverse transfection protocol. Seventy-two hours after transfection, the medium was removed from 6 cm dishes, and placed in 15 mL Falcon tubes to collect loosely attached cells undergoing mitosis or apoptosis. The dishes were washed once with 4 mL warm PBS and the wash was added to the Falcon tube. The remaining cells were trypsinized for 5 min at 37°C and resuspended in 3,5 mL fresh DMEM and then transferred to the 15 mL Falcon tube. This was centrifuged for 2 min, at 1000 rpm, at room temperature after which supernatant was removed. 6 mL of ice cold PBS was added to each Falcon tube which was then briefly vortexed and centrifuged for 2 min at 1000 rpm, RT. The supernatant was removed and 3 mL of ice cold PBS was added to each Falcon tube which was then briefly vortexed and resuspended. After this, 7 mL of ice cold 96% ethanol was added to each tube drop by drop and vortexed to ensure that the cells do not clump together. The tubes were rotated for 1 hour at 4°C and then stored at -20°C overnight. The cells were then centrifuged for 5 min at 3000 rpm, at 4°C and supernatant was discarded. The pellet was resuspended in 5 mL ice cold PBS and centrifuged for 5 min at 3000 rpm, at +4°C. The supernatant was discarded and 1 mL of cold PBS was added to each tube except for control sample. To the control sample 2 mL of PBS was added and this was then divided into 2 separate tubes: stained and non-stained.

Cells were resuspended and transferred to 1,5 mL eppendorf tubes. They were then centrifuged for 5 min at 3000 rpm, at 4°C. The supernatant was discarded and 1 mL of a solution containing 100 µg/mL of propidium iodided and RNAse in PBS was added to each eppendorf tube and resuspended. To the non-stained sample only 100 µg/mL of RNAse in PBS was added. This was then incubated for 30 min, at 37°C in the dark, with shaking. The samples were then transferred into polypropylene FACS tubes (Falcon, USA) through a 0,45 µm filter and the PI content and distribution throughout the cell cycle was evaluated by passing each sample on a flow cytometer (Beckton Dickinson, EPICS-FL-XL, USA). 20000 cells were analyzed per sample and graphs were obtained in the Beckton Dickinson EPICS-FL-XL Software. The results were presented as a histogram depicting propidium iodide fluorescence intensity against cell number.

3.12. MTT cell viability assay

To determine cell survival after exposure to different anticancer drugs, the standard MTT assay protocol was used with modifications to include cell knockdown. The MTT assay of determining cell viability is a colorimetric method based on the ability of cellular dehydrogenase enzymes to reduce the yellow tetrazolium dye MTT (3-(4,5-dimethylthiazol-2-yl)-2,5-diphenyltetrazolium bromide into its purple insoluble product, formazan (Mickisch et al., 1990).

Due to the different properties and origins of each used cell line, different numbers of cells were plated for MTT assay, in 96-well format. Number of cells plated for each cell line is listed in Table 3.12.1.

The cells were knocked down following the instructions from manufacturer of Lipofectamine RNAiMAX reagent which was used in all silencing experiments, as described previously. The forward transfection protocol was utilized. 24 hours after transfection, cells were trypsinized and resuspended in DMEM with FBS, counted using the Beckman Coulter counter and plated on 96 well plate in the appropriate density in 180 μL of DMEM per well. On the following day, 48 hours after transfection, cells in 96 well format were treated with 20 μL of anticancer drugs cisplatin, paclitaxel or vincristin added per well. Each compound was tested in a series of dilutions in quadriplicate. The cells were then incubated in the incubator at 37°C and 5% CO_2 for 72 hours.

Table 3.12.1. Cell numbers for each cell line used in MTT assay

Cell line	Cell number for MTT assay
HeLa	$2,5 \times 10^3$
HeLa CK	$2,5 \times 10^3$
CaCO-2	$9,5 \times 10^3$
HCT-116	$3,5 \times 10^3$
MDA-MB-231	1×10^4
MDA-MB-468	1×10^4
MCF-7	1×10^4

When this incubation was finished, 120 hours after transfection, the medium was removed from the wells and 20 μg of MTT dye in 40 μL of medium was added to each well. It is important to remove all residues of medium since lactate dehydrogenase is released from dead cells which have ruptured cell membranes, and it can also reduce MTT and contribute to the purple coloration. The cells with added MTT were incubated for 3 h at 37°C after which 170 μL of dimethyl sulfoxide (DMSO) was added per each well, to dissolve the purple formazan crystals. The 96 well plates were shaken for 15 to 20 minutes on a Vibromix 301EVT shaker (Tehtnica, Slovenia) at 500 rpm, to help dissolve the crystals. After this absorbance at 600 nm was measured on a StatFax 2100 spectrophotometric plate reader (Awareness Technology INC, USA). Measured absorbance is proportional to the number of viable cells and relative cell survival after treatment with drugs was calculated with respect to non treated (control) cells. Before calculating cell survival, absorbance of the ''blank'' sample well (background) was subtracted from all of the measured absorbances.

For easier following of this experimental procedure, which is also tied to other methods, all of the steps in consecutive order and knockdown duration are described in Table 3.12.2.

To check for knockdown efficiency, after collecting cells for seeding them in a 96 well plate on the third day of the experiment, the remainder of the cells was preserved and collected either for RNA isolation or protein extraction on the following day, 48 hours after knockdown. This specific time point is also the time point of treatment with drugs.

Table 3.12.2. Experimental procedure for MTT assay and related cell collecting

Day	Step	Knockdown duration
1	Plating cells for knockdown	-
2	Silencing (10 nM siRNA)	0 h
3	Plating for MTT assay in 96 well format	24 h
4	Treating with drugs / Isolation of RNA or proteins	48 h
5	Incubation	72 h
6	Incubation	96 h
7	MTT treatment and plate reading	120 h

3.13. Statistical analysis

The obtained results were statistically processed with one-way or two-way ANOVA with multiple comparsion and Bonferroni or Dunnett's post-hoc tests. The data are presented as mean values from representatives of at least 2 experiments +/- standard deviation. Statistical significance was calculated as $p<0,05$. The data were processed in Microsoft Excel or GraphPad Prism version 8.3.0 (GraphPad Software, 2020).

4. Results

4.1. Basal levels and causative relationship of RhoD and KIF20B in tumour cell lines

4.1.1. Basal levels of RhoD and KIF20B in tumour cell lines

To assess the basal levels of proteins RhoD and KIF20B in selected cell lines, and to subsequently analyse if there might be a causative relationship in their expressions after knockdown of each of them, first I analysed the expression of these proteins at transcriptional level using RT-qPCR. In all tested cell lines, relative RNA levels of RhoD and KIF20B were determined by comparing to levels of GAPDH in each sample (Figure 4.1.1.). The obtained results were compared to the relative relationships of expression shown in The Human Protein Atlas Database, version 18. In this database, the relationships of RhoD or KIF20B RNA levels are shown only for three out of seven tested cell lines: HeLa, CaCO-2 and MCF-7. Regarding HeLa and MCF-7, the relationships shown in Figure 4.1.1 correspond to the results in the database, while data for CaCO-2 is different for RhoD expression. Namely, in the database CaCO-2 shows lower RhoD expression as compared to HeLa and MCF-7 cell lines, while my results demonstrate similar levels to MCF-7 cell line. Interestingly, I have found that the cisplatin resistant cell line, HeLa CK (developed by Osmak and Eljuga, 1993), has approximately a double amount of RhoD mRNA when compared to its maternal cell line HeLa from which it was developed. In the colorectal carcinoma cell lines, CaCO-2 and HCT-116, there is a large difference in expression levels of RhoD mRNA, while for the three breast carcinoma cell lines (MCF-7, MDA-MB-231 and MDA-MB-468), these levels are comparable. On the other hand, the KIF20B mRNA levels are similar in HeLa, HeLa CK, CaCO-2, HCT-116 and MDA-MB-231 cell lines. They differ in MDA-MB-468 and MCF-7 cells, which express much lower level of KIF20B mRNA for this protein compared to other cell lines.

4.1.2. RhoD knockdown reduces KIF20B expression on the protein level in HeLa and HeLa CK cells

Since KIF20B was identified as an interacting partner of RhoD in a yeast two hybrid assay (Ishizaki et al., unpublished data), I analysed in HeLa cells whether knockdown of any of these proteins affects the expression of the other. Considering that the commercially available antibodies against RhoD yielded unsatisfactory results in all immunoassays
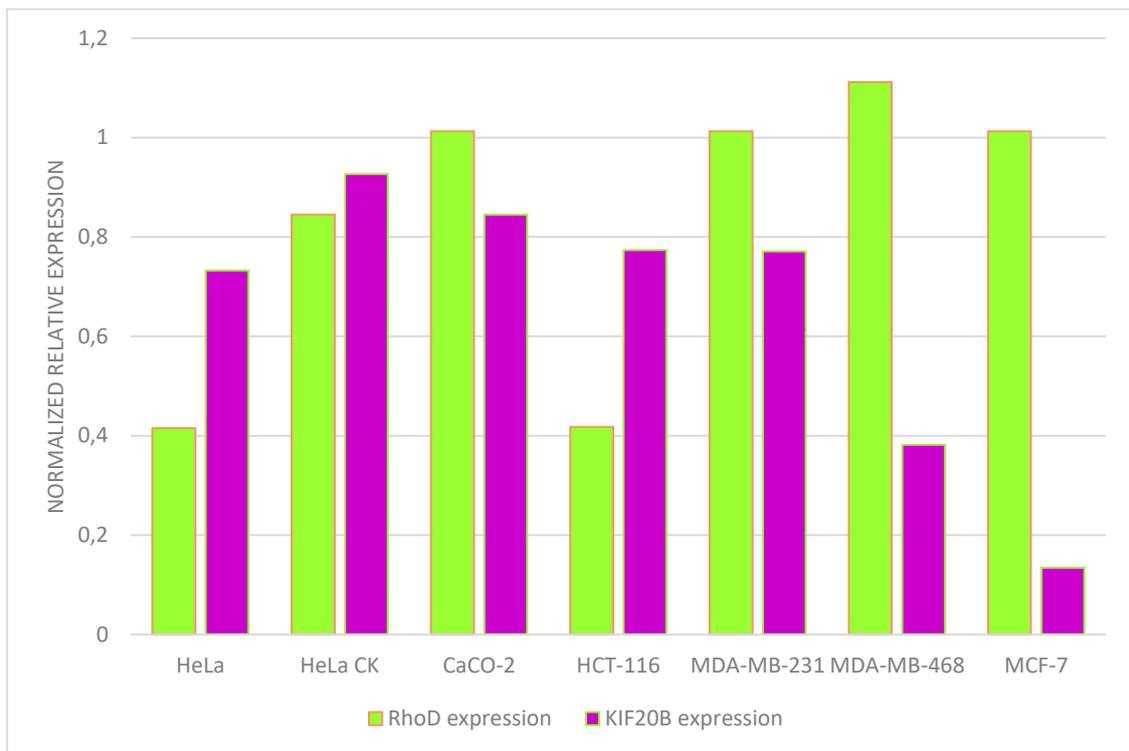
Figure 4.1.1. Expression levels of RhoD and KIF20B mRNA compared in all tested cell lines, relative to GAPDH mRNA expression. *The data was obtained from RT-qPCR experiments where GAPDH mRNA expression levels were measured based on relative fluorescence intensity of the reaction. The RhoD and KIF20B relative expression levels respectively, were obtained by subtracting the GAPDH levels. Finally, the GAPDH values for HeLa cells were used as means of comparison for other cell lines, and the resulting relationships between expressions of mRNA for both proteins across all cell lines are presented.*

performed, only RT-qPCR was used to assess RhoD expression levels. KIF20B was analysed at the mRNA level using RT-qPCR and at protein level using western blot.

Firstly, I analysed the potential of transfection of two different RhoD-specific and three different KIF20B-specific siRNAs to decrease corresponding targets in the cell. All analysed siRNAs were shown to be able to decrease mRNA and for KIF20B at the protein level of the corresponding gene (data shown where applicable).

In HeLa cells, all of the three tested KIF20B siRNAs show high efficieny of knockdown, as visible in Figure 4.1.2. A, B and D, both on transcriptional and translational level. The KIF20B protein band is not at all visible upon transfection with any of three siRNAs tested at 10 nM concentration. Transfection with one KIF20B siRNA (#1) increased the level of RhoD mRNA while transfection with the other two shows virtually no effect to RhoD expression levels. Conversely, knockdown of RhoD upon transfection with two different RhoD siRNAs decreases the levels of KIF20B in both, transcriptional and translational levels.
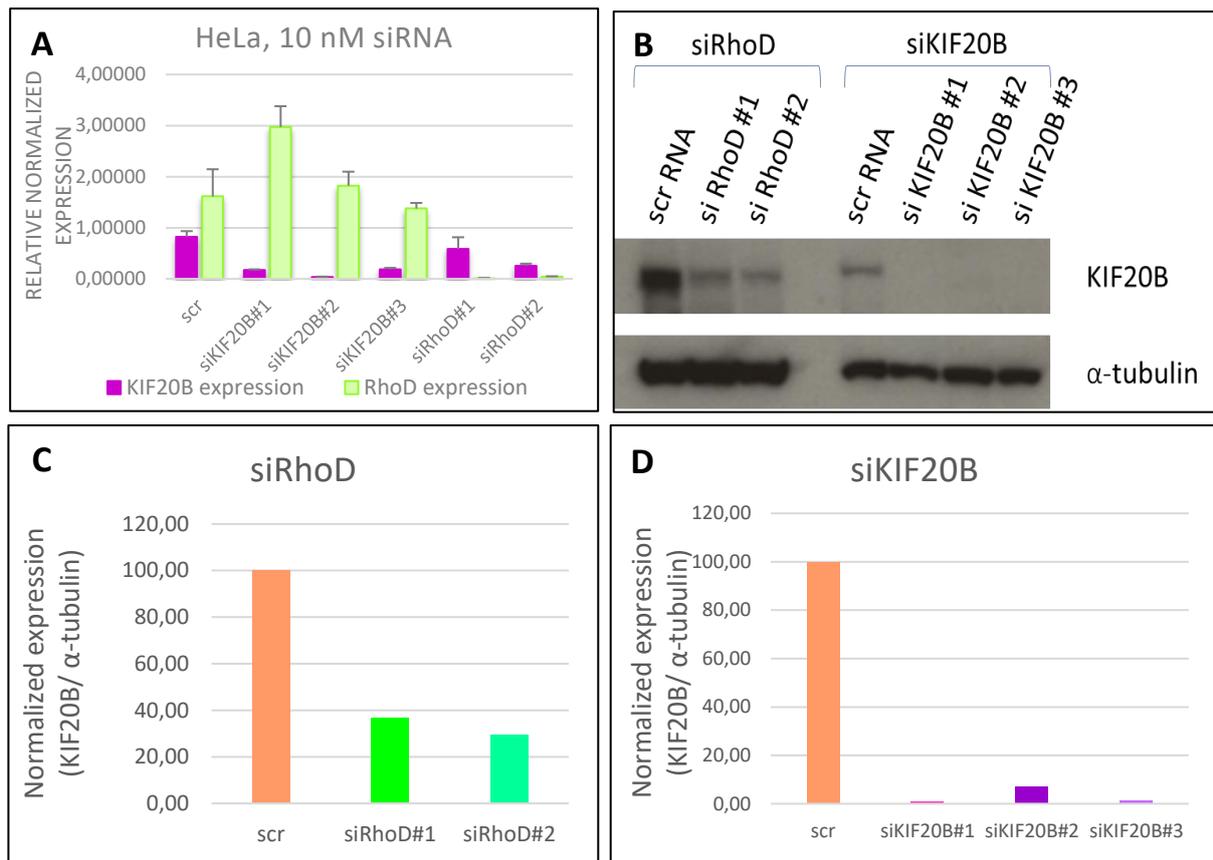
Figure 4.1.2. Knockdown of RhoD decreases expression of KIF20B on transcriptional (mRNA) and translational (protein) level in HeLa cells. A) RT-qPCR to RhoD and KIF20B in HeLa cells upon RhoD or KIF20B knockdown. Relative expression is shown, which was normalized to a GAPDH reference values. GAPDH was used as the ''housekeeping'' gene in the qPCR experiment. Error bars denote standard errors of the mean (SEM) of the sample duplicates. B) Western blot to KIF20B and α-tubulin in HeLa cells. Left sample set is knockdown of RhoD and right is knockdown of KIF20B. α-tubulin was used as a ''housekeeping'' gene, which shows that approximately equal amounts of cell lysates were loaded onto the gel. A) and B) are representative out of 3 experiments. Cells were harvested 48 hours after transfection, and a final concentration of siRNA used was 10 nM. C) and D) are densitometry data of the western blot in B). The KIF20B protein expression was normalized based on α-tubulin protein levels for each lane.

The effect seems more profound at protein level, judging from the western blot quantification data (Figure 4.1.2. C).

I have also analysed the efficacy of RhoD knockdown upon transfection with 1 nM siRNAs, to see if the degree of silencing is comparable to 10 nM siRNAs. The RhoD knockdown was still efficient even at siRNA concentration of 1 nM decreasing the levels of KIF20B protein (data not shown).

Next I analysed whether KIF20B or RhoD knockdown affects in the same manner the expression of RhoD or KIF20B, respectively, in cells resistant to cisplatin. A HeLa subline resistant to cisplatin, HeLa CK, was transfected with two different siRNAs specific for each, KIF20B or RhoD, respectively. KIF20B knockdown was efficient in HeLa CK, but to a lower degree than in HeLa cells, judging from both the RT-qPCR and western blot data (Figure 4.1.3.
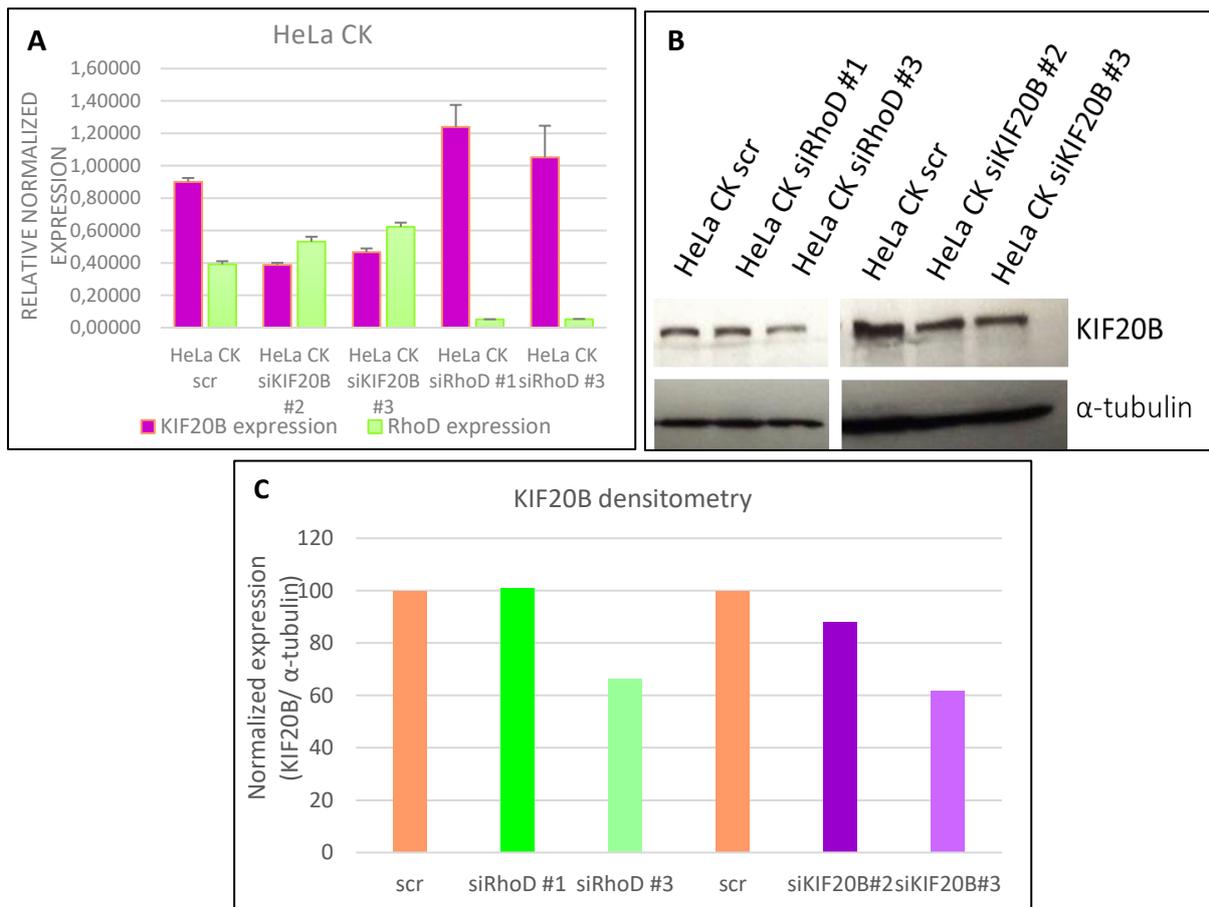
Figure 4.1.3. RhoD knockdown decreases KIF20B expression in HeLa CK cells only at the protein level upon transfection with one out of two RhoD siRNAs. A) *RT-qPCR to RhoD and KIF20B in HeLa CK cells. Relative expression is shown, normalized to GAPDH reference gene. Error bars denote standard errors of the mean (SEM) of the sample duplicates.* *B) Western blot to KIF20B and α-tubulin in HeLa CK cells. A) and B) are representative out of 3 experiments. Cells were harvested 48 hours after transfection, and a final concentration of siRNA used was 10 nM.* *C) is the quantification data of the western blot in B). The KIF20B protein expression was normalized based on α-tubulin protein levels for each lane.*

A – C). I have shown (Figure 4.1.1.) that HeLa CK cells express slightly more KIF20B than their maternal cell line HeLa. I hypothesize that this might be the reason why it is more difficult to reduce KIF20B expression using transfection of KIF20B siRNA. Interestingly, transfection with both KIF20B siRNAs increased the level of RhoD mRNA which is similar to result obtained in HeLa cells upon transfection with one out of three different KIF20B siRNA. On the other hand, the RhoD knockdown using two siRNAs in HeLa CK cells was as succesfull as in HeLa cells although HeLa CK cells express two-fold higher levels of RhoD mRNA than HeLa. However, unlike results obtained in HeLa cell line in which RhoD knockdown decreased expression of KIF20B at both transcriptional and translational levels, in HeLa CK cells I observed differential results at transcriptional and translational level. Namely, RhoD knockdown either slightly increases or does not affect the expression of KIF20B at the mRNA levels. However, western

blot results show that RhoD decreases KIF20B protein levels in one out of two RhoD siRNAs (Figure 4.1.3. A – C).

In conclusion, this results indicate a causative relationship between RhoD and KIF20B in HeLa and HeLa CK cells supporting results of Ishizaki and colleagues (unpublished data) obtained in a yeast two hybrid assay and identifying KIF20B and RhoD as interacting partners. Since RhoD antibodies are not available I decided to focus on the expression of KIF20B upon knockdown of RhoD for which specific antibodies are available. Another reason for this decision is that RhoD is strongly upregulated in cisplatin resistant HeLa CK compared to parental HeLa cells and therefore might be related to the mechanism of cisplatin resistance.

4.1.3. RhoD knockdown reduces KIF20B expression on the protein level in colorectal carcinoma cell lines CaCO-2 and HCT-116

As a model of colorectal carcinoma, I used the cell lines CaCO-2 and HCT-116. The cell lines are both colorectal adenocarcinoma, however with different properties and morphologies.
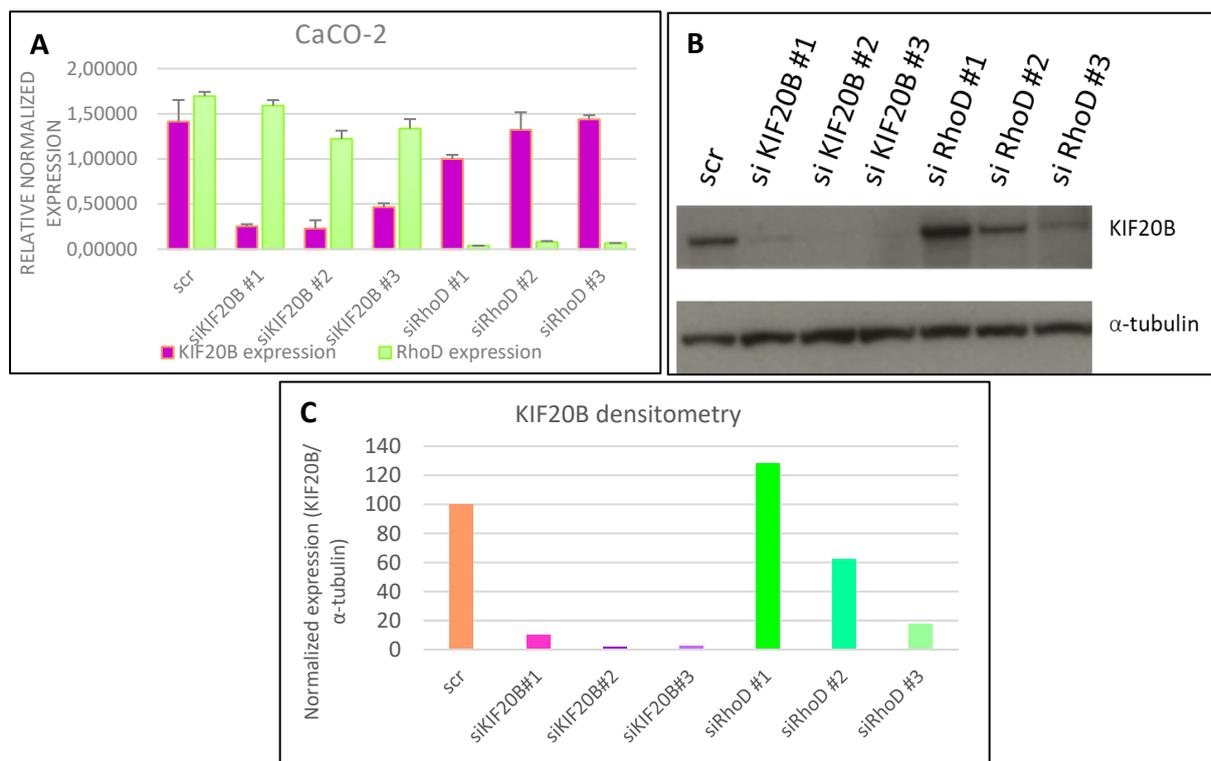
Figure 4.1.4. RhoD knockdown reduces KIF20B protein expression in CaCO-2 cells. A) RT-qPCR to RhoD and KIF20B in CaCO-2 cells. Relative expression is shown, normalized to GAPDH. Error bars denote standard errors of the mean (SEM) of the sample duplicates. B) Western blot to KIF20B and α-tubulin in CaCO-2 cells. A) and B) are representative out of 3 experiments. Cells were harvested 48 hours after transfection, and a final concentration of siRNA used was 1 nM. C) is the quantification data of the western blot in B). The KIF20B protein expression was normalized based on α-tubulin protein levels for each lane.

Since CaCO-2 cells were more sensitive to transfection, I have titrated the amount of siRNA used for knockdown and found that the 1 nM concentration was the least toxic at which I

have observed consistent results among different siRNAs for each gene. In CaCO-2 cells, knockdown of both RhoD and KIF20B was efficient at 1 nM concentration of siRNA, at transcriptional level (Figure 4.1.4. A and B). Succesfull knockdown of KIF20B was also confirmed on protein level (Fig. 4.1.4. B and C). Figure 4.1.4. shows that knockdown of KIF20B decreases the level of RhoD mRNA in two out of three KIF20B siRNAs. On the other hand differential effect, on transcriptional and translational level, was observed for the level of KIF20B upon transfection with RhoD siRNAs.
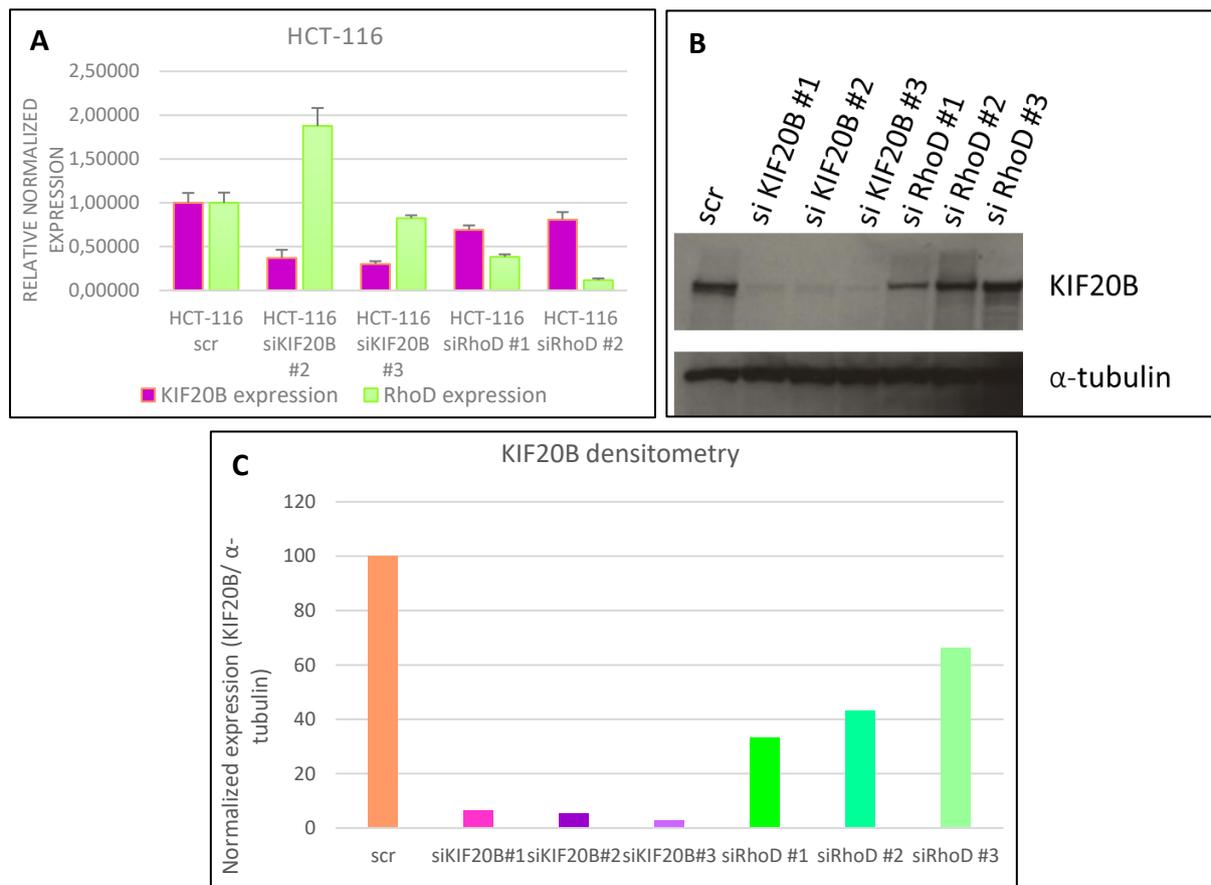
Figure 4.1.5. RhoD knockdown reduces KIF20B expression on the protein level in HCT-116 cells. A) *RT-qPCR to RhoD and KIF20B in HCT-116 cells. Relative expression is shown, normalized to GAPDH. Error bars denote standard errors of the mean (SEM) of the sample duplicates.* ***B)*** *Western blot to KIF20B and α-tubulin in HCT-116 cells. A) and B) are representative out of 3 experiments. Cells were harvested 48 hours after knockdown, and a final concentration of siRNA used was 10 nM.* ***C)*** *is the quantification data of the western blot in B). The KIF20B protein expression was normalized based on α-tubulin protein levels for each lane. Based on densitometry data, all three RhoD siRNAs induce a reduction of KIF20B expression on the protein level.*

Two RhoD siRNAs exhibited a reduction in KIF20B expression on the protein level, while on the mRNA level KIF20B expression was similar to control. For the third RhoD siRNA results show the opposite effect *i.e.* decreased KIF20B mRNA expression level and increased KIF20B protein level. However, two analysed siRNAs show consistent results and since the effect on

protein expression may not always reflect the mRNA expression levels, I conclude that in CaCO-2 cells knockdown of RhoD decreases the amount of KIF20B protein.

In HCT-116 cells, knockdown of both RhoD and KIF20B using specific siRNAs was efficient (Fig. 4.1.5. A). In addition, KIF20B protein expression is reduced for all three KIF20B siRNAs used (Fig. 4.1.5. B). Knockdown of KIF20B upon transfection with two different KIF20B siRNAs produced differential effects on the level of RhoD transcription *i.e.* increased and decreased mRNA expression (Fig. 4.1.5. A). However, knockdown of RhoD revealed much more consistent results of KIF20B expression. A reduction in KIF20B mRNA expression, as well as reduction in protein levels of KIF20B was observed upon transfection with all tested RhoD siRNAs. Two different RhoD siRNAs decrease transcriptional level of KIF20B and three different siRNAs decrease the amount of KIF20B protein (Figure 4.1.5. A, B and C).

In conclusion, in both colorectal carcinoma cell lines, CaCO-2 and HCT-116, RhoD knockdown induced a decrease in KIF20B protein expression.

4.1.4. RhoD knockdown differentially affects KIF20B expression in breast carcinoma cell lines MCF-7, MDA-MB-231 and MDA-MB-468

For breast carcinoma, three different cell lines were used: namely MDA-MB-231, MDA- MB-468 (both triple negative breast adenocarcinoma) and MCF-7 (estrogen receptor positive breast adenocarcinoma).

In MCF-7 cells RhoD mRNA expression is substantially higher than that of KIF20B (Figures 4.1.1. and 4.1.6. A). KIF20B knockdown was successfull at both mRNA and protein level (Figure 4.1.6. A and B). RhoD knockdown observed at mRNA level was also satisfactory (Figure 4.1.6. A). In MCF-7 cells, the KIF20B knockdown induced a decrease in RhoD mRNA levels, which was more prominent in one siRNA. The KIF20B mRNA levels are comparable to control for one RhoD siRNA, while for the other one they show an increase in KIF20B mRNA content (Figure 4.1.6. A). On the protein level (Figure 4.1.6. B and C) RhoD knockdown induces an increase in protein levels of KIF20B in both RhoD specific siRNAs, which is contrary to observations on HeLa and tested colorectal carcinoma cell lines.

In MDA-MB-231 cell line at the mRNA level and at the protein level KIF20B knockdown was efficient (Figure 4.1.7. A, C and D). RhoD knockdown was also satisfactory, as seen from the RT-qPCR data (Figure 4.1.7. A). At the mRNA level KIF20B knockdown interestingly

reduced levels of RhoD mRNA in both KIF20B specific siRNAs. RhoD knockdown showed a decrease in KIF20B expression at mRNA level for one RhoD siRNA, and no change in the other. On the protein level one RhoD siRNA was tested and it confirmed the result from RT-qPCR data, showing a reduction in the protein amount of KIF20B (RhoD siRNA #1, Figure 4.1.7. A, C and D).
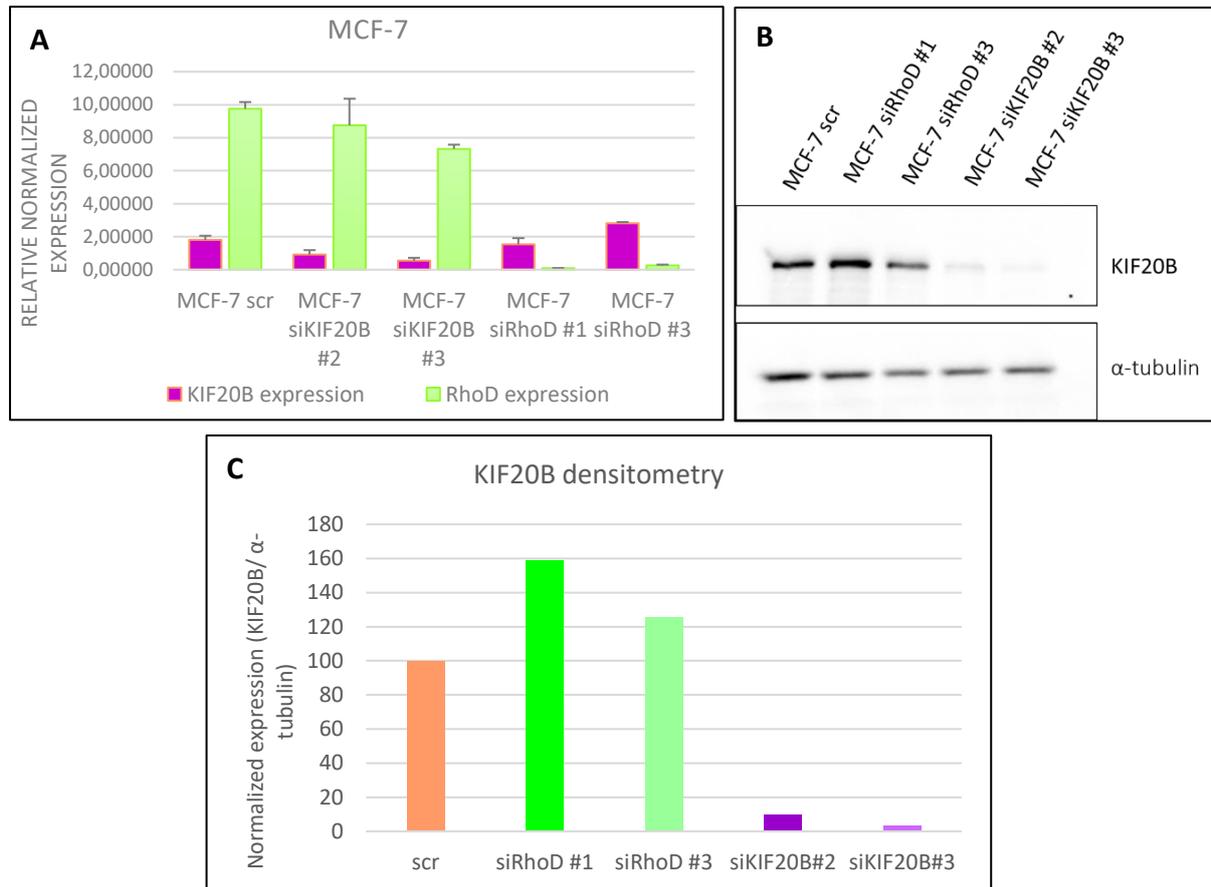
*Figure 4.1.6. RhoD knockdown increases KIF20B expression in MCF-7 cells on the protein level. **A)** RT-qPCR to RhoD and KIF20B in MCF-7 cells. Relative expression is shown, normalized to GAPDH. Error bars denote standard errors of the mean (SEM) of the sample duplicates. **B)** Western blot to KIF20B and α-tubulin in MCF-7 cells. A) and B) are representative out of 3 experiments. For both experiments cells were harvested 48 hours after silencing, and a final concentration of siRNA used was 10 nM. **C)** is the quantification data of the western blot in B). The KIF20B protein expression was normalized based on α-tubulin protein levels for each lane.*

In the MDA-MB-468 cell line two KIF20B specific siRNAs exhibited a satisfactory degree of knockdown at the mRNA level. RhoD knockdown was also very efficient at the mRNA level (Figure 4.1.7. B). On the protein level, KIF20B knockdown was also successfull, as shown for the tested KIF20B specific siRNA (Figure 4.1.7. C). Regarding the relationship of KIF20B and RhoD on the mRNA level, after KIF20B knockdown one KIF20B specific siRNA showed no change to the RhoD mRNA levels, while they were slightly reduced for the other
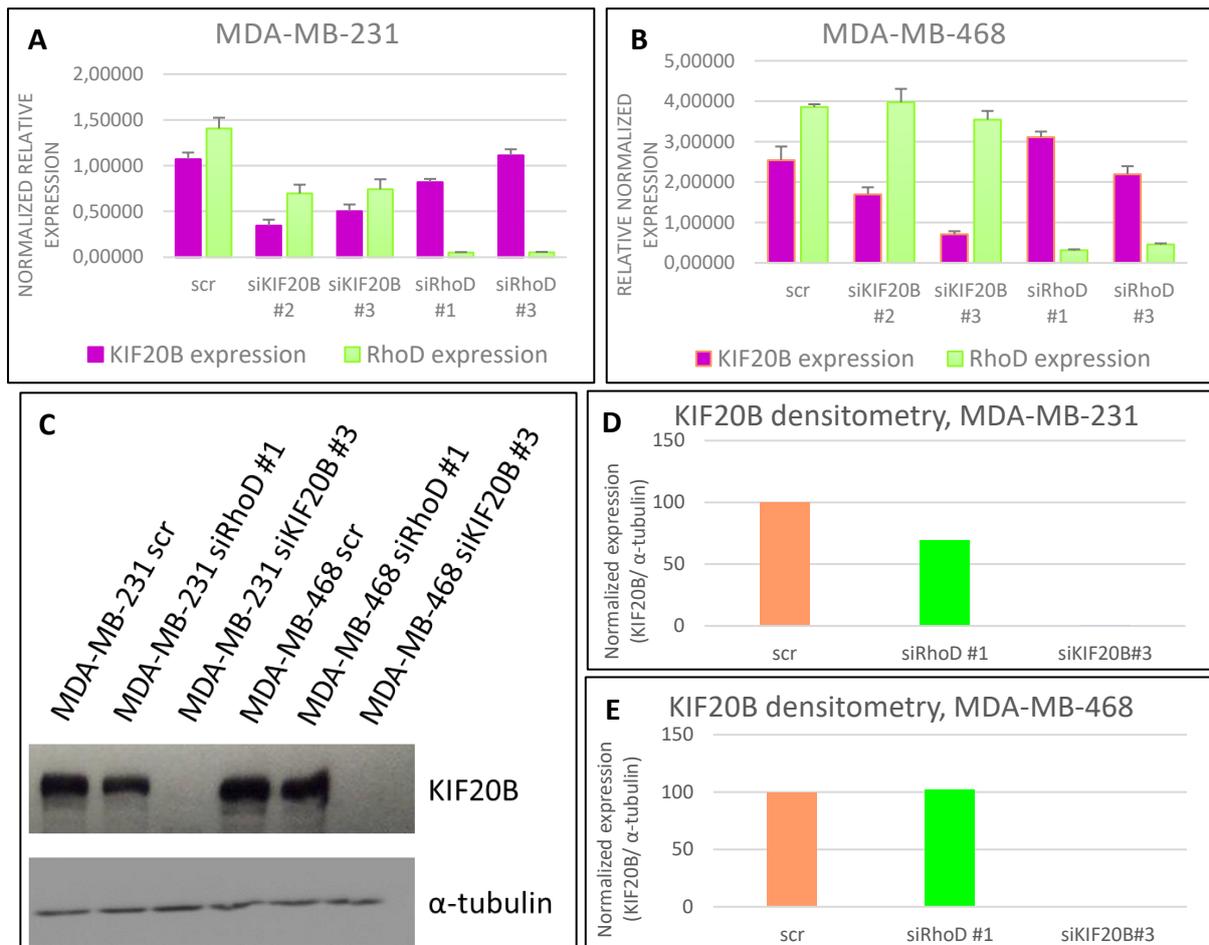
Figure 4.1.7. RhoD knockdown has a differential effect on KIF20B expression in MDA-MB-231 and MDA-MB-468 cells. A) *RT-qPCR to RhoD and KIF20B in MDA-MB-231 cells. Relative expression is shown, normalized to GAPDH.* ***B)*** *RT-qPCR to RhoD and KIF20B in MDA-MB-468 cells. Relative expression, normalized to GAPDH is displayed. Error bars denote standard errors of the sample duplicates in A) and B).* ***C)*** *Western blot to KIF20B and α-tubulin in MDA-MB-231 and MDA-MB-468 cells. A), B) and C) are representative out of 3 experiments. For all experiments cells were harvested 48 hours after silencing, and a final concentration of siRNA used was 10 nM.* ***D)*** *is the quantification of western blot data (C) for MDA-MB-231 cells and* ***E)*** *is the quantification data for MDA-MB-468 cells. The KIF20B protein expression was normalized based on α-tubulin protein levels for each lane.*

KIF20B siRNA. On the other hand, RhoD knockdown induced a slight increase in KIF20B mRNA levels for one RhoD specific siRNA, and a mild decrease for the other (Figure 4.1.7. B). On the protein level the one RhoD siRNA used showed no observable effect on KIF20B expression, *i.e.* the protein level of KIF20B was unchanged when compared to knockdown control (Figure 4.1.7. C and E).

Finally, altogether these data have shown that on the mRNA level both KIF20B and RhoD knockdown was successfull in all the tested cell lines. At the protein level KIF20B knockdown was confirmed in all cases. I can conclude that at the mRNA level RhoD knockdown affected the mRNA levels of KIF20B and vice versa. RhoD knockdown induced reduction in KIF20B mRNA levels in HeLa, CaCO-2, HCT-116 and MDA-MB-231 cells, and an increase in HeLa CK cells. On the other hand, knockdown of KIF20B has increased RhoD mRNA

levels in HeLa CK, and decreased in CaCO-2, MCF-7 and MDA-MB-231 cells. Also, RhoD knockdown has affected the protein levels of KIF20B, which was particularly observed in HeLa cells, where RhoD specific siRNAs caused a decrease in both mRNA and protein levels of KIF20B in most cases. In colorectal carcinoma cell lines CaCO-2 and HCT-116 a milder effect of KIF20B expression reduction was observed upon RhoD knockdown, but more prominently at the protein level. In the case of breast carcinoma models MCF-7, MDA-MB-231 and MDA-MB-468 a differential effect was observed in each of the three cell lines tested: RhoD knockdown induced an increase in KIF20B expression in MCF-7 cells, a decrease in MDA-MB-231 cells, and no change in MDA-MB-468 cells at the protein level. The results are summarized in Table 4.1.1. My results show the causative relationship between expression of KIF20B and RhoD supporting the hypothesis that these two proteins establish an interaction within the cell.

Table 4.2.1. Comparison of RhoD and KIF20B expression at the mRNA and protein level upon knockdown of the other gene, given for each tested cell line. The presented values correspond to data obtained from RT-qPCR and western blot, for each siRNA used. ↑ denotes an increase, ↓ denotes a decrease, and ○ denotes no observed change. The siRNAs used for each gene are marked accordingly (#1, #2 and #3). AVG represents the final outcome of knockdown on the expression of the other protein, based on results from each siRNA used. Blank cells indicate there are no results available for this particular siRNA.

Cell line	mRNA level								Protein level			
	RhoD expression (siKIF20B)				KIF20B expression (siRhoD)				KIF20B expression (siRhoD)			
siRNA / Cell line	#1	#2	#3	AVG	#1	#2	#3	AVG	#1	#2	#3	AVG
HeLa	↑	○	○	○	↓	↓		↓	↓	↓		↓
HeLa CK		↑	↑	↑	↑		↑	↑	○	↓		↓
CaCO-2	↓	↓	↓	↓	↓	↓	↓	↓	↑	↓	↓	↓
HCT-116		↑	↓	○	↓	↓		↓	↓	↓	↓	↓
MCF-7		↓	↓	↓	↓		↑	○	↑		↑	↑
MDA-MB-231		↓	↓	↓	↓		○	↓	↓			↓
MDA-MB-468		↑	↓	○	↑		↓	○	○			○

4.2. Localization of RhoD and KIF20B upon their knockdown using specific siRNA

After establishing that there is a causative relationship between the expression of KIF20B and RhoD at mRNA and protein level, I wanted to determine if their proposed interaction is also evident microscopically and to identify the cellular compartment or area where this interaction might be taking place. From published data, it is known that RhoD predominately localizes in the early endosome compartment (Murphy et al., 1996; Murphy et al., 2001; Gasman et al., 2003) and that the localization of KIF20B varies in the cell depending on the phase of mitosis that cell is currently undergoing (Kamimoto et al., 2001; Abaza et al., 2003; Kanehira et al., 2007). Knowing this I have first tested the knockdown efficiency of KIF20B in my model cell lines at various phases of cell division by immunofluorescence (IF) and confocal microscopy. Unfortunately, I was unable to do the same for RhoD, as cellular localization of endogenous RhoD is not clearly observed, because of specificity and titer of commercially available anti -human RhoD antibodies. The next step was to find if the localization of either protein changes when the other is knocked down. In the case of KIF20B this was achieved with knockdown by transfection with RhoD siRNAs and immunofluorescence against KIF20B. I found that the immunofluorescence signal of KIF20B in the cells treated with RhoD siRNA was not concentrated at the cleavege furrow and midbody during mitosis. As I was unable to perform the corresponding experiment for endogenous RhoD localization, I circumvented the issue of RhoD visualization by transfecting cells with EGFP tagged RhoD plasmid constructs. The constructs used were EGFP-RhoD^{WT} (wild type), EGFP-RhoD^{G26V} (Val mutant) and the EGFP-RhoD^{Q75L} (Lys mutant). These mutants were the constitutively active form of RhoD (RhoD-GTP form, as opposed to the inactive RhoD-GDP form). Since the proposed interaction of KIF20B and RhoD occurred when RhoD was in its active form, I have used the constitutively active mutants for further localization studies, especially the EGFP-RhoD^{Q75L} mutant since the EGFP-RhoD^{G26V} exhibited higher cell lethality upon its transfection.

4.2.1. RhoD knockdown elicits a reduction in intensity of KIF20B signals at the intercellular bridge of cytokinetic HeLa cells

To check if RhoD and KIF20B colocalize in any parts of the cell during cell division, I first had to evaluate KIF20B localization in the cell by immunofluorescence with the available antibody and compare it to previous reports. Thus far, localization of KIF20B in human cell
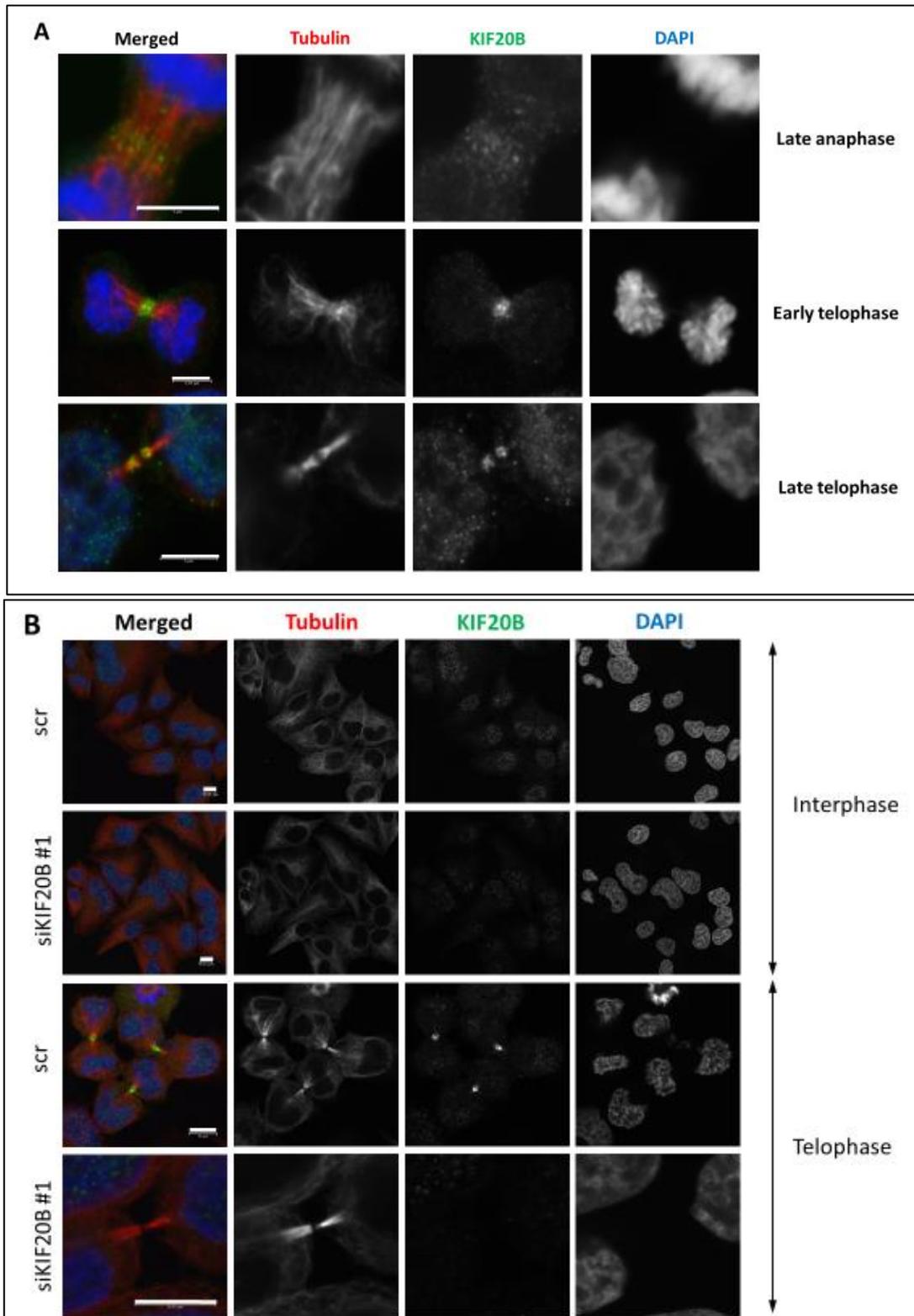
Figure 4.2.1. Localization of KIF20B in HeLa cells. A) KIF20B localizes in the spindle midzone during late anaphase, with the signal concentrating at the midbody with progression of telophase. The signal condenses in early telophase, finally appearing as two distinct foci in the midbody at late telophase. Scale bar = 5 µm. *B) KIF20B knockdown by specific siRNA effectively decreases KIF20B signal.* This is evident as absence of KIF20B signals from the interphase nuclei and the intercellular bridge region during telophase. Scale bar = 10 µm. Cells were collected after 48 hours in culture, fixed by PTEMF method and stained with primary antibodies against tubulin (red) and KIF20B (green). The nuclei were counterstained with DAPI (blue). Micrographs were taken at 630x, with variable zoom in individual photos, to observe the cell structures in better detail.

77

lines has been shown in HeLa cells (Abaza et al., 2003; Janisch et al., 2018), UM-UC-3 (Kanehira et al., 2007) bladder cancer cells, SW480 and LOVO colorectal carcinoma (W. F. Lin et al., 2018), at least in interphase.

In this research KIF20B localization patterns have been tested in respect to the stage of cell division. In general, KIF20B localizes on the nucleus in interphase cells, it is still present on the chromosomes during prometaphase and metaphase, while in early anaphase it moves from the chromosomes to the area of the central spindle, where it resides up until constriction of microtubules and formation of the contractile actin ring. At this stage, in early to late telophase, it is mostly localized on the midbody, between two newly forming daughter cells. After cytokinesis, the KIF20B midbody signals may still be visible with the daughter cell which inherited the midbody. This pattern of localization was observed in most of the tested cell lines in previous reports and in this research, but I will present here representative results obtained in HeLa, HCT-116 and CaCO-2 cell models.

In HeLa cells, except for KIF20B signals in nuclei during interphase (Figure 4.2.1. B), the most prominent observed localization of KIF20B after staining with specific antibody was during the final stages of cell division, *i.e.* from late anaphase to late telophase (cytokinesis), as shown in Figure 4.2.1. A. The signal is punctate in late anaphase at the area of the central spindle. As division progresses, the signal becomes denser at the midbody where it stays also during late telophase and cytokinesis, in the form of two distinct foci. These particular areas were of most interest to determine the efficiency of KIF20B knockdown in immunofluorescent imaging. The signals in central spindle and midbody are generally always absent from those areas upon KIF20B knockdown, indicating that knockdown was successful (as shown in Figure 4.2.1. B), when compared to negative control cells (labelled scr in Figure 4.2.1. B). These data are consistent with previous findings of KIF20B localization in HeLa cells with other antibodies against KIF20B (Janisch et al., 2018).

After confirming KIF20B localization and specificity of the antibody used for immunofluorescence, I was interested in finding if RhoD knockdown caused any changes in KIF20B localization patterns or signal intensity. To evaluate signal distribution, I have assessed KIF20B signals in general, encompassing signals on nuclei in interphase cells and signals in dividing cells which migrate from chromosomes to spindle midzone and intercellular bridge, depending on the stage of cell division.
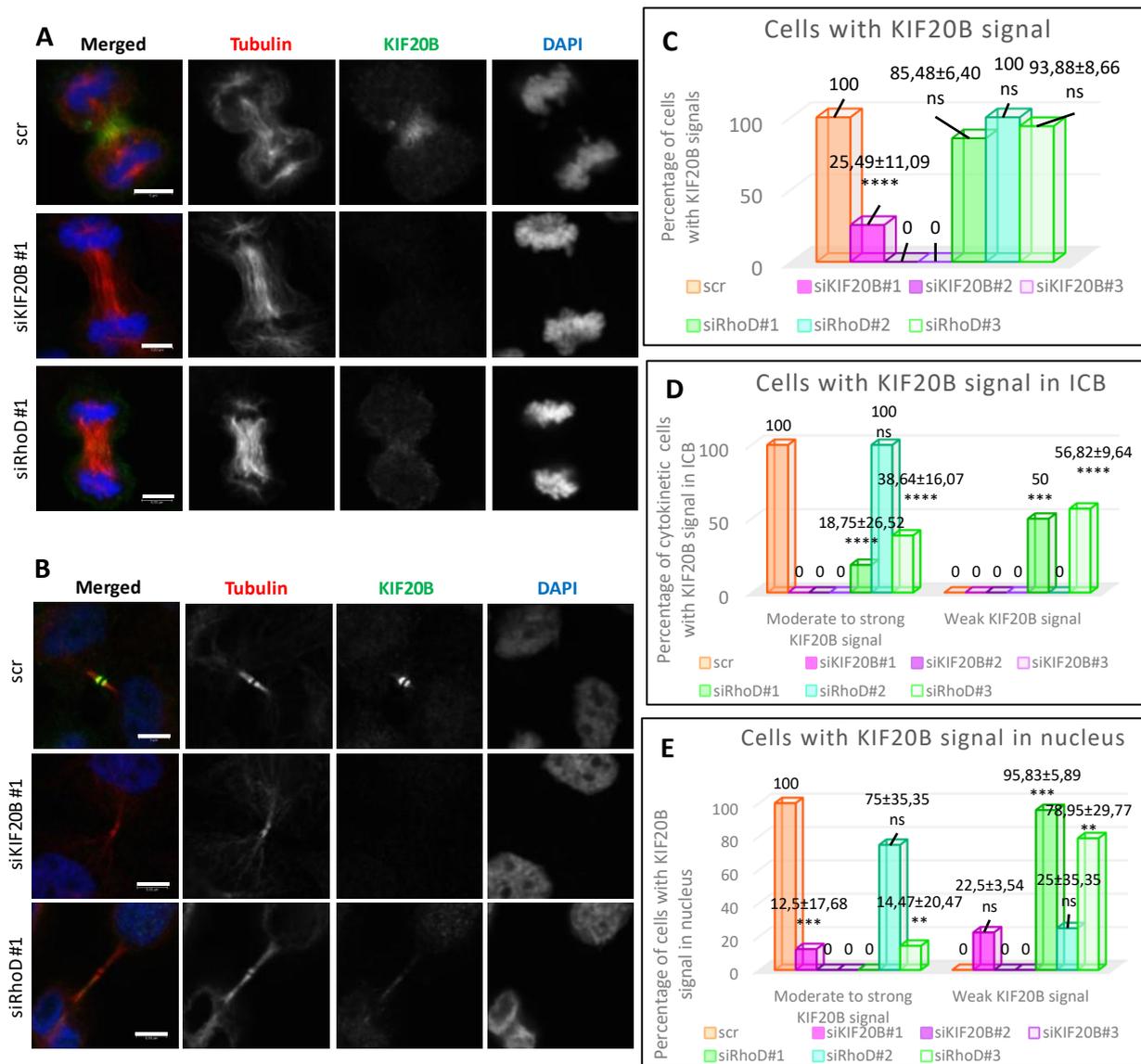
Figure 4.2.2. RhoD knockdown in HeLa cells elicits loss of KIF20B signal in the intercellular bridge (ICB) of cytokinetic cells. *A) KIF20B signals in early telophase are diminished upon RhoD knockdown. B) KIF20B signals in HeLa cells undergoing late telophase and cytokinesis. Cells were harvested 48 hours after transfection with 10 nM siRNAs and stained for tubulin (red), KIF20B (green) and counterstained with DAPI (blue). Micrographs shown are representative out of four individual experiments. Magnification: 630 x. **C)** Quantification of HeLa cells displaying KIF20B signals upon knockdown with either negative control, KIF20B or RhoD specific siRNAs. Statistical significance was calculated using one-way ANOVA with Dunnett's multiple comparison test. **D)** Quantification of cytokinetic HeLa cells displaying KIF20B signals only in the ICB, divided into moderate to strong and weak KIF20B signals. **E)** Quantification of HeLa cells displaying KIF20B signals in the nucleus, separating chromosomes and spindle midzone. Moderate to strong and weak signals are individually shown. In D) and E) statistical significance was calculated by two-way ANOVA with Dunnett's multiple comparison test. For C), D) and E) values in percentages are displayed upon each bar, with corresponding standard deviations between two experiments, where applicable. N > 50 cells. * denotes P<0,05; ** denotes P<0,005; *** denotes P<0,0005 and **** P<0,00005; ns = non significant. Scale bars = 5 µm.*

In two out of three RhoD siRNAs (#1 and #3) I have noticed a decrease in KIF20B signal intensity (Figure 4.2.2. A and B). When counting the number of cells displaying a KIF20B signal, 85,48 ± 6,40 % of cells where RhoD#1 siRNA was used and 93,88 ± 8,66 % cells where RhoD#3 siRNA was used, still exhibited KIF20B signals, but ANOVA test showed this signal reduction

was not significant (Figure 4.2.2. C). However, I have noticed that while KIF20B signals in the nuclei of interphase cells still lingered, even in cells transfected with KIF20B siRNA, KIF20B signals of cytokinetic cells (localized in the intercellular bridge (ICB) at the midbody), were significantly reduced. That is why I have separately evaluated cells with signals only in the nuclei up until late telophase, and cells in late telophase undergoing cytokinesis (Figure 4.2.2. D and E). I have also categorized signal intensity into moderate to strong, which was easily observable, and weak signal which I characterized as faint to non-existent. Two out of three RhoD siRNAs used in transfection of HeLa cells displayed 18,75 ± 26,52 % (siRhoD#1) and 38,64 ± 16,07 % (siRhoD#3) of cytokinetic cells with strong or moderate KIF20B signals in the ICB, while a larger portion exhibited weaker KIF20B signals in the same area (50,00 ± 0,00 and 56,82 ± 9,64 % respectively) (Figure 4.2.2. D). On the other hand, I have found that KIF20B signals persisted in the nucleus, even for one KIF20B siRNA (#1), where 12,5 ± 17,68 % of transfected cells still exhibited strong signals, and 22,5 ± 3,54 % exhibited weak signals. As for HeLa cells where RhoD was knocked down, one siRNA (#2) displayed a higher portion of strong signals in the nucleus (75 ± 35,35 %), while the other two (siRhoD#1 and siRhoD#3) exhibited a much lower percentage of cells with strong/moderate KIF20B signals (0,00 and 14,47 % respectively) and a higher portion of cells with weak to no signal (95,83 ± 5,89 % and 78,95 ± 29,77 %, respectively) (Figure 4.2.2. E). Altogether, I can conclude that there is a significant reduction in KIF20B signal intensity in HeLa cells upon RhoD knockdown, confirmed for two out of three tested siRNAs.

In HeLa CK cells I have observed the same cellular localization pattern of KIF20B throughout cell division, as in HeLa cells, however I have not noticed reductions in KIF20B signal intensity after transfection with RhoD siRNAs (data not shown).

4.2.2. KIF20B signals migrate from nuclei to microtubules in CaCO-2 and HCT-116 cells

In CaCO-2 cells, I have observed a very similar localization pattern of KIF20B as in HeLa cells, with indications of a more detailed signal migration than was described previously in literature for any tested cell line. Thus far, no data has either been published regarding localization of KIF20B in CaCO-2 cells, especially during cell division. Due to the multinuclear nature of the cell line, I have stained for the Zonula occludens (ZO)-1, residing in cell-cell
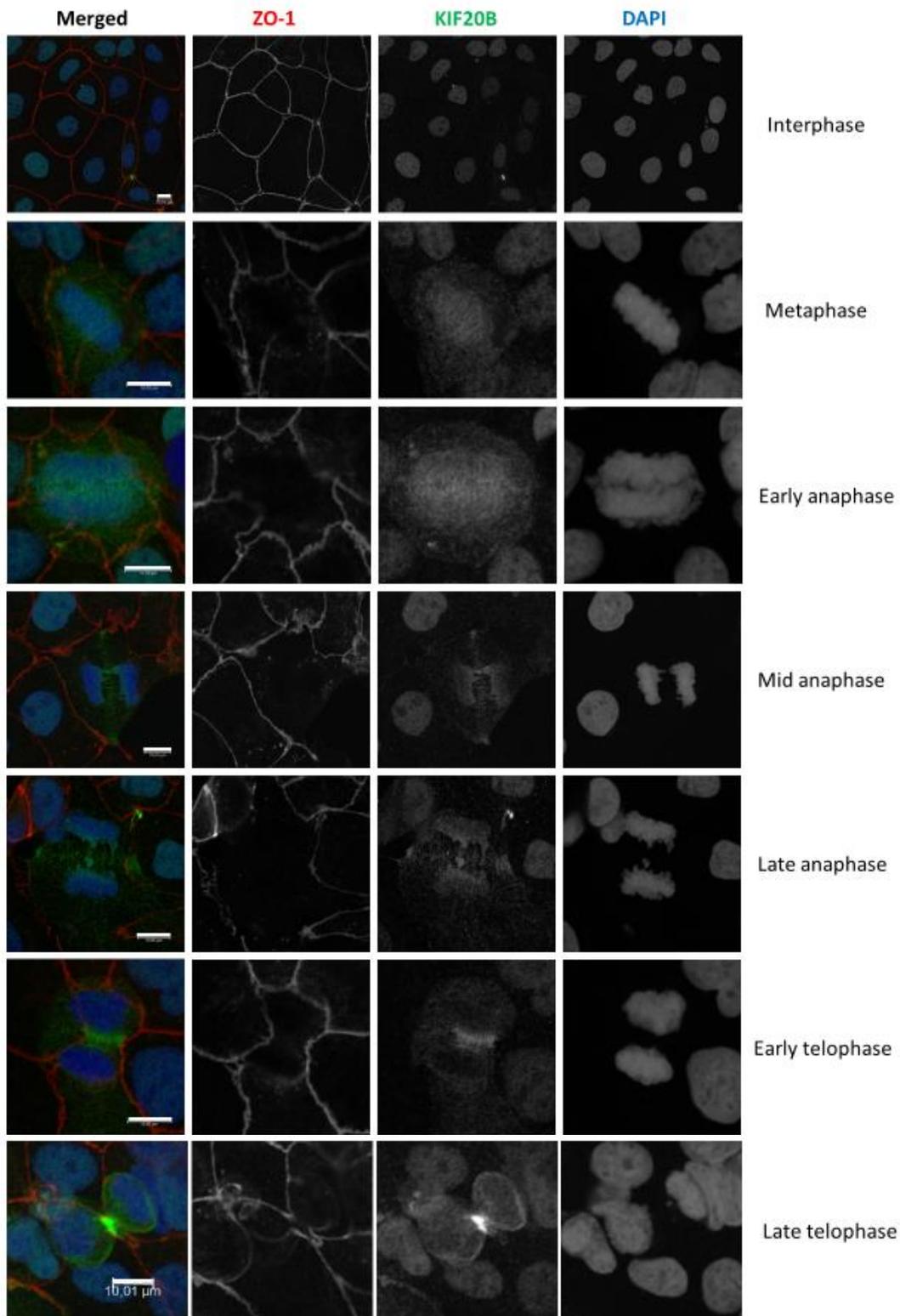
Figure 4.2.3. KIF20B signals migrate from nuclei to microtubules during the initial stages of cell division in CaCO-2 cells. Cells were collected after 48 hours in culture, fixed by PTEMF method and stained with primary antibodies against ZO-1 (red) and KIF20B (green). The nuclei were counterstained with DAPI (blue). Micrographs were taken at 630x, with variable zoom in individual photos, to observe the cell structures in better detail. Scale bar = 10 μm.

contacts, to better distinguish cell-cell boundaries, which was important to tell adjacent cells apart.

As shown in Figure 4.2.3., during interphase, the KIF20B signals are situated on the cell nuclei. During metaphase, these signals are also present on the metaphase chromosomes, but form an interlocking filamentous pattern which is not readily visible at first glance. This structure most likely follows the microtubules which are attached to the chromosomes. During anaphase, these signals are translocating from the chromosomes to the area in between two newly formed daughter nuclei, and also laterally, outlining the spindle midzone. In most of the observed cases, the KIF20B signals also persisted during anaphase on lingering chromosomes. In telophase, signals condensed at the intercellular bridge, visible as two distinct foci on either side of the midbody. During KIF20B knockdown in CaCO-2 cells, signals of KIF20B were absent from the described areas (chromosomes, spindle midzone, intercellular bridge) and knockdown was efficient for all tested KIF20B siRNAs. However, unlike as in HeLa cells, RhoD knockdown elicited no change in intensity of KIF20B signals, which were comparable to control (Figure 4.2.4.).
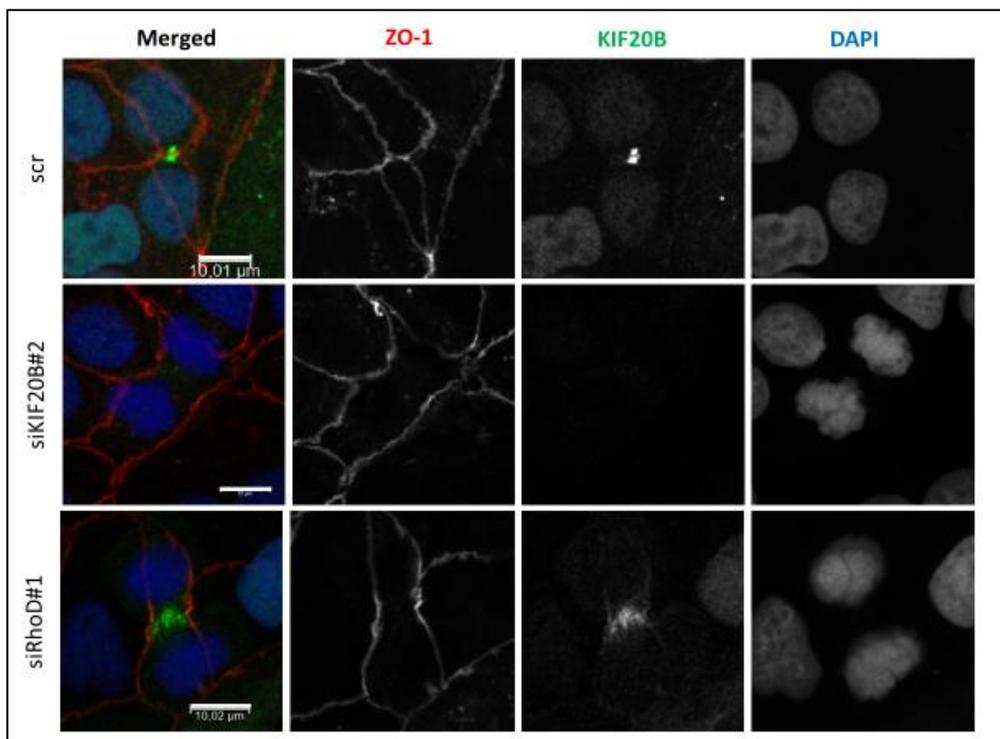
Figure 4.2.4. RhoD knockdown elicits no decrease in KIF20B signal intensity in CaCO-2 cells. Cells were harvested 48 hours after transfection with 1 nM siRNAs and stained for ZO-1 (red), KIF20B (green) and counterstained with DAPI (blue). Micrographs shown are representative out of two individual experiments. Magnification: 630 x. Scale bar = 10 µm.

The results displayed in Figure 4.2.4. were obtained by transfection with 1 nM siRNAs. The same results were obtained also with 10 nM siRNA.

In HCT-116 cells, another model of colorectal adenocarcinoma, a corresponding localization to the one in HeLa and CaCO-2 cells was observed during cell division, as shown in Figure 4.2.5.

Signals were on nuclei in interphase (visible in all panels of Figure 4.2.5.), migrating from chromosomes to spindle midzone during metaphase to anaphase transition and finally concentrating on the intercellular bridge. Absence of signals at designated areas was also observed upon KIF20B knockdown, tested with all three siRNAs against KIF20B (Figure 4.2.6.)
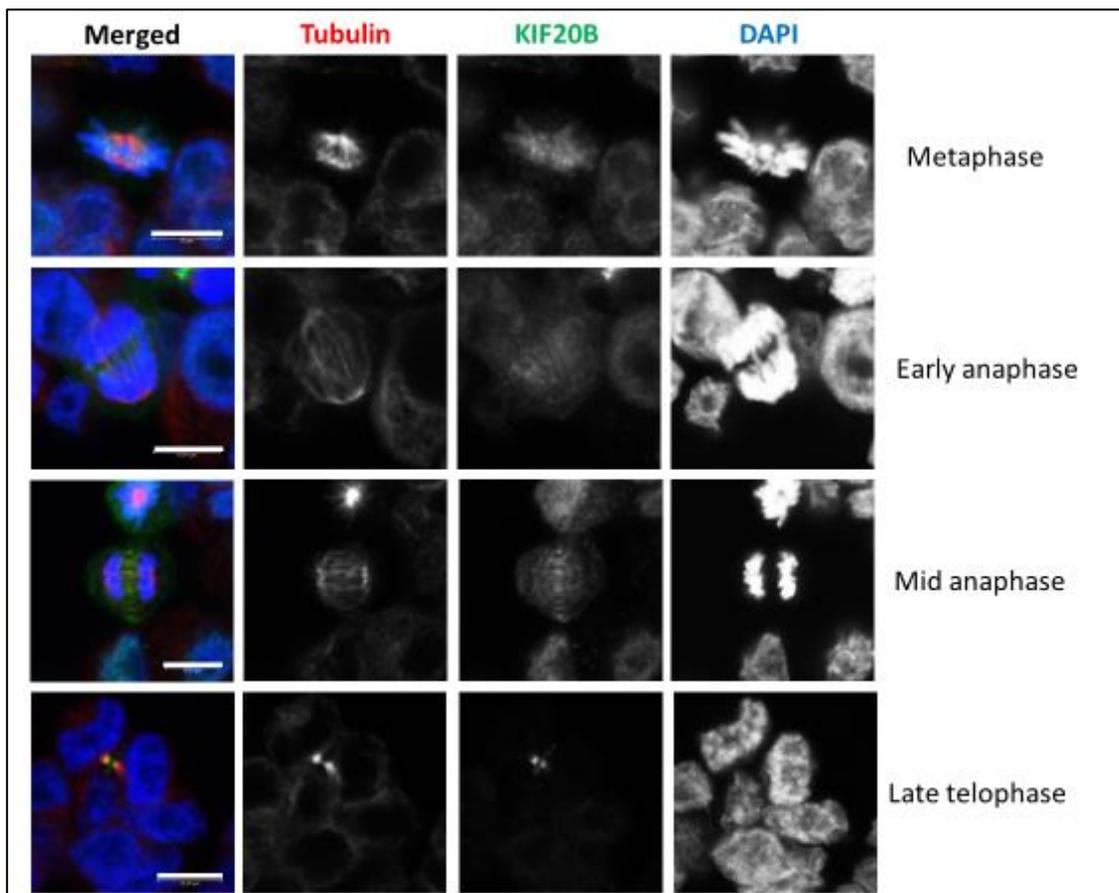
Figure 4.2.5. Localization of KIF20B (green) in HCT-116 cells during different stages of cell division. Cells were collected after 24 hours in culture, fixed by PTEMF method and stained with primary antibodies against tubulin (red) and KIF20B (green). The nuclei were counterstained with DAPI (blue). Micrographs were taken at 630x magnification. Scale bar = 10 µm.
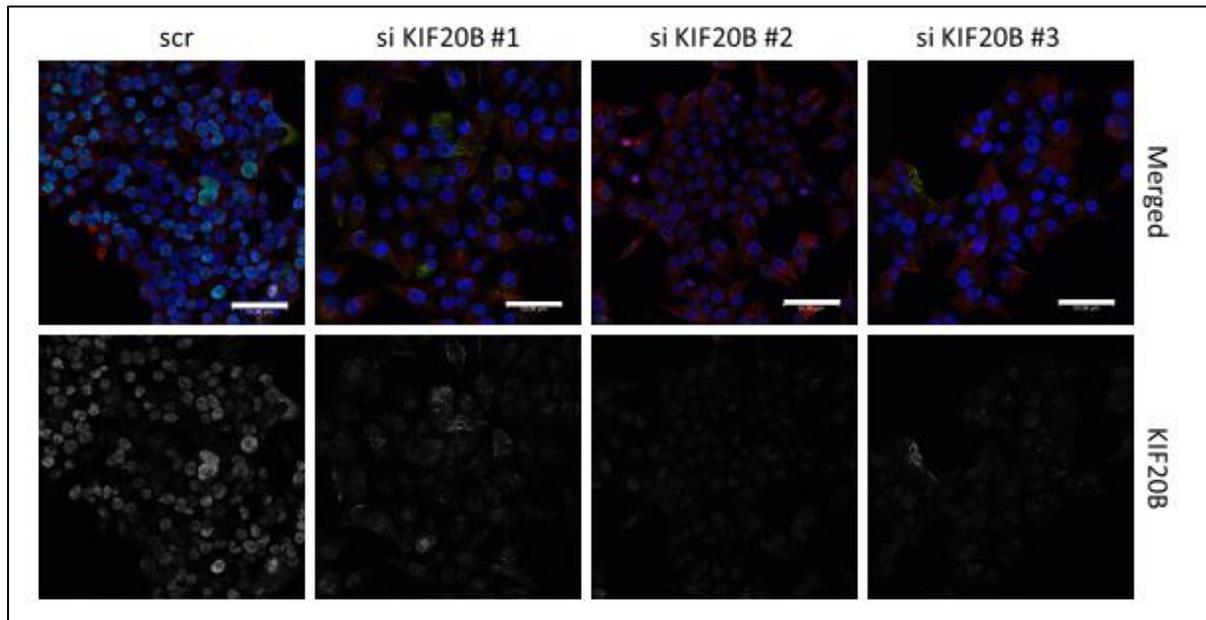
*Figure 4.2.6. **KIF20B knockdown by transfection with KIF20B siRNAs was successful in HCT-116 cells** for all three tested siRNAs. Cells were harvested 48 hours after transfection, fixed with PTEMF, stained for tubulin (red), KIF20B (green) and counterstained with DAPI (blue). Only the KIF20B signal is displayed in the subpanel below Merged, where signal is predominately localized to the cell nuclei. Micrographs were taken at 630x magnification, 1x zoom. Scale bar = 50 µm.*

4.2.3. KIF20B signals persist in the interphase nuclei and the intercellular bridge of RhoD silenced MDA-MB-231 and MDA-MB-468 breast carcinoma cells

In the final model, the breast carcinoma, I have also tested KIF20B localization in MDA-MB-231 and MDA-MB-468 cells. Localization of KIF20B corresponded to the other cell models
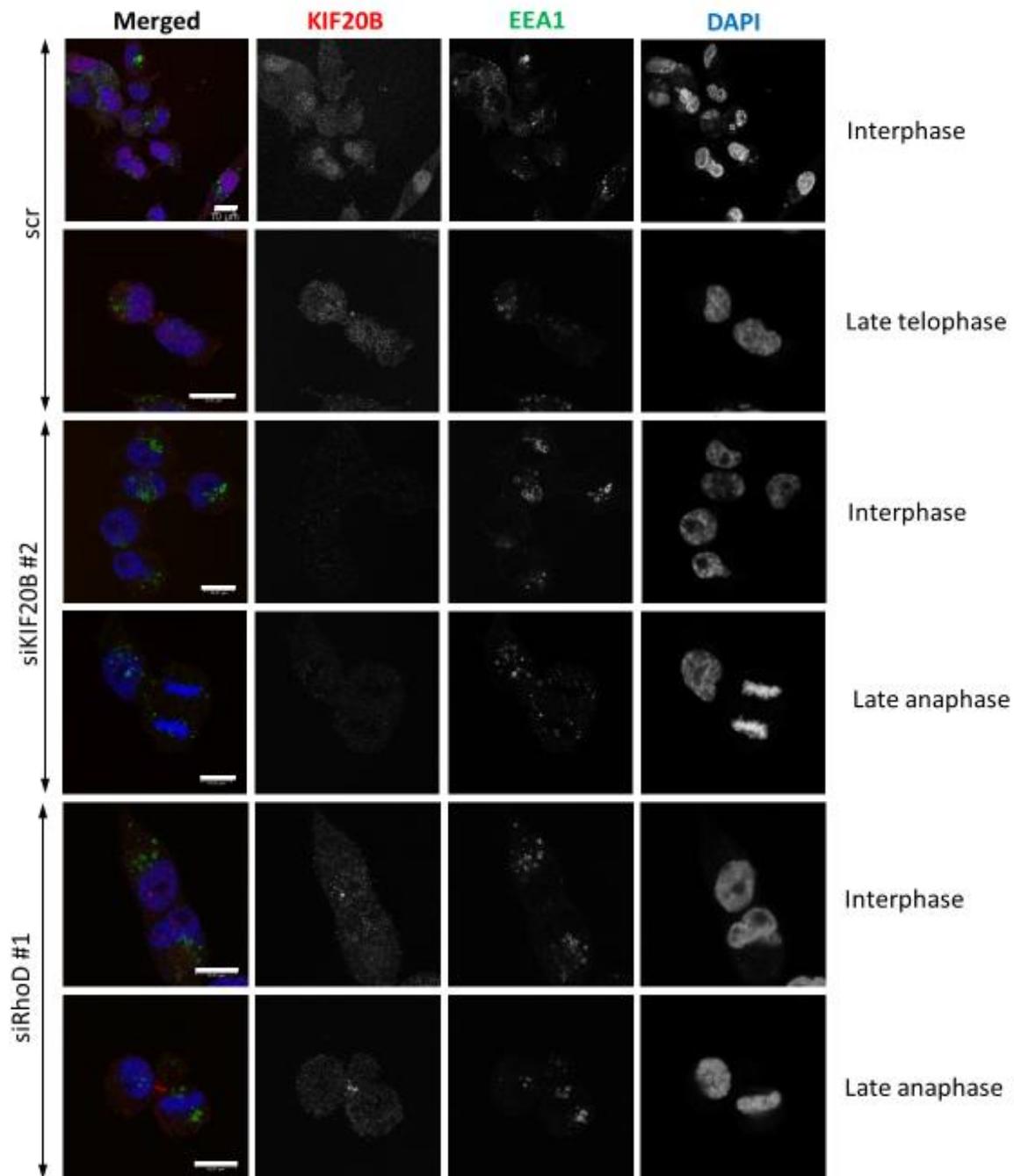
Figure 4.2.7. RhoD knockdown does not affect intensity of KIF20B signals in MDA-MB-231 cells and KIF20B knockdown was efficiently achieved. *Cells were collected 48 hours after knockdown, fixed and stained with primary antibodies against KIF20B (red) and EEA1 (green). The nuclei were counterstained with DAPI (blue). Micrographs were taken at 630x, with variable zoom. Scale bar = 10 µm.*

I used; namely on nucleus during interphase, and the spindle midzone and intercellular bridge during anaphase and telophase, respectively (Figures 4.2.7. and 4.2.8.). KIF20B knockdown
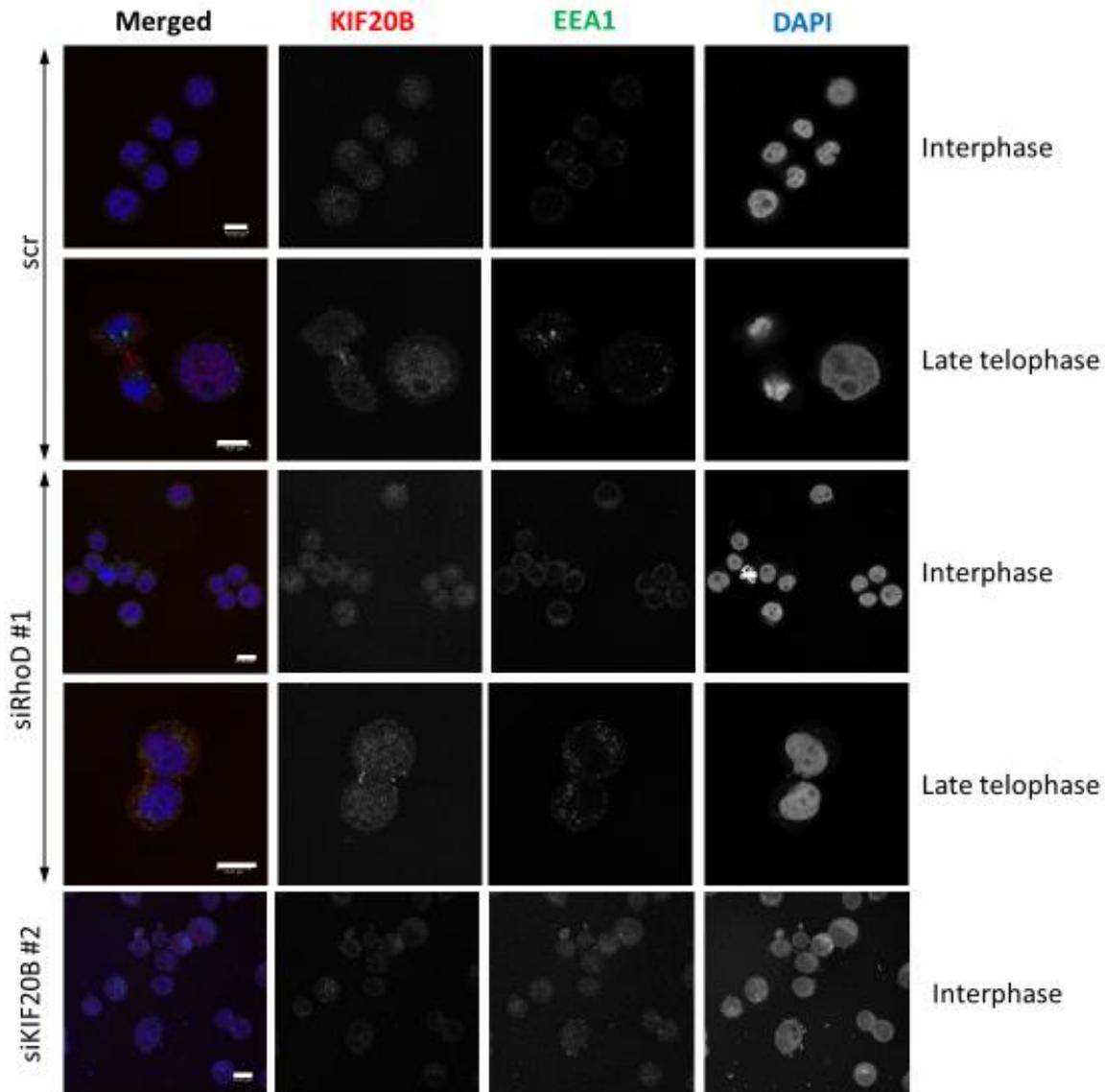
Figure 4.2.8. Localization of KIF20B (red) in MDA-MB-468 cells exhibits no change in KIF20B signal intensity after RhoD knockdown. *KIF20B knockdown was efficient, as established in the lower panel. Cells were collected 48 hours after knockdown, fixed and stained with primary antibodies against KIF20B (red) and EEA1 (green). The nuclei were counterstained with DAPI (blue). Micrographs were taken at 630x, with variable zoom. Scale bar = 10 μm.*

was also successfully confirmed as absence of KIF20B signals from these structures (Figure 4.2.7.), or a very mild dispersed signal observed in the cytoplasm of silenced cells (Figure 4.2.8.).

However, in the RhoD silenced cells, KIF20B signals were still present at the intercellular bridge (Figures 4.2.7. and 4.2.8., RhoD panels), and on interphase nuclei, as visible in the designated figures.

Alongside KIF20B, EEA1 (Early endosome antigen 1) was also stained to distinguish if there are any notable differences in the distribution, size or localization of early endosome structures upon KIF20B or RhoD knockdown, since RhoD is known to localize on early

endosomes. No striking differences were found. However, interestingly, the endosome structures appeared to be larger and more abundant in the MDA-MB-231 than in MDA-MB-468 cell line.

4.2.4. Exogenous RhoD localizes in the intercellular bridge of telophase HeLa cells

As mentioned previously, due to the poor detectability of commercially available RhoD antibodies, RhoD localization was examined by transfecting a plasmid containing a gene for RhoD, tagged with EGFP. As described in the Materials and methods section 3.10., plasmid constructs expressing RhoD wild type (WT) and constitutively active GTP mutants (RhoD ^{Q75L} and RhoD^{G26V}), tagged with EGFP, were developed (Ishizaki et al., unpublished results).

Since RhoD has been found to be a "fast acting" Rho GTPase, which is independent of classic GTP-GDP exchange process carried out by various Rho activating proteins (Rho-GEF, GAP and GDI), it is predominantly present in the cell in its GTPase form (Aspenström, 2017; Blom et al., 2018).

Beside the already published localization patterns of RhoD to early and recycling endosomes (Murphy et al., 1996) in interphase cells, here I found its novel localization in dividing cells, specifically in the latest stages of telophase.

In interphase HeLa cells the exogenous RhoD is not ubiquitously localized, with prominent localization to the boundaries between adjacent cells. The signal may also be present in a dotted manner perinuclearly, which I have observed in both constitutively active RhoD mutants; RhoD^{Q75L} and RhoD^{G26V} (Figure 2.9. A, and 2.10. A). I have noticed that the transfection rate is much greater in the RhoD^{Q75L} mutant, than in the RhoD^{G26V} mutant (29,85 ± 0,76% opposed to 2,95 ± 0,12% in the negative control, AVG N = 80 cells) (Figure 4.2.9. B). In Figure 4.2.9. A, F-actin was stained due to involvement of RhoD with the actin cytoskeleton (Murphy et al., 1996; Gasman et al., 2003).

On the other hand, in dividing HeLa cells, I have noticed that EGFP-RhoD signal appears in the middle of the intercellular bridge, inbetween or sometimes even overlapping with the two KIF20B foci at the midbody (Figure 4.2.10. A). I have confirmed this localization in the RhoD^{WT} transfectant and both constitutively active mutants used and attempted to quantify it in the negative control (scr) EGFP-RhoD transfected HeLa cells. Since there is a very low naturally occurring ratio of division in unsynchronized HeLa cells, it is difficult to find EGFP-positive

mitotic cells, especially cytokinetic cells, whose ratio is even lower. To illustrate this ratio I have quantified mitotic and cytokinetic cells in the negative control of non-transfected and EGFP-RhoD^{Q75L} transfected cells (Figure 4.2.10. B).
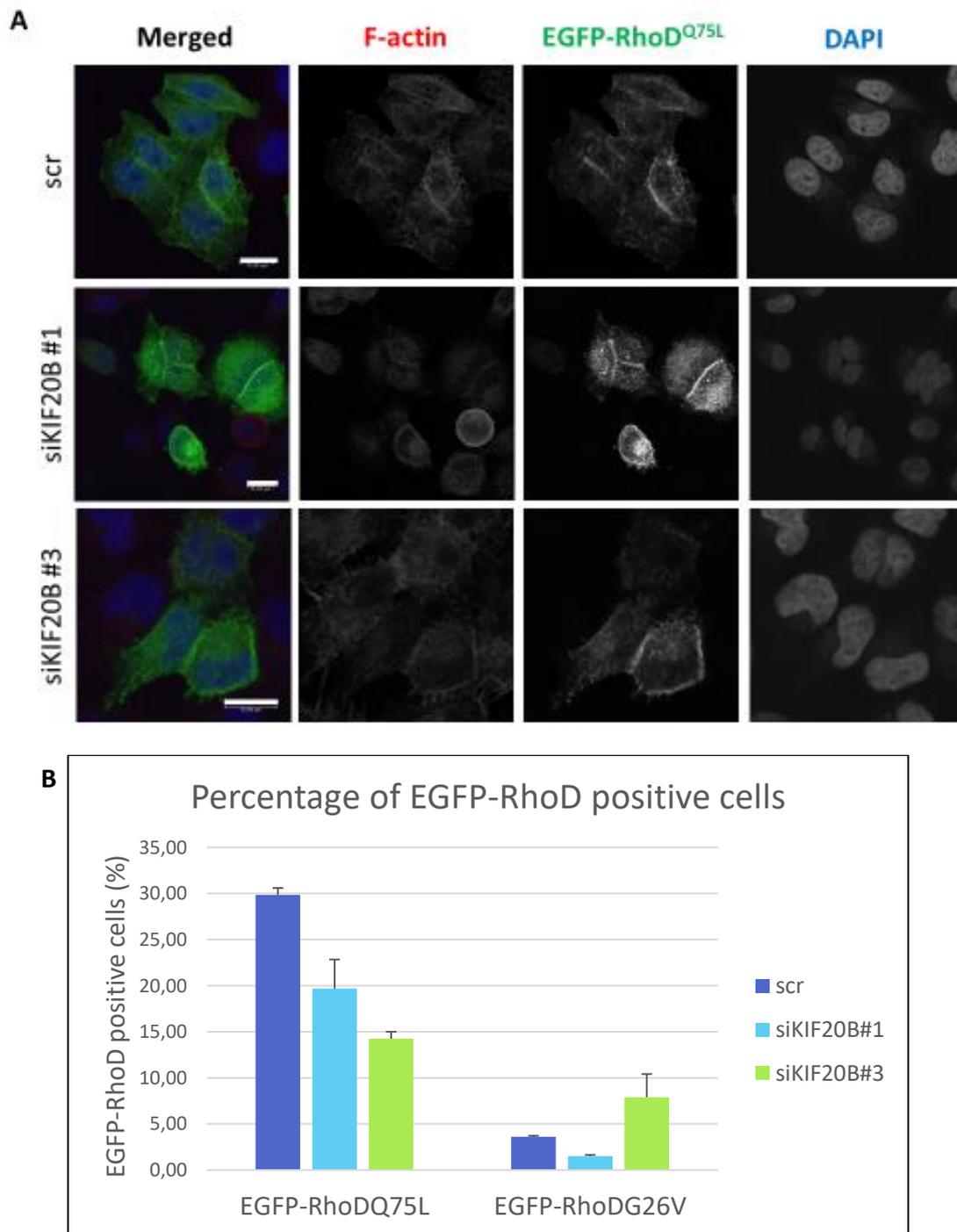
Figure 4.2.9. In interphase HeLa cells exogenous EGFP-RhoD localizes perinuclearly and at cell-cell junctions. A) *HeLa cells were cotransfected with plasmid expressing EGFP tagged RhoD mutant and siRNA directed at KIF20B or control siRNA (scr) at 10 nM final concentration. After 48 hours of incubation, cells were fixed and stained with antibodies against F-actin (red). The nuclei were counterstained with DAPI (blue).* **B)** *Transfection efficiency of EGFP-RhoD constitutively active mutants RhoD^{Q75L} and RhoD^{G26V} in negative control and KIF20B-silenced cells. Data from a representative out of two experiments is shown. Error bars denote standard deviation between two counting sessions on different parts of one slide. N (average cells counted) = 80. Scale bar = 15 μm.*

A Merged | KIF20B | EGFP-RhoD^Q75L | Rabaptin 5 | DAPI

Interphase

Metaphase

Early anaphase

Late telophase

B Ratio of mitotic and EGFP+ cytokinetic cells
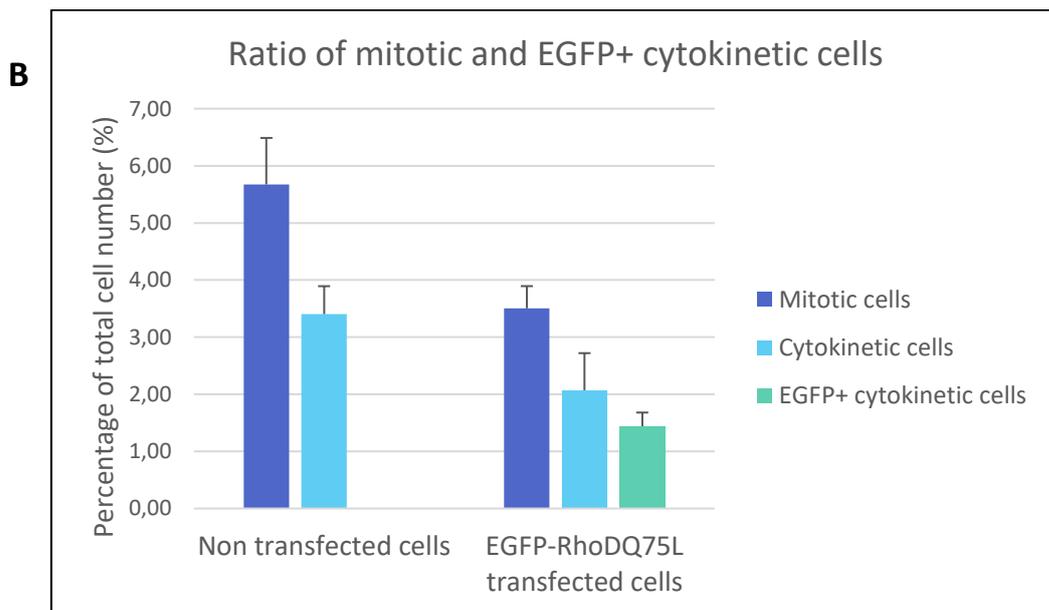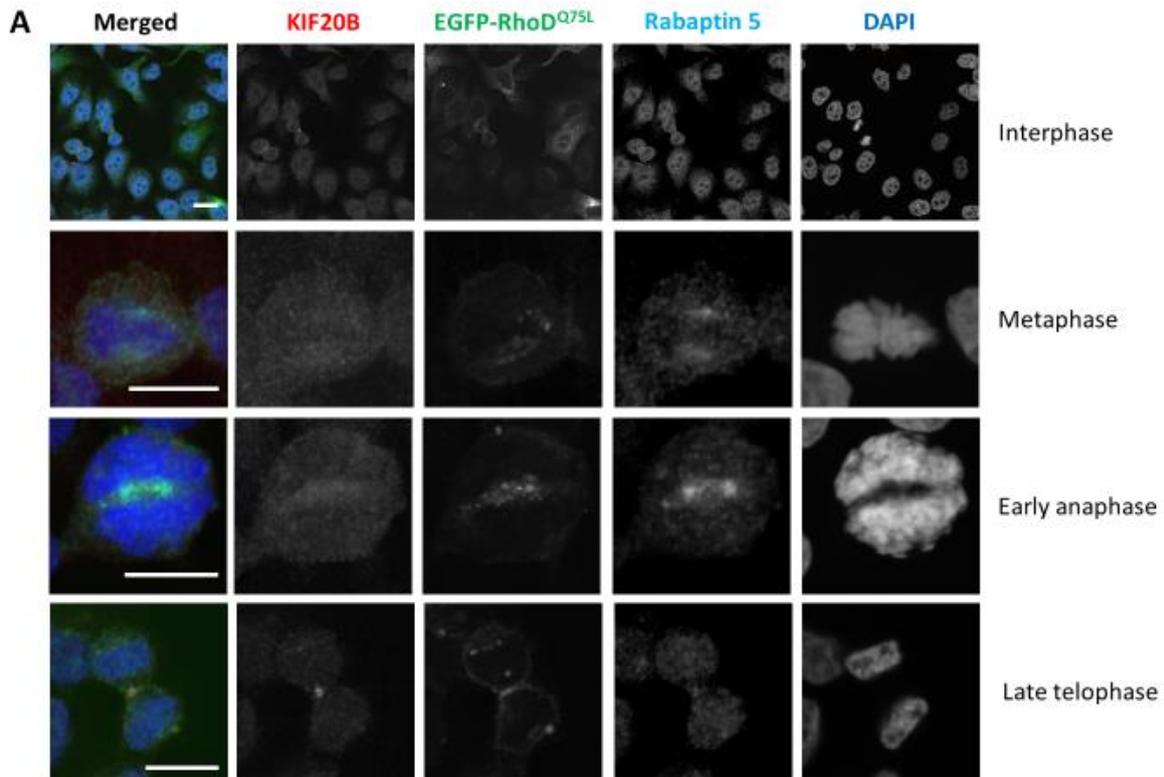
Figure 4.2.10. Exogenous RhoD localizes at the midbody of telophase HeLa cells, in between KIF20B foci. A) HeLa cells were transfected with plasmid expressing EGFP tagged RhoD^Q75L mutant (green). After 48 hours of incubation, cells were fixed and stained with antibodies against KIF20B (red) and Rabaptin 5 (cyan). The nuclei were counterstained with DAPI (blue). B) Ratio of mitotic and cytokinetic HeLa cells in non transfected and EGFP-RhoD^Q75L transfected cells. For EGFP-RhoD^Q75L transfected cells the percentage of EGFP-expressing cells in cytokinesis is also shown. Values shown are average from two different experiments. Error bars denote standard deviation between the experiments. N = 80. Scale bar = 15 µm.

The average amount of mitotic cells in the non-transfected HeLa population was 5,68 ± 0,81%, and the amount of cytokinetic cells was 3,41 ± 0,49%. Obviously, in non-transfected cells there were no EGFP-positive cells. I have compared these amounts to the EGFP-RhoD^Q75L transfected cells, which have about 30% of EGFP expression rate, as shown previously. In

these cells, the mitotic population was a bit lower, perhaps due to the transfection, namely 3,51 ± 0,39%. The ratio of cytokinetic cells was also lower than in control non-transfected cells, with 2,07 ± 0,65% cells. Out of all the cell population, only 1,44 ± 0,24% of cells were both in the cytokinesis stage of division and expressing the EGFP-RhoD construct (N = 80 cells). In the EGFP-RhoD^{G26V} transfected cells, the rate of EGFP-expressing cells is below the range of the mitotic cell ratio of HeLa cells, and sometimes only a few cells expressing the EGFP tagged RhoD protein can be found, that are in the desired stage of cell division. That is why here I presented data for only the EGFP-RhoD^{Q75L} construct. Interestingly, in every cytokinetic cell that was expressing either of the EGFP-RhoD constructs (WT, Q75L and G26V), I have found that the exogenous RhoD localizes at the midbody of cytokinetic cells, even in cells where KIF20B was knocked down by specific siRNAs (example in Figure 4.2.11.). From the data presented in Figures 4.2.8., 4.2.9. and 4.2.10., I can conclude that during cell division, the
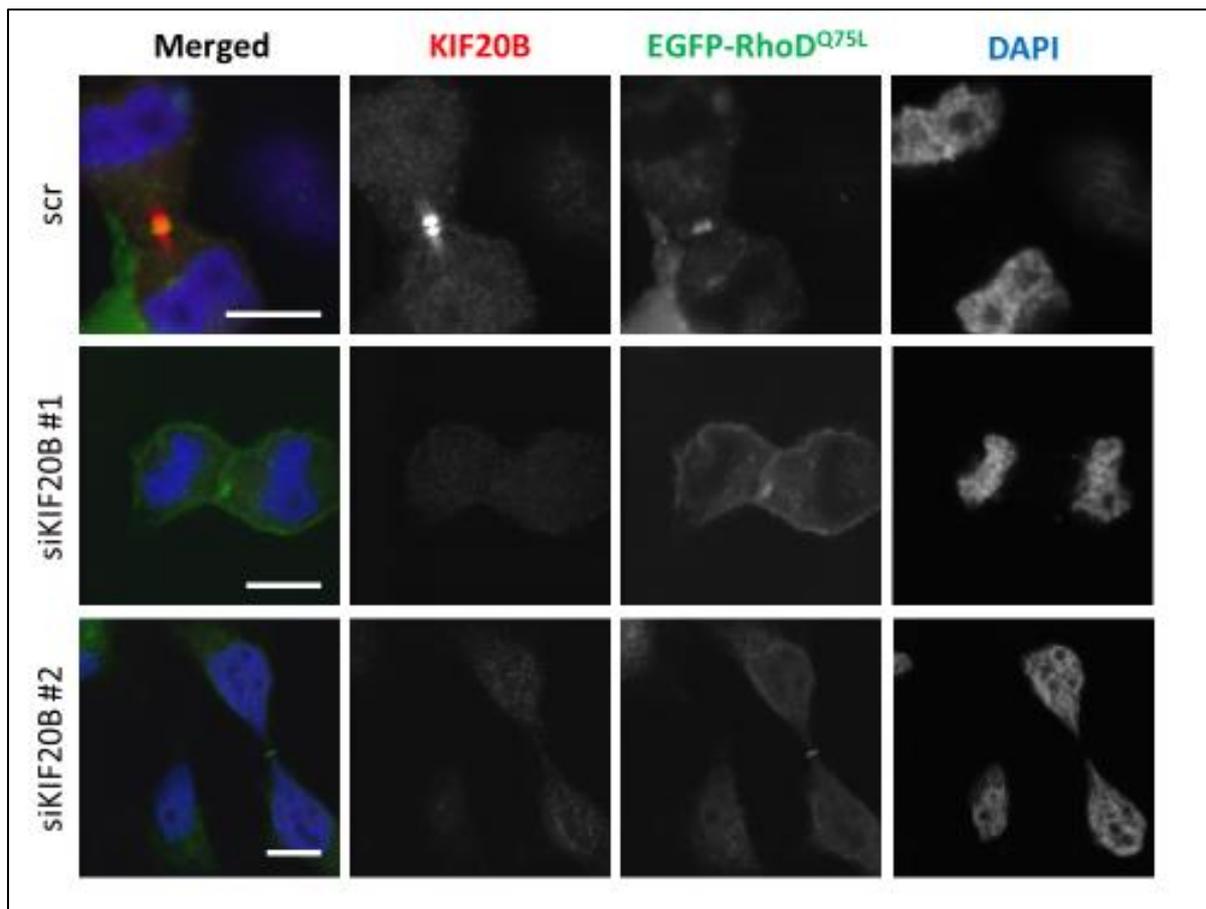
Figure 4.2.11. RhoD-EGFP localizes in the intercellular bridge of transfected cytokinetic cells even in the absence of KIF20B. *Cells were cotransfected with plasmid expressing EGFP tagged RhoD^{Q75L} mutant and siRNA directed at KIF20B or control siRNA (scr) at 10 nM final concentration. After 48 hours of incubation, cells were fixed and stained with antibodies against KIF20B (red). The nuclei were counterstained with DAPI (blue). Scale bar = 10 μm.*

localization of exogenous RhoD changes from concentrating at the perinuclear area of the interphase cell.

To follow the early endosome compartment, in which RhoD is also situated, I have stained cells for Rabaptin 5 (the interactor of Rab5, a protein which localizes to early endosomes) (Figure 4.2.10. A). In early anaphase, the localization of EGFP-RhoD^{Q75L} coincides with KIF20B and Rabaptin 5 in between the segregating chromosomes, and suggests that RhoD is situated in endosomal structures. During late anaphase there is no colocalization between RhoD and KIF20B as KIF20B migrates to microtubules and RhoD is present throughout the cell as a diffuse signal. However, the most striking localization of exogenous RhoD is that during telophase, when RhoD can be visualized as a prominent strip of signal in the intercellular bridge. Coincidentally, KIF20B signals frame the RhoD signal in this area, with some overlap suggesting colocalization (Figures 4.2.10. A, last row, and 4.2.11. first row). Thus far, the localization of RhoD has never before been described in the intercellular bridge during telophase, although a role for RhoD in cytokinesis has been speculated in its early research (Tsubakimoto et al., 1999). KIF20B knockdown, on the other hand, does not influence this localization, as shown in Figure 4.2.11., which was confirmed with two different KIF20B siRNAs. These results suggest that cellular localization of RhoD is dependent on its activation during mitosis. Moreover, KIF20B is not concentrated at midbody in the RhoD-depleted cells, suggesting that RhoD activity is indispensable for localization of KIF20B during mitosis. In HeLa CK cells, EGFP-RhoD signals were also found at the described area of the intercellular bridge, and were present in all the constructs and even in the absence of KIF20B (data not shown).

4.2.5. Exogenous RhoD localizes at the midbody of cytokinetic CaCO-2 cells

In CaCO-2 cells, the same localization for EGFP-RhoD was observed at cell-cell boundaries and perinuclearly in interphase cells, as in HeLa cells. This was verified for both EGFP-RhoD mutants, as shown in Figure 4.2.12. A. The transfection ratio of the EGFP-RhoD constructs was rather low, as demonstrated in Figure 2.12. B, however the transfection rate of the RhoD^{Q75L} was still better than that of the EGFP-RhoD^{G26V} construct (6,87 ± 4,43 % and 1,41 ± 0,70%, respectively). When compared to the overall transfection rate of the GFP-expressing plasmid, which has a transfection rate of 5,94 ± 3,17%, it is evident that the RhoD^{Q75L} construct has a better transfection efficiency than RhoD^{G26V}. For comparison, in

HeLa cells, the GFP-expressing plasmid alone has a transfection rate of 48,99%, even when cotransfected with negative control siRNA (data not shown).
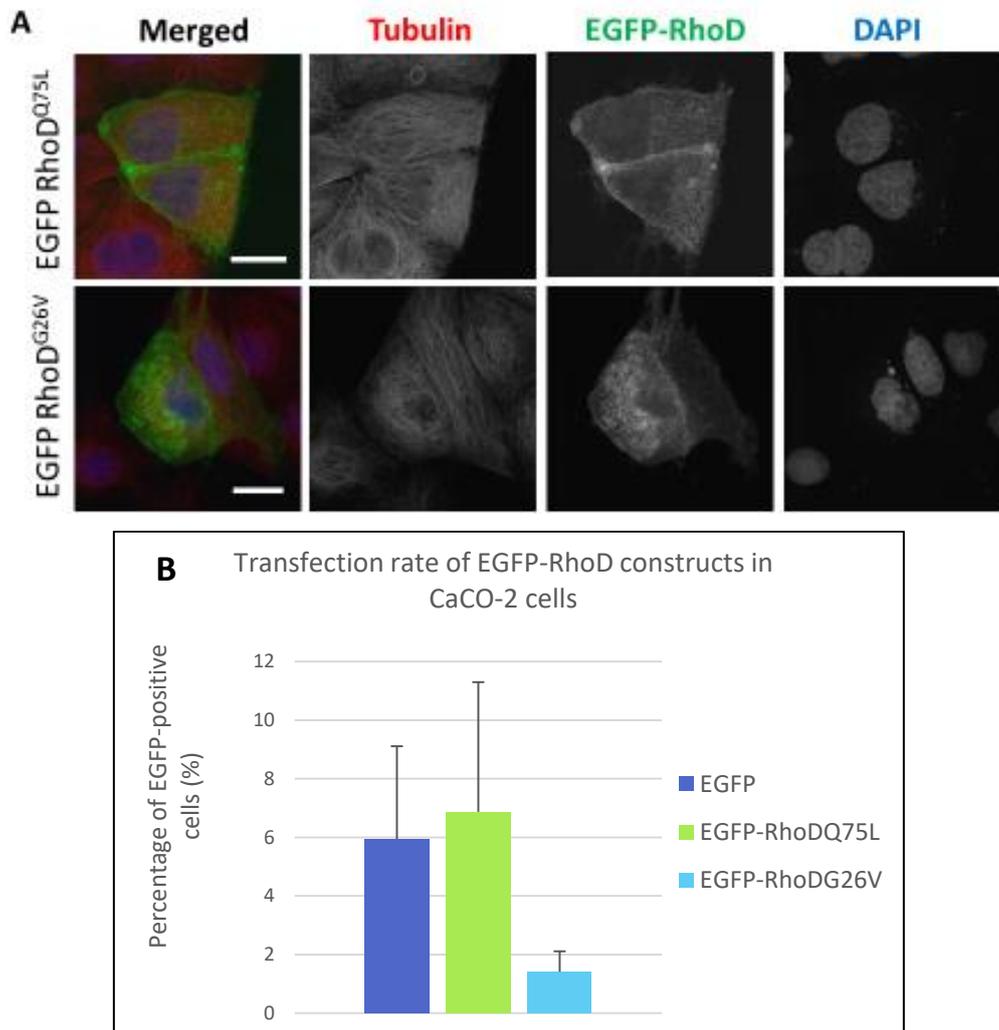
Figure 4.2.12. Exogenous RhoD localizes perinuclearly and in cell-cell contacts of interphase CaCO-2 cells. A) *CaCO-2 cells were transfected with plasmid expressing EGFP tagged RhoD^{Q75L} or RhoD^{G26V} mutant (green). After 48 hours of incubation, cells were fixed and stained with antibodies against tubulin (red). The nuclei were counterstained with DAPI (blue).* **B)** *Transfection rates of EGFP expressing plasmid and EGFP-RhoD constitutively active constructs. Values shown are average from two separate experiments. Error bars denote standard deviation between the experiments. N = 100 cells. Scale bar = 20 µm.*

As for EGFP-RhoD localization during cell division, it was very similar to one observed in HeLa cells (Figure 4.2.13., demonstrated on EGFP-RhoD^{Q75L} transfected CaCO-2 cells). During interphase, metaphase and anaphase, RhoD signal was overlapping with Rabaptin 5 signals, indicating this was indeed the early endosome compartment. During late telophase, the RhoD signal at intercellular bridge was clearly visible between KIF20B signals, and also colocalized with Rabaptin 5. Henceforth, the EGFP-RhoD signal at the intercellular bridge was confirmed in two cancer cell lines from different origins, implying that this newly found localization of active RhoD may have a global significance across cell lines.
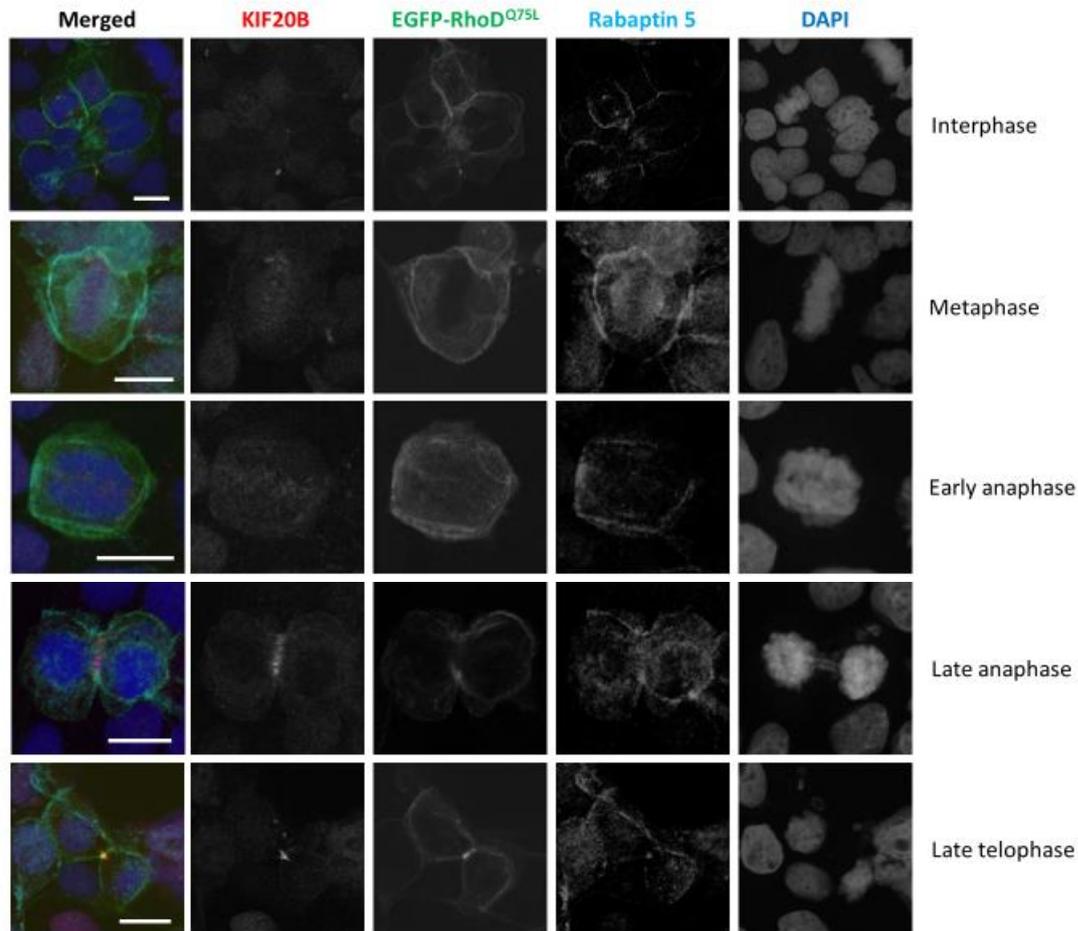
Figure 4.2.13. Exogenous RhoD^{Q75L} mutant localizes at the midbody of telophase CaCO-2 cells, in between KIF20B foci. *CaCO-2 cells were transfected with plasmid expressing EGFP tagged RhoD^{Q75L} mutant (green). After 48 hours of incubation, cells were fixed and stained with antibodies against KIF20B (red) and Rabaptin 5 (cyan). The nuclei were counterstained with DAPI (blue). Scale bar = 15 μm.*

4.2.6. Exogenous RhoD localizes at the cell-cell boundaries of MDA-MB-468 and MCF-7 cells

Since the transfection rates of EGFP-RhoD constructs in the breast carcinoma MDA-MB-468 and MCF-7 cells were rather low (Table 4.2.1.), I was only able to determine that in the interphase cells exogenous RhoD localizes in the cell-cell boundaries, as was previously established in HeLa and CaCO-2 cells (Figure 4.2.14.). In telophase cells the signal was diffused in the cytoplasm and the intercellular bridge, and not showing any particular concentration at or around the midbody, which was evident in both negative control and cells where KIF20B was knocked down (data not shown).

Table 4.3.1. Transfection rate of EGFP-RhoD^{WT} and EGFP-RhoD^{Q75L} constructs in MDA-MB-468 and MCF-7 breast carcinoma cells. The presented values are from a representative experiment.

Cell line	EGFP-RhoD^{WT}		EGFP-RhoD^{Q75L}	
	scr	siKIF20B	scr	siKIF20B
MDA-MB-468	7,86 %	7,61 %	11,54 %	9,09 %
MCF-7	20,07 %	23,11 %	13,92 %	10,99 %
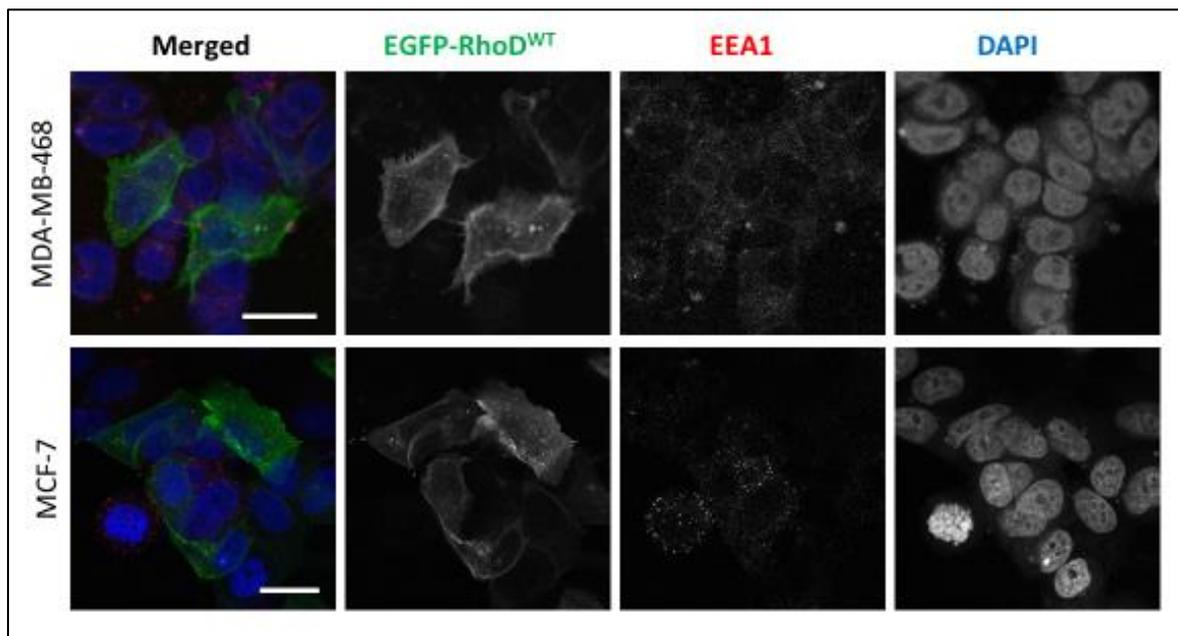
Figure 4.2.14. Exogenous RhoD^{WT} localizes at cell-cell junctions in interphase MDA-MB-468 and MCF-7 breast carcinoma cells. *Cells were transfected with plasmid expressing EGFP tagged RhoD^{WT} (green). After 48 hours of incubation, cells were fixed and stained with antibodies against EEA1 (red). The nuclei were counterstained with DAPI (blue). Scale bar = 20 µm.*

4.3. Cell synchronization and flow cytometry in HeLa cells upon RhoD and KIF20B knockdown reveal possible roles for RhoD in cell division

4.3.1. Synchronization of HeLa cells upon RhoD knockdown reveals an increase in the number of late telophase cells

Since I have observed the interaction of RhoD with KIF20B by the yeast-two-hybrid assay, and their mutual localization in the intercellular bridge during late telophase, I was interested in evaluating if RhoD or KIF20B knockdown caused arrests in cell division.
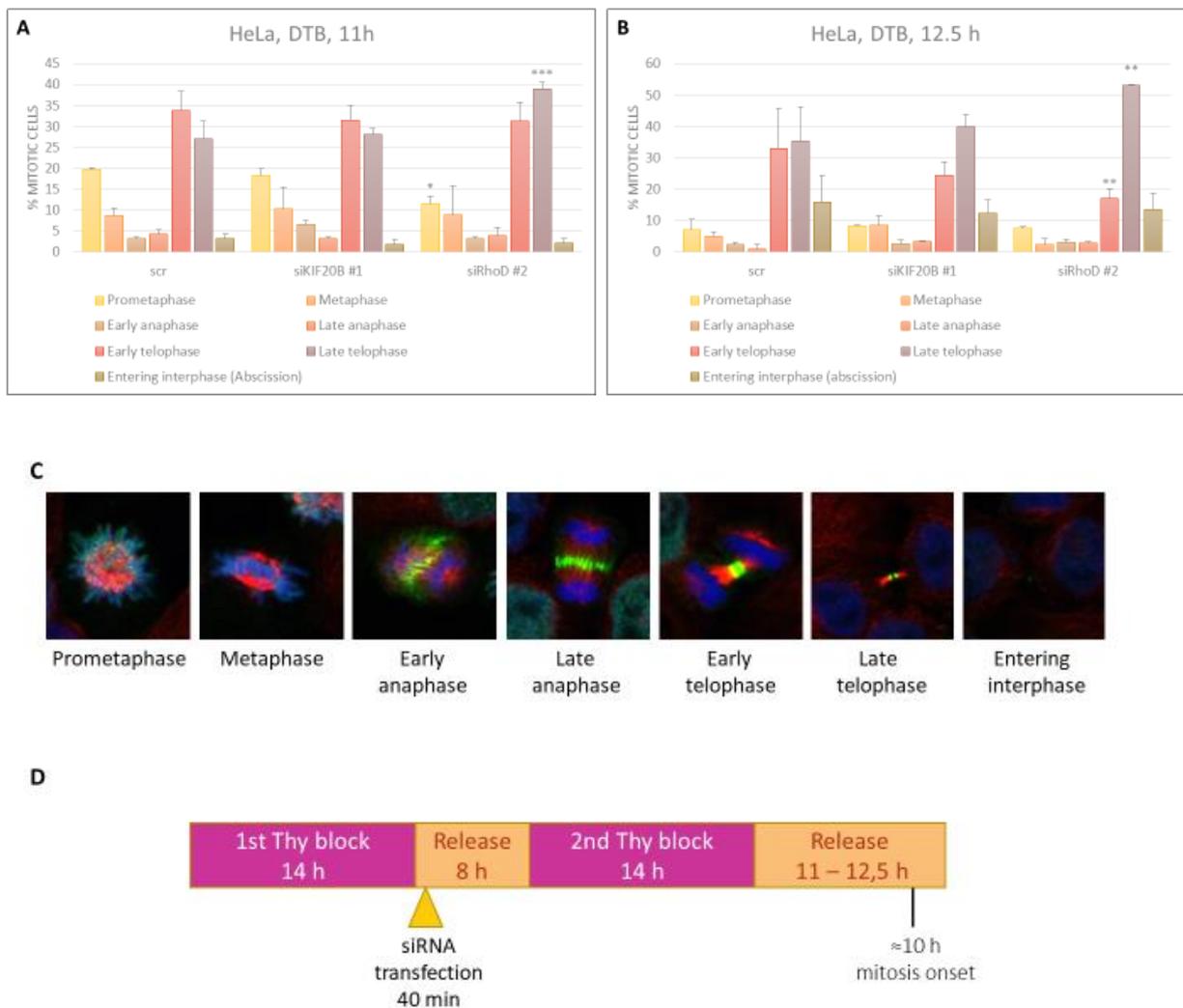
Figure 4.3.1. Following RhoD knockdown there is an increase in the number of late telophase HeLa cells. Cells were silenced during the second thymidine block with 1nM final concentration of siRNA, and fixed and stained A) 11 and B) 12,5 hours after release. Cells were counted under confocal microscope by assessing mitotic cell phenotypes. N > 100 cells. Error bars denote standard deviations between two separate experiments. Statistical significance was calculated using two-way ANOVA with Dunnett's multiple comparison test. *denotes P < 0,05; ** P <0,005 and *** P < 0,0005. C) Definition of mitotic phase species quantified in A and B. Cells were fixed and stained with antibodies against tubulin (red) and KIF20A (green). The KIF20A stained cells are depicted here for the sake of visualization. The nuclei were counterstained with DAPI (blue). D) Schematic representation of cell synchronization experiment.

To determine if there was a delay in some of the processes occurring during cell division, cell synchronization with double thymidine block (DTB) was performed on cells that were knocked down for KIF20B or RhoD.

In the DTB protocol cells are arrested early in S-phase, at the G1/S boundary, and then progress synchronously through G2 and mitotic (M) phase. Excess thymidine added to the culture medium inhibits DNA synthesis and arrests cells in late G1 or early S phase after second block, after which they synchronously progress through G2 and M phases of the cell cycle. This particular protocol of arrest, was chosen due to an increase in multinucleation phenotype 48 hours after knockdown with either RhoD or KIF20B specific siRNA and I wanted to see if there were any delays in the progression of mitosis. Since I found localization of RhoD in the intercellular bridge, with signals overlapping with KIF20B, and taking into consideration that KIF20B has a role in cytokinesis, I wanted to see if after knockdown of either of these genes, the mitotic profiles shared any similarities. Knockdown was performed during release from the first thymidine block and cells were fixed and stained 11 or 12,5 hours following the release from the second thymidine block. At these timepoints, the synchronized HeLa cells reach telophase (Yasuda and Narumiya, 2006), meaning that cell division is nearly finished in most of the treated cells. By counting the cells in different phases of cell division, it can be concluded if there was a delay in any of the mitotic phases after RhoD or KIF20B knockdown, when compared to control. At the 11 h time point, in the control sample (scr) it can be seen that most cells have reached the telophase stage of division (more than 50% of mitotic cells) (Figure 4.3.1. A). About 20% of mitotic cells is still in the prometaphase stage for the control sample. After KIF20B knockdown, the mitotic phase profiles are nearly the same as in control sample at the 11 h time point. However, the RhoD knockdown sample shows a significant increase in number of late telophase cells and decrease in prometaphase and metaphase cells, indicating that upon RhoD knockdown cell division progressed slightly faster than in control and KIF20B silenced cells.

At the 12,5 h time point (Figure 4.3.1. B), in control sample there are less prometaphase, metaphase and anaphase cells than in the 11 h time point, which is expected, meaning that mitosis has progressed forward and most cells are now at its final stages, telophase, and mitosis exit (marked as entering interphase/abscission on the graph and defined as cells which have resolved cytokinesis identifiable by midbody remnant or severed intercellular bridge). The amount of these cells has increased at the 12,5 h time point, when compared to

11h, which is also expected. Although the total number of telophase cells (early and late telophase combined) is similar between control cells and cells after KIF20B or RhoD knockdown, still in siRhoD sample there is a higher amount of late telophase than early telophase cells, suggesting that there is indeed a faster progression of RhoD knocked down cells through mitosis.

4.3.2. Cell cycle analysis in HeLa cells upon RhoD and KIF20B knockdown reveals a distinct G1/S phase gap

To further determine the role that RhoD might have during cell proliferation, and if there is a connection to KIF20B in this role, I have conducted cell cycle analysis of propidium iodide content by flow cytometry on HeLa cells after RhoD or KIF20B knockdown. Cells were collected 72 hours post transfection to procure enough time for cell division events, since the observed multinucleate phenotype still fell in the natural range of HeLa cells multinucleation rate.
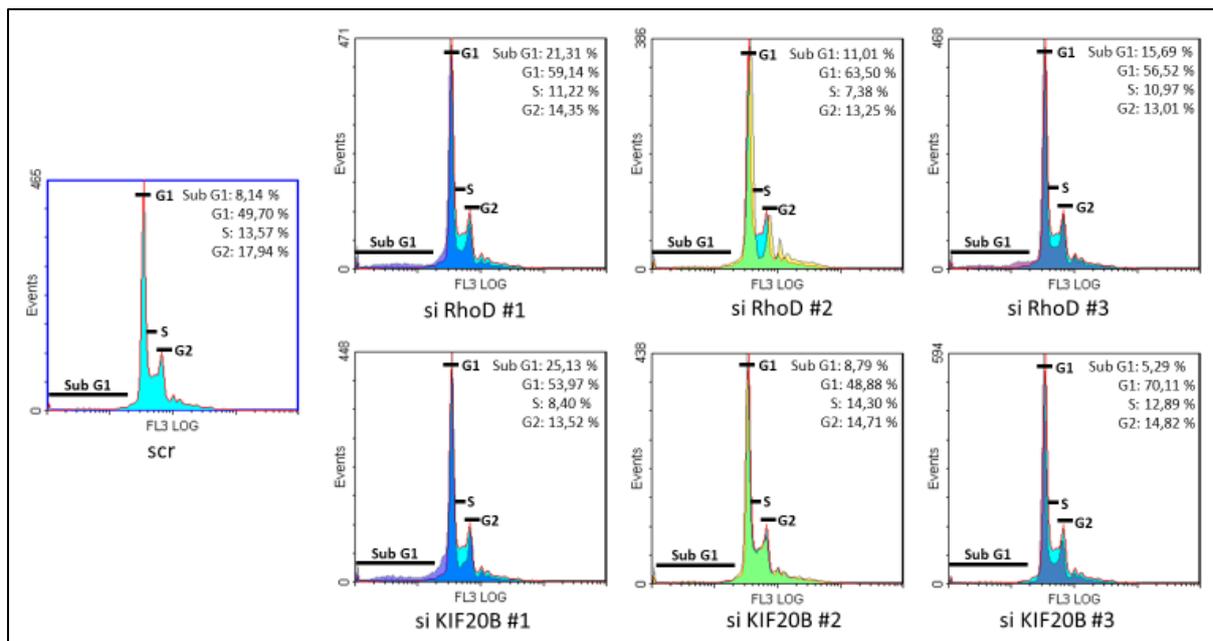
Figure 4.2.2. Cell cycle analysis in HeLa cells reveals a G1/S phase gap upon RhoD and KIF20B knockdown. Flow cytometry cell cycle analysis by PI incorporation on HeLa cells, 72 h post transfection with 10 nM final concentration of RhoD or KIF20B specific siRNAs. The data for each sample was obtained from 20000 cells. The negative control sample cell cycle histogram profile is shown on the left, and it was superimposed on histogram data from every tested sample, with a red outline. The data for siRhoD samples is shown in the upper, and for siKIF20B samples, in the lower row. The figure shown is representative data out of 2 experiments.

Similar to the results of Kyrkou et al. in 2012, who have obtained results 48 hours after transfection, I have also noticed a distinctive G1/S phase gap upon RhoD knockdown in all

three tested siRNA samples (Figure 4.3.2., upper panels). The RhoD siRNAs #1 and #3 also show a small portion of sub G1 population compared to control, indicating a low degree of apoptotic cells in the samples. Interestingly, a very similar cell cycle profile to that of HeLa cells after RhoD knockdown arose in two of the HeLa cells samples following KIF20B knockdown (Figure 4.3.2., lower panels). Thus far data pertaining cell cycle analysis of KIF20B silenced cells has only been published regarding HCT-116 cells (Abaza et al., 2003), and interpreted only in the context of a hypodiploid peak appearing 72 hours after knockdown, indicating an increase in the presence of apoptotic cells. This is the first time that data considering cell cycle analysis regarding different phase distribution upon KIF20B knockdown was reported. Coincidentally, I have observed a higher amount of apoptotic cells also upon knockdown with one KIF20B siRNA (#1).

Together, the cell cycle data for HeLa cells upon RhoD and KIF20B knockdown show an intriguingly similar pattern, with the distinct G1/S gap for all three tested RhoD siRNAs and two of the tested KIF20B siRNAs. These results also suggest that there is a functional relationship between RhoD and KIF20B, at least in the G1/S phase transition.

4.4. RhoD and KIF20B knockdown decreases proliferation in several tumor cell lines, and sensitizes HeLa cells to cisplatin

To assess if RhoD and KIF20B might have a role in sensitivity of tumor cell lines to anticancer drugs, gene knockdown of RhoD and KIF20B has been achieved by transfection of specific siRNAs and MTT assay, upon exposure of cells to cisplatin (cDDP), paclitaxel (PTX) or vincristine (VCR), was performed. CDDP is primarily a DNA damaging drug (Dasari and Tchounwou, 2014), although it has been shown that it induces the formation of reactive oxygen species which can trigger cell death (Brozović et al., 2008). PTX and VCR are both microtubule targeting agents which have opposing mechanisms of action to microtubules, i.e. PTX stabilizes while VCR destabilizes microtubules (Morris and Fornier, 2008). Since KIF20B was found to also be a microtubule stabilizing protein (Abaza et al., 2003), I hypothesized that these two microtubule targeting drugs might have an effect in KIF20B depleted cells, especially given that the area of cell response to anticancer drugs tied to KIF20B expression is beginning to emerge (Tan et al., 2012; X. Liu et al., 2014; X. Liu et al., 2018). The research regarding roles of RhoD in anticancer drug treatment comprises of a single paper showing a decrease in RhoD expression in MCF-7 breast adenocarcinoma cell line resistant to cisplatin (Watson et al., 2007) indicating that the expression of RhoD might be related to sensitivity to therapy.

4.4.1. RhoD or KIF20B knockdown increases sensitivity to cDDP in HeLa cells but decreases sensitivity in CaCO-2, HCT-116, MDA-MB-231, MDA-MB-468 and MCF-7 cells

In order to assess tumor cell sensitivity to cDDP upon RhoD or KIF20B knockdown, I measured cell proliferation in the presence of different concentrations of cDDP using MTT assay. Due to an apparent decrease in cell proliferation after knockdown of each gene, all of the MTT test data was statistically analyzed by the ANOVA two-way test coupled with Bonferroni post-hoc analysis. This particular statistical test takes into account the effect on proliferation upon transfection with siRNAs in evaluation whether knockdown affects the cells' response to the administered drug. Regardless of the graphical appearance of the response, ANOVA takes into consideration the differences between the raw absorbance data of the negative control (in this case the "scrambled" or negative control of silencing) and the absorbance data of the siRNA in question, for every drug concentration administered in the

MTT test. If these differences grow larger for each subsequent higher concentration of the drug administered, then it is a case where the knockdown and the drug have a synergistic effect which is interpreted as increase in sensitivity. Conversely, if the differences are diminishing upon drug exposure, then the drug and knockdown have opposing or antagonistic effect, which can be interpreted as a decrease in sensitivity upon knockdown, or emergence of resistance. When there are no discernible differences between the negative control and siRNA for each drug concentration, then there is no interaction observed between action of drug and knockdown of a specific gene expression. However, if the knockdown alone causes diminished cell proliferation, independently from the drug, then this is an additive effect to drug action (Motulsky, 2007).
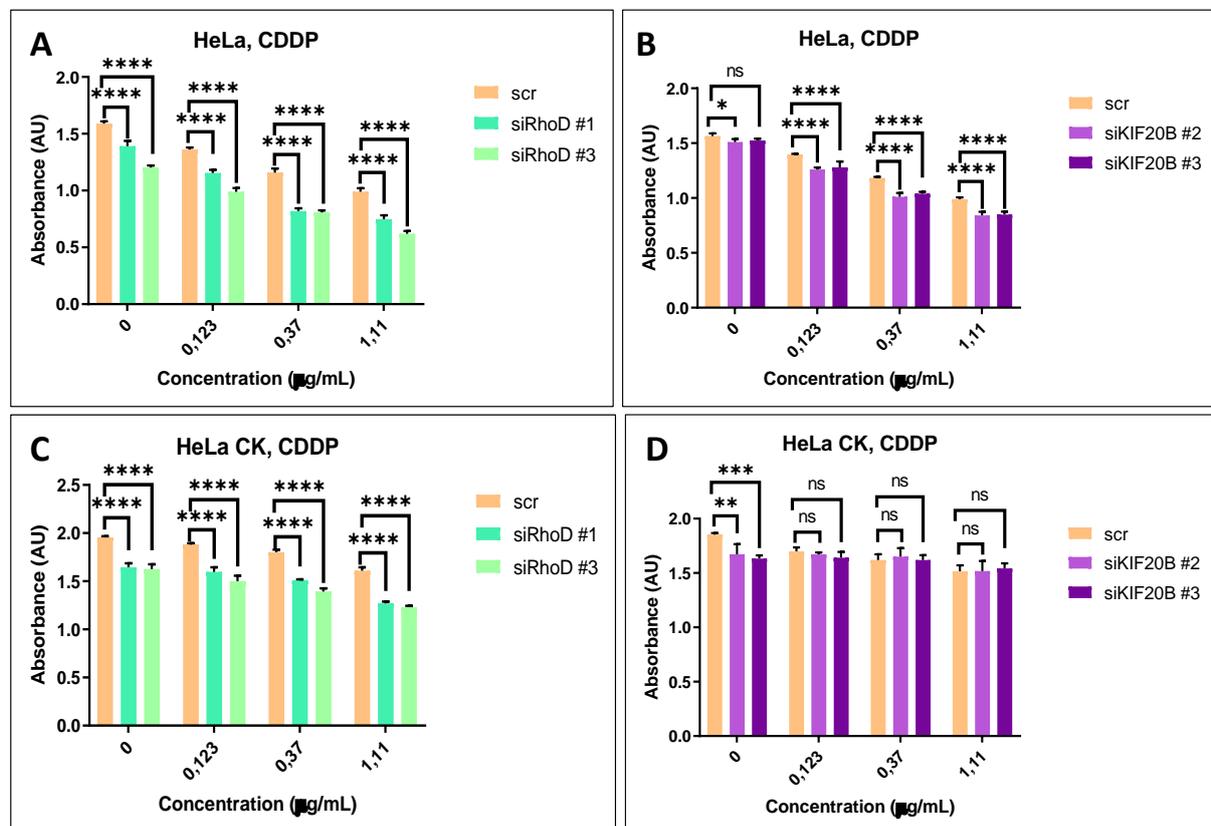
Figure 4.4.1. RhoD and KIF20B individual knockdown confers sensitivity to cDDP in HeLa cells. *MTT assay of HeLa and HeLa CK cells 72 h after treatment with cisplatin and 120 h post transfection.* ***A)*** *Response to cDDP in HeLa cells after RhoD knockdown and* ***B)*** *KIF20B knockdown.* ***C)*** *Response to cDDP in HeLa CK cells upon RhoD and* ***D)*** *KIF20B knockdown. The data shown are representative from a minimum of two experiments. Error bars signify standard deviations of triplicate absorbance values in a single experiment. Statistical significance was calculated by using two-way ANOVA with Bonferroni's post-hoc analysis test. * denotes P<0,05; ** denotes P<0,005; *** denotes P<0,0005 and **** P<0,00005; ns = non significant.*

HeLa cells have demonstrated an increase in sensitivity to cDDP after knockdown of either gene; RhoD or KIF20B (Figure 4.4.1. A and B). However, a similar result was not obtained in HeLa CK cells which were obtained by exposure of Hela cells to cisplatin and which, compared to parental cells, demonstrate cDDP resistance. This may indicate that the preferential pathway of cDDP toxicity is different in HeLa CK cells to that observed in HeLa cells. In HeLa CK there is no interaction of RhoD knockdown on sensitivity to cDDP (Figure 4.4.1. C). In the case of KIF20B knockdown, however, there is a decrease in sensitivity to cDDP in HeLa CK cells (Figure 4.4.1. D). Since the response to cDDP exhibits the same directionality (an increase in cDDP sensitivity) in HeLa cells which was observed with both RhoD and KIF20B knockdown, these two proteins might share the same downstream effectors.
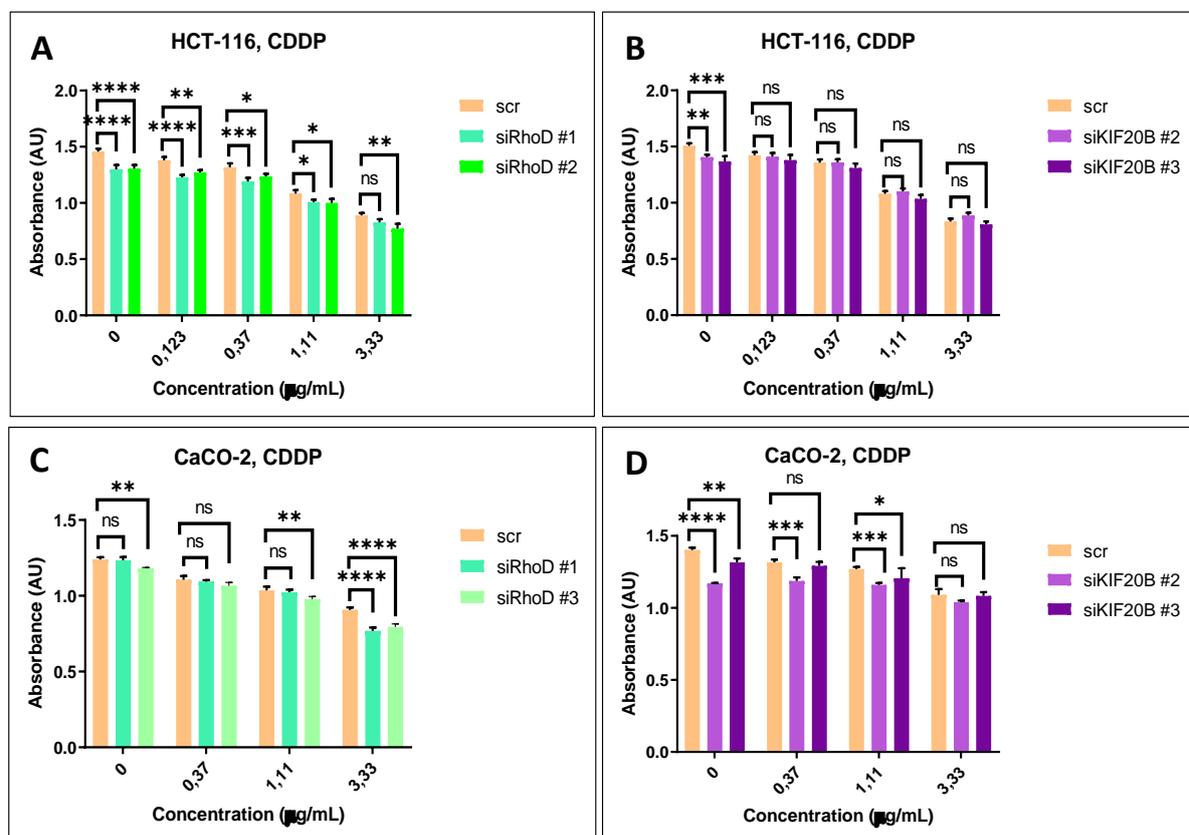
Figure 4.4.2. RhoD and KIF20B individual knockdown confers a decrease in sensitivity to cDDP in HCT-116 cells, no interaction for RhoD knockdown and a decrease in sensitivity to cDDP upon KIF20B knockdown in CaCO-2 cells. MTT assay of HCT-116 and CaCO-2 cells 72 h after treatment with cisplatin and 120 h post transfection. *A)* Response to cDDP in HCT-116 cells after RhoD and *B)* KIF20B knockdown. *C)* Response to cDDP in CaCO-2 cells silenced with RhoD and *D)* KIF20B. The data shown are representative from a minimum of two experiments. Error bars signify standard deviations of triplicate absorbance values in a single experiment. Statistical significance was calculated by using two-way ANOVA with Bonferroni's post-hoc analysis test. * denotes $P<0,05$; ** denotes $P<0,005$; *** denotes $P<0,0005$ and **** $P<0,00005$; ns = non significant.
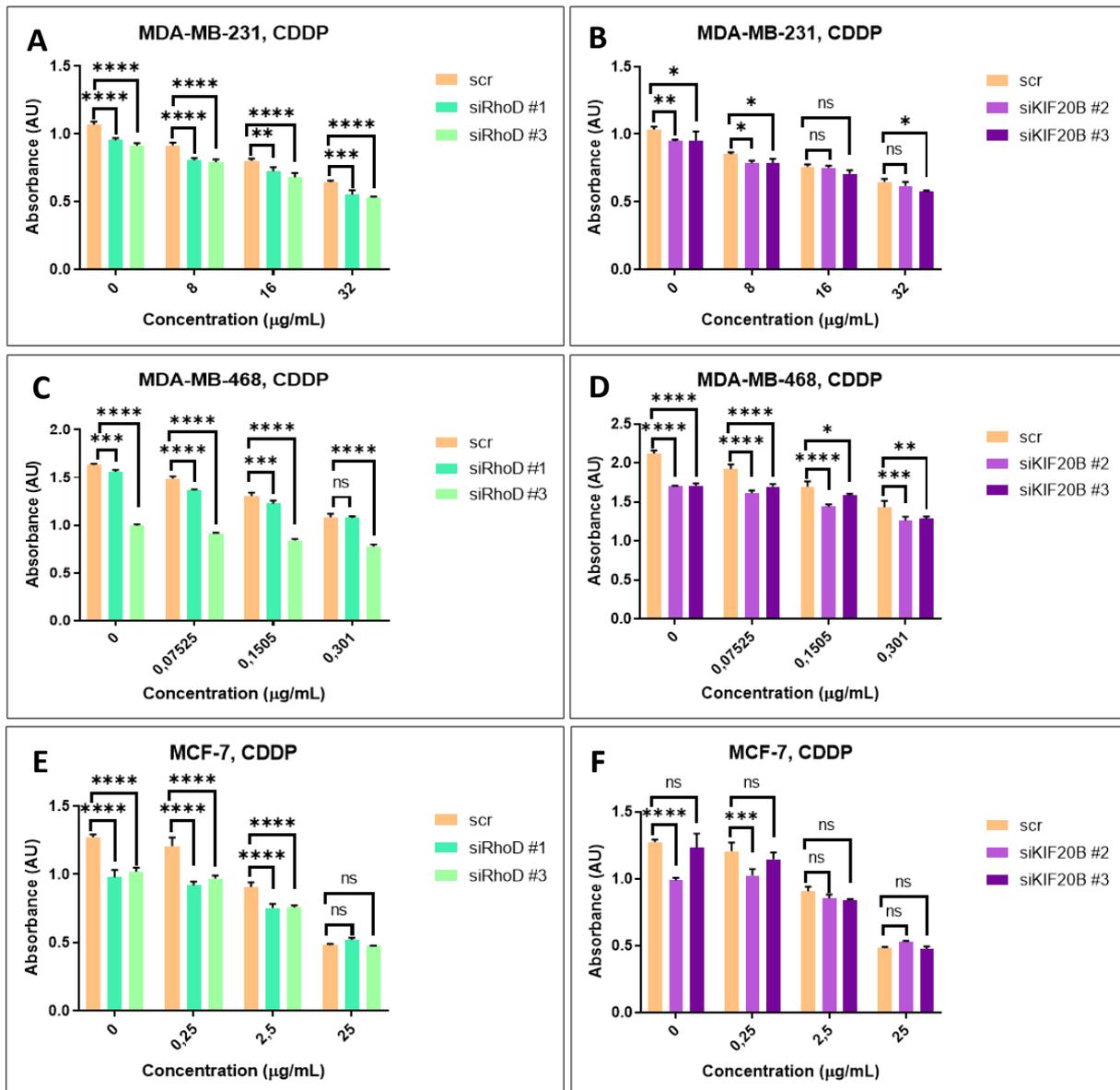
Figure 4.4.3. RhoD knockdown confers a decrease in sensitivity to cDDP in MDA-MB-231, MDA-MB-468 and MCF-7 cells, while KIF20B silencing causes the same effect in MDA-MB-468 and MCF-7 cells. *MTT assay of MDA-MB-231, MDA-MB-468 and MCF-7 cells 72 h after treatment with cisplatin and 120 h post transfection.* **A)** *Response to cDDP in MDA-MB-231 cells silenced for and* **B)** *KIF20B.* **C)** *Response to cDDP in MDA-MB-468 RhoD silenced cells and* **D)** *KIF20B silenced cells.* **E)** *Response to cDDP in MCF-7 cells upon RhoD and* **F)** *KIF20B knockdown. The data shown are representative from a minimum of two experiments. Error bars signify standard deviations of triplicate absorbance values in a single experiment. Statistical significance was calculated by using two-way ANOVA with Bonferroni's post-hoc analysis test. * denotes P<0,05; ** denotes P<0,005; *** denotes P<0,0005 and **** P<0,00005; ns = non significant.*

In HCT-116, the situation is different. The RhoD knockdown decreases sensitivity to cDDP (Figure 4.4.2. A). The same happens also for KIF20B knockdown in HCT-116 cells (Figure 4.4.2. B). On the other hand, in CaCO-2 cells there is no interaction between the cDDP exposure and RhoD k nockdown (Figure 4.4.2. C). However, similarly to HCT-116 cells, when KIF20B is knocked down in CaCO-2 cells a decrease in sensitivity to cDDP is observed (Figure 4.4.2. D). Considering HCT-116 and CaCO-2 cells are both colorectal adenocarcinoma, this similar

response to cisplatin upon KIF20B knockdown may indicate a different mechanism of cDDP toxicity when compared to HeLa cells, which originate from an entirely different tissue.

In the case of three breast adenocarcinoma cell lines, MDA-MB-231, MDA-MB-468 and MCF-7, all three cell lines exhibit a decrease in sensitivity to cDDP upon RhoD knockdown (only for one out of two RhoD siRNAs in MDA-MB-468 cells) (Figure 4.4.3. A, C and E). As for KIF20B knockdown, a decrease in sensitivity to cDDP was in MDA-MB-468 cells (Figure 4.4.3. D), while ambiguous results were obtained for two KIF20B siRNAs in case of MCF-7 cells (Figure 4.4.3. F), showing both no interaction and a decrease in sensitivity to cDDP.

The outcome of combined RhoD or KIF20B knockdown to cDDP sensitivity in different cell lines is summarized in Table 4.4.1. It appears that only in HeLa cells RhoD and KIF20B knockdown induces an increase in sensitivity to cDDP. Recent expression profiling in many tumor cell lines, as compared to normal tissues (Abaza et al., 2003; X. R. Liu et al., 2012; Kanehira et al., 2007; X. Liu et al., 2014; Ansari et al., 2015; X. Liu et al., 2018; W. F. Lin et al., 2018; G. Li et al., 2019; Z. Y. Li et al., 2019), demonstrated increased expression of KIF20B in tumor tissue. Therefore my hypothesis that their knockdown might increase sensitivity to cDDP proved correct only in HeLa cells. For RhoD this is a novel find, which may or may not be linked with KIF20B knockdown-induced response. Thus far RhoD was found to be downregulated in three melanoma cell lines (M14, A375 and MV3), when compared to normal melanocyte cells (Wen et al., 2017).

Table 4.4.1. Summary of response to cisplatin (CDDP) after knockdown of either RhoD or KIF20B. *Data was gathered from assessment of MTT assay results, according to ANOVA statistical analysis. S = increased sensitivity to the drug upon knockdowby specific siRNA; R = decreased sensitivity (induced resistance) to drug after knockdown by specific siRNA; NI = no interaction between drug and siRNA. *denotes different effects to the drug sensitivity in two siRNAs used for the single gene.*

Cell line	Response to CDDP after siRhoD	Response to CDDP after siKIF20B
HeLa	S	S
HeLa CK	NI	R
HCT-116	R	R
CaCO-2	NI	R
MDA-MB-231	R	NI
MDA-MB-468	R/NI*	R
MCF-7	R	R/NI*

Another study found that RhoD was overexpressed in tumor plasma cells of multiple myeloma patient samples, compared to normal (healthy) plasma cells (Andrade et al., 2010). Consistently with the paper reporting that in cisplatin resistant MCF-7 cells RhoD expression was decreased (Watson et al., 2007), I would expect that knocking down RhoD might elicit a decrease in sensitivity to cDDP in MCF-7 cells, which it did.

In conclusion, I showed that in the majority of tumor cell lines knockdown of either RhoD or KIF20B affects the sensitivity to cDDP. Increased sensitivity was observed in HeLa cells while decreased sensitivity in all other tested cell lines. However, the mechanism of this observation remains to be determined.

4.4.2. RhoD knockdown induces a decrease in sensitivity to PTX in all tested cell lines
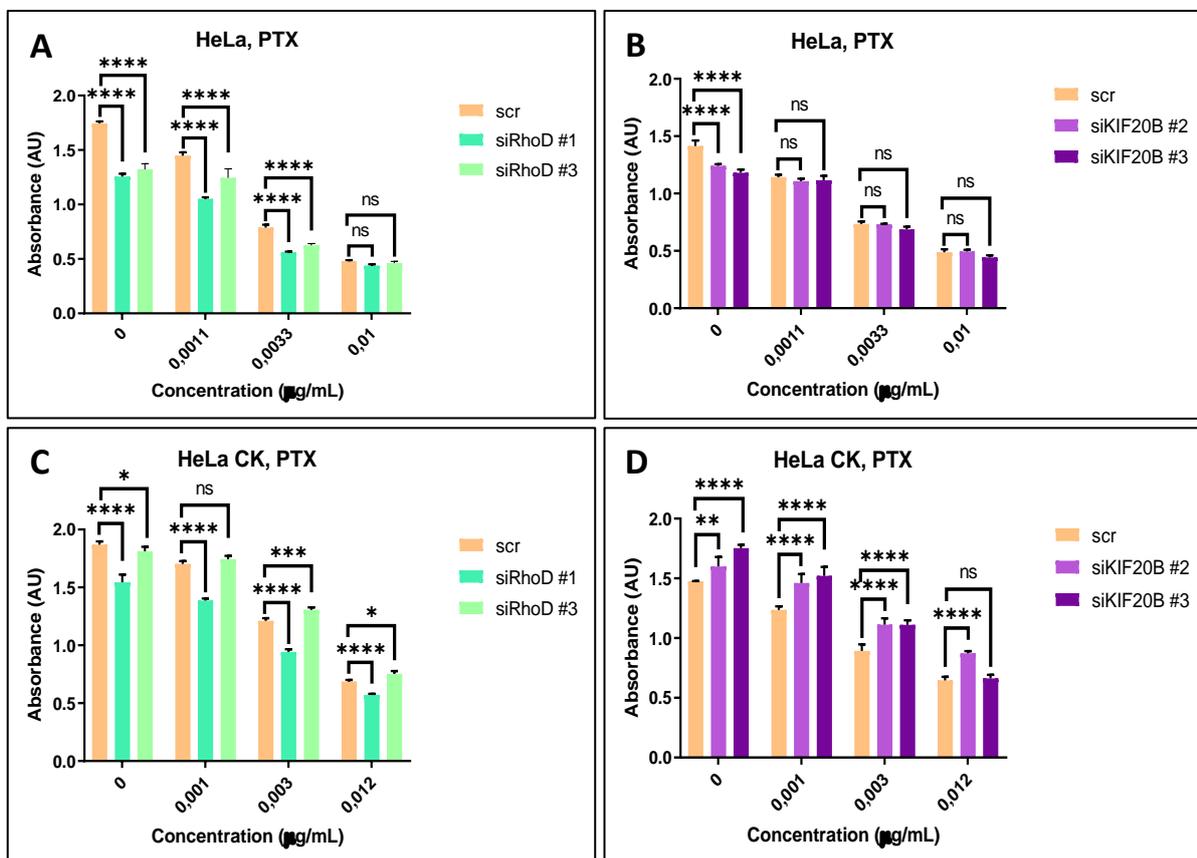
*Figure 4.4.4. RhoD knockdown confers decrease in sensitivity to PTX in HeLa and HeLa CK cells. MTT assay of HeLa and HeLa CK cells 72 h after treatment with PTX and 120 h post transfection. **A)** Response to PTX in HeLa cells upon RhoD and **B)** KIF20B knockdown. **C)** Response to PTX in HeLa CK cells after RhoD and **D)** KIF20B knockdown. The data shown are representative from a minimum of two experiments. Error bars signify standard deviations of triplicate absorbance values in a single experiment. Statistical significance was calculated by using two-way ANOVA with Bonferroni's post-hoc analysis test. * denotes P<0,05; ** denotes P<0,005; *** denotes P<0,0005 and **** P<0,00005; ns = non significant.*

In HeLa, RhoD knockdown decreased sensitivity to PTX (Figure 4.4.4. A) while in HeLa CK one RhoD siRNA decreased and the other showed no interaction with PTX sensitivity

(Figure 4.4.4. C). In the case of KIF20B knockdown in HeLa cells, a decrease in sensitivity to PTX appeared in one tested siRNA (Figure 4.4.4. B). In HeLa CK cells knockdown of KIF20B, there is no interaction between the drug and the siRNAs used (Figure 4.4.4. D).

In colorectal carcinoma cell lines HCT-116 and CaCO-2, knockdown of RhoD decreased sensitivity to PTX in one out of two RhoD siRNAs (Figure 4.4.5. A and C). In HCT-116 cells KIF20B knockdown shows no interaction to PTX (Figure 4.4.5. B).

Figure 4.4.5. RhoD knockdown induces a decrease in sensitivity to PTX in HCT-116 and CaCO-2 cells. *MTT assay of HCT-116 and CaCO-2 cells 72 h after treatment with PTX and 120 h post transfection. **A)** Response to PTX in HCT-116 cells silenced for RhoD and **B)** KIF20B. **C)** Response to PTX in CaCO-2 cells silenced with RhoD and **D)** KIF20B. The data shown are representative from a minimum of two experiments. Error bars signify standard deviations of triplicate absorbance values in a single experiment. Statistical significance was calculated by using two-way ANOVA with Bonferroni's post-hoc analysis test. * denotes P<0,05; ** denotes P<0,005; *** denotes P<0,0005 and **** P<0,00005; ns = non significant.*

In CaCO-2 cells knockdown of both RhoD and KIF20B displays a decrease in sensitivity to PTX with one siRNA, while the other shows no interaction with the drug (Figure 4.4.5. D).

As for breast carcinoma cells, in all three model cell lines, MDA-MB-231, MDA-MB-468 and MCF-7, RhoD knockdown decreases sensitivity to PTX (Figure 4.4.6. A, C and E). In MDA-MB-231 cells, KIF20B knockdown does not affect sensitivity to PTX (Figure 4.4.6. B). In the other

breast cancer cell lines, MDA-MB-468 and MCF-7, KIF20B knockdown induces a decrease in sensitivity to PTX (Figure 4.4.6. D and F).

This ambiguous response of decrease in sensitivity/no interaction in cells upon KIF20B
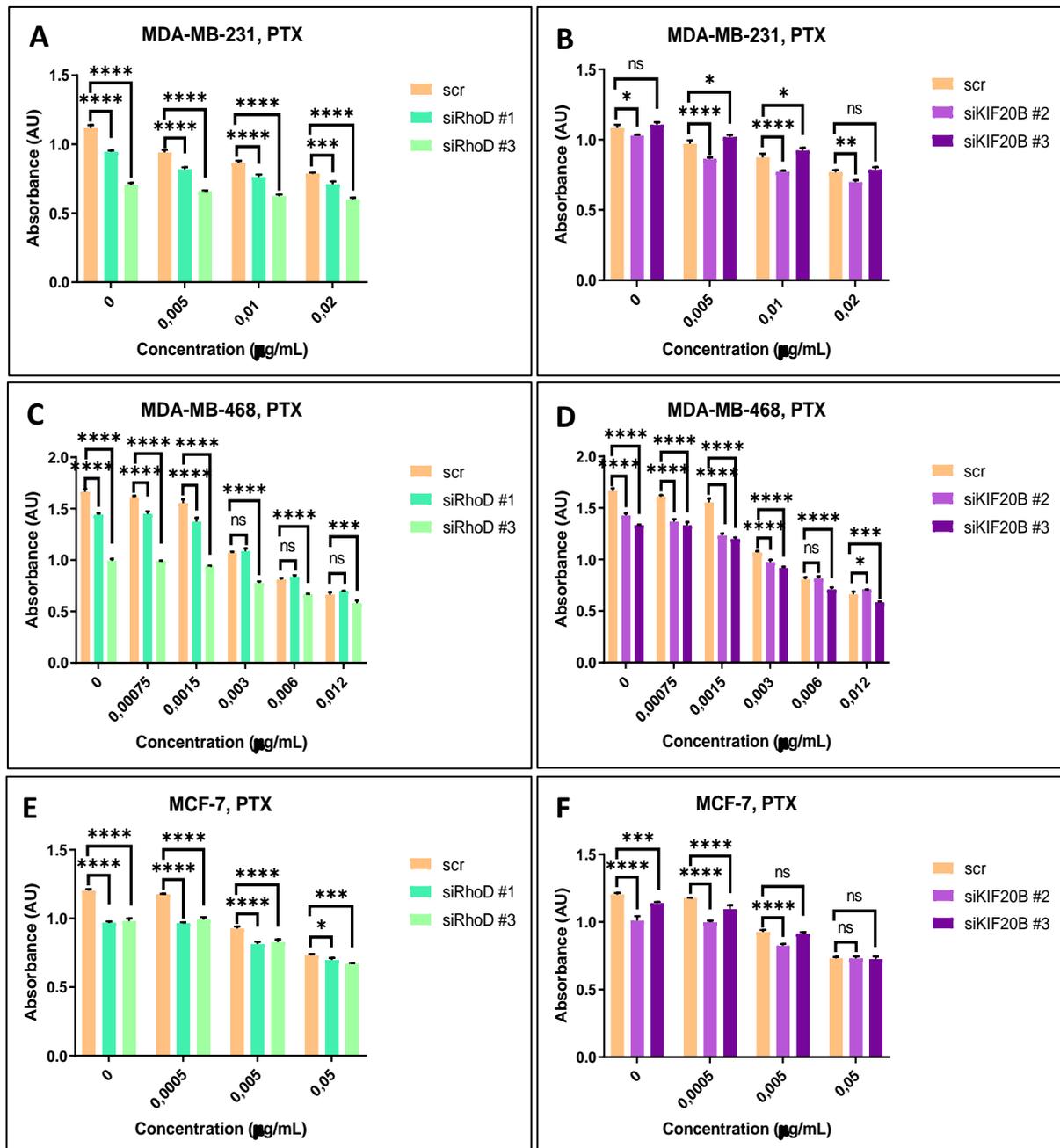
Figure 4.4.6. RhoD knockdown confers a decrease in sensitivity to PTX in MDA-MB-231, MDA-MB-46 and MCF-7 cells, while KIF20B silencing causes this effect only in MDA-MB-468 and MCF-7 cells. *MTT assay of MDA-MB-231, MDA-MB-468 and MCF-7 cells 72 h after treatment with PTX and 120 h post transfection. **A)** Response to PTX in MDA-MB-231 cells silenced for RhoD and **B)** KIF20B. **C)** Response to PTX in MDA-MB-468 cells upon RhoD and **D)** KIF20B knockdown. **E)** Response to PTX in MCF-7 cells upon RhoD and **F)** KIF20B knockdown. The data shown are representative from a minimum of two experiments. Error bars signify standard deviations of triplicate absorbance values in a single experiment. Statistical significance was calculated by using two-way ANOVA with Bonferroni's post-hoc analysis test. * denotes P<0,05; ** denotes P<0,005; *** denotes P<0,0005 and **** P<0,00005; ns = non significant.*

knockdown might be due to knockdown efficiency, which was not as prominent as RhoD knockdown, at least according to the RT-qPCR data.

The results of RhoD and KIF20B knockdown on PTX response across all tested cell lines are summarized in Table 4.4.2.

Table 4.4.2. Summary of response to paclitaxel (PTX) after knockdown of either RhoD or KIF20B. Data was gathered from assessment of MTT assay results, according to ANOVA statistical analysis. S = increased sensitivity to the drug upon knockdown by specific siRNA; R = decreased sensitivity (induced resistance) to drug after knockdown by specific siRNA; NI = no interaction between drug and siRNA. *denotes different effects to the drug sensitivity in two siRNAs used for the single gene.

Cell line	Response to PTX after siRhoD	Response to PTX after siKIF20B
HeLa	R	R/NI*
HeLa CK	R/NI*	NI
HCT-116	R/NI*	NI
CaCO-2	R/NI*	R/NI*
MDA-MB-231	R	NI
MDA-MB-468	R	R
MCF-7	R	R

4.4.3. RhoD knockdown induces a decrease in sensitivity to VCR in HeLa, HCT-116 and MCF-7 cells

In HeLa cells there is a decrease in sensitivity to VCR upon RhoD knockdown (Figure 4.4.7. A), and also upon KIF20B knockdown, although displayed only in one KIF20B siRNA (Figure 4.4.7. B). On the other hand, in HeLa CK cells, there is no interaction with the drug VCR for either RhoD or KIF20B knockdown (Figure 4.4.7. C and D).

In colorectal carcinoma cell line HCT-116 knockdown of RhoD decreased sensitivity to VCR (Figure 4.4.8. A), while in the other colorectal carcinoma cell line CaCO-2 no interaction was observed (Figure 4.4.8. B). KIF20B knockdown in both, HCT-116 and CaCO-2 cells, did not change sensitivity to VCR (Figure 4.4.8. C and D).

Upon RhoD knockdown in the breast carcinoma model cell lines MDA-MB-231, MDA-MB-468 and MCF-7, decreased sensitivity to VCR was observed only in MCF-7 cells (Figure 4.4.9. E), while in other two cell lines no interaction was observed. KIF20B knockdown did not change sensitivity of any of breast carcinoma cell lines to VCR (Figure 4.4.9. B, D and F).

Some similarities were encountered in HeLa cells, regarding the decrease in sensitivity to VCR and PTX upon RhoD or KIF20B knockdown, and also in HCT-116 cells, where RhoD knockdown

also induced decreased sensitivity to VCR and PTX. The results from VCR response to RhoD or KIF20B knockdown are summarized in Table 4.4.3.
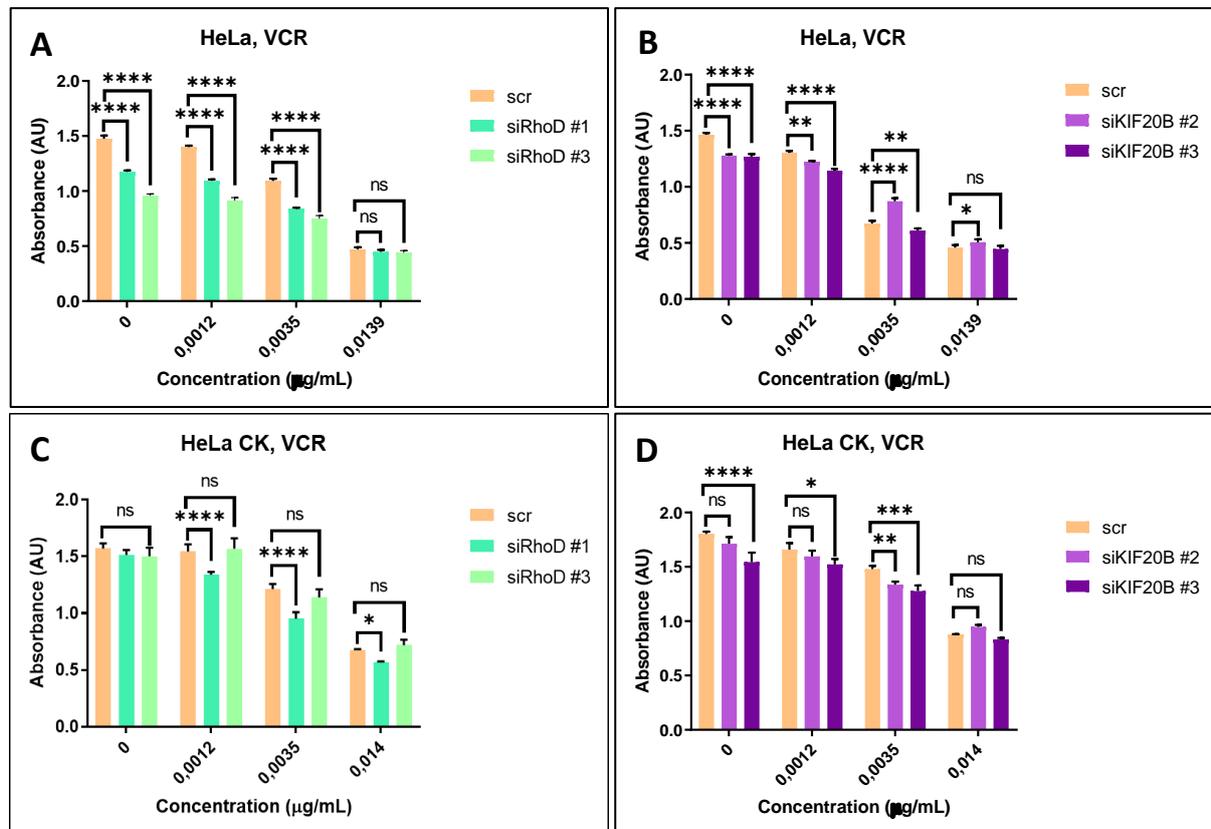
Figure 4.4.7. RhoD and KIF20B individual knockdown confers a decreased sensitivity to VCR in HeLa and no effect in HeLa CK cells. *MTT assay of HeLa and HeLa CK cells 72 h after treatment with VCR and 120 h post transfection.* ***A)*** *Response to VCR in HeLa cells after RhoD and* ***B)*** *KIF20B knockdown.* ***C)*** *Response to VCR in HeLa CK cells silenced for RhoD and* ***D)*** *KIF20B. The data shown are representative from a minimum of two experiments. Error bars signify standard deviations of triplicate absorbance values in a single experiment. Statistical significance was calculated by using two-way ANOVA with Bonferroni's post-hoc analysis test. * denotes P<0,05; ** denotes P<0,005; *** denotes P<0,0005 and **** P<0,00005; ns = non significant.*
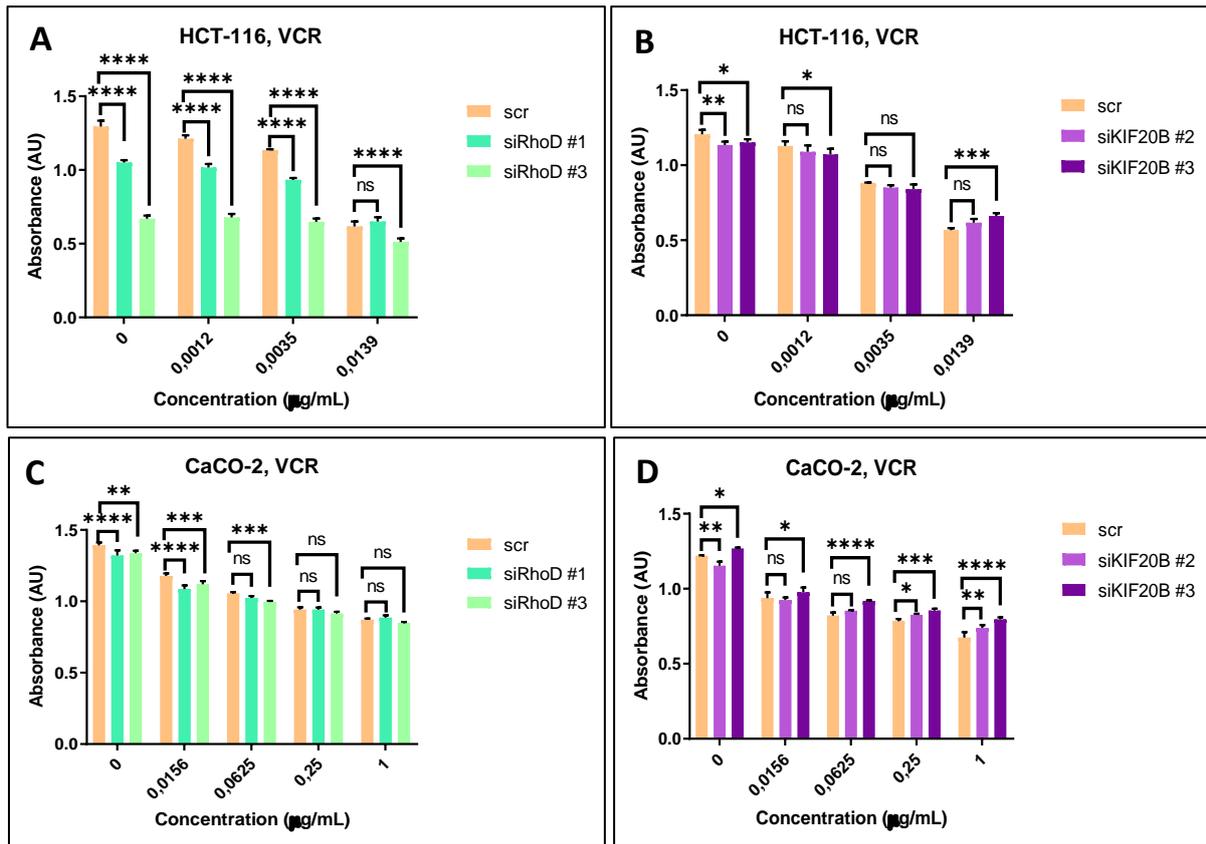
Figure 4.4.8. RhoD knockdown induces a decrease in sensitivity to VCR in HCT-116 cells. *MTT assay of HCT-116 and CaCO-2 cells 72 h after treatment with VCR and 120 h post transfection.* ***A)*** *Response to VCR in HCT-116 cells silenced for RhoD or* ***B)*** *KIF20B.* ***C)*** *Response to VCR in CaCO-2 cells silenced with RhoD or* ***D)*** *KIF20B specific siRNA. The data shown are representative from a minimum of two experiments. Error bars signify standard deviations of triplicate absorbance values in a single experiment. Statistical significance was calculated by using two-way ANOVA with Bonferroni's post-hoc analysis test. * denotes P<0,05; ** denotes P<0,005; *** denotes P<0,0005 and **** P<0,00005; ns = non significant.*

Table 4.4.3. Summary of response to vincristine (VCR) after knockdown of either RhoD or KIF20B. *Data was gathered from assessment of MTT assay results, according to ANOVA statistical analysis. S = increased sensitivity to the drug upon knockdown by specific siRNA; R = decreased sensitivity (induced resistance) to drug after knockdown by specific siRNA; NI = no interaction between drug and siRNA. *denotes different effects to the drug sensitivity in two siRNAs used for the single gene.*

Cell line	Response to VCR after siRhoD	Response to VCR after siKIF20B
HeLa	R	R/NI*
HeLa CK	NI	NI
HCT-116	R	NI
CaCO-2	NI	NI
MDA-MB-231	NI	NI
MDA-MB-468	NI	R/NI*
MCF-7	R	NI
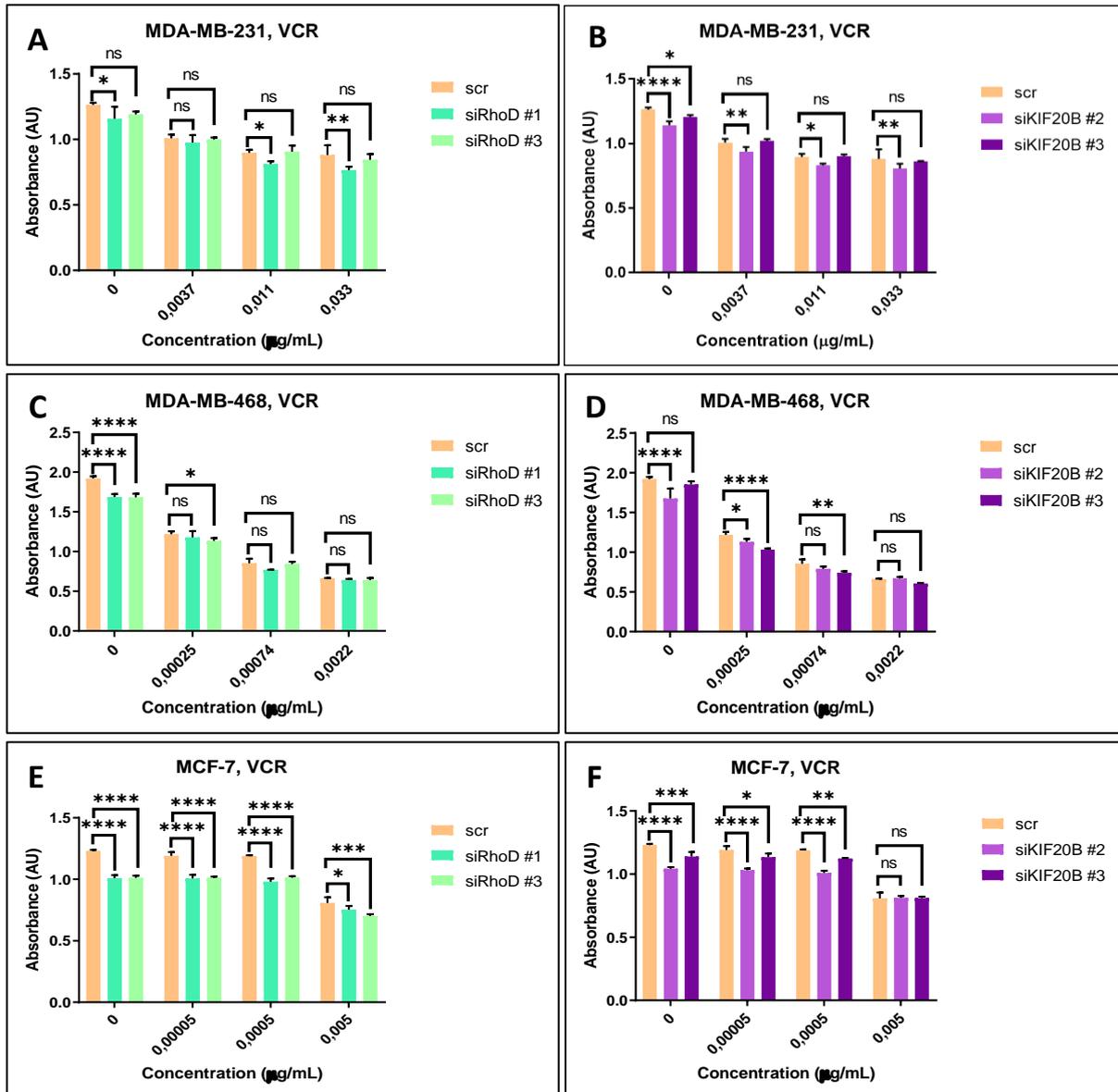
Figure 4.4.9. RhoD knockdown confers decreased sensitivity to VCR in the MCF-7 cell line. *MTT assay of MDA-MB-231, MDA-MB-468 and MCF-7 cells 72 h after treatment with VCR and 120 h post transfection.* ***A)*** *Response to VCR in MDA-MB-231 cells silenced with RhoD or* ***B)*** *KIF20B specific siRNA.* ***C)*** *Response to VCR in MDA-MB-468 cells after RhoD or* ***D)*** *KIF20B knockdown.* ***E)*** *Response to VCR in MCF-7 cells following RhoD or* ***F)*** *KIF20B knockdown. The data shown are representative from a minimum of two experiments. Error bars signify standard deviations of triplicate absorbance values in a single experiment. Statistical significance was calculated by using two-way ANOVA with Bonferroni's post-hoc analysis test. * denotes P<0,05; ** denotes P<0,005; *** denotes P<0,0005 and **** P<0,00005; ns = non significant.*

5. Discussion

5.1. Rho GTPase significance in cancer

Rho family of GTPase proteins are involved in many cellular processes, notably cell cycle progression (Bustelo, 2018). As such, Rho GTPase proteins and their regulators (Rho GEFs and GAPs) have a significant role in tumorigenesis, and it is not surprising that they have become interesting targets of tumor therapy (Bustelo, 2018). For example, RhoA and RhoC are overexpressed in certain human cancers (G. Fritz et al., 2002; Orgaz et al., 2014), while RhoB is a known tumor suppressor (Prendergast, 2001; Huang & Prendergast, 2006). The Rho GTPase regulator protein RhoGAP7/DLC1 (Deleted in Liver Cancer 1) activates GTPase states of RhoA, RhoB, RhoC and Cdc42, and it has become a tumor suppressor candidate molecule (Wang et al., 2016). The Rho GEF TIAM1 (T-cell lymphoma invasion and metastasis-inducing protein 1) activates Rac1, Cdc42 and RhoA and is considered an oncogene (Michiels et al., 1995; Marei & Malliri, 2017). RhoB and RhoD are the two Rho family members found on endosomes (Ellis and Mellor, 2000). Taking into consideration the tumor suppressor role of RhoB and the RhoA-antagonistic properties of RhoD (Tsubakimoto et al., 1999), these two proteins may share a common role in tumor progression. The endosomes and the ESCRT complex have been recognized as vital components of cell division finalization and there is high interest in impact of the endosomal compartment in cytokinesis (Schiel et al., 2013). This may be a novel aspect to understanding cancer cell biology and the implications of RhoD on cancer are worth exploring. However, the impact of RhoD on cancer and tumor therapy has been largely unexplored. By finding novel interacting partners of RhoD, its involvement in tumor progression may be further elucidated.

KIF20B, a kinesin associated with cell division, was identified as one of RhoD interacting partners (Ishizaki et al., unpublished data). Interestingly, mitotic kinesins have emerged as valuable targets in cancer treatment (Rath and Kozielski, 2012), especially since they are associated to microtubules and implicated in cell division (Chandrasekaran et al., 2015). This research was initiated to find the physiological significance of the RhoD and KIF20B interaction in cancer cells. Considering their cancer-associated properties, I speculated the relationship of RhoD and KIF20B might also have implications in tumor treatment and anticancer drug sensitivity.

5.2. RhoD and KIF20B expression in cancer

The research published on RhoD thus far does not offer clear evidence of its role in tumorigenesis. RhoD was found to be downregulated in melanoma cell lines (Wen et al., 2017). and overexpressed in multiple myeloma (Andrade et al., 2010). Although the most published data on RhoD indicates it may have tumor-suppressor like properties (Murphy et al., 1996; Tsubakimoto et al., 1999; Nguyen et al., 2002), individual data from independent analyses submitted by researchers suggest a different role. Some databases like OncoMX and HIVE offer insight into mutations of RhoD that may be associated with cancer (https://oncomx.org/searchview/?gene=O00212#details; (https://hive.biochemistry.gwu.edu/ biomuta/proteinview/O00212). They show that mutations were mostly located around amino acid residues which are not associated with active or inactive GTP state. The highest frequency of mutations was found in stomach, melanoma and liver cancer. According to this data, RhoD was mostly found to be overexpressed in cancer, which is opposite to my expectations that it might have a tumor-suppressor role, as in the case of RhoB. However, the functional roles of the RhoD mutations listed in these repositories are not clear. Thus, further investigation is needed on RhoD tumorigenesis and the pathophysiological significance of its mutations.

Kinesins have come into the spotlight as inhibitor targets of tumor therapy because of their roles in cell division and cell cycle progression (Rath and Kozielski, 2012). KIF20B is no exception. A clinical trial for bladder cancer therapy using peptide vaccine containing epitopes from KIF20B showed promising results, suggesting that KIF20B may indeed be a valuable target for oncotherapy (Obara et al., 2012). Many studies have reported that KIF20B is usually overexpressed in cancer and that higher expression leads to poorer prognosis/outcomes in clinic. This was demonstrated on many cancer cell lines and patient samples (Abaza et al., 2003; Kanehira et al., 2007; X. R. Liu et al., 2012; X. Liu et al., 2014; Ansari et al., 2015; W. F. Lin et al., 2018; X. Liu et al., 2018; G. Li et al., 2019; Z. Y. Li et al., 2019). The known role of KIF20B in cancer progression has made its interaction with RhoD more interesting to this research.

5.3. The causal relationship of RhoD and KIF20B

In this research I have addressed the postulated interaction between RhoD and KIF20B (De Zan and Ishizaki, unpublished data). I further wanted to investigate the relationship of

these molecules regarding protein expression and localization, and later the significance of their interaction in the context of sensitivity to antitumor treatments.

First I wanted to see if there was a causal relationship behind the interaction of RhoD and KIF20B, so I evaluated expression at the mRNA level for both genes, after knocking down each of the interacting partner molecules. By comparing the data obtained from RT-qPCR and western blots from eight different cell lines, I concluded that there is a causative relationship between the expression of RhoD and KIF20B. In HeLa cells, I found a reduction of KIF20B at both mRNA and protein level, upon transfection with RhoD specific siRNAs. In HeLa CK cells (the cDDP-resistant HeLa subline; Osmak and Eljuga, 1993), however, at the mRNA level I found an increase in KIF20B expression after RhoD knockdown.

Interestingly, I determined that HeLa CK cells contain two-fold of the RhoD mRNA amount than in the parental cell line, HeLa. This upregulation of RhoD in HeLa CK cells might be related to the mechanism of cDDP resistance. Previous research has shown that RhoB expression was decreased more than two-fold on the protein level in HeLa CK cells, when compared to HeLa cells. On the mRNA level, there was no difference between expression of RhoB in HeLa and HeLa CK cells (Čimbora-Zovko et al., 2010). In a paper by Kyrkou and associates (2012), it was found in Human Umbilical Vein Endothelial cells (HUVEC) that RhoD knockdown induced increased expression of RhoB mRNA. I have also evaluated RhoB protein expression in HeLa cells upon RhoD (and KIF20B) knockdown, and found that it is also increased (data not shown). Interestingly, beside RhoF, the closest phylogenetic Rho family member to RhoD is RhoB, and the two proteins share similarities in function and localization (Narumiya and Thumkeo, 2018). It is likely there is a redundancy in expression levels of RhoB and RhoD. This would explain why in HeLa CK cells, where RhoB is downregulated on the protein level, RhoD expression was found to be increased on the mRNA level. This relationship between RhoB and RhoD is worth further investigation in the future, especially considering the tumor suppressor role of RhoB (Fritz et al., 1995; Liu et al., 2000).

In other tested cell lines, I found that RhoD knockdown decreases KIF20B expression at least on the protein level in CaCO-2, HCT-116 and MDA-MB-231 cells. Regarding KIF20B knockdown influence on RhoD mRNA expression, I have found increased RhoD mRNA levels in HeLa CK, and decreased in CaCO-2, MCF-7 and MDA-MB-231 cells. Since I haven't been able to determine the influence of KIF20B knockdown on the protein level of RhoD by western blot, it is difficult to come to conclusions about that relationship based singularly on RT-qPCR

data. It is plausible that this relationship varies upon different tissue types and also other cellular properties. For example I observed variable KIF20B expression upon RhoD knockdown in three different breast carcinoma cell lines. Also, the amount of RhoD in each cell line may be crucial in influencing KIF20B protein levels, as interaction with RhoD might stabilize KIF20B. If a cell line would have a higher amount of RhoD than KIF20B, then KIF20B amount would be severely impacted upon RhoD knockdown.

These findings have led to the conclusion that there is indeed a causative relationship between proteins RhoD and KIF20B, and the significance of their interaction needs to be further elucidated.

5.4. RhoD and KIF20B localization patterns

After analyzing expression data, I wanted to check if the two proteins colocalized, which might further explain the significance of their interaction. Protein localization patterns can offer valuable insight into their physiological roles, which may be altered in cancer. Some of these changes in localization may be direct consenquences of chromosomal instability (CIN), DNA damage, chromosome separation defects, aberrant vesicular trafficking or altered protein interactions, to name a few (Wang and Li, 2014; McClelland, 2017; Wang et al., 2017; Bakhoum and Cantley, 2019).

Since localization of proteins is an important determinant of their functional properties, I wanted to check if knockdown of either RhoD or KIF20B caused aberrant localization of each interacting partner. Considering that KIF20B is a mitotic protein and its localization varies upon mitotic phase, I observed both mitotic and interphase cells (Kamimoto et al., 2001; Abaza et al., 2003; Kanehira et al., 2007). First I checked RhoD and KIF20B localization in unaltered cells.

KIF20B localization in all tested cell lines was similar to the already published results in HeLa cells (Abaza et al., 2003; Janisch et al., 2018), HeLa S3 cells (Kamimoto et al., 2001), UM-UC-3 bladder cancer cells (Kanehira et al., 2007) and colorectal cancer SW480 and LOVO cells (Lin et al., 2018). In all of my tested cell lines (HeLa, HeLa CK, CaCO-2, HCT-116, MDA-MB-231, MDA-MB-468 and MCF-7), I observed the usual KIF20B localization at the spindle midzone in anaphase and at the intercellular bridge (the midbody) in telophase, indicating that KIF20B role in this stage of cell division is probably conserved among various cell lines and tissues. However, I managed to demonstrate on HeLa, HCT-116 and CaCO-2 cells, that

KIF20B is longer associated with the chromosomes than previously thought. Until now nobody reported that the association of KIF20B with nucleus proceeds through metaphase until early anaphase, when the signal is gradually transferred to the microtubules of early mitotic spindle. Such localization is reminiscent of the Chromosome Passenger Complex proteins Aurora kinase B or Survivin (Carmena et al., 2012). I also used immunofluorescence to inspect KIF20B knockdown with specific siRNAs. As expected, upon knockdown there was a lack of KIF20B signals on the cell nuclei in interphase, and a complete absence of KIF20B signals in the spindle midzone, the intercellular bridge and midbody during anaphase to telophase in my tested cell lines.

Since I have noticed the reduction in KIF20B expression after RhoD knockdown in western blot analysis in HeLa, CaCO-2, HCT-116 and MDA-MB-231 cells, I wanted to confirm these results by analysing immunofluorescent staining of KIF20B upon RhoD knockdown. Only in HeLa cells, I confirmed this finding in two out of three used RhoD specific siRNAs. For RhoD siRNAs #1 and #3 I found a significant reduction of KIF20B signals in both nucleus and midbody areas. Why is there such an obvious discrepancy between different RhoD siRNAs in HeLa cells? The siRNA#1 has the best efficiency in abrogating KIF20B signal. The possible answer may lie in the specificity of RhoD siRNAs to the mRNA sequence segments they bind, and which are subsequently degraded. Three siRNAs that were used target different portions of the RhoD mRNA and interestingly, the RhoD siRNA#1 is the only one which falls into a sequence position outside of the RhoD exon 3. Today only two splice variants of RhoD are known, and one of them is missing the exons 2 and 3, which are precisely the sites which siRNAs #2 and #3 target (Figure 5.1). This means that RhoD siRNA#1 would be able to knockdown both RhoD splice variants and abolish the signal of KIF20B at the plausible KIF20B interaction site on RhoD protein better than the other siRNAs. However, off-target effects of the siRNAs cannot be ruled out. To confirm this role of RhoD, a rescue experiment should be performed in the future, where after RhoD knockdown, RhoD insensitive to siRNA is overexpressed, and KIF20B expression is then checked.

After testing KIF20B localization upon RhoD knockdown, I also wanted to inspect if there was a similar impact of KIF20B knockdown on RhoD expression and localization in cells. I have tested this by immunofluorescence, using exogenous RhoD in its active form, in control and KIF20B silenced cells.
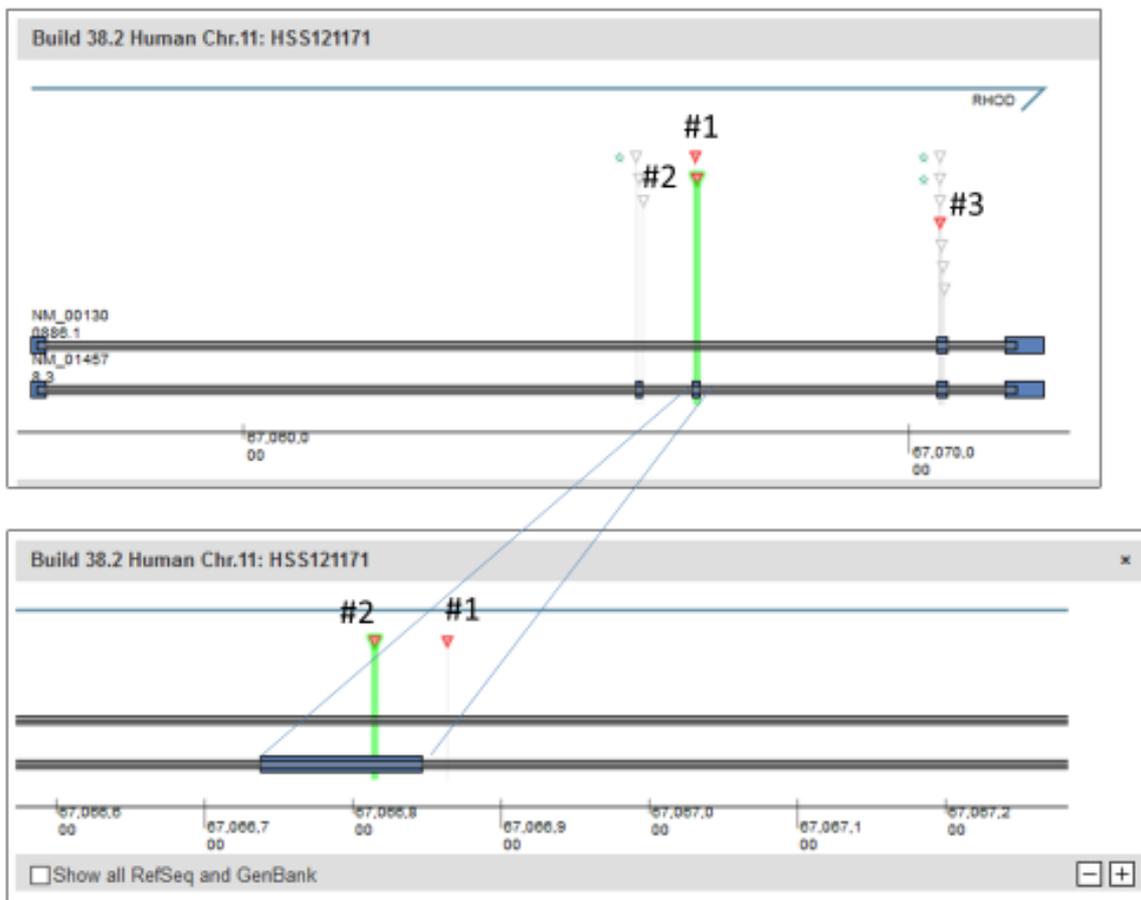
Figure 5.3. Data from the ThermoFisher Scientific webpage regarding sequence specificity of RhoD stealth siRNAs #1, #2 and #3 to the transcriptome sequence of RhoD. The figure below is the magnified portion of target sequence from the upper figure. Red triangles mark where the specific RhoD siRNAs bind the target sequence.

I found a RhoD localization previously unreported in literature: RhoD localizes in the midbody of telophase cells, surrounded or overlapped by KIF20B signals. The examples are shown on HeLa and CaCO-2 cells for EGFP-RhoD^{Q75L} construct. I quantified the number of EGFP-RhoD^{Q75L} positive cells in cytokinesis which exhibit RhoD signal in the midbody and found that exogenous RhoD localized at the midbody in every EGFP-RhoD positive cell observed, including the cases where constructs EGFP-RhoD^{WT} and EGFP-RhoD^{G26V} were used. RhoD localization during cell division that was reported previously was inspected upon overexpression of RhoD in HeLa cells (Kyrkou et al., 2012).

However, the authors didn't find the localization of RhoD at the intercellular bridge in telophase. Since they used the myc-tagged protein, they had to combine it with the primary antibody against myc, 9E10. The midbody is a very dense structure and sometimes it is more difficult to visualize it by staining with antibodies (Hu et al., 2012), rather than using a fluorescent tag, like EGFP in my case. This is probably why, to this day, the localization of RhoD at the midbody was never reported.

Interestingly, RhoD expression has been linked to CIN. The CIN phenotype is a hallmark of human cancer and results from chromosome segregation errors, causing structural and numerical chromosome abnormalities. It was also found to positively correlate with tumor stage and poor prognosis, metastasis and resistance to therapy (McClelland, 2017; Wang et al., 2017; Bakhoum and Cantley, 2019). RhoD overexpression induces decreased differentiation and centrosomal amplification that lead to aberrant multipolar spindles and abnormal chromosome segregation. These abnormalities are hallmarks of CIN, indicating that RhoD might be implicated in cancer progression (Kyrkou et al., 2012).

Since I found an overlap of KIF20B and RhoD signals at the midbody, I assumed this may be an area of their interaction. It is known that KIF20B is implicated in cell division (Kamimoto et al., 2001; Abaza et al., 2003; Kanehira et al., 2007) and it was recently confirmed that it is required for efficient cytokinetic furrowing and timely abscission in human cells (Janisch et al., 2018). Thus far, RhoD was linked with cytokinesis in a paper by Keisuke Tsubakimoto and associates (1999). By using the constitutively active GTPase RhoD^{G26V} mutant they found that active RhoD overexpression interrupted cytokinesis and caused multinucleation in NIH-3T3 cells. The authors have speculated that RhoD interferes with cytokinesis by interfering with RhoA action. RhoA has a role in maintaining the contractile actin ring that constricts throughout anaphase and telophase. This happens probably through direct sequestration of RhoA by RhoD or by regulation of RhoA regulators by RhoD. Also, RhoD has been reported in the same research to have antagonistic properties to RhoA in formation of stress fibers and focal adhesions (Tsubakimoto et al., 1999).

My results showed that KIF20B knockdown has no effect on the newly characterized exogenous RhoD localization by either intensity or misplacement. However, I have noticed an increase in perinuclear accumulation of RhoD positive vesicles (endosomes) by knockdown with KIF20B siRNAs in HeLa cells (data not shown). It was previously reported that in transiently transfected cells RhoD colocalizes with Rab5 positive cytoplasmic vesicles, which correspond to early endosomes (Murphy et al., 1996). The authors have shown that overexpression of a constitutively active Rab5^{Q79L} GTPase mutant can induce a perinuclear accumulation of large endosomes, which was repressed by simultaneous expression of the constitutively active RhoD^{G26V} (Murphy et al., 1996). Taking into consideration this interaction between Rab5 and RhoD, and a similar phenotype induced by KIF20B knockdown, there might also be a connection between KIF20B and perinuclear endosome accumulation. In CaCO-2

and HeLa cells, I have also found that there is a colocalization between RhoD, KIF20B and Rabaptin 5, a Rab5 effector molecule, in the midbody during telophase.

Recently a new role has emerged for Rab proteins in control of tumor progression as they were found to be deregulated in cancer. In tumor cells Rab proteins are involved in delivery and recycling of integrins during cell migration, secretion of proteases during tissue invasion, secretion of exosomes that mediate communication with stromal cells, trafficking of receptors and control of their signaling, impact on cell cycle and survival, and resistance to anticancer drugs (Recchi and Seabra, 2012). Interestingly, the same Rabs may act as oncoproteins or tumor suppressors in different cancers, which may be due to the interaction of specific Rab protein with different effectors or cargos in various tumors (Tzeng and Wang, 2016). Considering the implications of Rab proteins in tumorigenesis, it is not surprising that they might have important roles in sensitivity to anticancer drugs. For example, the GTPase-regulated endocytosis is an important factor in drug resistance, as it contributes to drug uptake into cells. Downregulation of Rab5C-mediated endocytosis contributes to reduction of cellular cisplatin accumulation and drug resistance (Jin et al., 2014).

5.5. Influence of RhoD and KIF20B on cell cycle entry

After taking into consideration published data on RhoD roles in cytokinesis and cell division, its interaction with KIF20B and my localization data, I wanted to check if there were similarities between cell division phenotypes after RhoD and KIF20B knockdown. To evaluate this I have performed cell synchronization and cell cycle analysis. Cell synchronization has been thoroughly explored in HeLa cells, so I used this model in my experiment (Yasuda and Narumiya, 2006; Wee & Wang, 2017). I examined the progress of mitotic exit in HeLa cells following either RhoD or KIF20B knockdown. However, I did not notice any substantial differences between control samples and KIF20B knockdown samples, indicating that the KIF20B knockdown phenotype was mild. In the case of RhoD knockdown, there were less cells in metaphase and more cells in telophase, especially late, compared to control. This means that upon RhoD knockdown the cells progressed through mitosis faster compared to control and KIF20B knocked down samples. Previously reported results from cell cycle experiments in HeLa cells demonstrated that RhoD[WT] is most activated in prometaphase stage, which gradually decreases through anaphase and telophase (Kyrkou et al., 2012). The same research confirmed that RhoD overexpression leads to multinucleation, as established earlier

(Tsubakimoto et al., 1999). Upon RhoD knockdown, I observed no clear changes in choromosome structure. The same study as mentioned above, focused on centrosome integrity and duplication and revealed that RhoD knockdown produced cells with no visible centrosomes, which leads to formation of multipolar spindles and abnormal chromosome segregation, adding weight to the CIN phenotype (Kyrkou et al., 2012).

Alongside previous research, my finding that HeLa cells progress through mitosis faster upon RhoD knockdown, strengthens the hypothesis that RhoD has functions antagonistic to RhoA: RhoD dissolutes stress fibers and focal adhesions, while RhoA is essential in forming those structures. Overexpressed RhoD^{G26V} also restricts endosome motility in endothelial cells (Murphy et al., 2001). It was later discovered that this restriction is mediated through hDia2C and Src tyrosine kinase. The Diaphanous related formin hDia2C is an actin nucleator and a Rho effector protein. A novel signal transduction pathway was identified where hDia2C and c-Src are sequentially activated by RhoD. This activation regulates endosome motility through interactions with the actin cytoskeleton (Gasman et al., 2003). Src, which controls endosome motility, binds to the activated hDia2C. The hDia2C protein is also bound to a Rab5 positive endosome via activated RhoD. RhoD tethers the endosome to the F-actin filaments, thereby restricting its motility (Randazzo, 2003). Perhaps my finding that cells upon RhoD knockdown are progressing faster through mitosis can be interpreted by this same signaling cascade. Since activated RhoD is involved in tethering endosomes to the actin cytosekeleton thereby slowing them down, the machinery that enables abscission in late telophase (the endosomal sorting complex – ESCRT) is not impeded and that may be why mitotic exit is faster in RhoD silenced cells. This is also how the failure of cytokinesis in RhoD overexpressed cells may be explained (Tsubakimoto et al., 1999). Since there is an abundance of RhoD which can cause the signaling cascade to tether Rab5 positive endosomes to the actin cytoskeleton, the abscission is somehow prevented from happening which may lead to cytokinesis failure and multinucleation. Recently, it was found that Rab5 is essential for the delivery of components of the membrane-severing ESCRT III machinery to complete cytokinesis (Kumar et al., 2019), supporting this hypothesis.

Since I was interested to find if the RhoD-KIF20B interaction had any influence on the cell cycle, I performed the analysis by flow cytometry 72 hours post transfection in HeLa cells. For all three tested RhoD siRNAs, I found a distinct "gap" in the G1/S phase cell content, and the same phenotype was found in two of the tested KIF20B sRNAs. Similar results were

obtained by Kyrkou and colleagues (2012). Another research group performed cell cycle analysis upon KIF20B knockdown in HCT-116 cells and reported a hypodiploid peak appearing 72 hours after knockdown, indicating an increase in the presence of apoptotic cells (Abaza et al., 2003). Interestingly, I also observed a higher number of apoptotic cells in one KIF20B siRNA (#1). In my research, however, it is the first time that data regarding cell cycle analysis in HeLa cells following KIF20B knockdown was reported. Considering that the cell cycle data for HeLa cells upon RhoD and KIF20B knockdown show the distinct G1/S gap, this indicates the two proteins might have a common role during the G1/S transition. Coincidentally, I also found a decrease in proliferation upon RhoD knockdown, which I observed in cultured cells 120 hours post transfection. This was evident from MTT assay data, by comparing proliferation rates of control and RhoD silenced cells.

In my experiments RhoD knockdown does not lead to failure of cell division, but accelerates entry into telophase during mitosis. There are proteins with similar localization to RhoD, which also show some similar properties. For example, the protein Kaiso, a transcriptional repressor, localizes to centrosomes and midbody in telophase, same as RhoD. Its overexpression leads to mitotic arrest and cell death. However, knockdown of Kaiso in SK-LMS-1 cells induced a shorter cell cycle, and this protein is more associated with tumorigenesis than RhoD (Soubry et al., 2010). Another protein, the tumor suppressor CYLD, is also required for timely entry into mitosis. It localizes to microtubules in interphase and the midbody during telophase, and its protein levels decrease as cells exit from mitosis. CYLD down-regulation delays but does not entirely block the G2/M progression, causing only a subtle proliferative disadvantage (Stegmeier et al., 2007), similar to situation with RhoD. Many proteins that have crucial functions in cytokinesis are also involved in CIN. One of them is the protein regulator of cytokinesis (PRC1). PRC1 accumulates at the spindle midzone, binds and bundles microtubules and its deregulation can cause cytokinesis failure. This can then lead to abnormal distribution of chromosomes to daughter cells, which further increases CIN and promotes intratumor heterogeneity in cancer. Resistance to antitumor therapy may arise from such changes (Li et al., 2017). Comparing RhoD localization and roles to these proteins, suggests that RhoD may indeed have a function in tumorigenesis which needs to be further unveiled and it may also be important in providing new understanding of drug sensitivity in cancer cells.

5.6. Role of RhoD and KIF20B to tumor cell sensitivity to drugs cDDP, PTX and VCR

Since RhoD and KIF20B displayed connections in cell cycle progression, expression and localization studies, I proposed they also might have a role in cancer and sensitivity of tumor cells to anticancer agents. By using cell models of different origins, I analyzed if RhoD knockdown induces a similar response in tumor cells to anticancer agents, as KIF20B. If so, this may indicate that the RhoD/KIF20B interaction might have a role in response to anticancer drugs. To test this I have used cDDP, an alkylating like agent extensively used in tumor therapy, and two microtubule targeting agents (MTAs) PTX and VCR. The MTAs were especially interesting to me since KIF20B itself stabilizes microtubules and arrests cells at telophase (Abaza et al., 2003). Thus far, no research has been published on the influence of RhoD knockdown on sensitivity to anticancer drugs.

When treating cells with cDDP upon RhoD or KIF20B knockdown, I found different responses across different cell types. In HeLa cells, RhoD knockdown induced sensitization to cDDP, and KIF20B knockdown induced comparable levels of sensitization at the same concentrations of cDDP. Interestingly, in HeLa CK cells, at the same concentrations of cDDP, the response was nearly the same to control values for RhoD knockdown and displayed a decrease in sensitivity for KIF20B knockdown. Intriguingly, HeLa CK cells contain twofold RhoD mRNA amount than parental HeLa cells, and also have higher mRNA amounts of KIF20B. This may indicate that the mechanisms of resistance to cDDP involve changes in levels of RhoD and KIF20B proteins. In the other cell lines I found a decreased sensitivity to cDDP after KIF20B knockdown. The only literature data regarding RhoD's role in response to cytotoxic drugs are based on its cancerogenic properties or lack thereof in melanoma cell lines (Wen et al., 2017) and multiple myeloma (Andrade et al., 2010). Another research found that in cDDP resistant MCF-7 cells RhoD expression was decreased (Watson et al., 2007). My observations have demonstrated the same direction of cDDP response after RhoD knockdown in MCF-7 cells, where I expected that RhoD knockdown would induce a decrease in sensitivity to cDDP, which it did. In conclusion, I showed that for the majority of tumor cell lines tested knockdown of RhoD or KIF20B affects the sensitivity to cDDP. Increased sensitivity was observed in HeLa cells while decreased sensitivity in all other tested cell lines. However, the mechanism of this response remains to be determined.

In the case of PTX, I expected to see sensitization to the drug, especially after KIF20B knockdown, since recent research found KIF20B downregulation leads to induced sensitivity

to MTAs. However, I have demonstrated either a decrease in sensitivity or no interaction with PTX after KIF20B knockdown in tested cell lines. KIF20B knockdown decreased sensitivity to PTX in MDA-MB-468 and MCF-7. I found no interaction with PTX after KIF20B knockdown in HeLa CK, HCT-116 and MDA-MB-231 cells. On the other hand, in already published research, KIF20B expression in breast cancer patient samples was found to inversely correlate with PTX response, indicating that KIF20B was overexpressed in tumor tissues resistant to PTX, compared to normal breast tissues (Tan et al., 2012). The same research group found that an oncolytic adenoviral vector with KIF20B shRNA initiated hepatocellular carcinoma (HCC) proliferation arrest, induction of apoptosis and increased sensitivity to PTX. The group tried to unravel the mechanism behind this response, and they discovered that KIF20B depletion stabilized p53, blocked STAT3 phosphorylation and prolonged mitotic arrest (Liu et al., 2014). Their further research on HCC cell models found that KIF20B depletion by shRNA oncolytic adenoviral vector induced sensitivity to PTX and acted synergistically with two other MTAs; Epothilone B and VCR (Liu et al., 2018). The influence of KIF20B knockdown on response to PTX I obtained is difficult to explain. KIF20B is a microtubule stabilizing protein (Abaza et al., 2003), and MTAs like PTX and EpoB are microtubule stabilizing drugs. PTX suppresses mitosis at metaphase, while KIF20B knockdown was shown to affect mitosis at telophase (Liu et al., 2018). Thus, an additive effect of the two would be expected. PTX and many MTAs induce cell death by activating the Spindle Assembly Checkpoint, which induces mitotic arrest and apoptosis (Silva et al., 2017). Some cancer cells can bypass the SAC activation and become insensitive to its activation by MTAs. That is why an effective mitosis blockade by targeting other checkpoints beside SAC may lead to increased sensitivity to MTAs (Bargiela-Iparraguirre et al., 2014; Liu et al., 2018).

In the case of RhoD knockdown, I observed a decrease in sensitivity to PTX in HeLa, MDA-MB-231, MDA-MB-468 and MCF-7 cells, and an ambiguous response with tendency to decrease in sensitivity to PTX was observed in HeLa CK, HCT-116 and CaCO-2 cells. Since generally RhoD knockdown induced a decrease in sensitivity to PTX in tested cell lines, it is likely that an increased amount of RhoD would lead to an increase in sensitivity in these cell lines. This assumption goes in hand with the RhoA-antagonistic properties of RhoD (Murphy et al, 1996; Tsubakimoto et al., 1999; Murphy et al., 2001; Nguyen et al., 2002; Gasman et al., 2003; Randazzo, 2003). Perhaps in my tested cell lines where the response is borderline

decrease in sensitivity to PTX the quantity of the RhoD protein is rather low, which led to a corresponding low decrease in sensitivity to PTX.

VCR is a microtubule destabilizing drug, so the already antagonistic effect it has to microtubule polymerization would most likely increase after knockdown of the microtubule-stabilizing KIF20B. The only research regarding KIF20B knockdown and increase in sensitivity to VCR was conducted on HCC models (Liu et al., 2018). Conversely, the predominant response to VCR after KIF20B knockdown that I observed was no interaction with sensitivity to VCR.

RhoD knockdown induced no interaction with VCR in most of my tested cell lines, with a decrease in sensitivity in HeLa, HCT-116 and MCF-7 cells. Just like with PTX, this effect may be ascribed to the anti-tumorigenic properties of RhoD. The effect may be more pronounced in HeLa and HCT-116, because they have the least amount of RhoD mRNA out of all tested cell lines. MCF-7 with the highest RhoD mRNA content, may be more susceptible to the damage induced by VCR.

Judging by my proliferation assay results, the responses to cDDP, PTX and VCR may not be linked to the same mechanisms for RhoD and KIF20B. However, with the exception of HeLa cells, RhoD knockdown elicited mostly decrease in sensitivity to all of these drugs, reinforcing its role as a molecule antagonistic to the oncogene RhoA. In the future perhaps a combination of RhoD and RhoB knockdown might induce even a stronger response to drugs, considering their common properties. Regarding influence of KIF20B knockdown on response to cDDP, PTX and VCR, I only managed to show sensitization to cDDP in HeLa cells. The response was not always similar to that induced after RhoD knockdown, indicating there is no clear connection between RhoD and KIF20B when it comes to response to drugs cDDP, PTX and VCR.

6. Conclusions

Altogether, these results confirm that there is a causative relationship between RhoD and KIF20B, which I can corroborate with expression studies on the mRNA and protein level; localization studies and cell cycle data. The most likely location for this interaction is the intercellular bridge, specifically the midbody, where both proteins localize, and where I found the most prominent absence of KIF20B signals after RhoD knockdown. Another member of the Kinesin-6 family, KIF20A, was also found to interact with a protein specific for recycling endosomes, Rab6A and it may act as a motor required for RAB6 regulated transport of Golgi associated vesicles along microtubules (Echard et al., 1998). Similar to KIF20A, KIF20B may also recruit RhoD-positive endosomes, especially during telophase. It is still necessary to further determine the nature and impact this interaction might have on cell division and endosomal transport. Considering the mild multinucleation phenotypes knockdown of both proteins elicited and considering their mutually exclusive roles in terms of carcinogenicity, perhaps their interaction has a significance in cell division which does not essentially contribute to known mechanisms of response to cytotoxic drugs. That is why this physiological and functional interaction should be observed in the future from a different aspect.

This research has demonstrated that the relationship between RhoD and KIF20B is worth exploring further, especially in the context of the function of their interaction during cell division. Other than this, the role of RhoD as a possible tumor-suppressor molecule is interesting and may prove important in future studies about tumor cell sensitivity to drugs and mechanisms of carcinogenesis. Small Rho GTPases are versatile proteins that have an impact on multiple cellular processes, and a greater understanding of their roles in cancer progression and therapy may lead to development of promising new drugs.

7. References

Abaza, A., Soleilhac, J. M., Westendorf, J., Piel, M., Crevel, I., Roux, A., & Pirollet, F. (2003). M phase phosphoprotein 1 is a human plus-end-directed kinesin-related protein required for cytokinesis. *Journal of Biological Chemistry*, *278*(30), 27844–27852. https://doi.org/10.1074/jbc.M304522200

Acker, T., & Plate, K. H. (2003). Role of hypoxia in tumor angiogenesis - Molecular and cellular angiogenic crosstalk. *Cell and Tissue Research*, *314*(1), 145–155. https://doi.org/10.1007/s00441-003-0763-8

Adams, R. R., Tavares, A. A. M., Salzberg, A., Bellen, H. J., & Glover, D. M. (1998). Pavarotti Encodes a Kinesin-Like Protein Required To Organize the Central Spindle and Contractile Ring for Cytokinesis. *Genes and Development*, *12*(10), 1483–1494. https://doi.org/10.1101/gad.12.10.1483

Agarwal, R., & Kaye, S. B. (2003). Ovarian cancer: Strategies for overcoming resistance to chemotherapy. *Nature Reviews Cancer*, *3*(7), 502–516. https://doi.org/10.1038/nrc1123

Aggarwal, S. K. (1998). Calcium modulation of toxicities due to cisplatin. *Metal-Based Drugs*, *5*(2), 77–81. https://doi.org/10.1155/MBD.1998.77

Alexandre, J., Hu, Y., Lu, W., Pelicano, H., & Huang, P. (2007). Novel action of paclitaxel against cancer cells: Bystander effect mediated by reactive oxygen species. *Cancer Research*, *67*(8), 3512–3517. https://doi.org/10.1158/0008-5472.CAN-06-3914

Andrade, V. C. C., Vettore, A. L., Panepucci, R. A., Almeida, M. S. S., Yamamoto, M., De Carvalho, F., Caballero, O. L., Zago, M. A., & Colleoni, G. W. B. (2010). Number of expressed cancer/testis antigens identifies focal adhesion pathway genes as possible targets for multiple myeloma therapy. *Leukemia and Lymphoma*, *51*(8), 1543–1549. https://doi.org/10.3109/10428194.2010.491136

Ansari, D., Andersson, R., Bauden, M. P., Andersson, B., Connolly, J. B., Welinder, C., Sasor, A., & Marko-Varga, G. (2015). Protein deep sequencing applied to biobank samples from patients with pancreatic cancer. *Journal of Cancer Research and Clinical Oncology*, *141*(2), 369–380. https://doi.org/10.1007/s00432-014-1817-x

Aoki, Y., Niihori, T., Kawame, H., Kurosawa, K., Ohashi, H., Tanaka, Y., Filocamo, M., Kato, K., Suzuki, Y., Kure, S., & Matsubara, Y. (2005). Germline mutations in HRAS proto-oncogene cause Costello syndrome. *Nature Genetics*, *37*(10), 1038–1040. https://doi.org/10.1038/ng1641

Arora, S., Kothandapani, A., Tillison, K., Kalman-Maltese, V., & Patrick, S. M. (2010). Downregulation of XPF-ERCC1 enhances cisplatin efficacy in cancer cells. *DNA Repair*, *9*(7), 745–753. https://doi.org/10.1016/j.dnarep.2010.03.010

Aspenström, P. (2017). Fast-cycling Rho GTPases. *Small GTPases*, *1248*, 00–00. https://doi.org/10.1080/21541248.2017.1391365

Aspenström, P. (2018). Activated rho GTPases in cancer—the beginning of a new paradigm. *International Journal of Molecular Sciences*, *19*(12). https://doi.org/10.3390/ijms19123949

Aspenström, P., Fransson, Å., & Saras, J. (2004). Rho GTPases have diverse effects on the organization of the actin filament system. *Biochemical Journal*, *377*(2), 327–337. https://doi.org/10.1042/BJ20031041

Aspenström, P., Ruusala, A., & Pacholsky, D. (2007). Taking Rho GTPases to the next level: The cellular functions of atypical Rho GTPases. *Experimental Cell Research*, *313*(17), 3673–3679.

https://doi.org/10.1016/j.yexcr.2007.07.022

Bakhoum, S. F., & Cantley, L. C. (2019). The multifaceted role of chromosomal instability in cancer and its microenvironment Samuel. *Cell*, *174*(6), 1347–1360. https://doi.org/10.1016/j.cell.2018.08.027

Barbuti, A. M., & Chen, Z. S. (2015). Paclitaxel through the ages of anticancer therapy: Exploring its role in chemoresistance and radiation therapy. *Cancers*, *7*(4), 2360–2371. https://doi.org/10.3390/cancers7040897

Bargiela-Iparraguirre, J., Prado-Marchal, L., Pajuelo-Lozano, N., Jiménez, B., Perona, R., & Sánchez-Pérez, I. (2014). Mad2 and BubR1 modulates tumourigenesis and paclitaxel response in MKN45 gastric cancer cells. *Cell Cycle*, *13*(22), 3590–3601. https://doi.org/10.4161/15384101.2014.962952

Barr, F. A., & Gruneberg, U. (2007). Cytokinesis: Placing and Making the Final Cut. *Cell*, *131*(5), 847–860. https://doi.org/10.1016/j.cell.2007.11.011

Bastos, R. N., Gandhi, S. R., Baron, R. D., Gruneberg, U., Nigg, E. A., & Barr, F. A. (2013). Aurora B suppresses microtubule dynamics and limits central spindle size by locally activating KIF4A. *Journal of Cell Biology*, *202*(4), 605–621. https://doi.org/10.1083/jcb.201301094

Basu, A., & Krishnamurthy, S. (2010). Cellular responses to cisplatin-induced DNA damage. *Journal of Nucleic Acids*, *2010*. https://doi.org/10.4061/2010/201367

Belotti, D., Vergani, V., Drudis, T., Borsotti, P., Pitelli, M. R., Viale, G., Giavazzi, R., & Taraboletti, G. (1996). The Drug Paclitaxel Has Antiangiogenic. *Clinical Cancer Research*, *2*(November), 1843–1849.

Bieling, P., Telley, I. A., & Surrey, T. (2010). A minimal midzone protein module controls formation and length of antiparallel microtubule overlaps. *Cell*, *142*(3), 420–432. https://doi.org/10.1016/j.cell.2010.06.033

Blom, M., Reis, K., & Aspenström, P. (2018). RhoD localization and function is dependent on its GTP/GDP-bound state and unique N-terminal motif. *European Journal of Cell Biology*, *97*(6), 393–401. https://doi.org/10.1016/j.ejcb.2018.05.003

Blom, M., Reis, K., Heldin, J., Kreuger, J., & Aspenström, P. (2017). The atypical Rho GTPase RhoD is a regulator of actin cytoskeleton dynamics and directed cell migration. *Experimental Cell Research*, *352*(2), 255–264. https://doi.org/10.1016/j.yexcr.2017.02.013

Blom, M., Reis, K., Nehru, V., Blom, H., Gad, A. K. B., & Aspenström, P. (2015). RhoD is a Golgi component with a role in anterograde protein transport from the ER to the plasma membrane. *Experimental Cell Research*, *333*(2), 208–219. https://doi.org/10.1016/j.yexcr.2015.02.023

Breuninger, L. M., Aaronson, A., & Kruh, G. D. (1995). Expression of Multidrug Resistance-associated Protein in NIH/3T3 Cells Confers Multidrug Resistance Associated with Increased Drug Efflux and Altered Intracellular Drug Distribution. *Cancer Research*, *55*, 5342–5347.

Brozovic, A., Ambriović-Ristov, A., & Osmak, M. (2010). The relationship between cisplatin-Induced reactive oxygen species, glutathione, and BCL-2 and resistance to cisplatin. *Critical Reviews in Toxicology*, *40*(4), 347–359. https://doi.org/10.3109/10408441003601836

Brozović, A., Majhen, D., Roje, V., Mikac, N., Jakopec, S., Fritz, G., Osmak, M., & Ambriović-Ristov, A. (2008). Avβ3 Integrin-Mediated Drug Resistance in Human Laryngeal Carcinoma Cells Is Caused By Glutathione-Dependent Elimination of Drug-Induced Reactive Oxidative Species. *Molecular Pharmacology*, *74*(1), 298–306. https://doi.org/10.1124/mol.107.043836

Bustelo, X. R. (2018). RHO GTPases in cancer: known facts, open questions, and therapeutic challenges. *Biochemical Society Transactions*, *46*(3), 741–760. https://doi.org/10.1042/BST20170531

Camlin, N. J., McLaughlin, E. A., & Holt, J. E. (2017). Motoring through: The role of kinesin superfamily proteins in female meiosis. *Human Reproduction Update*, *23*(4), 409–420. https://doi.org/10.1093/humupd/dmx010

Carmena, M., Wheelock, M., Funabiki, H., & Earnshaw, W. C. (2012). The chromosomal passenger complex (CPC): From easy rider to the godfather of mitosis. *Nature Reviews Molecular Cell Biology*, *13*(12), 789–803. https://doi.org/10.1038/nrm3474

Cesario, J. M., Jang, J. K., Redding, B., Shah, N., Rahman, T., & McKim, K. S. (2006). Kinesin 6 family member Subito participates in mitotic spindle assembly and interacts with mitotic regulators. *Journal of Cell Science*, *119*(22), 4770–4780. https://doi.org/10.1242/jcs.03235

Chandrasekaran, G., Tátrai, P., & Gergely, F. (2015). Hitting the brakes: Targeting microtubule motors in cancer. *British Journal of Cancer*, *113*(5), 693–698. https://doi.org/10.1038/bjc.2015.264

Chatterjee, M., & Van Golen, K. L. (2011). Farnesyl transferase inhibitor treatment of breast cancer cells leads to altered RhoA and RhoC GTPase activity and induces a dormant phenotype. *International Journal of Cancer*, *129*(1), 61–69. https://doi.org/10.1002/ijc.25655

Chavrier, P., Simons, K., & Zerial, M. (1992). The complexity of the Rab and Rho GTP-binding protein subfamilies revealed by a PCR cloning approach. *Gene*, *112*(2), 261–264. https://doi.org/10.1016/0378-1119(92)90387-5

Čimbora-Zovko, T., Fritz, G., Mikac, N., & Osmak, M. (2010). Downregulation of RhoB GTPase confers resistance to cisplatin in human laryngeal carcinoma cells. *Cancer Letters*, *295*(2), 182–190. https://doi.org/10.1016/j.canlet.2010.02.025

Croft, D. R., & Olson, M. F. (2011). Transcriptional regulation of Rho GTPase signaling. *Transcription*, *2*(5), 211–215. https://doi.org/10.4161/trns.2.5.16904

Cuadrado, A., Lafarga, V., Cheung, P. C. F., Dolado, I., Llanos, S., Cohen, P., & Nebreda, A. R. (2007). A new p38 MAP kinase-regulated transcriptional coactivator that stimulates p53-dependent apoptosis. *EMBO Journal*, *26*(8), 2115–2126. https://doi.org/10.1038/sj.emboj.7601657

D'Avino, P. P., Giansanti, M. G., & Petronczki, M. (2015). Cytokinesis in animal cells. *Cold Spring Harbor Perspectives in Biology*, *7*(4), 1–17. https://doi.org/10.1101/cshperspect.a015834

D'Avino, P. P., Savoian, M. S., Capalbo, L., & Glover, D. M. (2006). RacGAP50C is sufficient to signal cleavage furrow formation during cytokinesis. *Journal of Cell Science*, *119*(21), 4402–4408. https://doi.org/10.1242/jcs.03210

Dasari, S., & Tchounwou, P. B. (2015). *Cisplatin in cancer therapy : molecular mechanisms of action*. 364–378. https://doi.org/10.1016/j.ejphar.2014.07.025.Cisplatin

De, S., Cipriano, R., Jackson, M. W., & Stark, G. R. (2009). Overexpression of kinesins mediates docetaxel resistance in breast cancer cells. *Cancer Research*, *69*(20), 8035–8042. https://doi.org/10.1158/0008-5472.CAN-09-1224

Dehaan, R. D., Yazlovitskaya, E. M., & Persons, D. L. (2001). Regulation of p53 target gene expression by cisplatin-induced extracellular signal-regulated kinase. *Cancer Chemotherapy and Pharmacology*, *48*(5), 383–388. https://doi.org/10.1007/s002800100318

Desoize, B., & Madoulet, C. (2002). Particular aspects of platinum compounds used at present in cancer treatment. *Critical Reviews in Oncology/Hematology*, *42*(3), 317–325.

https://doi.org/10.1016/S1040-8428(01)00219-0

Duan, Z., Foster, R., Bell, D. A., Mahoney, J., Wolak, K., Vaidya, A., Hampel, C., Lee, H., & Seiden, M. V. (2006). Signal transducers and activators of transcription 3 pathway activation in drug-resistant ovarian cancer. *Clinical Cancer Research*, *12*(17), 5055–5063. https://doi.org/10.1158/1078-0432.CCR-06-0861

Dumontet, C., & Jordan, M. A. (2010). *Microtubule-binding agents: a dynamic field of cancer therapeutics*. *9*(10), 790–803. https://doi.org/10.1038/nrd3253

Durkin, C. H., Leite, F., Cordeiro, J. V., Handa, Y., Arakawa, Y., Valderrama, F., & Way, M. (2017). RhoD Inhibits RhoC-ROCK-Dependent Cell Contraction via PAK6. *Developmental Cell*, *41*(3), 315-329.e7. https://doi.org/10.1016/j.devcel.2017.04.010

Echard, A., Jollivet, F., Martinez, O., Lacapère, J. J., Rousselet, A., Janoueix-Lerosey, I., & Goud, B. (1998). Interaction of a Golgi-associated kinesin-like protein with Rab6. *Science*, *279*(5350), 580–585. https://doi.org/10.1126/science.279.5350.580

Ellis, S., & Mellor, H. (2000). Regulation of endocytic traffic by Rho family GTPases. *Trends in Cell Biology*, *10*(March 2000), 85–88.

Espinosa, E., Zamora, P., Feliu, J., & González Barón, M. (2003). Classification of anticancer drugs - A new system based on therapeutic targets. *Cancer Treatment Reviews*, *29*(6), 515–523. https://doi.org/10.1016/S0305-7372(03)00116-6

Fidyk, N., Wang, J. Bin, & Cerione, R. A. (2006). Influencing cellular transformation by modulating the rates of GTP hydrolysis by Cdc42. *Biochemistry*, *45*(25), 7750–7762. https://doi.org/10.1021/bi060365h

Fink, D., Nebel, S., Aebi, S., Zheng, H., Cenm, B., Nehmã, A., Christen, D., & Howell, S. B. (1996). The Role of DNA Mismatch Repair in Platinum Drug Resistance. *Cancer Research*, *56*(619), 4881–4886.

Florian, S., Mitchison, T. J., Florian, S., & Mitchison, T. J. (2016). Chapter 25 Anti-Microtubule Drugs. In *The Mitotic Spindle: Methods and Protocols, Methods in Molecular Biology* (Vol. 1413). Springer Science+Business Media New York. https://doi.org/10.1007/978-1-4939-3542-0

Fontijn, R. D., Goud, B., Echard, A., Jollivet, F., van Marle, J., Pannekoek, H., & Horrevoets, A. J. (2001). The human kinesin-like protein RB6K is under tight cell cycle control and is essential for cytokinesis. *Molecular and Cellular Biology*, *21*(8), 2944–2955. https://doi.org/10.1128/MCB.21.8.2944-2955.2001

Fratta, E., Coral, S., Covre, A., Parisi, G., Colizzi, F., Danielli, R., Marie Nicolay, H. J., Sigalotti, L., & Maio, M. (2011). The biology of cancer testis antigens: Putative function, regulation and therapeutic potential. *Molecular Oncology*, *5*(2), 164–182. https://doi.org/10.1016/j.molonc.2011.02.001

Fritz, G., Brachetti, C., Bahlmann, F., Schmidt, M., & Kaina, B. (2002). Rho GTPases in human breast tumours: Expression and mutation analyses and correlation with clinical parameters. *British Journal of Cancer*, *87*(6), 635–644. https://doi.org/10.1038/sj.bjc.6600510

Fritz, G., Kaina, B., & Aktories, K. (1995). The Ras-related small GTP-binding protein RhoB is immediate-early inducible by DNA damaging treatments. *Journal of Biological Chemistry*, *270*(42), 25172–25177. https://doi.org/10.1074/jbc.270.42.25172

Fritz, Gerhard, Just, I., & Kaina, B. (1999). Rho GTPases are over-expressed in human tumors. *International Journal of Cancer*, *81*(5), 682–687. https://doi.org/10.1002/(SICI)1097-

0215(19990531)81:5<682::AID-IJC2>3.0.CO;2-B

Fuller, B. G., Lampson, M. A., Foley, E. A., Rosasco-Nitcher, S., Le, K. V., Tobelman, P., Brautigan, D. L., Stukenberg, P. T., & Kapoor, T. M. (2008). Midzone Activation of Aurora B in Anaphase Produces an Intracellular Phosphorylation Gradient. *Nature*, *453*(7198), 1132–1136. https://doi.org/10.1038/nature06923

Gad, A. K. B., Nehru, V., Ruusala, A., & Aspenstrom, P. (2012). RhoD regulates cytoskeletal dynamics via the actin nucleation-promoting factor WHAMM. *Molecular Biology of the Cell*, *23*, 4807–4819. https://doi.org/10.1091/mbc.E12-07-0555

Galluzzi, L., Vitale, I., Michels, J., Brenner, C., Szabadkai, G., Harel-Bellan, A., Castedo, M., & Kroemer, G. (2014). Systems biology of cisplatin resistance: Past, present and future. *Cell Death and Disease*, *5*(5), e1257-18. https://doi.org/10.1038/cddis.2013.428

Ganguly, A., Yang, H., & Cabral, F. (2010). Paclitaxel dependent cell lines reveal a novel drug activity. *Molecular Cancer Therapeutics*, *9*(11), 2914–2923. https://doi.org/10.1158/1535-7163.MCT-10-0552

Ganguly, A., Yang, H., Pedroza, M., Bhattacharya, R., & Cabral, F. (2011). Mitotic Centromere-associated Kinesin (MCAK) mediates paclitaxel resistance. *Journal of Biological Chemistry*, *286*(42), 36378–36384. https://doi.org/10.1074/jbc.M111.296483

Gasman, S., Kalaidzidis, Y., & Zerial, M. (2003). RhoD regulates endosome dynamics through Diaphanous-related Formin and Src tyrosine kinase. *Nature Cell Biology*, *5*(3), 195–204. https://doi.org/10.1038/ncb935

Georges, A., Coyaud, E., Marcon, E., Greenblatt, J., Raught, B., & Frappier, L. (2019). USP7 Regulates Cytokinesis through FBXO38 and KIF20B. *Scientific Reports*, *9*(1), 1–16. https://doi.org/10.1038/s41598-019-39368-y

Giannakakou, P., Sackett, D. L., Kang, Y. K., Zhan, Z., Buters, J. T. M., Fojo, T., & Poruchynsky, M. S. (1997). Paclitaxel-resistant human ovarian cancer cells have mutant β-tubulins that exhibit impaired paclitaxel-driven polymerization. *Journal of Biological Chemistry*, *272*(27), 17118–17125. https://doi.org/10.1074/jbc.272.27.17118

Gidding, C. E. M., Kellie, S. J., Kamps, W. A., & De Graaf, S. S. N. (1999). Vincristine revisited. *Critical Reviews in Oncology/Hematology*, *29*(3), 267–287. https://doi.org/10.1016/S1040-8428(98)00023-7

Go, R. S., & Adjei, A. A. (1999). Review of the comparative pharmacology and clinical activity of cisplatin and carboplatin. *Journal of Clinical Oncology*, *17*(1), 409–422. https://doi.org/10.1200/jco.1999.17.1.409

Green, R. A., Paluch, E., & Oegema, K. (2012). Cytokinesis in Animal Cells. *Annual Review of Cell and Developmental Biology*, *28*, 29–58. https://doi.org/10.1146/annurev-cellbio-101011-155718

Gromley, A., Yeaman, C., Rosa, J., Redick, S., Chen, C. T., Mirabelle, S., Guha, M., Sillibourne, J., & Doxsey, S. J. (2005). Centriolin anchoring of exocyst and SNARE complexes at the midbody is required for secretory-vesicle-mediated abscission. *Cell*, *123*(1), 75–87. https://doi.org/10.1016/j.cell.2005.07.027

Gruneberg, U., Neef, R., Honda, R., Nigg, E. A., & Barr, F. A. (2004). Relocation of Aurora B from centromeres to the central spindle at the metaphase to anaphase transition requires MKlp2. *Journal of Cell Biology*, *166*(2), 167–172. https://doi.org/10.1083/jcb.200403084

Guminski, A. D., Balleine, R. L., Chiew, Y. E., Webster, L. R., Tapner, M., Farrell, G. C., Harnett, P. R., &

DeFazio, A. (2006). MRP2 (ABCC2) and cisplatin sensitivity in hepatocytes and human ovarian carcinoma. *Gynecologic Oncology*, *100*(2), 239–246. https://doi.org/10.1016/j.ygyno.2005.08.046

Haga, R. B., & Ridley, A. J. (2016). Rho GTPases: Regulation and roles in cancer cell biology. *Small GTPases*, *7*(4), 207–221. https://doi.org/10.1080/21541248.2016.1232583

Hall, M. D., Okabe, M., Shen, D. W., Liang, X. J., & Gottesman, M. M. (2008). The role of cellular accumulation in determining sensitivity to platinum-based chemotherapy. *Annual Review of Pharmacology and Toxicology*, *48*, 495–535. https://doi.org/10.1146/annurev.pharmtox.48.080907.180426

Harmon, B. V., Takano, Y. S., Winterford, C. M., & Potten, C. S. (1992). Cell death induced by vincristine in the intestinal crypts of mice and in a human Burkitt's lymphoma cell line. *Cell Proliferation*, *25*(6), 523–536. https://doi.org/10.1111/j.1365-2184.1992.tb01457.x

Hayakawa, J., Ohmichi, M., Kurachi, H., Kanda, Y., Hisamoto, K., Nishio, Y., Adachi, K., Tasaka, K., Kanzaki, T., & Murata, Y. (2000). Inhibition of BAD phosphorylation either at serine 112 via extracellular signal-regulated protein kinase cascade or at serine 136 via Akt cascade sensitizes human ovarian cancer cells to cisplatin. *Cancer Research*, *60*(21), 5988–5994.

Heim, A., Rymarczyk, B., Malhotra, S., & Mayer, T. U. (2017). Regulation of cell division. In *Advances in Experimental Medicine and Biology* (Vol. 953). https://doi.org/10.1007/978-3-319-46095-6_3

Hill, E., Clarke, M., & Barr, F. A. (2000). The Rab6-binding kinesin, Rab6-KIFL, is required for cytokinesis. *Embo J*, *19*(21), 5711–5719. https://doi.org/10.1093/emboj/19.21.5711

Hirokawa, N., & Tanaka, Y. (2015). Kinesin superfamily proteins (KIFs): Various functions and their relevance for important phenomena in life and diseases. *Experimental Cell Research*, *334*(1), 16–25. https://doi.org/10.1016/j.yexcr.2015.02.016

Hodge, R. G., & Ridley, A. J. (2016). Regulating Rho GTPases and their regulators. *Nature Reviews Molecular Cell Biology*, *17*(8), 496–510. https://doi.org/10.1038/nrm.2016.67

Honkawa, H., Masahashi, W., Hashimoto, S., & Hashimoto-Gotoh, T. (1987). Identification of the principal promoter sequence of the c-H-ras transforming oncogene: deletion analysis of the 5'-flanking region by focus formation assay. *Molecular and Cellular Biology*, *7*(8), 2933–2940. https://doi.org/10.1128/mcb.7.8.2933

Howell, S. B., Safaei, R., Larson, C. A., & Sailor, M. J. (2010). Copper transporters and the cellular pharmacology of the platinum-containing cancer drugs. *Molecular Pharmacology*, *77*(6), 887–894. https://doi.org/10.1124/mol.109.063172

Hu, C.-K., Coughlin, M., Field, C. M., & Mitchinson, T. J. (2011). KIF4 Regulates Midzone Length during Cytokinesis Chi-Kuo. *Current Biology*, *21*(10), 815–824. https://doi.org/10.1016/j.cub.2011.04.019

Hu, C. K., Coughlin, M., & Mitchison, T. J. (2012). Midbody assembly and its regulation during cytokinesis. *Molecular Biology of the Cell*, *23*(6), 1024–1034. https://doi.org/10.1091/mbc.E11-08-0721

Hu, Y., Zhu, Q. N., Deng, J. L., Li, Z. X., Wang, G., & Zhu, Y. S. (2018). Emerging role of long non-coding RNAs in cisplatin resistance. *OncoTargets and Therapy*, *11*, 3185–3194. https://doi.org/10.2147/OTT.S158104

Huang, M., & Prendergast, G. C. (2006). RhoB in cancer suppression. *Histology and Histopathology*, *21*(1–3), 213–218. https://doi.org/10.14670/HH-21.213

Hümmer, S., & Mayer, T. U. (2009). Cdk1 Negatively Regulates Midzone Localization of the Mitotic Kinesin Mklp2 and the Chromosomal Passenger Complex. *Current Biology*, *19*(7), 607–612. https://doi.org/10.1016/j.cub.2009.02.046

Ishida, S., Lee, J., Thiele, D. J., & Herskowitz, I. (2002). Uptake of the anticancer drug cisplatin mediated by the copper transporter Ctr1 in yeast and mammals. *Proceedings of the National Academy of Sciences of the United States of America*, *99*(22), 14298–14302. https://doi.org/10.1073/pnas.162491399

Iwasaki, Y., Nagata, K., Nakanishi, M., Natuhara, A., Kubota, Y., Ueda, M., Arimoto, T., & Hara, H. (2005). Double-cycle, high-dose ifosfamide, carboplatin, and etoposide followed by peripheral blood stem-cell transplantation for small cell lung cancer. *Chest*, *128*(4), 2268–2273. https://doi.org/10.1378/chest.128.4.2268

Jaffe, A. B., & Hall, A. (2005). Rho GTPases: Biochemistry and biology. *Annual Review of Cell and Developmental Biology*, *21*, 247–269. https://doi.org/10.1146/annurev.cellbio.21.020604.150721

Janisch, K. M., Vock, V. M., Fleming, M. S., Shrestha, A., Grimsley-Myers, C. M., Rasoul, B. A., Neale, S. A., Cupp, T. D., Kinchen, J. M., Liem, K. F., & Dwyer, N. D. (2013). The vertebrate-specific Kinesin-6, Kif20b, is required for normal cytokinesis of polarized cortical stem cells and cerebral cortex size. *Development*, *140*(23), 4672–4682. https://doi.org/10.1242/dev.093286

Janisch, Kerstin M., McNeely, K. C., Dardick, J. M., Lim, S. H., & Dwyer, N. D. (2018). Kinesin-6 KIF20B is required for efficient cytokinetic furrowing and timely abscission in human cells. *Molecular Biology of the Cell*, *29*(2), 166–179. https://doi.org/10.1091/mbc.E17-08-0495

Jansen, S., Gosens, R., Wieland, T., & Schmidt, M. (2018). Paving the Rho in cancer metastasis: Rho GTPases and beyond. *Pharmacology and Therapeutics*, *183*, 1–21. https://doi.org/10.1016/j.pharmthera.2017.09.002

Jin, L., Huo, Y., Zheng, Z., Jiang, X., Deng, H., Chen, Y., Lian, Q., Ge, R., & Deng, H. (2014). Down-regulation of ras-related protein rab 5C-dependent endocytosis and glycolysis in cisplatin-resistant ovarian cancer cell lines. *Molecular and Cellular Proteomics*, *13*(11), 3138–3151. https://doi.org/10.1074/mcp.M113.033217

Jones, E. V., Dickman, M. J., & Whitmarsh, A. J. (2007). Regulation of p73-mediated apoptosis by c-Jun N-terminal kinase. *Biochemical Journal*, *405*(3), 617–623. https://doi.org/10.1042/BJ20061778

Jordan, M. A., Thrower, D., & Wilson, L. (1991). Mechanism of Inhibition of Cell Proliferation by Vinca Alkaloids. *Cancer Research*, *51*(8), 2212–2222.

Kamimoto, T., Zama, T., Aoki, R., Muro, Y., & Hagiwara, M. (2001). Identification of a Novel Kinesin-related Protein, KRMP1, as a Target for Mitotic Peptidyl-prolyl Isomerase Pin1. *Journal of Biological Chemistry*, *276*(40), 37520–37528. https://doi.org/10.1074/jbc.M106207200

Kampan, N. C., Madondo, M. T., McNally, O. M., Quinn, M., & Plebanski, M. (2015). Paclitaxel and its evolving role in the management of ovarian cancer. *BioMed Research International*, *2015*. https://doi.org/10.1155/2015/413076

Kanehira, M., Katagiri, T., Shimo, A., Takata, R., Shuin, T., Miki, T., Fujioka, T., & Nakamura, Y. (2007). Oncogenic role of MPHOSPH1, a cancer-testis antigen specific to human bladder cancer. *Cancer Research*, *67*(7), 3276–3285. https://doi.org/10.1158/0008-5472.CAN-06-3748

Kartalou, M., & Essigmann, J. M. (2001). Mechanisms of resistance to cisplatin. *Mutation Research*, *478*, 23–43. https://doi.org/10.1016/s0027-5107(01)00141-5

Kavallaris, M., Kuo, D. Y. S., Burkhart, C. A., Regl, D. L., Norris, M. D., Haber, M., & Horwitz, S. B. (1997). Taxol-resistant epithelial ovarian tumors are associated with altered expression of specific β-tubulin isotypes. *Journal of Clinical Investigation*, *100*(5), 1282–1293. https://doi.org/10.1172/JCI119642

Kavallaris, M., Tait, A. S., Norris, M. D., Haber, M., Walsh, B. J., He, L., & Horwitz, S. B. (2001). Multiple microtubule alterations are associated with Vinca alkaloid resistance in human leukemia cells. *Cancer Research*, *61*(15), 5803–5809.

Klauber, N., Parangi, S., Flynn, E., Hamel, E., & D'Amato, R. J. (1997). Inhibition of angiogenesis and breast cancer in mice by the microtubule inhibitors 2-methoxyestradiol and taxol. *Cancer Research*, *57*(1), 81–86.

Klinman, E., & Holzbaur, E. L. F. (2018). Walking Forward with Kinesin. *Trends in Neurosciences*, *41*(9), 555–556. https://doi.org/10.1016/j.tins.2018.07.006

Koch, M., Krieger, M. L., Stölting, D., Brenner, N., Beier, M., Jaehde, U., Wiese, M., Royer, H. D., & Bendas, G. (2013). Overcoming chemotherapy resistance of ovarian cancer cells by liposomal cisplatin: Molecular mechanisms unveiled by gene expression profiling. *Biochemical Pharmacology*, *85*(8), 1077–1090. https://doi.org/10.1016/j.bcp.2013.01.028

Koizumi, Kazuhisa, Takano, K., Kaneyasu, A., Watanabe-Takano, H., Tokuda, E., Abe, T., Watanabe, N., Takenawa, T., & Endo, T. (2012). RhoD activated by fibroblast growth factor induces cytoneme-like cellular protrusions through mDia3C. *Molecular Biology of the Cell*, *23*(23), 4647–4661. https://doi.org/10.1091/mbc.E12-04-0315

Kosmas, C., Tsavaris, N. B., Malamos, N. A., Vadiaka, M., & Koufos, C. (2001). Phase II study of paclitaxel, ifosfamide, and cisplatin as second-line treatment in relapsed small-cell lung cancer. *Journal of Clinical Oncology*, *19*(1), 119–126. https://doi.org/10.1200/JCO.2001.19.1.119

Kuboyama, T., Yokoshima, S., Tokuyama, H., & Fukuyama, T. (2004). Stereocontrolled Total Synthesis of (+)-Vincristine. *Pnas*, *101*(33), 11966–11970. https://doi.org/10.1073/pnas.0401323101

Kumar, H., Pushpa, K., Kumari, A., Verma, K., Pergu, R., & Mylavarapu, S. V. S. (2019). The exocyst complex and Rab5 are required for abscission by localizing ESCRT III subunits to the cytokinetic bridge. In *Journal of cell science* (Vol. 132, Issue 14). https://doi.org/10.1242/jcs.226001

Kurasawa, Y., Earnshaw, W. C., Mochizuki, Y., Dohmae, N., & Todokoro, K. (2004). Essential roles of KIF4 and its binding partner PRC1 in organized central spindle midzone formation. *EMBO Journal*, *23*(16), 3237–3248. https://doi.org/10.1038/sj.emboj.7600347

Kyrkou, A., Soufi, M., Bahtz, R., Ferguson, C., Bai, M., Parton, R. G., Hoffmann, I., Zerial, M., Fotsis, T., & Murphy, C. (2012). RhoD participates in the regulation of cell-cycle progression and centrosome duplication. *Oncogene*, *32*(14), 1831–1842. https://doi.org/10.1038/onc.2012.195

Laemmli, U. K. (1970). Cleavage of Structural Proteins during the Assembly of the Head of Bacteriophage T4. *Nature*, *227*(August), 680–685. https://doi.org/10.1038/227680a0

Li, G., Xie, Z. K., Zhu, D. S., Guo, T., Cai, Q. L., & Wang, Y. (2019). KIF20B promotes the progression of clear cell renal cell carcinoma by stimulating cell proliferation. *Journal of Cellular Physiology*, *234*(9), 16517–16525. https://doi.org/10.1002/jcp.28322

Li, J., Dallmayer, M., Kirchner, T., Musa, J., & Grünewald, T. G. P. (2017). PRC1: Linking Cytokinesis, Chromosomal Instability, and Cancer Evolution. *Trends in Cancer*, *4*(1), 59–73. https://doi.org/10.1016/j.trecan.2017.11.002

Li, Z. Y., Wang, Z. X., & Li, C. C. (2019). Kinesin family member 20B regulates tongue cancer

progression by promoting cell proliferation. *Molecular Medicine Reports*, *19*(3), 2202–2210. https://doi.org/10.3892/mmr.2019.9851

Lin, R., Bagrodia, S., Cerione, R., & Manor, D. (1997). A novel Cdc42Hs mutant induces cellular transformation. *Current Biology*, *7*(10), 794–797. https://doi.org/10.1016/S0960-9822(06)00338-1

Lin, W. F., Lin, X. L., Fu, S. W., Yang, L., Tang, C. T., Gao, Y. J., Chen, H. Y., & Ge, Z. Z. (2018). Pseudopod-associated protein KIF20B promotes Gli1-induced epithelial-mesenchymal transition modulated by pseudopodial actin dynamic in human colorectal cancer. *Molecular Carcinogenesis*, *57*(7), 911–925. https://doi.org/10.1002/mc.22812

Ling, G., Zhang, P., Zhang, W., Sun, J., Meng, X., Qin, Y., Deng, Y., & He, Z. (2010). Development of novel self-assembled DS-PLGA hybrid nanoparticles for improving oral bioavailability of vincristine sulfate by P-gp inhibition. *Journal of Controlled Release*, *148*(2), 241–248. https://doi.org/10.1016/j.jconrel.2010.08.010

Liu, A., Du, W., Liu, J.-P., Jessell, T. M., & Prendergast, G. C. (2000). RhoB Alteration Is Necessary for Apoptotic and Antineoplastic Responses to Farnesyltransferase Inhibitors. *Molecular and Cellular Biology*, *20*(16), 6105–6113. https://doi.org/10.1128/mcb.20.16.6105-6113.2000

Liu, Q., Kaneko, S., Yang, L., Feldman, R. I., Nicosia, S. V., Chen, J., & Cheng, J. Q. (2004). Aurora-A abrogation of p53 DNA binding and transactivation activity by phosphorylation of serine 215. *Journal of Biological Chemistry*, *279*(50), 52175–52182. https://doi.org/10.1074/jbc.M406802200

Liu, X., Gong, H., & Huang, K. (2013). Oncogenic role of kinesin proteins and targeting kinesin therapy. *Cancer Science*, *104*(6), 651–656. https://doi.org/10.1111/cas.12138

Liu, X., Li, Y., Zhang, X., Liu, X.-Y., Peng, A., Chen, Y., Meng, L., Chen, H., Zhang, Y., Miao, X., Zheng, L., & Huang, K. (2018). Inhibition of kinesin family member 20B sensitizes hepatocellular carcinoma cell to microtubule-targeting agents by blocking cytokinesis. *Cancer Science*, *May*, 1–11. https://doi.org/10.1111/cas.13794

Liu, X. R., Cai, Y., Cao, X., Wei, R. C., Li, H. L., Zhou, X. M., Zhang, K. J., Wu, S., Qian, Q. J., Cheng, B., Huang, K., & Liu, X. Y. (2012). A new oncolytic adenoviral vector carrying dual tumour suppressor genes shows potent anti-tumour effect. *Journal of Cellular and Molecular Medicine*, *16*(6), 1298–1309. https://doi.org/10.1111/j.1582-4934.2011.01396.x

Liu, X., Zhou, Y., Liu, X., Peng, A., Gong, H., Huang, L., Ji, K., Petersen, R. B., Zheng, L., & Huang, K. (2014). MPHOSPH1: A potential therapeutic target for hepatocellular carcinoma. *Cancer Research*, *74*(22), 6623–6634. https://doi.org/10.1158/0008-5472.CAN-14-1279

Liu, Y. M., Chen, H. L., Lee, H. Y., & Liou, J. P. (2014). Tubulin inhibitors: A patent review. *Expert Opinion on Therapeutic Patents*, *24*(1), 69–88. https://doi.org/10.1517/13543776.2014.859247

Lo, I. F. M., Brewer, C., Shannon, N., Shorto, J., Tang, B., Black, G., Soo, M. T., Ng, D. K. K., Lam, S. T. S., & Kerr, B. (2008). Severe neonatal manifestations of Costello syndrome. *Journal of Medical Genetics*, *45*(3), 167–171. https://doi.org/10.1136/jmg.2007.054411

Long, M., & Simpson, J. C. (2017). Rho GTPases operating at the Golgi complex: Implications for membrane traffic and cancer biology. *Tissue and Cell*, *49*(2), 163–169. https://doi.org/10.1016/j.tice.2016.09.007

Ma, P., Xiao, H., Li, C., Dai, Y., Cheng, Z., Hou, Z., & Lin, J. (2015). Inorganic nanocarriers for platinum drug delivery. *Materials Today*, *18*(10), 554–564. https://doi.org/10.1016/j.mattod.2015.05.017

Machuy, N., Rajalingam, K., & Rudel, T. (2004). Requirement of caspase-mediated cleavage of c-Abl during stress-induced apoptosis. *Cell Death and Differentiation*, *11*(3), 290–300. https://doi.org/10.1038/sj.cdd.4401336

Madaule, P., & Axel, R. (1985). A novel ras-related gene family. *Cell*, *41*(1), 31–40. https://doi.org/10.1016/0092-8674(85)90058-3

Majhen, D., Stojanović, N., Vukić, D., Pichon, C., Leduc, C., Osmak, M., & Ambriović-Ristov, A. (2014). Increased adenovirus type 5 mediated transgene expression due to RhoB down-regulation. *PLoS ONE*, *9*(1), 1–11. https://doi.org/10.1371/journal.pone.0086698

Marei, H., & Malliri, A. (2017). GEFs: Dual regulation of Rac1 signaling. *Small GTPases*, *8*(2), 90–99. https://doi.org/10.1080/21541248.2016.1202635

Martino, E., Casamassima, G., Castiglione, S., Cellupica, E., Pantalone, S., Papagni, F., Rui, M., Siciliano, A. M., & Collina, S. (2018). Vinca alkaloids and analogues as anti-cancer agents: Looking back, peering ahead. *Bioorganic and Medicinal Chemistry Letters*, *28*(17), 2816–2826. https://doi.org/10.1016/j.bmcl.2018.06.044

McClelland, S. E. (2017). *Role of Chromosomal Instability in Cancer Progression*. *13*(July), 1–14.

McGuire, W., Rowinsky, E., Rosenhein, N., Grumbine, F., Ettinger, D., Armstrong, D., & Donehower, R. (1990). Taxol: A unique antineoplastic agent with significant activity in advanced ovarian epithelial neoplasms. *International Journal of Gynecology & Obstetrics*, *31*(3), 298–298. https://doi.org/10.1016/0020-7292(90)91032-l

Mckay, H. F., & Burgess, D. R. (2011). "Life is a Highway": Membrane Trafficking During Cytokinesis. *Traffic*, *12*(3), 247–251. https://doi.org/10.1111/j.1600-0854.2010.01139.x

Michiels, F., Habets, G. G. M., Stam, J. C., Habets, G. G. M., Van Der Kammen, R. A., & Collard, J. G. (1995). A role for Rac in Tiaml-induced membrane ruffling and invasion. In *Nature* (Vol. 375, Issue 6529, pp. 338–340). https://doi.org/10.1038/375338a0

Mickisch, G., Fajta, S., Keilhauer, G., Schlick, E., Tschada, R., & Alken, P. (1990). Chemosensitivity testing of primary human renal cell carcinoma by a tetrazolium based microculture assay (MTT). *Urological Research*, *18*(2), 131–136. https://doi.org/10.1007/BF00302474

Miki, H., Okada, Y., & Hirokawa, N. (2005). Analysis of the kinesin superfamily: Insights into structure and function. *Trends in Cell Biology*, *15*(9), 467–476. https://doi.org/10.1016/j.tcb.2005.07.006

Mishima, M., Kaitna, S., & Glotzer, M. (2002). Central spindle assembly and cytokinesis require a kinesin-like protein/RhoGAP complex with microtubule bundling activity. *Developmental Cell*, *2*(1), 41–54. https://doi.org/10.1016/S1534-5807(01)00110-1

Morgan, D. O. (1997). Cyclin-dependent kinases: Engines, clocks, and microprocessors. *Annual Review of Cell and Developmental Biology*, *13*, 261–291. https://doi.org/10.1146/annurev.cellbio.13.1.261

Morita, E., Sandrin, V., Chung, H. Y., Morham, S. G., Gygi, S. P., Rodesch, C. K., & Sundquist, W. I. (2007). Human ESCRT and ALIX proteins interact with proteins of the midbody and function in cytokinesis. *EMBO Journal*, *26*(19), 4215–4227. https://doi.org/10.1038/sj.emboj.7601850

Morris, P. G., & Fornier, M. N. (2008). Microtubule active agents: Beyond the taxane frontier. *Clinical Cancer Research*, *14*(22), 7167–7172. https://doi.org/10.1158/1078-0432.CCR-08-0169

Motulsky, H. J. (2007). Prism 5 Statistics Guide. In *GraphPad Software, Inc. All*.

Mozzetti, S., Ferlini, C., Concolino, P., Filippetti, F., Raspaglio, G., Prislei, S., Gallo, D., Martinelli, E.,

Ranelletti, F. O., Ferrandina, G., & Scambia, G. (2005). Class III β-tubulin overexpression is a prominent mechanism of paclitaxel resistance in ovarian cancer patients. *Clinical Cancer Research*, *11*(1), 298–305.

Murphy, C., Saffrich, R., Grummt, M., Gournier, H., Rybin, V., Rubino, M., Auvinen, P., Lutcke, A., Parton, R. G., & Zerial, M. (1996). Endosome dynamics regulated by a Rho protein. *Nature*, *384*, 427–432.

Murphy, C., Saffrich, R., Olivo-Marin, J. C., Giner, A., Ansorge, W., Fotsis, T., & Zerial, M. (2001). Dual function of rhoD in vesicular movement and cell motility. *European Journal of Cell Biology*, *80*(6), 391–398. https://doi.org/10.1078/0171-9335-00173

Narumiya, S., & Thumkeo, D. (2018). Rho signaling research: history, current status and future directions. *FEBS Letters*, *592*(11), 1763–1776. https://doi.org/10.1002/1873-3468.13087

Neef, R., Klein, U. R., Kopajtich, R., & Barr, F. A. (2006). Cooperation between mitotic kinesins controls the late stages of cytokinesis. *Current Biology*, *16*(3), 301–307. https://doi.org/10.1016/j.cub.2005.12.030

Neef, R., Preisinger, C., Sutcliffe, J., Kopajtich, R., Nigg, E. A., Mayer, T. U., & Barr, F. A. (2003). Phosphorylation of mitotic kinesin-like protein 2 by polo-like kinase 1 is required for cytokinesis. *Journal of Cell Biology*, *162*(5), 863–875. https://doi.org/10.1083/jcb.200306009

Nehru, V., Almeida, F. N., & Aspenström, P. (2013). Interaction of RhoD and ZIP kinase modulates actin filament assembly and focal adhesion dynamics. *Biochemical and Biophysical Research Communications*, *433*(2), 163–169. https://doi.org/10.1016/j.bbrc.2013.02.046

Nehru, V., Voytyuk, O., Lennartsson, J., & Aspenström, P. (2013). Rhod binds the rab5 effector rabankyrin-5 and has a role in trafficking of the platelet-derived growth factor receptor. *Traffic*, *14*(12), 1242–1254. https://doi.org/10.1111/tra.12121

Neto, H., Collins, L. L., & Gould, G. W. (2011). Vesicle trafficking and membrane remodelling in cytokinesis. *Biochemical Journal*, *437*(1), 13–24. https://doi.org/10.1042/BJ20110153

Nguyen, Q.-D. (2002). RhoA- and RhoD-dependent regulatory switch of Galpha subunit signaling by PAR-1 receptors in cellular invasion. *The FASEB Journal*, *16*(6), 565–576. https://doi.org/10.1096/fj.01-0525com

Noble, R. L., Beer, C. T., & Cutts, J. H. (1958). ROLE OF CHANCE OBSERVATIONS I N Noble et al . : Chance Observations in Chemotherapy. *Ann. N.Y. Acad. Sci.*, *76*, 882–894.

Obara, W., Ohsawa, R., Kanehira, M., Takata, R., Tsunoda, T., Yoshida, K., Takeda, K., Katagiri, T., Nakamura, Y., & Fujioka, T. (2012). Cancer peptide vaccine therapy developed from oncoantigens identified through genome-wide expression profile analysis for bladder cancer. *Japanese Journal of Clinical Oncology*, *42*(7), 591–600. https://doi.org/10.1093/jjco/hys069

Orgaz, J. L., Herraiz, C., & Sanz-Moreno, V. (2014). Rho GTPases modulate malignant transformation of tumor cells. *Small GTPases*, *5*(4). https://doi.org/10.4161/sgtp.29019

Osmak, M., & Eljuga, D. (1993). The characterization of two human cervical carcinoma HeLa sublines resistant to cisplatin. *Research in Experimental Medicine*, *193*(1), 389–396. https://doi.org/10.1007/BF02576247

Pei, P. G., Pasquier, E., & Kavallaris, M. (2007). Class III Beta-tubulin mediates sensitivity to chemotherapeutic drugs in non-small cell lung cancer. *Cancer Research*, *67*(19), 9356–9363. https://doi.org/10.1158/0008-5472.CAN-07-0509

Piccart, M. J., & Cardoso, F. (2003). Progress in systemic therapy for breast cancer: An overview and

perspectives. *European Journal of Cancer, Supplement*, *1*(2), 56–69. https://doi.org/10.1016/S1359-6349(03)00009-0

Porter, A. P., Papaioannou, A., & Malliri, A. (2016). Deregulation of Rho GTPases in cancer. *Small GTPases*, *7*(3), 123–138. https://doi.org/10.1080/21541248.2016.1173767

Prekeris, R., & Gould, G. W. (2008). Breaking up is hard to do – membrane traffic in cytokinesis. *Journal of Cell Science*, *121*(0 10), 1569–1576. https://doi.org/10.1242/jcs.018770

Prendergast, G. C. (2001). Farnesyltransferase inhibitors define a role for RhoB in controlling neoplastic pathophysiology. *Histology and Histopathology*, *16*(1), 269–275. https://doi.org/10.14670/HH-16.269

Prendergast, G. C., Khosravi-Far, R., Solski, P. A., Kurzawa, H., Lebowitz, P. F., & Der, C. J. (1995). Critical role of Rho in cell transformation by oncogenic Ras. *Oncogene*, *10*(12), 2289–2296.

Randazzo, P. A. (2003). RhoD, Src, and hDia2C in Endosome Motility. *Developmental Cell*, *4*, 287–293. https://doi.org/10.1038/ncb935.Murphy

Rath, O., & Kozielski, F. (2012). Kinesins and cancer. *Nature Reviews Cancer*, *12*(August), 527–539. https://doi.org/10.1038/nrc3310

Recchi, C., & Seabra, M. C. (2012). Novel functions for Rab GTPases in multiple aspects of tumour progression. *Biochemical Society Transactions*, *40*(6), 1398–1403. https://doi.org/10.1042/BST20120199

Rohwer, N., & Cramer, T. (2011). Hypoxia-mediated drug resistance: Novel insights on the functional interaction of HIFs and cell death pathways. *Drug Resistance Updates*, *14*(3), 191–201. https://doi.org/10.1016/j.drup.2011.03.001

Rojas, A. M., Fuentes, G., Rausell, A., & Valencia, A. (2012). The Ras protein superfamily: Evolutionary tree and role of conserved amino acids. *Journal of Cell Biology*, *196*(2), 189–201. https://doi.org/10.1083/jcb.201103008

Saad, S. Y., Najjar, T. A. O., & Alashari, M. (2004). Role of non-selective adenosine receptor blockade and phosphodiesterase inhibition in cisplatin-induced nephrogonadal toxicity in rats. *Clinical and Experimental Pharmacology and Physiology*, *31*(12), 862–867. https://doi.org/10.1111/j.1440-1681.2004.04127.x

Said, R., & Tsimberidou, A. M. (2014). Pharmacokinetic evaluation of vincristine for the treatment of lymphoid malignancies. *Expert Opinion on Drug Metabolism and Toxicology*, *10*(3), 483–494. https://doi.org/10.1517/17425255.2014.885016

Sandilands, E., Brunton, V. G., & Frame, M. C. (2007). The membrane targeting and spatial activation of Src, Yes and Fyn is influenced by palmitoylation and distinct RhoB/RhoD endosome requirements. *Journal of Cell Science*, *120*(15), 2555–2564. https://doi.org/10.1242/jcs.003657

Sapir, T., Levy, T., Sakakibara, A., Rabinkov, A., Miyata, T., & Reiner, O. (2013). Shootin1 Acts in Concert with KIF20B to Promote Polarization of Migrating Neurons. *Journal of Neuroscience*, *33*(29), 11932–11948. https://doi.org/10.1523/JNEUROSCI.5425-12.2013

Schiel, J. A., Childs, C., & Prekeris, R. (2013). Endocytic transport and cytokinesis: From regulation of the cytoskeleton to midbody inheritance. *Trends in Cell Biology*, *23*(7), 319–327. https://doi.org/10.1016/j.tcb.2013.02.003

Schiel, J. A., & Prekeris, R. (2013). Membrane Dynamics during Cytokinesis. *Current Opinion in Cell Biology*, *25*(1), 92–98. https://doi.org/10.1016/j.ceb.2012.10.012

Schiff, P. B., Fant, J., & Horwitz, S. B. (1979). Promotion of microtubule assembly in vitro by taxol [19]. In *Nature* (Vol. 277, Issue 5698, pp. 665–667). https://doi.org/10.1038/277665a0

Sevko, A., Kremer, V., Falk, C., Umansky, L., Shurin, M. R., Shurin, G. V., & Umansky, V. (2012). Application of paclitaxel in low non-cytotoxic doses supports vaccination with melanoma antigens in normal mice. *Journal of Immunotoxicology*, *9*(3), 275–281. https://doi.org/10.3109/1547691X.2012.655343

Silva, P. M. A., Ribeiro, N., Lima, R. T., Andrade, C., Diogo, V., Teixeira, J., Florindo, C., Tavares, Á., Vasconcelos, M. H., & Bousbaa, H. (2017). Suppression of spindly delays mitotic exit and exacerbates cell death response of cancer cells treated with low doses of paclitaxel. *Cancer Letters*, *394*(March), 33–42. https://doi.org/10.1016/j.canlet.2017.02.024

Simonian, P. L., Grillot, D. A. M., & Nuñez, G. (1997). Bcl-2 and Bcl-XL can differentially block chemotherapy-induced cell death. *Blood*, *90*(3), 1208–1216. https://doi.org/10.1182/blood.v90.3.1208.1208_1208_1216

Soubry, A., Staes, K., Parthoens, E., Noppen, S., Stove, C., Bogaert, P., Van Hengel, J., & Van Roy, F. (2010). The transcriptional repressor Kaiso localizes at the mitotic spindle and is a constituent of the pericentriolar material. *PLoS ONE*, *5*(2), 1–18. https://doi.org/10.1371/journal.pone.0009203

Stegmeier, F., Sowa, M. E., Nalepa, G., Gygi, S. P., Harper, J. W., & Elledge, S. J. (2007). The tumor suppressor CYLD regulates entry into mitosis. *Proceedings of the National Academy of Sciences of the United States of America*, *104*(21), 8869–8874. https://doi.org/10.1073/pnas.0703268104

Stengel, K., & Zheng, Y. (2011). Cdc42 in oncogenic transformation, invasion, and tumorigenesis. *Cell Signal*, *23*(9), 1415–1423. https://doi.org/10.1016/j.cellsig.2011.04.001

Subramanian, R., Wilson-Kubalek, E. M., Arthur, C. P., Bick, M. J., Campbell, E. A., Darst, S. A., Milligan, R. A., & Kapoor, T. M. (2010). Insights into antiparallel microtubule crosslinking by PRC1, a conserved nonmotor microtubule binding protein. *Cell*, *142*(3), 433–443. https://doi.org/10.1016/j.cell.2010.07.012

Takahashi, S., Fusaki, N., Ohta, S., Iwahori, Y., Iizuka, Y., Inagawa, K., Kawakami, Y., Yoshida, K., & Toda, M. (2012). Downregulation of KIF23 suppresses glioma proliferation. *Journal of Neuro-Oncology*, *106*(3), 519–529. https://doi.org/10.1007/s11060-011-0706-2

Takano, Y., Okudaira, M., & Harmon, B. V. (1993). Apoptosis Induced by Microtubule Disrupting Drugs in Cultured Human Lymphoma Cells: Inhibitory Effects of Phorbol Ester and Zinc Sulphate. *Pathology Research and Practice*, *189*(2), 197–203. https://doi.org/10.1016/S0344-0338(11)80092-0

Tan, M.-H., De, S., Bebek, G., Orloff, M. S., Wesolowski, R., Downs-Kelly, E., Budd, T. G., Stark, G. R., & Eng, C. (2012). Specific kinesin expression profiles associated with taxane resistance in breast cancer. *Breast Cancer Resistance Treatment*, *131*(3), 849–858. https://doi.org/10.1007/s10549-011-1500-8

Taniuchi, K., Nakagawa, H., Nakamura, T., Eguchi, H., & Ohigashi, H. (2005). Down-regulation of RAB6KIFL / KIF20A , a Kinesin Involved with Membrane Trafficking of Discs Large Homologue 5 , Can Attenuate Growth of Pancreatic Cancer Cell Membrane Trafficking of Discs Large Homologue 5 , Can Attenuate Growth of Pancreatic Cancer Cel. *Cancer Research*, *1*, 105–112.

Tong, Y., Chugha, P., Hota, P. K., Alviani, R. S., Li, M., Tempel, W., Shen, L., Park, H.-W., & Buck, M. (2007). Binding of Rac1, Rnd1, and RhoD to a Novel Rho GTPase Interaction Motif Destabilizes

Dimerization of the Plexin-B1 Effector Domain. *Journal of Biological Chemistry*, *282*(51), 37215–37224. https://doi.org/10.1074/jbc.M703800200

Traut, T. W. (1994). Physiological concentrations of purines and pyrimidines. *Molecular and Cellular Biochemistry*, *140*(1), 1–22. https://doi.org/10.1007/BF00928361

Truong, D., Boddy, K. C., Canadien, V., Brabant, D., Fairn, G. D., D'Costa, V. M., Coyaud, E., Raught, B., Pérez-Sala, D., Park, W. S., Heo, W. Do, Grinstein, S., & Brumell, J. H. (2018). Salmonella exploits host Rho GTPase signalling pathways through the phosphatase activity of SopB. *Cellular Microbiology*, *20*(10). https://doi.org/10.1111/cmi.12938

Tsimberidou, A. M., Braiteh, F., Stewart, D. J., & Kurzrock, R. (2009). Ultimate fate of oncology drugs approved by the US food and drug administration without a randomized trial. *Journal of Clinical Oncology*, *27*(36), 6243–6250. https://doi.org/10.1200/JCO.2009.23.6018

Tsubakimoto, K., Matsumoto, K., Abe, H., Ishii, J., Amano, M., Kaibuchi, K., & Endo, T. (1999). Small GTPase RhoD suppresses cell migration and cytokinesis. *Oncogene*, *18*(15), 2431–2440. https://doi.org/10.1038/sj.onc.1202604

Turner, N., Stewart, J., Barnett, F., & White, S. (2012). Syndrome of inappropriate anti-diuretic hormone secretion secondary to carboplatin after docetaxel-carboplatin-trastuzumab combination for early stage HER-2 positive breast cancer. *Asia-Pacific Journal of Clinical Oncology*, *8*(3), 10–12. https://doi.org/10.1111/j.1743-7563.2012.01526.x

Tzeng, H. T., & Wang, Y. C. (2016). Rab-mediated vesicle trafficking in cancer. *Journal of Biomedical Science*, *23*(1), 1–7. https://doi.org/10.1186/s12929-016-0287-7

Van Der Burgt, I., Kupsky, W., Stassou, S., Nadroo, A., Barroso, C., Diem, A., Kratz, C. P., Dvorsky, R., Ahmadian, M. R., & Zenker, M. (2007). Myopathy caused by HRAS germline mutations: Implications for disturbed myogenic differentiation in the presence of constitutive HRas activation. *Journal of Medical Genetics*, *44*(7), 459–462. https://doi.org/10.1136/jmg.2007.049270

Vega, F. M., Colomba, A., Reymond, N., Thomas, M., & Ridley, A. J. (2012). RhoB regulates cell migration through altered focal adhesion dynamics. *Open Biology*, *2*(MAY). https://doi.org/10.1098/rsob.120076

Vega, F. M., & Ridley, A. J. (2008). Rho GTPases in cancer cell biology. *FEBS Letters*, *582*(14), 2093–2101. https://doi.org/10.1016/j.febslet.2008.04.039

Verhey, K. J., & Hammond, J. W. (2009). Traffic control: Regulation of kinesin motors. *Nature Reviews Molecular Cell Biology*, *10*(11), 765–777. https://doi.org/10.1038/nrm2782

Vicente, J. J., & Wordeman, L. (2015). Mitosis, Microtubule Dynamics and the Evolution of Kinesins. *Experimental Cell Research*, *334*(1), 61–69. https://doi.org/10.1016/j.yexcr.2015.02.010

Wang, D., Qian, X., Rajaram, M., Durkin, M. E., & Lowy, D. R. (2016). DLC1 is the principal biologically-relevant down-regulated DLC family member in several cancers. *Oncotarget*, *7*(29), 45144–45157. https://doi.org/10.18632/oncotarget.9266

Wang, H., Spang, A., Sullivan, M. A., Hryhorenko, J., & Hagen, F. K. (2005). The Terminal Phase of Cytokinesis in the Caenorhabditis elegans Early Embryo Requires Protein Glycosylation. *Molecular Biology of the Cell*, *16*(September), 4202–4213. https://doi.org/10.1091/mbc.E05-05–0472

Wang, L., Yang, L., Luo, Y., & Zheng, Y. (2003). A Novel Strategy for Specifically Down-regulating Individual Rho GTPase Activity in Tumor Cells. *Journal of Biological Chemistry*, *278*(45), 44617–

44625. https://doi.org/10.1074/jbc.M308929200

Wang, W., Zhang, Y., Chen, R., Tian, Z., Zhai, Y., Janz, S., Gu, C., & Yang, Y. (2017). Chromosomal instability and acquired drug resistance in multiple myeloma. *Oncotarget*, *8*(44), 78234–78244. https://doi.org/10.18632/oncotarget.20829

Wang, X., & Li, S. (2014). Protein mislocalization: Mechanisms, functions and clinical applications in cancer. In *Biochimica et Biophysica Acta - Reviews on Cancer* (Vol. 1846, Issue 1). https://doi.org/10.1016/j.bbcan.2014.03.006

Wani, M. C., & Horwitz, S. B. (2014). Nature as a Remarkable Chemist: A Personal Story of the Discovery and Development of Taxol®. *Anticancer Drugs*, *25*(5), 482–487. https://doi.org/10.1097/CAD.0000000000000063

Watson, M. B., Lind, M. J., Smith, L., Drew, P. J., & Cawkwell, L. (2007). Expression microarray analysis reveals genes associated with in vitro resistance to cisplatin in a cell line model. *Acta Oncologica*, *46*(5), 651–658. https://doi.org/10.1080/02841860601156157

Wee, P., & Wang, Z. (2017). Cell cycle synchronization of hela cells to assay EGFR pathway activation. *Methods in Molecular Biology*, *1652*, 167–181. https://doi.org/10.1007/978-1-4939-7219-7_13

Wen, S.-J., Zhang, W., Ni, N.-N., Wu, Q., Wang, X.-P., Lin, Y.-K., & Sun, J.-F. (2017). Expression of Rho GTPases family in melanoma cells and its influence on cytoskeleton and migration. *Oncotarget*, *8*(18), 30112–30122. https://doi.org/10.18632/oncotarget.15618

Wennerberg, K., & Der, C. J. (2004). Rho-family GTPases: It's not only Rac and Rho (and i like it). *Journal of Cell Science*, *117*(8), 1301–1312. https://doi.org/10.1242/jcs.01118

Westendorf, J. M., Rao, P. N., & Gerace, L. (1994). Cloning of cDNAs for M-phase phosphoproteins recognized by the MPM2 monoclonal antibody and determination of the phosphorylated epitope. *Proceedings of the National Academy of Sciences USA*, *91*(2), 714–718. https://doi.org/10.1073/pnas.91.2.714

Wherlock, M., Gampel, A., Futter, C., & Mellor, H. (2004). Farnesyltransferase inhibitors disrupt EGF receptor traffic through modulation of the RhoB GTPase. *Journal of Cell Science*, *117*(15), 3221–3231. https://doi.org/10.1242/jcs.01193

Wiernik, P. H., Schwartz, E. L., Strauman, J. J., Dutcher, J. P., Lipton, R. B., & Paietta, E. (1987). Phase I Clinical and Pharmacokinetic Study of Taxol. *Cancer Research*, *47*(9), 2486–2493.

Wu, X., & Frost, J. A. (2006). Multiple Rho proteins regulate the subcellular targeting of PAK5. *Biochemical and Biophysical Research Communications*, *351*(2), 328–335. https://doi.org/10.1016/j.bbrc.2006.09.172

Yang, Z. (2002). Small GTPases: Versatile signaling switches in plants. *Plant Cell*, *14*(SUPPL.), 375–388. https://doi.org/10.1105/tpc.001065

Yasuda, S., & Narumiya, S. (2006). Analysis of a mitotic role of Cdc42. *Methods in Enzymology*, *406*(06), 656–665. https://doi.org/10.1016/S0076-6879(06)06051-4

Zhang, I., Alter, N., Reed, J. C., Borner, C., Obeid, L. M., & Hannun, Y. A. (1996). Bcl-2 interrupts the ceramide-mediated pathway of cell death. *Proceedings of the National Academy of Sciences of the United States of America*, *93*(11), 5325–5328. https://doi.org/10.1073/pnas.93.11.5325

Zhang, Y., Yang, S. H., & Guo, X. L. (2017). New insights into Vinca alkaloids resistance mechanism and circumvention in lung cancer. *Biomedicine and Pharmacotherapy*, *96*(44), 659–666. https://doi.org/10.1016/j.biopha.2017.10.041

Zhu, C., Bossy-Wetzel, E., & Jiang, W. (2005). Recruitment of MKLP1 to the spindle midzone/midbody by INCENP is essential for midbody formation and completion of cytokinesis in human cells. *Biochemical Journal*, *389*(2), 373–381. https://doi.org/10.1042/BJ20050097

Zhu, C., & Jiang, W. (2005). Cell cycle-dependent translocation of PRC1 on the spindle by Kif4 is essential for midzone formation and cytokinesis. *Proceedings of the National Academy of Sciences of the United States of America*, *102*(2), 343–348. https://doi.org/10.1073/pnas.0408438102

Zhu, C., Lau, E., Schwarzenbacher, R., Bossy-Wetzel, E., & Jiang, W. (2006). Spatiotemporal control of spindle midzone formation by PRC1 in human cells. *Proceedings of the National Academy of Sciences of the United States of America*, *103*(16), 6196–6201. https://doi.org/10.1073/pnas.0506926103

8. Summary

RhoD is the less known member of Rho protein family with roles antagonistic to those of RhoA transforming protein. The potential interacting partner of RhoD, kinesin KIF20B, is overexpressed in several tumor cell lines. Until now, only one study has shown influence of RhoD expression on tumor cell resistance to cisplatin and the topic of KIF20B in tumor cell resistance to antitumor drugs has not been fully adressed.

In this research we have addressed the plausible interaction between RhoD and KIF20B, which we have supported with western blot and localization data. In the western blot data, in most cell lines tested there is a reduction of KIF20B protein band in the RhoD silenced samples, at least for one tested siRNA.

Regarding KIF20B localization, we have managed to demonstrate on HeLa and CaCO-2 cells, that KIF20B is associated with the chromosomes longer than previously thought. Since we have noticed there was considerable reduction in KIF20B signals after RhoD silencing on the western blot samples, we wanted to check this phenomenon by immunofluorescent staining of KIF20B in RhoD silenced cells and we have managed to corroborate this find in HeLa cells.

Using exogenous RhoD in its active forms in control and KIF20B silenced cells, we have come across a RhoD localization which was previously unreported in literature. In every cell line tested, we have found that RhoD always localized in the midbody of telophase cells, surrounded or overlapped by KIF20B signals. We have also confirmed that KIF20B knockdown has no effect on this newly characterized exogenous RhoD localization in either intensity or misplacement.

To see if there were delays in mitosis, we have synchronized HeLa cells and we noticed that in the case of RhoD silenced sample, the cells progressed through mitosis faster than in both control and KIF20B silenced sample. To study the influence RhoD might have on cell cycle in HeLa cells, we have stained non-synchronized RhoD or KIF20B silenced HeLa cells with propidium iodide and analyzed their distribution in cell cycle by flow cytometry. We have found that in all three tested RhoD siRNAs, there was a distinct gap in the G1/S phase cell content, and the same phenotype was found in the two of the tested KIF20B sRNAs.

Since RhoD and KIF20B have shown mutual roles and properties in cell cycle progression, expression and localization studies, we have proposed that they also might have a role in sensitivity of tumor cells to anticancer agents.

When treating RhoD or KIF20B silenced cells with cisplatin, we have found different responses across different cell types. In HeLa cells, we have found that RhoD knockdown significantly induces sensitization to cisplatin, and that siKIF20B also induces comparable levels of sensitization at the same concentrations of cisplatin.

Across all tested cell lines, upon RhoD knockdown there is a readily visible effect of a slightly decreased cell proliferation, of about 20%, when compared to silencing negative control. The effect of KIF20B knockdown on cell proliferation is somewhat similar to that of RhoD, yet not as pronounced. So far, our results demonstrate sensitization to cisplatin only in HeLa cells when silenced by either RhoD or KIF20B siRNA. While our other results are indicative of a mild sensitivity across all cell lines, in response to paclitaxel and vincristine treatment, the ANOVA statistical analysis reveals mostly antagonistic effects between the drugs and both siRNAs.

Overall, we have demonstrated that RhoD has a novel localization in the intercellular bridge which was previously unknown, and might indicate a deeper involvement in the final steps of cytokinesis, possibly through the interaction with KIF20B.

This raises an interesting observation that KIF20B and RhoD might indeed be worth of a more insightful approach in terms of anticancer drug research as potential targets, especially RhoD.

9. Sažetak

RhoD je manje poznati član obitelji Rho proteina te ima uloge u staničnim procesima koje su suprotne onima RhoA transformirajućeg proteina. Primjerice, RhoD ograničava kretanje endosoma u stanici i suzbija migraciju. KIF20B, potencijalni interakcijski partner iz obitelji kinesina 6, povećano je eksprimiran u nekoliko tumorskih staničnih linija, posebno u stanicama raka mjehura. Nedavno su mitotski kinesini postali veoma zanimljive nove mete u istraživanju tumora (Rath and Kozielski, 2012), posebno zbog njihove povezanosti uz mikrotubule. Mikrotubuli su ključne strukture prilikom mitoze, što ih čini dobrim metama za protumitotske lijekove (Chandrasekaran et al., 2015).

Do sada je samo jedna studija pokazala mogući utjecaj ekspresije proteina RhoD na otpornost tumorskih stanica na protutumorske lijekove, dok je ista tematika za protein KIF20B tek nedavno načeta.

U ovom istraživanju bavili smo se mogućom interakcijom između proteina RhoD i KIF20B (Ishizaki et al., neobjavljeni podaci), što smo poduprli podacima o ekspresiji te lokalizacije. Podaci western blotova pokazuju da kod većine ispitanih staničnih linija (osim kod MCF-7 i MDA-MB-468), prilikom utišavanja proteina RhoD s 10 nM specifičnom siRNA dolazi do smanjenja intenziteta ekspresije proteina KIF20B. Na nivou mRNA, ovi pronalasci se uglavnom slažu s podacima dobivenim kvantitativnom reakcijom lančane polimeraze, kojom smo također primijetili prilično visoku eksprimiranost RhoD mRNA u ispitanim staničnim linijama.

S obzirom na lokalizaciju KIF20B, u svim ispitanim staničnim linijama ona odgovara već objavljenim rezultatima na stanicama HeLa (Abaza et al., 2003, Janisch et al., 2018), HeLa S3 (Kamimoto et al., 2001), UM-UC-3 stanicama karcinoma mjehura (Kanehira et al., 2007) te stanicama kolorektalnog karcinoma SW480 i LOVO (Lin et al., 2017). Međutim, na HeLa, HCT-116 i CaCO-2 stanicama smo u našoj studiji imunofluorescencijom uspjeli pokazati da KIF20B ostaje pridružen kromosomima dulje nego što se do sada mislilo, odnosno da je pridužen kromosomima dulje od same interfaze, kroz metafazu pa sve do rane anafaze, kada se signal proteina KIF20B postepeno prenosi na početno mitotsko vreteno. Također smo ispitali i utišavanje KIF20B putem imunofluorescencije te potvrdili kako je KIF20B signal slabiji na interfaznim jezgrama u utišanim stanicama te potpuno nestaje u središnjem dijelu mitotskog vretena i međustaničnom mostu tokom anafaze i telofaze.

Na podacima dobivenima iz western blota primijetili smo kako u većini ispitanih stanica prilikom utišavanja RhoD dolazi do smanjenja intenziteta ekspresije KIF20B, te smo taj pronalazak željeli potvrditi i s imunofluorescencijom, što smo uspjeli na primjeru HeLa stanica. Također smo htjeli ispitati i obrnuti učinak, odnosno ima li ekspresija KIF20B proteina utjecaj na lokalizaciju ili ekspresiju RhoD u stanicama, što smo učinili utišavanjem KIF20B u stanicama transfeciranim s aktivnom formom proteina RhoD. Primijetili smo da utišavanje KIF20B nema nikakav utjecaj na drugačiju lokalizaciju ili intenzitet signala proteina RhoD, no primijetili smo i novu, do sada nepotvrđenu lokalizaciju proteina RhoD. U ispitanim staničnim linijama, pronašli smo da se RhoD uvijek lokalizira na Flemingovo tjelešce u međusaničnom mostu telofaznih stanica, te je uokviren ili se preklapa sa signalom KIF20B.

Kako bismo ispitali ima li RhoD utjecaja na odgađanje ili zastoj mitoze, s obzirom da je pronađen u međustaničnom mostu, obavili smo utišavanje na sinkroniziranim HeLa stanicama pomoću dvostrukog timidinskog blokiranja mitoze te ispitali postotak stanica u pojedinoj fazi mitoze imunofluorescencijom. Nismo primijetili velike razlike između kontrolnih uzoraka i KIF20B utišanih stanica, što je ukazalo na blagi fenotip koji pokazuju stanice s utišanim KIF20B, no primijetili smo da u slučaju utišavanja RhoD stanice brže prolaze kroz mitozu u odnosu na kontrolni uzorak te KIF20B utišane stanice. Kako bismo provjerili utjecaj koji bi RhoD mogao imati na stanični ciklus u HeLa stanicama, obojali smo nesinkronizirane HeLa stanice propidij jodidom i analizirali njihovu raspodjelu u staničnom ciklusu protočnom citometrijom 72 sata nakon transfekcije. Pronašli smo specifičnu „prazninu" na granici faza G1/S za sve 3 ispitane RhoD siRNA, a isti fenotip nađen je i na dvije od tri testirane KIF20B siRNA. Slični rezultati za RhoD objavljeni su i prije, ali za stanice 48 sati nakon utišavanja (Kyrkou et al., 2012). Ovaj pronalazak specifične „praznine" u G1/S fazi u RhoD i KIF20B utišanim HeLa stanicama ukazuje na to da postoji mogućnost kako RhoD i KIF20B imaju sličnu ulogu tokom G1/S prijelaza staničnog ciklusa.

S obzirom da smo pronašli dokaze kako bi RhoD i KIF20B mogli imati zajedničku ulogu tokom odvijanja staničnog ciklusa, te uz brojne literaturne podatke o sudjelovanju KIF20B u staničnoj diobi te saznanju da je sličan onkoproteinima, naši podaci i literatura o RhoD ukazuju na mogućnost da RhoD ima ulogu u raku, posebice u osjetljivosti tumorskih stanica na protutumorske lijekove. Ovu mogućnost ispitali smo analizom stanične proliferacije pomoću MTT testa. Obradom stanica s utišanim RhoD ili KIF20B proteinima citostaticima cisplatinom, paklitakselom i vinkristinom, našli smo drugačije odgovore u različitim tipovima stanica.

U svim ispitanim staničnim linijama nakon utišavanja RhoD uočili smo učinak blagogo smanjenja stanične proliferacije, oko 20% u odnosu na negativnu kontrolu utišavanja. Utjecaj utišavanja KIF20B na staničnu proliferaciju bio je ponešto sličan onom od RhoD, ali ne tako izražajan kao u RhoD utišanih stanica. Radi uočene smanjene stanične proliferacije kod utišavanja ovih molekula, sve podatke iz MTT testova analizirali smo pomoću ANOVA statističkog testa, koji uzima u obzir ovo smanjenje.

U HeLa stanicama pomoću MTT testa smo primijetili da utišavanje RhoD ili KIF20B doprinosi blagoj osjetljivosti stanica na cisplatinu. U HeLa CK stanicama, otpornima na cisplatinu, RhoD je također pridonio blagoj osjetljivosti, no u slučaju KIF20B utišavanja gotovo nikakav učinak nije zapažen, što znači da nema interakcije između lijeka i siRNA koja bi rezultirala sinergističkim ili antagonističkim efektom. Kada su HeLa stanice obrađene paklitakselom i vinkristinom, primijetili smo antagonistički efekt između lijekova i siRNA na RhoD ili KIF20B, što ukazuje na to da utišavanje RhoD ili KIF20B doprinosi blagoj otpornosti ovih stanica na ove lijekove. U HeLa CK stanicama ANOVA je pokazala blagu otpornost na paklitaksel prilikom utišavanja RhoD i slabu osjtljivost kod utišavanja KIF20B. Kod odgovora na vinkristin, situacija je u HeLa CK bila obrnuta i samo je rubna osjetljivost na vinkristin nađena u RhoD utišanim stanicama, i blaga otpornost u KIF20B utišanim stanicama.

Kod HCT-116 stanica odgovori na cisplatinu u stanicama utišanim na RhoD i KIF20B bili su veoma slični, ali neznačajni i pokazivali su blagu otpornost. U CaCO-2 stanicama nije pronađena interakcija između lijeka i utišanog RhoD ili KIF20B, a isto je primijećeno i kada su HCT-116 stanice obrađene s paklitakselom, dok su CaCO-2 stanice pokazale blagu, ali neznačajnu rezistenciju na paklitaksel. Slični rezultati dobiveni su i obrađivanjem stanica vinkristinom, gdje je utišavanje RhoD i KIF20B u HCT-116 stanicama pridonijelo neznačajnoj otpornosti, a kod CaCO-2 nije bilo jasne interakcije.

U modelima stanica raka dojke MDA-MB-231, MDA-MB-468 i MCF-7 primijećen je antagonistički učinak obje siRNA na lijek cisplatinu, pokazujući da siRhoD i siKIF20B pridonose blagoj otpornosti na cisplatinu, koja nije bila značajna. U MCF-7 stanicama uočena otpornost na cisplatinu prilikom utišavanja RhoD može se povezati s prethodno obavljenim literaturnim podacima gdje je nađeno da je ekspresija RhoD smanjena u MCF-7 stanicama otpornima na cisplatinu (Watson et al. 2007). Prilikom obrade paklitakselom, razlika između tretiranih i netretiranih stanica je drastičnija te ukazuje na to da utišavanje RhoD i KIF20B ima antagonistički utjecaj na lijek. Na kraju, prilikom obrade vinkristinom, antagonistički

efekt/otpornost također je primijećen u svim ispitanim staničnim linijama raka dojke za oba utišana gena, gdje su MCF-7 stanice pokazale najizraženiji učinak.

Što se tiče proteina KIF20B, iako grafički prikaz podataka iz MTT testa uglavnom ukazuje na blagu osjetljivost na paklitaksel i vinkristin kod većine ispitanih staničnih linija, dublja analiza pomoću ANOVA statističkog testa otkriva kako se već zbog učinka utišavanja KIF20B na staničnu proliferaciju zapravo radi o antagonističkom utjecaju lijeka i KIF20B siRNA molekula, što znači da utišavanje KIF20B pridonosi blagoj otpornosti na lijekove paklitaksel i vinkristin. Kada se ovi podaci usporede s trenutačno dostupnom literaturom, uviđa se da je prethodno nađeno kako je KIF20B povećano eksprimiran u tkivima raka dojke otpornima na spojeve taksane, u odnosu na normalna tkiva dojke (Tan et al., 2012). S obzirom na ove podatke, očekivali bismo da utišavanje KIF20B poveća osjetljivost na taksane, prije nego da blago poveća otpornost, kao što smo mi pokazali.

Druge studije koje govore o tome kako utišavanje KIF20B povećava osjetljivost na spojeve taksane obuhvaćaju dva istraživanja na staničnim linijama hepatocelularnog karcinoma (HCC). Prva priopćuje kako shRNA na KIF20B pokreće zastoj proliferacije HCC stanica, početak apoptoze te povećanu osjetljivost na paklitaksel, što su pokazali na staničnim linijama HepG2 i Hep3B (Liu et al., 2014). Druga studija iste skupine pokazuje na staničnim linijama HepG2, Hep3B i HuH-7, kako utišavanje KIF20B pomoću shRNA onkolitičkog adenovirusnog vektora povećava osjetljivost stanica na paklitaksel te ima sinergistički učinak s dva druga lijeka koji se vežu na mikrotubule; epotilon B i vinkristin (Liu et al., 2018). Ovi podaci nisu u skladu s našim opažanjima, no treba naglasiti kako smo koristili drugačiji tip utišavanja te smo koristili druge stanične modele.

Sveukupno, pokazali smo kako RhoD ima novu lokalizaciju u međustaničnom mostu koja do sada nije bila zabilježena te može ukazivati na dublju uključenost RhoD u posljednjim koracima citokineze, moguće preko interakcije s proteinom KIF20B. KIF20B je nedavno postao zanimljiva ciljna molekula za liječenje raznih tipova tumora, što ukazuje na njegovu bitnu ulogu tokom stanične diobe. Sve više istraživanja koristi sve više različitih vrsta stanica kako bi se saznalo utječe li utišavanje KIF20B u tumorskim stanicama na povećanje osjetljivosti istih na protutumorske lijekove. Za sada naši rezultati pokazuju povećanje osjetljivosti na cisplatinu i to samo u HeLa stanicama u kojima je utišan RhoD ili KIF20B. Dok naši drugi rezultati upućuju na blagu osjetljivost na paklitaksel i vinkristin u ispitanim staničnim linijama, ANOVA statistička analiza otkriva uglavnom antagonističke efekte između tih lijekova i obje siRNA.

Unatoč tome, sva ova opažanja ukazuju na to da bi KIF20B, a pogotovo RhoD, bili vrijedni daljnjih istraživanja odgovora na protutumorske lijekove. Kako bi se u budućnosti postigao jači učinak utišavanja te kako bi se zaobišli tzv. „off-target" efekti koje mogu imati molekule siRNA, tehnologija CRISPR-Cas9 bi mogla biti prikladnija u istraživanjima uključenosti RhoD i KIF20B u osjetljivost na protutumorske lijekove, također kao i u studijama o njihovim ulogama tokom stanične diobe.

10. Curriculum Vitae

I was born on July 24th 1985 in Zagreb, Croatia. After finishing high school, I enrolled in the Molecular Biology diploma course at the Department of Biology, of the Faculty of Science, University of Zagreb. As a student I was a demonstrating assistant for the course Microbiology, under the supervision of Prof. Božidar Stilinović, PhD, and later Prof. Jasna Hrenović, PhD. I finished the diploma program by graduating fourth in my class, on April 16th 2009. I performed experiments for my diploma thesis "Retargeting Adenovirus type 5 to integrin $\alpha_4\beta_1$" at the Laboratory for Genotoxic Agents of the Ruđer Bošković Institute, Zagreb, under the mentorship of Prof. Andreja Ambriović-Ristov, PhD. Later I was employed by the Ruđer Bošković Institute to work on the project "Cell response to cytotoxic compounds and resistance development" under leadership of Prof. Maja Osmak, PhD. Soon after I enlisted in the Molecular Biosciences PhD program of University of J. J. Strossmayer, Osijek, Croatia. I was also an Assistant in the doctoral course of Resistance of tumour cells to therapy, under supervision of Professor Maja Osmak, PhD.

In 2011 I participated in the Croatian final of the Fame Lab competition, hosted by British Council, which promotes popularization of science.

I was awarded a MEXT Scholarship for year 2012 by Ministry of Education, Culture, Sports, Science and Technology of Japan, which funded my Scholastic stay in Laboratory of Professor Shuh Narumiya, MD, PhD, Department of Pharmacology, Faculty of Medicine of University of Kyoto, Japan and Medical Innovation Center of Faculty of Medicine of University of Kyoto from April 2012 until August 2013. During this stay I have actively participated in the publication of two scientific research papers published in Journal of Cell Science and Cell Reports. At the University of Kyoto, I have started performing experiments for my PhD thesis, which I resumed and completed under the mentorships of Prof. Toshimasa Ishizaki, PhD, and Prof. Andreja Ambriović-Ristov, PhD, at the Laboratory for Cell Biology and Signal Transduction, upon my return to Croatia.

I participated in three international and three national Congress presentations and published five research papers in peer-reviewed journals.

I am happily married and a mother of three.

Publication List

1. Burja, Bojan; Čimbora-Zovko, Tamara; Tomić, Sanja; **Jelušić, Tihana**; Kočevar, Marijan; Polanc, Slovenko; Osmak, Maja; Pyrazolone-fused combretastatins and their precursors : synthesis, cytotoxicity, antitubulin activity and molecular modeling studies // Bioorganic & medicinal chemistry, 18 (2010), 7; 2375-2387 doi:10.1016/j.bmc.2010.03.006

2. Majhen, Dragomira; Stojanović, Nikolina; Špeljko, Tea; Brozović, Anamaria; **De Zan, Tihana**; Osmak, Maja; Ambriović-Ristov, Andreja; Increased expression of the coxsackie and adenovirus receptor downregulates alpha v beta 3 and alpha v beta 5 integrin expression, reduces cell adehesion and migration // Life sciences, 89 (2011), 7/8; 241-249 doi:10.1016/j.lfs.2011.06.009

3. Watanabe, Sadanori; **De Zan, Tihana**; Ishizaki, Toshimasa; Narumiya, Shuh; Citron kinase mediates transition from constriction to abscission through its coiled-coil domain. // Journal of cell science, 126 (2013), 8; 1773-1784 doi:10.1242/jcs.116608

4. Watanabe, Sadanori; **De Zan, Tihana**; Ishizaki, Toshimasa; Yasuda, Shingo; Kamijo, Hiroshi; Yamada, Daisuke; Aoki, Tomohiro; Kiyonari, Hiroshi; Kaneko, Hiroshi; Shimizu, Ritsuko et al. ; Loss of a Rho-Regulated Actin Nucleator, mDia2, Impairs Cytokinesis during Mouse Fetal Erythropoiesis // Cell reports, 5 (2013), 4; 926-932 doi:10.1016/j.celrep.2013.10.021

5. Rak, Sanjica; **De Zan, Tihana**; Štefulj, Jasminka; Kosović, Marin; Gamulin, Ozren; Osmak, Maja; FTIR spectroscopy reveals lipid droplets in drug resistant laryngeal carcinoma cells through detection of increased ester vibrational bands intensity // Analyst, 139 (2014), 13; 3407-3415 doi:10.1039/c4an00412d